The geology and genesis of the Kencana epithermal Au-Ag deposit, Gosowong Goldfield, Halmahera Island, Indonesia

by
Lindsey V. Clark
MSci

Submitted in fulfilment of the requirements
For the degree of Doctor of Philosophy

UNIVERSITY
OF TASMANIA

Australia

August, 2012

This thesis is dedicated to my parents

Gavin and Helen Clark

who encouraged me to study the Earth
whilst reaching for the stars

STATEMENT

This thesis contains no material which has been accepted for the award of any other degree or diploma in any tertiary institution and, to the best of my knowledge and belief, contains no copy or paraphrase material previously published or written by another person, except where due reference is made in the text of the thesis.

Date: 30th August 2012

Signature: 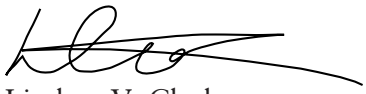

Lindsey V. Clark

AUTHORITY OF ACCESS

This thesis is not to be made available for loan or copying for a period of 24 months from the date this statement was signed; after that time limited copying is permitted in accordance with the Copyright Act 1968.

Date: 30th August 2012

Signature: 

Lindsey V. Clark

ABSTRACT

The Kencana Au-Ag low-sulfidation epithermal deposit, situated in the Neogene magmatic arc of Halmahera, Eastern Indonesia, has an estimated resource of 4.4 Mt @ 27.9 g/t Au, containing 4 Moz Au. The deposit, forming part of the Gosowong Goldfield, is the third, and most recently discovered (2002) deposit in the goldfield, after the Gosowong and Toguraci deposits.

The Gosowong goldfield is situated on the eastern side of the NW arm of Halmahera, which is composed of four superimposed volcanic arcs, produced as a result of subduction of the Molucca sea plate beneath Halmahera since the Palaeogene. Lithologies are dominated by andesite to basaltic andesite volcanic and volcaniclastic rocks and diorite intrusions.

Epithermal mineralization is hosted by the upper Miocene Gosowong Formation, a series of interbedded volcaniclastic rocks, ignimbrites and coherent andesitic volcanic flows and diorite intrusions. Andesites and diorites are closely temporally related, with andesite emplacement at 3.73 ± 0.22 Ma followed by diorite intrusion at ~3.50 Ma. Epithermal mineralization post-dates andesite and diorite emplacement with $^{40}Ar/^{39}Ar$ dating of hydrothermal adularia giving a mean age of 2.925 ± 0.026 Ma for the Kencana deposit.

The deposit is hosted by two main sub-parallel NW-trending fault structures, (namelyK1 and K2) with a strike length of 400 m, a vertical extent of 200 m and dipping ~46°E; joined by link structures, such as K-Link (KL). Bonanza Au-grade zones are located in dilational zones above hematitic volcaniclastic mudstone packages. The deposit does not crop out, but displays a weak surface expression represented by carbonate veining and faults filled with clay and pyrite.

Kencana (K1 vein) shows a complex, multiphase history of formation with numerous brecciation and opening events. Eleven infill types are recognized at Kencana, including

wallrock (1), quartz stockwork (2), wallrock breccias with crystalline quartz cement (3), red chalcedony infill (4), massive crystalline quartz (5), massive crystalline quartz breccias (6), cockade-banded quartz-chlorite breccias (7), banded quartz-chlorite (8), banded quartz-adularia (9), grey cryptocrystalline quartz stringer veins (10) and black quartz-molybdenite infill (11). Infill types 1, 2 and 3 are distributed throughout the deposit and are particularly prevalent on the margins of the vein. Types 7, 8 and 9 are the main ore-bearing stages and form the bulk of the central section of the vein. Type 11 infill is most prevalent to the north. Types 4, 5, 6 and 10 are variably and sporadically distributed across the vein.

Ore assemblages are dominated by high-fineness electrum and sulfides, with selenides and lesser tellurides and sulfosalts. Chalcopyrite is the most common sulfide mineral, with selenian-galena, sphalerite, bornite and pyrite in order of decreasing abundance. Other accessory minerals include aguilarite and molybdenite, with trace tennantite, arsenian-pyrite, silver and lead tellurides, naummanite and rare bismuth minerals. Gangue minerals are crystalline, microcrystalline and cryptocrystalline quartz, adularia, chlorite and calcite.

Ore deposition is interpreted to be the result of a combination of processes (mixing, boiling and cooling), with mixing processes inferred to be of particular importance, based on the presence of high-fineness electrum and selenium-bearing minerals. Evidence for boiling processes is present at Kencana after deposition of infill type 5, including bladed carbonate pseudomorphs and abundant adularia. A general transition from early coarse crystalline quartz to micro- and cryptocrystalline quartz is observed in the paragenetic sequence of the K1 vein, reflecting an increase in the rate of silica precipitation in silica-saturated fluids.

Fluid inclusion data indicate that early crystalline quartz (type 2c) was precipitated from near-neutral, hot, low salinity, low CO_2 (203.0 to 248.8°C, 0.1 to 0.5 wt% NaCl (equiv.), <0.015 m CO_2) fluids. Temperatures and salinities increase during formation of the main ore-bearing stages of the deposit. Fluids associated with precious metal deposition in type 7 and 8 infill are 202.7 to 306.9°C, 0.0 to 1.0 wt% NaCl (equiv.), <0.015 m CO_2, with fluids in quartz-adularia (type 9) mineralization forming at (95.8 to 258.7°C, 0.0 to 0.8 wt% NaCl (equiv.), and <0.015 m CO_2). Pressure estimates used to calculate minimum depth of

entrapment infer that most fluid inclusions were trapped 50 to 200 m deeper than their current location.

Mineralizing fluids are strongly dominated by meteoric water, with a marginally increased magmatic input during formation of type 7 and 8 infill. Gold hydrosulfides (in particular, $Au(HS)_2$ are most significant in terms of gold transport at Kencana. Metal-bearing fluids were sourced from the down-dip extension of the K1 vein, flowing upwards through the dilating structure. Metal distribution is vertically and laterally zoned at the Kencana deposit, with precious metals enriched at shallow levels of the system, and base metal values increasing systematically with depth. Lateral zonation implies a hydrothermal fluid temperature gradient with a metal source to the north of the Kencana deposit.

Ten alteration facies are recognized: SCG (Argillic 1) facies, ISP (Argillic 2) facies, IC (Argillic 3) facies, QAS (Phyllic) facies, EC (Propylitic 1) facies, CEP (Propylitic 2) facies, P (Sub-propylitic) facies, BM (Calc-potassic) facies, IDP (Intermediate-advanced argillic) facies, and KH (Advanced argillic) facies. Zonation is also observed in the distribution of alteration facies: (1) phyllic alteration (QAS facies) in the form of pervasive silicification and quartz-adularia-sericite alteration in the immediate vein zone, (2) argillic alteration (IC facies) enveloping the vein zone, (3) high-temperature propylitic alteration (CEP facies) filling fractures, extending up to 50 m from the vein, and (4) low-temperature argillic alteration and regional propylitic alteration (SCG, ISP and IC facies) distal to the vein. Supergene advanced argillic alteration (KH facies) blankets the top 5 m of stratigraphy at Kencana and represents intense tropical surface weathering. The geochemical signature of altered rocks hosting the Kencana deposit is variable depending on position relative to the mineralized structure, either within the vein, in the upflow zone, in the outflow zone or in the alteration halo.

It is proposed that a sub-class of low sulfidation epithermal deposits (Se-rich low sulfidation epithermals), characterized by bonanza-grade Au, bimodal volcanism and a Se-rich ore mineral assemblage, such as Midas (USA), Hishikari (Japan), and Broken Hills (New Zealand), be considered, and that Kencana is a classic example of such a deposit. It

is suggested that as well as similarities in their general geological setting, these deposits may form under similar physiochemical conditions, including the relatively more oxidized conditions than typical for low sulfidation systems.

The volcanic-hydrothermal evolution of the Kencana deposit is relevant to understanding the genesis of, and exploring, for other low sulfidation epithermal gold deposits in volcanic settings. Several geological and geochemical features observed in the Kencana deposit may be useful for helping to vector towards mineralized zones in the Gosowong Goldfield, and other low sulfidation epithermal districts, including zonation of chlorite chemistry from Fe-rich to Mg-rich with increasing proximity to mineralization, lateral metal zonation from high to low temperature assemblages, elevated Pb and Sb values in altered host rocks with strong zonation around the ore zone, and the quantitative increase of potassium metasomatism (represented by mK/(2Ca+Na+K) values) towards the Kencana deposit. High As and Sb values relative to mK/(2Ca+Na+K) values can be used as distal pathfinders to ore mineralization, as these elements are enriched at low mK/(2Ca+Na+K) values, where precious metals (e.g. Au) are enriched at higher mK/(2Ca+Na+K) values.

ACKNOWLEDGEMENTS

I have benefited greatly from the knowledge, assistance, support and friendship of many people over the course of this research and the following list attempts to thank all of those involved. I extend my gratitude to any that I may have overlooked.

First and foremost, I would like to thank my principal supervisor Prof. Bruce Gemmell, who has been unrelenting in his guidance, enthusiasm and belief in me over the course of this project. Bruce spent hours translating my thoughts and questions into expressions and theories fit for a thesis. Thank you Bruce for imparting so much knowledge on epithermal geology and for your patience, constructive help and advice - we've come a long way from the first week when I asked you what "epithermal" meant! Not to mention keeping me well supplied with Bombay Sapphire through many long months in the jungle.

I would also like to thank my secondary supervisor Prof. Dave Cooke, who was always willing to provide advice and support whenever it was required, and my research advisor Dr. Steven Micklethwaite.

To all the academic staff and researchers at CODES and the School of Earth Sciences at UTAS for many insightful discussions, inspiration and for opening my eyes to the world of ore deposits. I would also like to thank all the researchers and staff at CODES and the Central Science Laboratory who aided my project, took care of administrative and financial matters and taught me many new techniques in analysis: Karsten Goemann, Sandrin Feig, Sarah Gilbert, Marcel Guillong, Katie McGoldrick, Ian Little, Phil Robinson, Zhaoshan Chang, Huayong Chen, Izzy von Lichtan, Peter Cornish, Karen Mollross, Rose Pongratz, Helen Scott, Christine Higgins, Caroline Mordaunt, Claire Rutherford, Deborah Macklin and Nilar Hlaing. Thanks to June Pongratz for her assistance with printing and to Keith Dobson for IT and technical support.

This project was supported logistically and financially by Newcrest Mining Ltd., and thanks go to all those who were involved in setting up this project and for giving me the

opportunity to study such an incredible ore deposit. Special thanks to Dean Collett, Kylie Braund, Trinity Gilmore and Chris Chambers for many meetings, helpful discussions and direction. To all the geologists and staff on site at Gosowong, thank you for your assistance, friendship, badminton matches and all logistical support I received whilst in Indonesia. I'm eternally grateful for all the extra work put in to get me to the places I needed to be, and for putting up with my dubious Bahasa Indonesia. Thanks to Dadan Wardiman, Daud Silitonga, Sidik Purnama, Junita Siregar, Ketut Suyadnya, Joko Nugroho, Keke, Yulastriani Aci, Sanjaya Bekti, Fintje Mangalo, Rachel Benton, Jeremy Simpson, Brian Koster, Nick Fitzgerald, Colin McMillan and Mark Menzies.

Thanks for financial support provided to this project by the Society of Economic Geologists in the form of research grants and fellowship awards.

To all the friends I have made at CODES over the past 4 years, thank you for all the great times and for being there during the harder ones. I have had the opportunity to meet so many wonderful people and I am certain that our friendships will only continue to grow over the years. To Jamie and Clara Wilkinson, for endless advice, guidance, a beautiful friendship and bubbling (in all its forms). To Victoria Braniff, for all the tea breaks and for keeping me British. To Sarah Quine and Martin Jutzeler, for being our family away from home. To my family and friends at home for understanding when I decided to uproot myself to the other side of the globe and for always being there when I needed you. Thank you so much for the countless emails and calls, for keeping me going and for always telling me I could do it.

To Mathieu, without whom this thesis would not have been finished. I do not know how you managed to help get me across the line whilst writing your own thesis and yet remaining your calm and collected self. Your patience and encouragement have been unwavering and I cannot tell you how much I have valued your love, advice, friendship and your ability to always make laugh these past years. This thesis isn't for you, it's because of you.

And finally, to Bun. I cannot wait to share with you all the beauty in the world, and the magic in how it was made.

TABLE OF CONTENTS

Chapter 3: Deposit geology

Chapter 4: Vein geology

Chapter 5: Alteration facies, distribution and geochemistry

LIST OF FIGURES

Chapter 4: Vein geology

Chapter 5: Alteration facies, distribution and geochemistry

LIST OF TABLES

CHAPTER 1

INTRODUCTION

1.1 Background

The term 'epithermal' was first used by Lindgren (1933) as a low temperature and low pressure classification for a group of shallow crustal hydrothermal ore deposits. The classification was based on stratigraphic relationships in volcanic sequences and analogy with mineral occurrences and textures in modern geothermal systems. Lindgren (1933) proposed that epithermal deposits form at low pressures (< 100 bars) and low temperatures (< 200°C). Based on fluid inclusion and stable isotope studies (e.g. Nash, 1972; Casadevall and Ohmoto, 1977; Kamilli and Ohmoto, 1977; Sawkins et al., 1979; Buchanan, 1981), the temperature of formation was extended up to 300°C and meteoric water is recognized as a dominant component of the ore-forming fluids.

Several workers have subdivided epithermal deposits based on a variety of textural and compositional features (e.g. Sillitoe, 1977; Heald et al., 1987). Hedenquist (1987) subdivided the epithermal ore-forming domains into high and low sulfidation end- members. The term "sulfidation" was used to describe the oxidation state of sulfur species in the ore-forming fluids (Hedenquist, 1987; White and Hedenquist, 1990; Hedenquist and Lowerstern, 1994). The definition was later revised (Hedenquist et al., 2000) to categorize sulfur-bearing minerals in terms of sulfur fugacity, consistent with the usage of Einaudi (1977), Barton and Skinner (1979), and Einaudi et al. (2003), where low sulfidation deposits contain pyrite-pyrrhotite-arsenopyrite and high-Fe sphalerite, in contrast to pyrite-tetrahedrite/ tennantite-chalcopyrite and low-Fe sphalerite in intermediate sulfidation deposits (Hedenquist et al., 2000).

Low sulfidation epithermal deposits are characterized by (1) Au- Ag mineralization with anomalies of Cu-Pb-Zn-As-Sb-Hg, (2) a distal association with a magmatic fluid source, (3) quartz-calcite-adularia-sericite alteration, (4) a predominantly meteoric source of water with a magmatic volatile component, and (5) near neutral pH, moderate temperature

(< 300°C) and low salinity fluids (< 3.5 wt% NaCl eq.) (Cooke and Simmons, 2000; Simmons et al., 2005). High sulfidation epithermal deposits are characterised by (1) Au-Ag-(Cu) mineralization with anomalies of As-Sb-Bi-Pb-Hg-Te-Sn, (2) a close spatial association with a degassing magmatic source, (3) vuggy quartz and advanced argillic alteration assemblages, (4) a predominantly magmatic fluid source (low pH, low salinity (< 5 wt% NaCl eq.); Cooke and Simmons, 2000; Simmons et al., 2005).

Low sulfidation epithermal deposits are spatially associated with subaerial bimodal (basalt-rhyolite) magmas in a wide range of tectonic settings (Gemmell, 2004; Fig. 1.1). Crustiform and colloform banding, along with platy calcite pseudomorphs, are common textural features of low sulfidation deposits (Cooke and Simmons, 2000). At the shallow levels associated with epithermal deposit formation, precipitation of metals is favoured by boiling and/ or mixing, and is facilitated by changes in temperature, pressure and chemical gradient (White and Hedenquist, 1990; Cooke and Simmons, 2000).

The island arcs of Indonesia are known to host a large number of economic epithermal Au-Ag deposits. However, the Halmahera arc remains relatively unexplored due to the difficulty of access and the dense equatorial jungle cover. Kencana is the third low sulfidation epithermal Au-Ag deposit discovered in the Gosowong goldfield, after the Gosowong and Toguraci deposits (Fig. 1.1 A). This area, although relatively small, holds huge potential as an epithermal district, and it is highly probable that economic, high-grade epithermal veins remain undiscovered in the region. Due to the difficulty of the terrain and the propensity for 'blind' deposits in the goldfield, it is essential that exploration targets can be based on solid geological understanding arising from characterization of the existing deposits.

This PhD study was created out of the need to determine exploration vectors to mineralization in the goldfield, as well as the ideal opportunity to study a bonanza-grade Au-Ag epithermal deposit, including the volcanic facies, structural setting, metal distribution, vein textures, fluid chemistry and alteration, with the aim of furthering the understanding of deposit formation in the epithermal class.

1.2 Study Objectives

The main objectives of this research project were to determine and describe the geological, mineralogical and geochemical characteristics of the Kencana deposit. Of particular

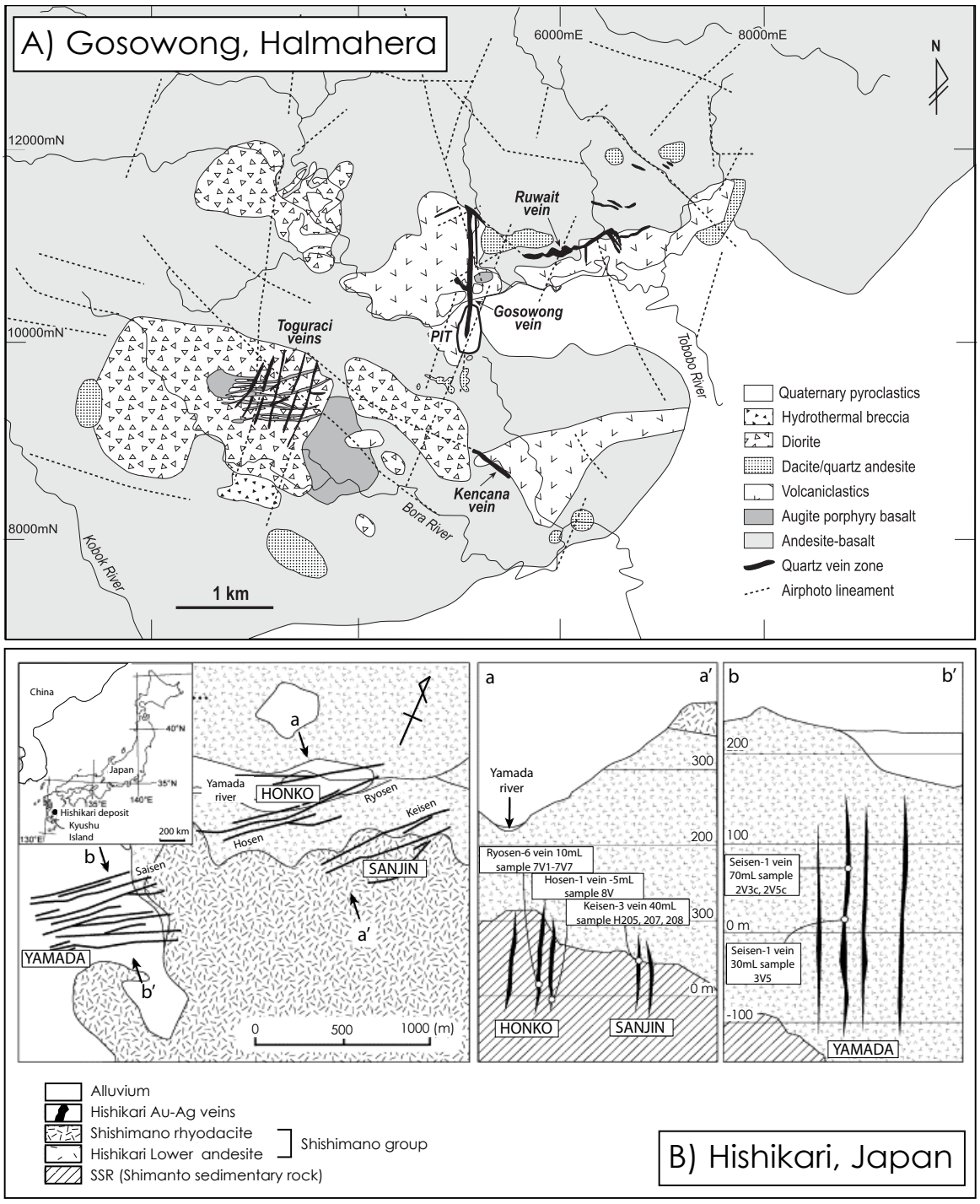

Fig. 1.1 District and deposit geology of selected low sulfidation epithermal Au-Ag deposits. A) Gosowong Goldfield, Halmahera, Indonesia (Gemmell, 2007); **B)** Hishikari deposit, Kyushu, Japan (modified after Ibaraki and Suzuki, 1993); **C)** Midas, Nevada, USA (Leavitt et al., 2004); **D)** Golden Cross, Coromandel Peninsula, New Zealand (Simmons et al., 2000; Begbie, 2007).

Fig. 1.1 continued.

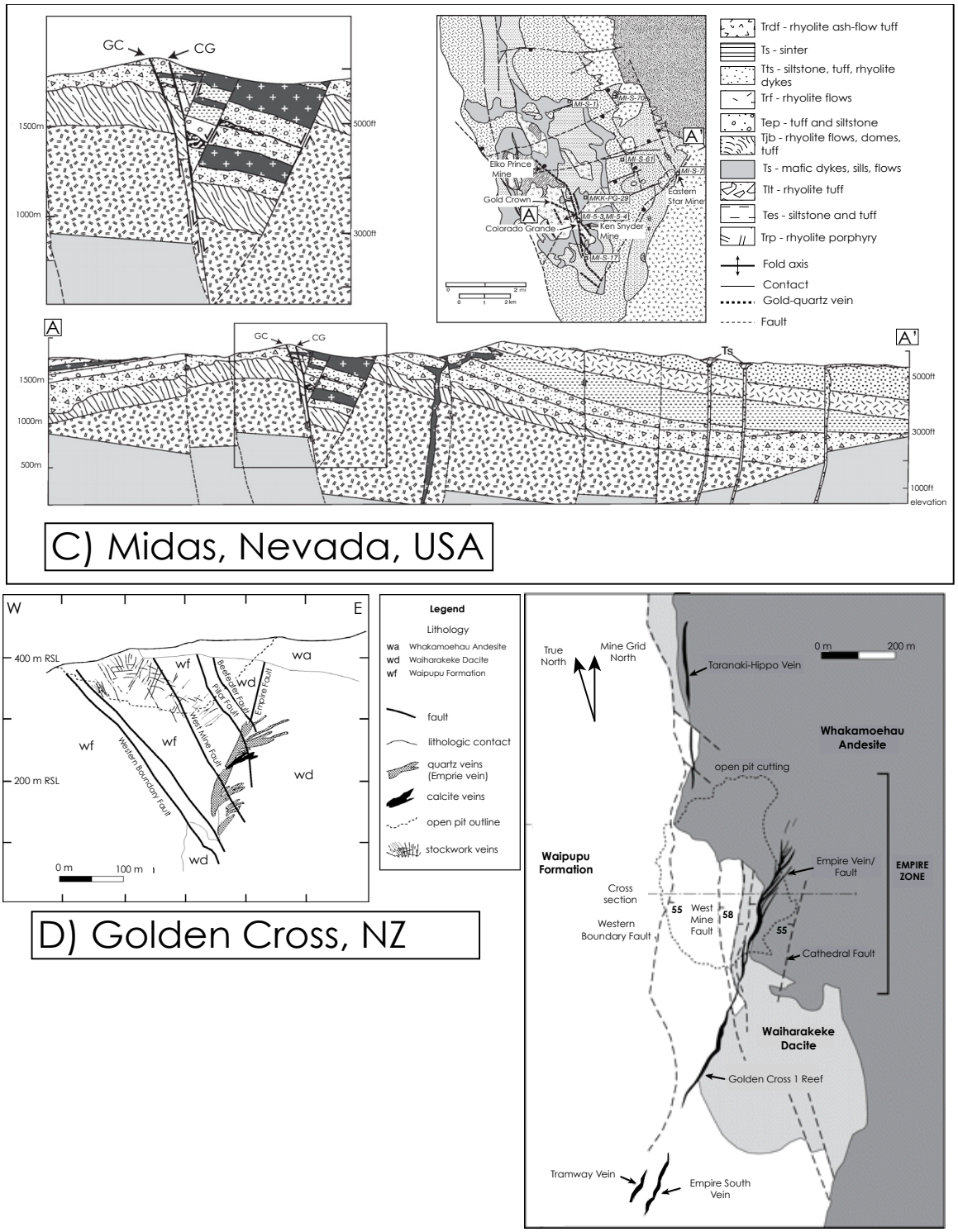

importance was the investigation and characterization of the vein textures and their distribution, alteration facies and their distribution, and determination of metal zonation, both laterally and vertically throughout the deposit.

The overall aim was to establish an ore genesis model for the deposit, which could be used to assist the exploration team in generating successful new targets in the Gosowong goldfield. Comparisons between the features described at Kencana and those from the deposits at Gosowong (and to a lesser extent, Toguraci) allow the generation of regional exploration vectoring models.

Specific objectives of the study are as follows:

1) Characterise the geological setting of the Kencana deposit
2) Define the hydrothermal alteration assemblages and zonation
3) Describe the ore and gangue mineralogy, assemblages, textures and zonation
4) Determine the geochemical (major and trace element) characteristics and signature of the hydrothermal alteration and ore
5) Construct models of the mineral, metal and alteration zonation associated with the K1 vein
6) Propose an ore genesis model for the Kencana deposit
7) Develop useful criteria for further epithermal exploration in the Gosowong goldfield

1.3 Approach and methods

This PhD study included three fields seasons of fieldwork for a total of six months at the Gosowong mine site (July-September 2008, December-February 2009, and June-July 2010). Geologic relationships were documented mainly through diamond core logging. Underground mapping and sampling were restricted to available areas of the mine and thus a systematic sampling program could not be established. Surface mapping was not undertaken due to the lack of outcrop and cover by Recent volcanics in the vicinity of the Kencana deposit.

The primary focus for logging was six cross sections traversing the length of the K1 vein. Representative cross sections were chosen that intersected the margins and central areas of the vein, including high grade mineralization and barren zones. Due to rapid drillcore degradation in the tropical weathering environment, five to seven representative drill cores

were selected along each cross section and graphic core logging was conducted based on modified logging codes already in place on site at Gosowong. Cores were logged for geology, paragenesis, mineralization and alteration. Samples were collected approximately each 10m for geochemical analysis and samples displaying the range of rock characteristics from each drill hole were collected to record coherent units, contact relationships, breccia characteristics, veining, alteration, mineralogy, textural features and stratigraphic relationships. In addition to petrographic analyses undertaken during this study at CODES, supplementary petrographic and geochemical data were obtained from internal company reports of Newcrest Mining Ltd. and PT. Nusa Halmahera Minerals (PT. is a common Indonesian company abbreviation of Perusahan Terbatas, an approximate translation of a limited company).

Laboratory-based methods were used to supplement observations made during core logging and thin section petrography. Scanning electron microscopy (SEM) coupled with an Energy Dispersive Spectrometer (EDS) analyses and back-scattered electron (BSE) imaging were used to identify micron-sized ore minerals. Electron probe microanalysis (EPMA) was used to determine the composition of various sulfides, selenides end electrum. These analyses were undertaken at the Central Science Laboratory (CSL) at the University of Tasmania (UTAS) under the supervision of Dr. Karsten Goemann and Dr. Sandrin Feig.

Portable shortwave infra-red spectroscopy (SWIR) analyses were used to assist with identification of clays (illite, montmorillonite, kaolinite etc.), micas (biotite, muscovite, phengite etc.) and carbonates in the alteration assemblages. Staining of rock slabs with sodium cobaltinitrite was used to assist with identification of K-feldspar. This work was undertaken at CODES.

Fluid inclusion analyses were conducted on a Linkam MSD600 motor-driven stage at Imperial College, London under the supervision of Dr. Jamie Wilkinson, and at CODES. Additional fluid inclusion data were obtained from internal company reports of Newcrest Mining Ltd.

X-ray fluorescence (XRF) and inductively-coupled plasma mass spectrometry (ICP-MS) were used to obtain major and trace element geochemical data for altered rocks. This work was undertaken at CODES under the supervision of Dr. Ian Little, Dr. Phil Robinson

and Katie McGoldrick.

$^{40}Ar/^{39}Ar$ geochronology was used to constrain the age of epithermal mineralization at the Kencana, Gosowong and Toguraci deposits. Adularia samples from vein material for each deposit were analysed at the University of Melbourne by Prof. David Phillips.

1.4 Location, access and physiography

The Kencana deposit is located in the Gosowong Goldfield, on the north-west arm of the island of Halmahera in the North Maluku Province of Eastern Indonesia, at an approximate latitude of 1° 09' N 127° 42'E (Fig. 1.2). The Halmahera island group includes Halmahera Island, which stretches over 300 km from north to south, and 125 km from east to west, in a distinctive 'K' shape (Hakim and Hall, 1991) covering a total area of 18,400 km^2, surrounded by the smaller islands of Morotai, Ternate, Bacan, Obi and Gebe (Darman and Sidi, 2000). Halmahera island is intersected by the Halmahera volcanic arc, which includes a chain of volcanic islands off the western shore of Halmahera and volcanoes on the NW arm of the island (Figs. 1.3 A, D, and F).

The deposit is situated approximately 2400 km northeast of the Indonesian national capital, Jakarta, and 55 km to the east of the provincial capital, Ternate. Access to the Gosowong mine is via a 90 minute private charter helicopter flight from Manado, the provincial capital of North Sulawesi (Fig. 1.3 C) The deposit is situated 15 km inland from the coastal town of Malifut (Carlile et al., 1998). The topography of the area is steep and densely forested (Fig. 1.3 E), with elevations between 80-260 m above sea level. The area experiences a tropical climate, with a wet season from October to April, and a drier season from May to September. Annual rainfall is in the region of 3000 mm, and an average temperature of 28-32°C. 575,000 people are settled on Halmahera Island. Tobelo, located in North Halmahera, is the largest settlement on the main island, with 35,000 inhabitants.

Newcrest Mining Limited, an Australian public company, holds an 82.5% interest in the PT. Nusa Halmahera Minerals seventh generation contract of work (CoW), which includes the Gosowong goldfield. The Indonesian state-owned mining enterprise, PT. Aneka Tambang, holds the remaining 17.5% interest.

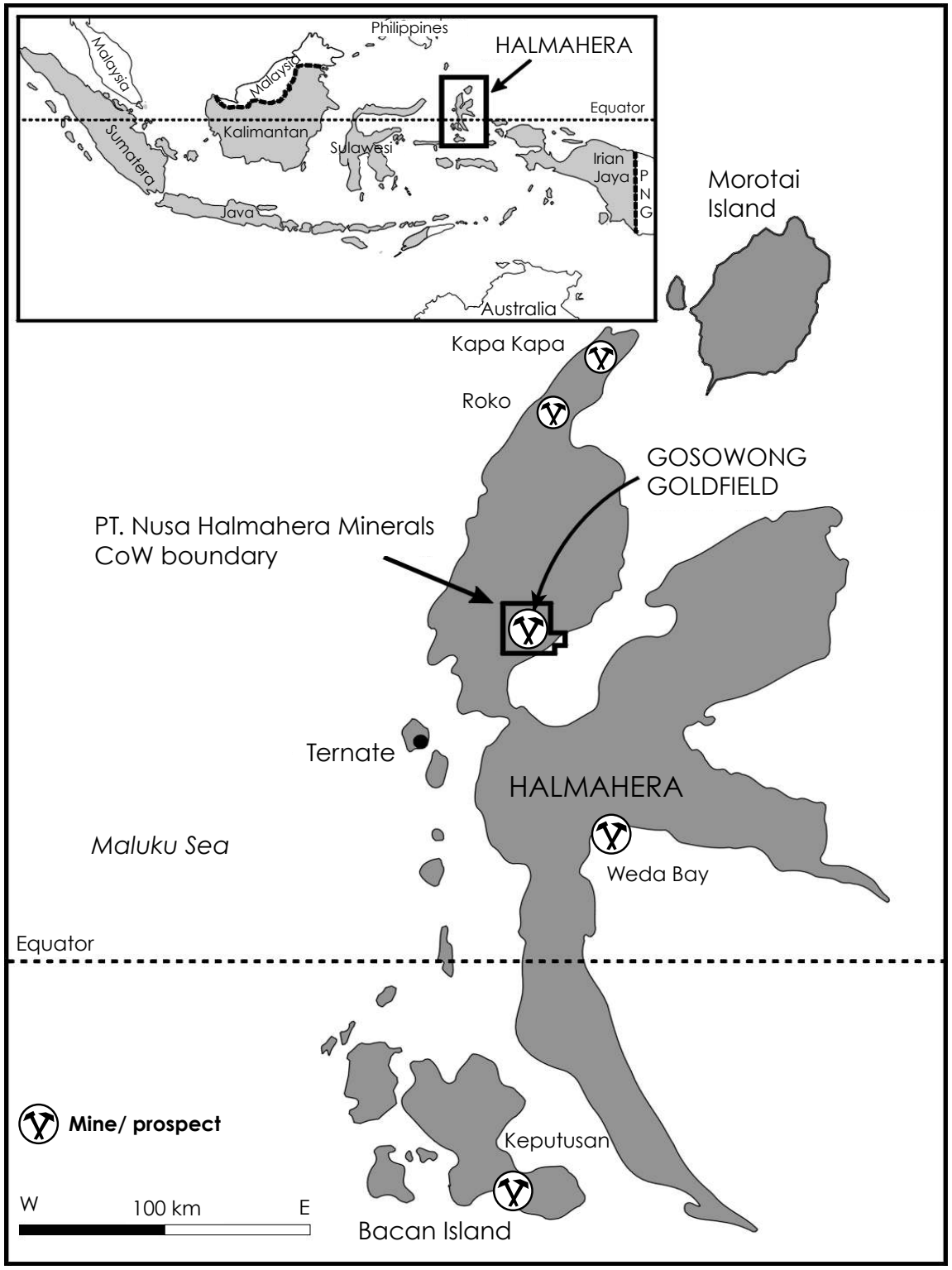

Fig. 1.2 Location of the Gosowong goldfield Halmahera is situated in Eastern Indonesia (inset), approximately 90 minutes by air from Manado, Sulawesi. The Gosowong goldfield is located within the Contract of Work (CoW) area (black box) on the western arm of Halmahera island. Modified after Newcrest, 2009.

Fig. 1.3 Views around NW Halmahera

A) Ibu volcano towards the northern end of the Halmahera arc, looking to the southeast (summit elevation 1325 m). All Halmahera arc volcanoes are active, with the last eruption of Ibu in 2004.

B) World War II debris is scattered across much of the island, including wrecks and artillery turrets.

C) AirFast Bell 204B helicopter used for the 90 minute private charter flight from Manado, Sulawesi to Gosowong mine, Halmahera.

D) Modern geothermal activity on the NW arm of Halmahera, including mudpools and steaming ground. Photograph taken from private charter helicopter, Gosowong.

E) The Tobobo River flows past the mine camp, and is the site of the Gosowong discovery outcrop (Fig. 1.3 F).

F) Gamalama volcano (1715m) dominates Ternate island, location of the North Malaku province captial. Recent eruptions include pyroclastic flow activity in 2003, and ash and steam plumes in 2008.

1.5 Exploration and mining history

Halmahera has a relatively short mineral exploration and mining history, mainly due to the rugged, deeply forested terrain, poor outcrop and difficulty of access. There is no history of gold mining, either legal or illegal. Prior to the Gosowong discovery, there was only one significant gold occurrence known in the Halmahera region - the Kaputusan Cu-Au porphyry deposit on the island of Bacan, where a resource of 77 Mt at 0.25 g/t Au and 0.33% Cu was determined by the Geological Survey of Indonesia, Federal Institute for Geosciences and Natural Resources in the late 1970's (Davey et al., 1997).

PT. Rio Tinto Bethlehem (CRA) and PT. Citra Maluku Mining (CSR) conducted reconnaissance sampling in the general coastal Gosowong area in 1985-1987. Both companies were targeting porphyry copper style mineralization, and as a result CRA did not assay for gold. CSR described some BLEG anomalies of 3-4 ppb Au in stream sediments from the Gosowong area, and despite describing quartz vein float in the Tobobo River both companies withdrew from Halmahera (Davey et al., 1997).

A review of the geology and mineralization of Indonesia carried out in 1991 by Newcrest Mining Ltd. determined that all major Au and Cu-Au deposits occur within Neogene magmatic arcs, where those of Plio-Pleistocene age were the most prospective (Carlile et al., 1998). The Halmahera arc was targeted as it provided an opportunity for Newcrest to obtain essentially a complete prospective arc in largely unexplored terrain.

Gosowong gold mineralization was discovered by Newcrest in May 1994 after a program of extensive ground reconnaissance in Northern Halmahera, targeting copper-gold porphyry and epithermal gold-silver mineralization. The deposit was discovered and tested using basic exploration techniques commonly used in the rugged tropical terrain of Indonesia (Davey et al., 1997; Carlile et al., 1998). Follow-up stream sediment and pan concentrate sampling (with later ridge and spur soil sampling) and geological mapping led to the discovery of the deposit. Reconnaissance stream sediment (Tobobo River) and float sampling produced strong positive gold anomalies 6.5 km downstream of the deposit.

In September 1993, gold-bearing quartz stockworking was discovered in the Tobobo River (Fig. 1.3 E; Fig. 1.4 F) (Carlile et al., 1998). The high-grade vein zone, which was exposed in hand-dug trenches, returned bonanza grade assay results, and the first drill hole produced an intercept of 18 m at 125.7 g/t Au. Construction of mine infrastructure com-

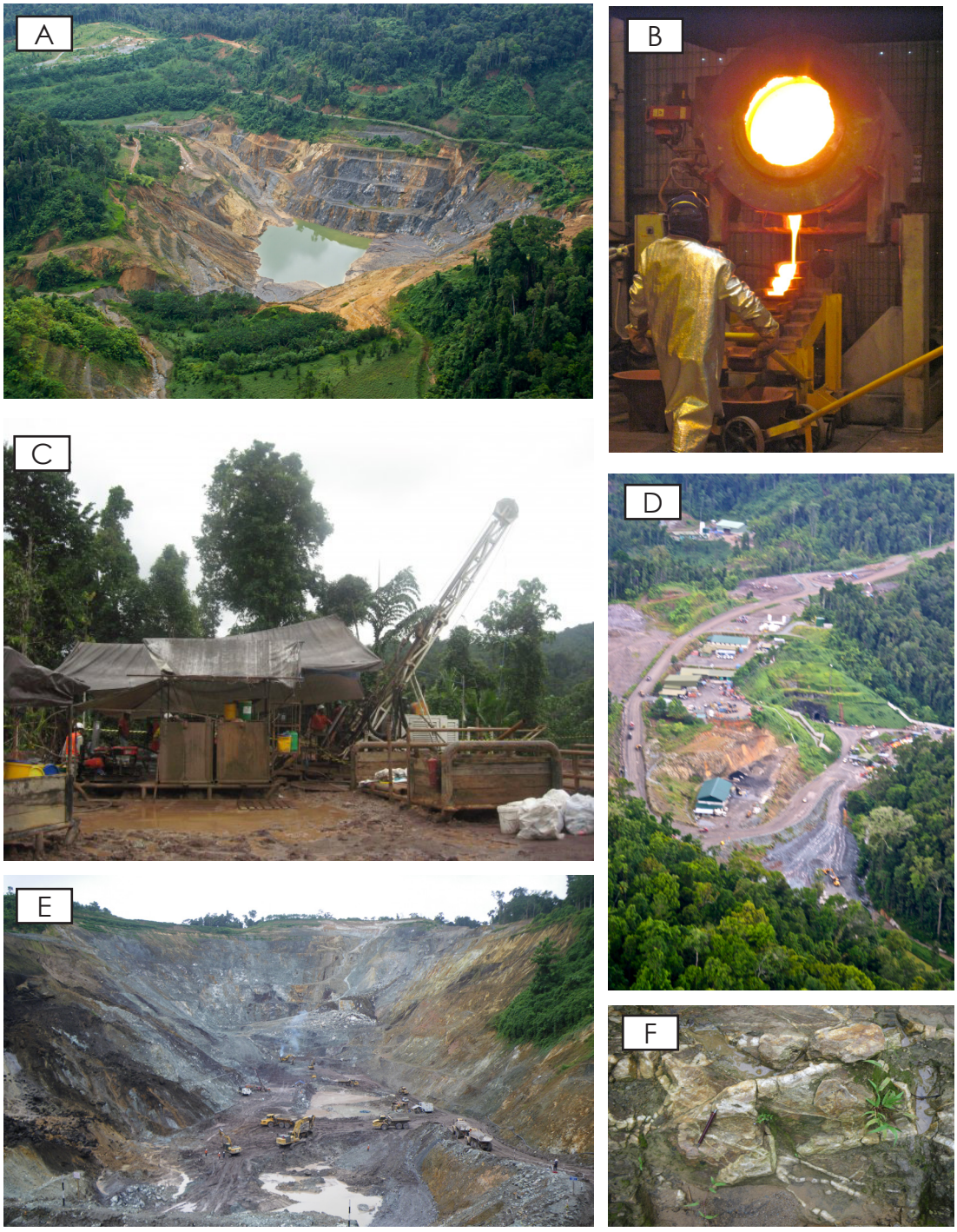

Fig. 1.4 Views around Gosowong Goldfield

A) Toguraci pit looking south east, taken in 2010 prior to development of the Toguraci North underground mine.
B) Gold pour at the on site mill
C) Drilling in the Gosowong goldfield requires innovative pad design and rig transport
D) Kencana underground portal with paste plant, geology office and haul road leading to the ROM pad
E) Gosowong pit in production in April 2012 (re-opened after initial closure in 2002), looking south. The vein can be identified on the far south wall, with slumping to the left of the image and minor advanced argillic alteration (white) at the top of the south wall (photo courtesy of J. B. Gemmell, 2012).
F) Gosowong discovery outcrop in the Tobobo river, crystalline quartz and chalcedony stockwork (pen for scale, photo courtesy of J. B. Gemmell, 2012).

menced in 1998. Production began in July 1999, and mining ceased in 2002. Total production from the Gosowong deposit was 880,000 tonnes at 27 g/t Au and 28 g/t Ag (760,000 oz Au) (Richards et al., 2005). The Gosowong pit was re-opened in early 2012 for extraction of further Au resources that are economic in the current climate (Fig. 1.4 E).

During 1999-2000, a program of 1:25,000 geological mapping within a 5 km radius of the Gosowong deposit led to the successful discovery of the Toguraci deposit, which represents high-grade low sulfidation epithermal Au-Ag mineralization overprinting earlier, uneconomic porphyry Cu-Au mineralization (Fig. 1.4 A).

Mineralization at Kencana was discovered in early 2003 as part of an ongoing exploration program in the Gosowong goldfield, targeting low sulfidation epithermal mineralization after the successful discovery and recovery of the Gosowong and Toguraci deposits. Olberg (2001) proposed a "Prospectivity Index" based on Gosowong mineralization that indicated the southerly extension of the Gosowong fault zone (GVZ) as a potential target for further epithermal mineralization. In January 2003, the first drill hole planned for the program intersected 7.25 m at 29 g/t Au, including 1 m at 140 g/t Au. This mineralization was not hosted in the GVZ, which was intersected further down-hole at 342.8 m, returning 15.1 m at 0.5 g/t Au (Richards et al., 2005), but instead corresponds to the intersection of a structure known as the T-fault. The current resource estimate at Kencana is 3.7 Mt at 24 g/t Au (2.8 Moz Au), with a mine life forecast until 2015. A number of epithermal deposits and prospects have been recognized to date in the Gosowong goldfield following an extensive exploration program, including Gosowong, Toguraci, Toguraci North, Gosowong North, Dongak, Tobobo, Langsat, Batu Api and Kencana.

1.6 Previous work

There has been little previous detailed work on the Kencana deposit, limited to preliminary petrographic studies and predominantly confidential internal company reports. Richards et al. (2005) described the discovery, exploration history and basic geology of the deposit. A preliminary SWIR-based study on the characterization of alteration assemblages at the Kencana deposit was the subject of an B.Sc thesis by Silitonga, 2006. Internal company reports by Coote (2003, 2005) documented preliminary observations on the ore mineral assemblages, vein textures and fluid inclusions.

The Gosowong deposit has been the subject of more comprehensive study, including a detailed investigation into the geology, geochemistry, fluid characteristics and alteration zonation as part of an M.Econ Geol. thesis by Olberg (2001). The deposit discovery was described in Davey et al. (1997) and Carlile et al. (1998). The geology of the deposit is outlined in Olberg et al. (1999) and Olberg (2001). Gemmell (2007) described the hydrothermal alteration zonation and whole rock geochemical signature surrounding the GVZ, resulting in the development of geochemical vectors to mineralization.

Geochronology studies in the goldfield were previously restricted to a preliminary study on $^{40}Ar/^{39}Ar$ at Gosowong (Vasconcelos, 1998), which yielded magmatism ages of 5.4-2.6 Ma with a best estimate of 3.7 Ma, and epithermal mineralization ages of 2.4-2.9 Ma, with a best estimate of 2.9 Ma, based on adularia analyses. New geochronology data for the Gosowong district are presented in Chapter 3.2.

1.7 Thesis structure

This thesis is organised in to seven chapters. Chapters 3-6 address one or more of the principal aims of the project.

Chapter 1 details the aims and objectives of the project, the location and physiography of the study area and the mining history and exploration history. The approach and methods utilized in this study are discussed, and the layout of the thesis is summarized.

Chapter 2 concerns the regional tectonics, structure, stratigraphy, metallogeny, and geochronology of the Gosowong goldfield and the deposits contained therein.

Chapter 3 focuses on the detailed stratigraphy of the Kencana deposit, including descriptions of the major intrusive and volcano-sedimentary lithofacies, their distribution and relationships; the depositional settings and sequence, and the deposit structure.

Chapter 4 documents the detailed geological features of the K1 vein, including descriptions of the gangue and ore mineral assemblages and their distribution, characterization of vein types and their distribution, vein paragenesis, fluid inclusion study and metal zonation. Chapter 5 focuses on the determination and distribution of the hydrothermal alteration facies (including SWIR analysis), as well as the geochemical signature and zonation of the alteration assemblages.

Chapter 6 synthesizes data from preceding chapters and reconstructs the geologic history and hydrothermal evolution of the Kencana deposit.

A summary of conclusions and implications for epithermal exploration in the Gosowong goldfield is provided in Chapter 7.

CHAPTER 2

REGIONAL AND DISTRICT GEOLOGY

2.1 Introduction

This chapter provides an overview of the regional tectonics, stratigraphy and volcanic activity contributing to the formation of the Kencana epithermal deposit. A review of the geology of Halmahera is given, including metallogeny, structure and stratigraphy. Detailed geology of the Gosowong goldfield including structure, metallogeny, detailed stratigraphy and geochronology is also documented in this chapter.

Indonesia represents an amalgamation of several arc complexes dating from the Mesozoic to the present day (Fig. 2.1 A; Wurst, 2004). All major mining operations within Indonesia are located within these volcanic arcs (Fig. 2.1 B). The Kencana deposit is located within the late Miocene to Pliocene Halmahera arc, which transects the western side of the island of Halmahera in the Maluku province of eastern Indonesia.

2.2 Regional Tectonics

Halmahera is situated to the east of the Molucca Sea Collision Zone, where the opposing Sangihe and Halmahera Arcs have been actively converging since the late Pliocene (Hall, 2000). This double convergence zone is a globally unique example of arc-arc collision. The Molucca Sea plate dips eastwards beneath Halmahera and west beneath the Sangihe Arc, forming an inverted U-shape (Fig. 2.2). Seismic evidence implies that 200-300 km of lithosphere has been subducted beneath Halmahera, and approximately 600 km beneath the Sangihe Arc (Hall, 2002). It is known that the surface thrusts on each side of the Molucca Sea are oriented toward the adjacent arcs, in the opposite direction to the dip of the subducting slabs beneath (Figs. 2.2, 2.3) (Hall, 2002). The west dipping thrust observed in the Molucca sea has been interpreted by Hall (1987) as the frontal thrust of the Sangihe fore-arc, where the east-dipping thrust on the west side of the Molucca sea has been interpreted as a back thrust developing in the overthrust wedge.

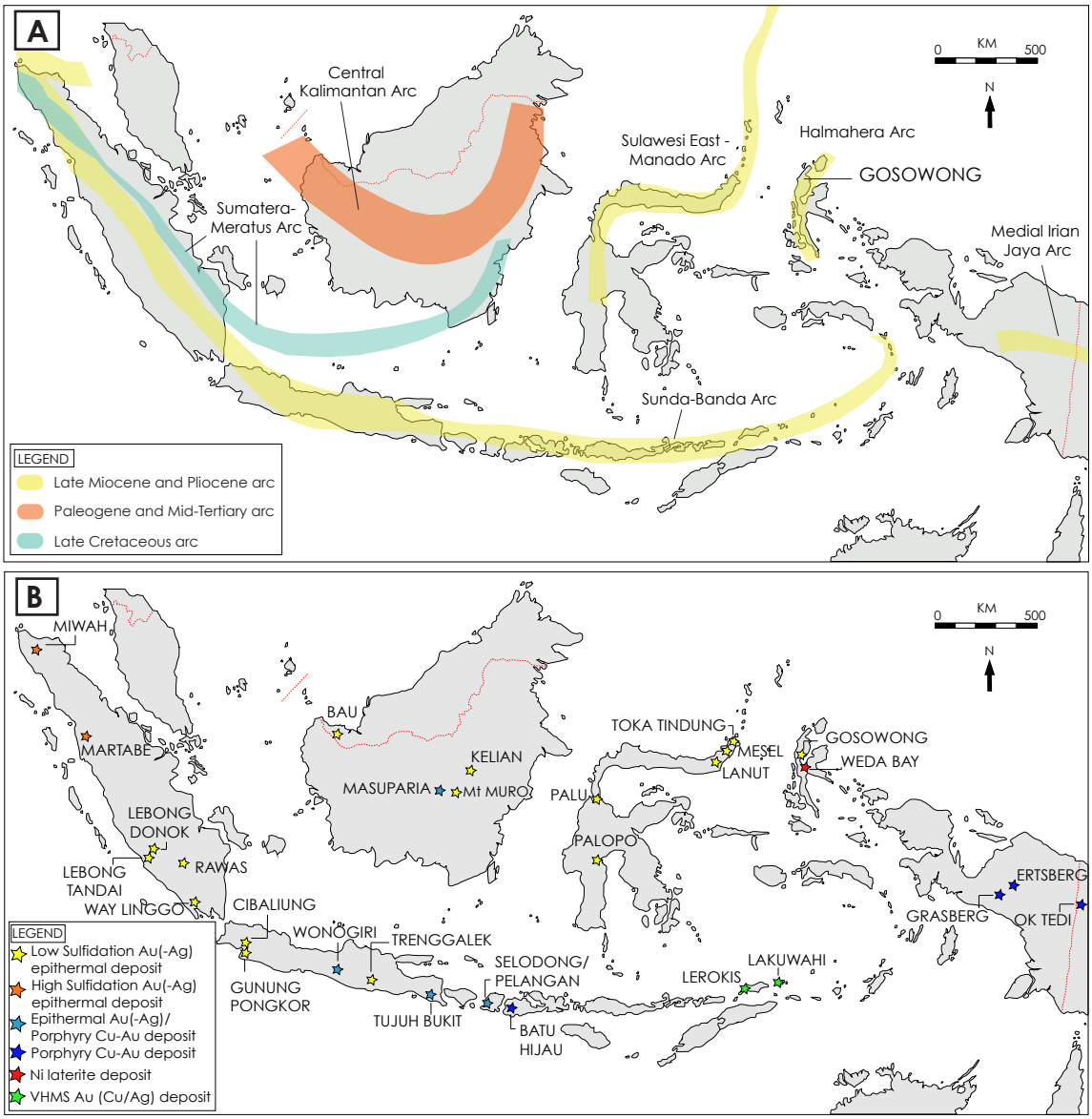

Fig. 2.1 Indonesian magmatic arcs

A) Location and age of the major volcanic arcs in Indonesia. Gosowong goldfield is situated within the Late Miocene - Pliocene Halmahera Arc. Diagram modified from Van Leeuwen, (1994); Wurst, (2004).

B) Location and deposit style of the major mine sites and prospects in Indonesia. Mine locations correlate with the position of the volcanic arcs in Fig 2.1 A. Modified from Golden Peaks Resources, (2010).

The Halmahera Thrust can be traced southward from the Philippines (Fig. 2.3), and has been interpreted by Hall (2002) as the base of the Sangihe fore-arc, which now overrides the Halmahera arc. However, the Sangihe thrust cannot be traced northward of Siau and is not present in the northern section of the Sangihe forearc (Fig. 2.3). To the north east of Halmahera, the Philippine Trench extends northward from approximately 2° N. Known to

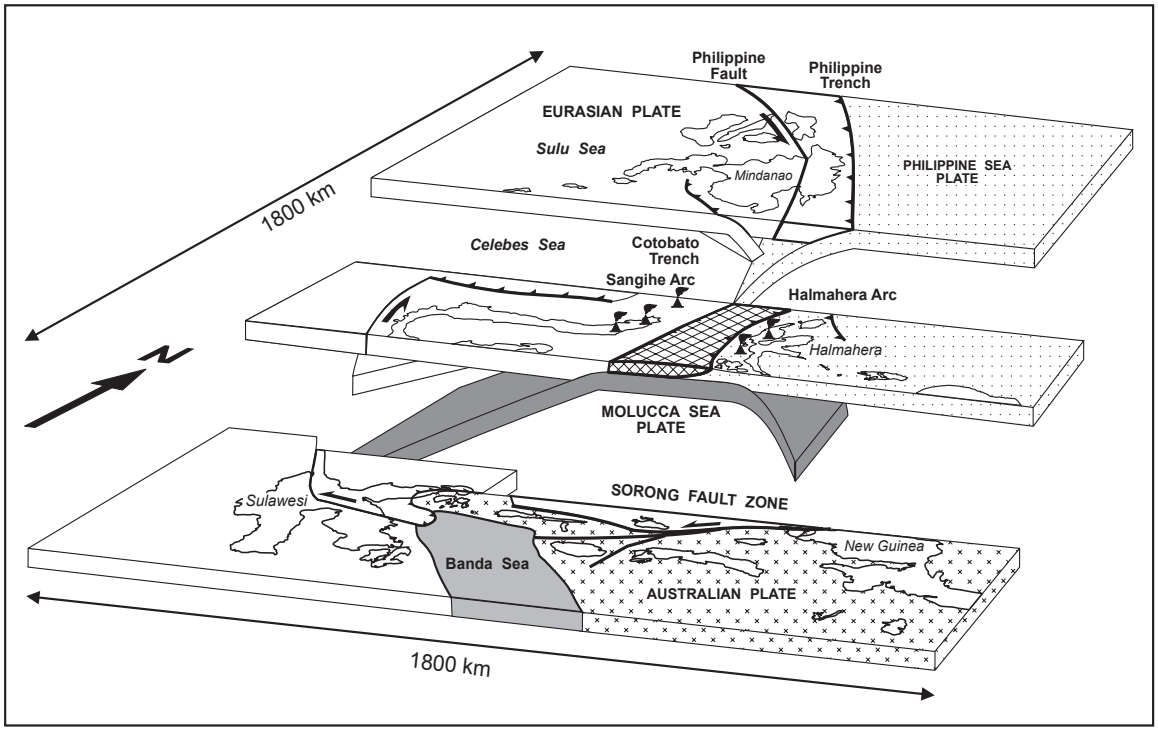

Fig. 2.2 Molucca Sea plate tectonics The Molucca Sea region, showing the converging Halmahera and Sangihe Arcs, displayed in a simplified 3D diagram that represents the geometry of the converging plates in east Indonesia. From Hall et al., (1995), Hall and Smyth, (2008).

be very young, less than 150 km of lithosphere is thought to have been subducted (Cardwell et al., 1980).

In the Northern Molucca Sea, the Halmahera arc has been completely over-ridden by the Sangihe fore-arc and it is proposed that the entire Halmahera arc will disappear within a few million years (Hall, 2002). Volcanic activity in the Halmahera arc ceases at Morotai, to the north of Halmahera, and has no known Neogene equivalent in the east Philippines (Hall, 2002).

As subduction proceeded through the Pliocene, Australia is known to have moved obliquely northward with respect to the Pacific, but the past position of Halmahera relative to Australia is as yet undetermined (Hall et al., 1988).

The Sorong fault system is a major left-lateral fault system to the south of Halmahera (Fig. 2.2), which separates the westward-moving plates to the northern side from the Australian plate to the south, with the Philippine Sea plate currently moving westward with respect to the Australian plate at a rate of 12 cm/year with a total displacement estimated to

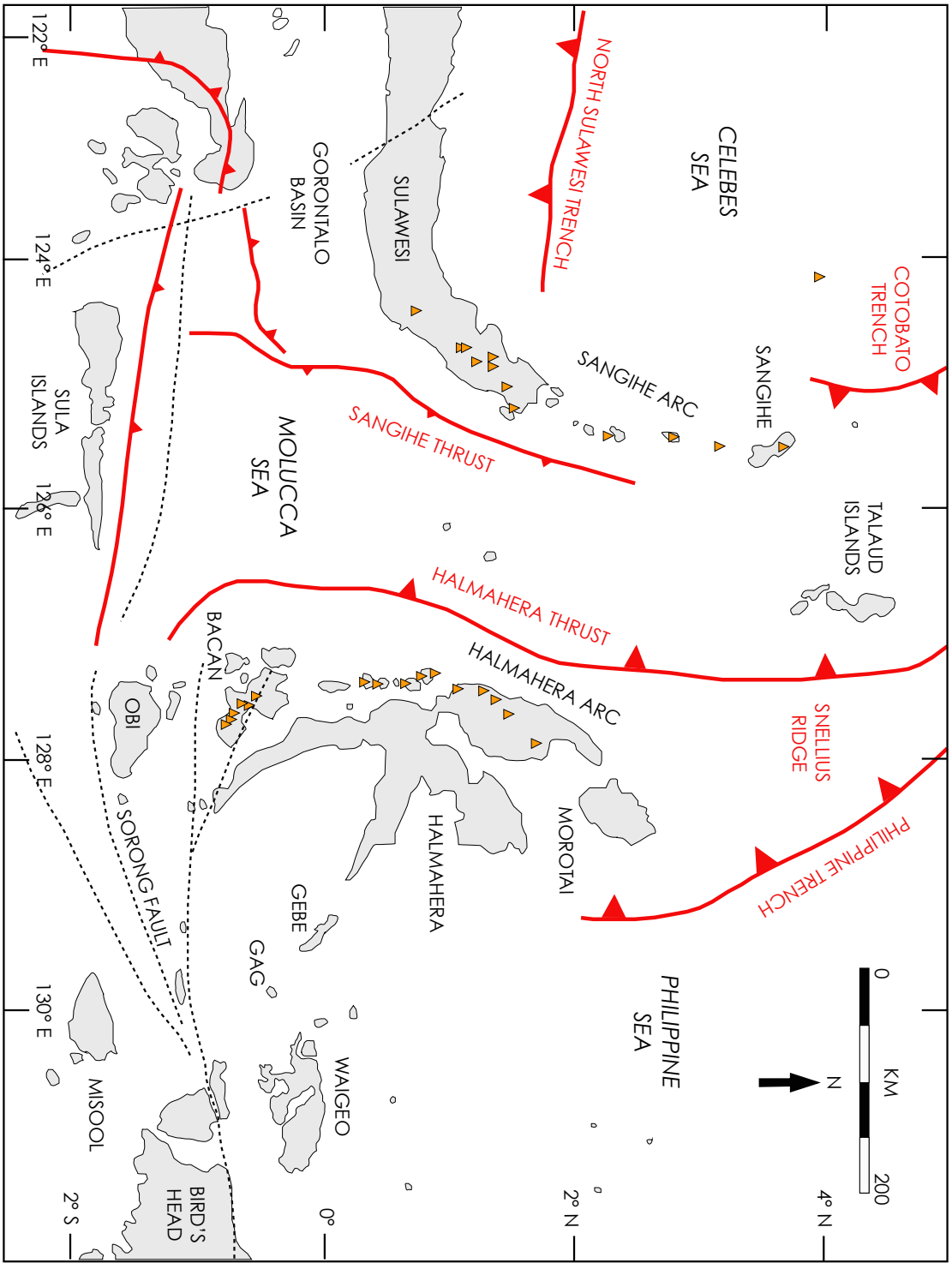

Fig. 2.3 Regional tectonic setting of Halmahera Island

Map showing subduction zones (large barbed lines) and thrusts (small barbed lines) in the Molucca Sea region. Orange triangles represent active volcanoes from the Smithsonian database. Modified from Mcpherson and Hall, (2002).

be as great as 600 km. The system extends eastward from New Guinea more than 1500 km along the northern margin of Irian Jaya, and 800 km to the west toward Sulawesi (Hamilton, 1979). The major change in plate boundaries at the beginning of the Miocene (~25 Ma) following arc-continent collision of the Australian margin with the Philippine Sea plate caused initiation of the Sorong fault system, leading to westward movement of continental fragments, which were subsequently accreted to Sulawesi during the Neogene (Hall, 1996).

The island of Bacan is unique in the Maluku islands, in that the southern part of the island has a continental metamorphic basement associated with a deformed ophiolitic complex which is significantly different to the ophiolitic basement complex of eastern Halmahera (Fig. 2.4; Hall et al., 1988). The ophiolitic basement of Bacan is interpreted to be part of the north Australian continental margin basement, separated from the Halmahera basement by the Molucca-Sorong fault, one of several splays of the Sorong fault zone, and represents magmatism in the fault zone (Hall et al., 1988).

2.3 Overview of the Geology of Halmahera

Halmahera can be generally divided into two geologic domains, the eastern and western provinces, reflecting the separate geological histories of these two sections of the island. The western province, in which the Gosowong goldfield is situated, includes the islands of Morotai, Ternate, Tidore, Bacan and western Halmahera; and represents an active volcanic arc situated above an eastward-dipping subduction zone (Fig. 2.4; Gemmell, 2007). This province is dominantly composed of Pliocene-Recent volcanics, forming the NW and SW arms, on a basement of Mesozoic to early Palaeogene volcanics, overlain by Neogene intrusions and volcanic rocks, with local cover by Recent volcanics (Gemmell, 2007).

The current arc volcanoes are stratiform calc-alkaline cones (situated in northwest and central Halmahera, and to the west of the western arm; Fig. 2.4), producing porphyritic basaltic to andesitic lavas and pyroclastics (Hall et al., 1988), with plagioclase, olivine, clinopyroxene, hornblende and magnetite phenocrysts in a glassy to granular groundmass, which is variably devitrified (Hakim and Hall, 1991). The present day arc can be divided into a normal oceanic segment and a continental segment (Morris et al., 1983).

The normal oceanic segment, including the volcanoes of northwest and central Hal-

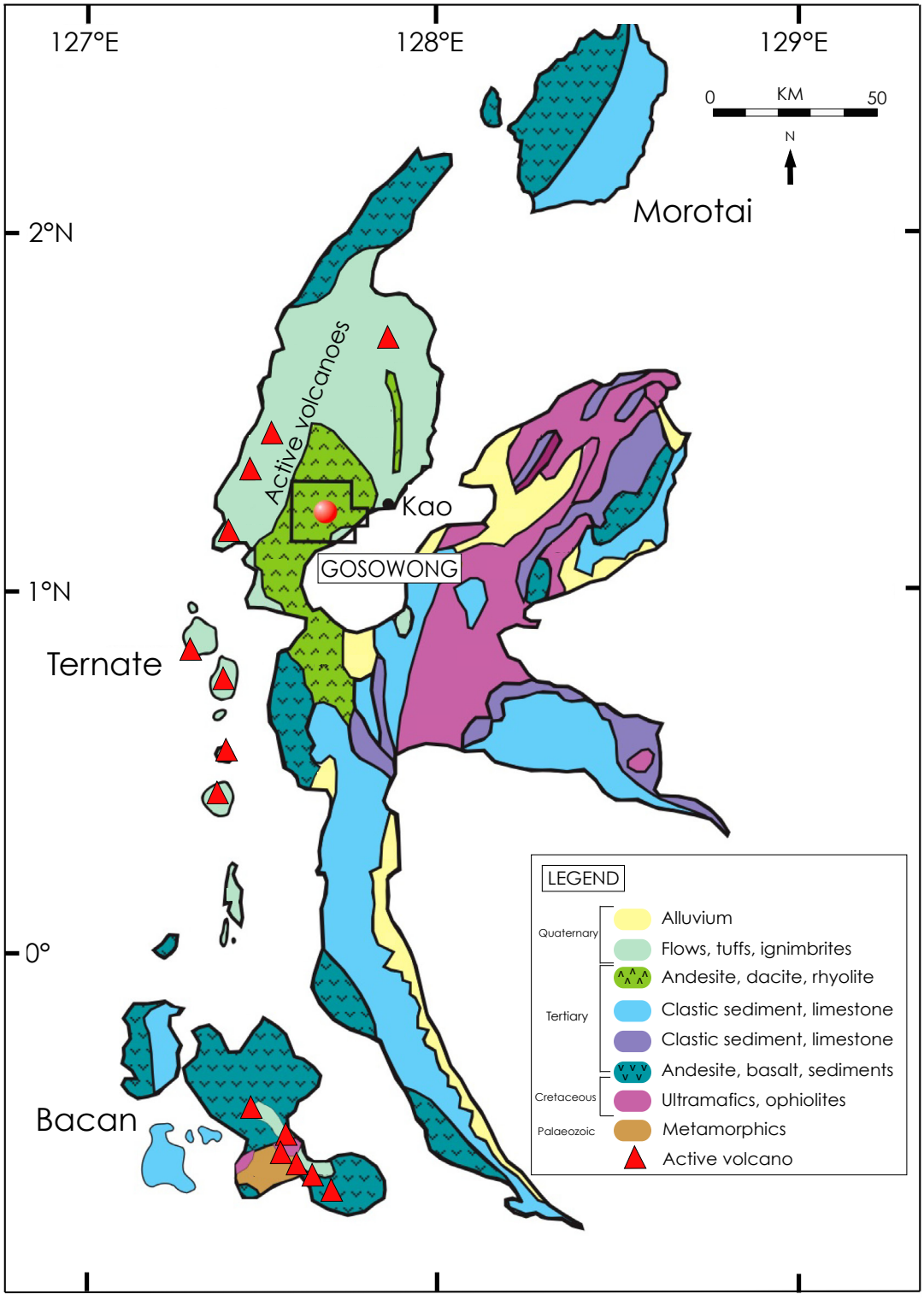

Fig. 2.4 Geological map of Halmahera Simplified geology of Halmahera showing major lithologies and the lithological distinction between the eastern and western provinces. Red triangles denote active volcanoes. Gosowong is situated in Late Palaeogene calc-alkaline volcanics, volcaniclastics and sedimentary host rocks on the NW arm of the island. Black polygon outline represents the PT. Nusa Halmahera Minerals contract of work (CoW) area. Modified from PT. Nusa Halmahera Minerals, 2008.

mahera, produces petrographically similar basalts and andesites (as studied from Tidore and Ternate), the andesitic compositions caused by the presence of an acid glass (Kuenen, 1935). Lava chemistry is typical of calc-alkaline intra-oceanic arc suites, with most rocks falling in the range of 53-63 weight percent SiO_2, with high Al_2O_3, low TiO_2 and K_2O contents representative of medium-K suites (Gill, 1981).

Element concentrations vary with SiO_2 content, while the HFSE and compatible elements are typically depleted. $^{87}Sr/^{86}Sr$ values suggest that the rocks are similar to those of many island arcs, but Pb isotope ratios suggest minor sediment contamination (Hakim and Hall, 1991).

The island of Bacan in the south is exceptional in that the lavas produced here are considered to have undergone considerable continental crust contamination, from the underlying ophiolitic basement of Australian continental crust (Hall et al., 1988). Bacan is considered the continental segment of the arc, reflected in elevated alkali element concentrations, and high $^{87}Sr/^{86}Sr$ (0.7198-0.7240) and $^{207}Pb/^{204}Pb$ ratios (~40.2) (Morris et al., 1983; Hakim and Hall, 1991).

2.4 Regional Stratigraphy

The north-western arm is composed of four superimposed volcanic arcs, produced as a result of subduction of the Molucca sea plate beneath Halmahera since the Palaeogene. These four volcano-sedimentary formations have been named the Bacan Formation (Palaeogene), the Gosowong Formation (Upper Miocene), the Kayasa Formation (Pliocene) and the overlying Quaternary Volcanic Formation, which is currently being deposited (Olberg et al., 1999). These formations are separated by major regional angular unconformities that represent significant hiatuses (Marjoribanks, 1997).

The eastern province has an ophiolitic basement complex forming the NE and SE arms of the island, unconformably overlain by Neogene sediments, which can be traced into the western province, and under the Pliocene volcanics through a junction zone which forms a topographic depression between the two provinces (Hall et al., 1988).

The ophiolitic basement, which has been interpreted as a pre-Oligocene fore-arc lacking an accretionary complex, contains slices of Mesozoic and Eocene sediments unconformably overlain by mid-Oligocene and younger sedimentary and volcanic rocks, indicating that

the ophiolitic basement must be at least late Eocene-early Oligocene in age material deposited in a proximal position (Darman and Sidi, 2000), and is thought to rest unconformably on the ophiolitic basement (Hall et al., 1988). Thus, this early-Palaeogene fore-arc is now situated in a back-arc position relative to the present day arc in western Halmahera (Hall et al., 1988). The ophiolitic basement comprises strongly sheared and brecciated mafic and ultramafic rocks, including serpentinized peridotite, gabbro, basalt and diabase (Sukamto et al., 1981), and can be traced northwards at least as far as eastern Mindanao in the Philippines, and extends eastward, through the islands of Gebe and Gag, toward the northern part of Irian Jaya.

At the end of the Eocene the arc and fore-arc terrain forming the Halmahera basement was strongly deformed, causing imbrication and uplift (Hall et al., 1988). The cause of the deformation remains unspecified, but it is suggested that it may be related to a major change in the motion of the Pacific Plate at around 40 Ma (Uyeda and Ben-Avraham, 1972). The length of subducted lithosphere indicated by seismic profiles suggest that the basement complex of the eastern province must have been situated at least 1000 km to the east of north Sulawesi before subduction commenced.

Initiation of subduction caused basin subsidence in eastern Halmahera, followed by the formation of a volcanic arc in the Western province, which is represented in the stratigraphy as a change from stable carbonate deposition in central and eastern Halmahera, through marls and siliciclastic debris, and finally calc-alkaline volcanic debris in the mid-Pliocene. Increasing amounts of volcanic debris appear in the stratigraphy, including volcanic tuffs and eventually calc-alkaline lavas, marking the increase of activity on the arc and the shallowing of the sedimentary basin (Hall et al., 1988).

Descriptions of the sedimentary units of southern and eastern Halmahera are derived from fieldwork undertaken by the 1987, 1990 and 1993 GRDC Halmahera Expeditions (Darman and Sidi, 2000), and their relative positions in the stratigraphy are shown in Fig. 2.5. The oldest dated sedimentary rocks are within the Buli group, which includes formations ranging from Cretaceous to Eocene in age, including the Gau Limestone, Dodaga Breccia, and the Paniti, Gowonli and Sagea Formations (Hall et al., 1988; Fig. 2.5). The Gowonli Fm (SE arm) is interpreted as a basin-fill deposit situated in the forearc of an active arc,

where the lower part of the sequence contains early, coarse volcaniclastic material deposited in a proximal position (Darman and Sidi, 2000), and is thought to rest unconformably on the ophiolitic basement.

The Gau limestone (NE arm) is interpreted as a deep-water carbonate formation deposited in an equatorial ocean basin with minor incorporated volcaniclastic material derived from active arc volcanism at the basin margin (Hall et al., 1988). The top of the formation is a gradational transition to the Dodaga breccia (Fig. 2.5).

The oldest known rocks from the SW arm are the Cretaceous to Eocene Oha Volcanic Group, composed of basaltic to basaltic andesite lavas with trachytic textures. The basement volcanics have undergone pervasive zeolite, chlorite and epidote alteration.

The unconformable contact at the end of the Eocene below the late Palaeogene and Neogene sediments (the Onat Marl Fm, Jawali Conglomerate and Subaim Limestone of the NE arm; and the Gemaf Conglomerate Fm of the SE arm; Fig. 2.5) is the result of the major imbrication and uplift event between the mid-Eocene and mid Oligocene (Hall et al., 1988).

The Subaim Limestone Formation, which unconformably overlies the Buli Group, is a massive or well-bedded limestone of reef or reef-derived material with rare clastic interbeds (Darman and Sidi, 2000). On the SW arm and the central zone, the Subaim Limestone is only present as small outcrops and pebbles in younger sediments. On the SE arm the Gemaf Conglomerate underlies the Subaim Limestone. This formation consists of dark conglomeritic clasts of ophiolitic material and well-sorted sands of littoral origin (Darman and Sidi, 2000).

Subsidence during the late Miocene, triggered by the onset of subduction, provided the setting for the conformable deposition of the Saolat Fm over the Subaim Limestone on the SE arm, a thick sequence of fossiliferous calcareous mudstones and micritic limestones with local ophiolitic sandstone interbeds (Darman and Sidi, 2000). The top of the formation is not seen on the SE arm, but the Wassile sandstone conformably overlies the Saolat Formation in the NE arm, a turbiditic sandstone and conglomerate unit which is interpreted as part of a prograding submarine fan, with the higher beds representing upper-fan channel deposits (Hall et al., 1988).

The SW arm and central zone display a different stratigraphy, where the mid-Miocene is represented by the Loku formation, a mudstone to conglomeritic unit deposited as turbidity flows of arc derived material and reef limestones (Fig. 2.5). The overlying units (Superak, Akelamo and Dufuk) are a sequence of conformable sandstones, siltstones, conglomerates and increasingly organic-rich mudstones deposited in shallowing marine conditions (Darman and Sidi, 2000). Re-initiation of volcanism in the central zone is represented by the Tapaya and Tafonga Volcanic Formations, which contain fragments of conglomerate and sandstone, though the upper part of the sequence is dominated by extrusive basalts and andesites (Fig. 2.5; Hall et al., 1988). A period of deformation and uplift and subsequent erosion preceded deposition of the Quaternary reef limestones, alluvium and volcanic rocks, which are unconformable on the underlying sequences.

2.5 Regional Structure

The nature of deformation is more complex in the western province than the eastern, where faults are typically vertical, and a major angular unconformity is present at the base of the Late Palaeogene and Neogene limestones overlying the imbricated basement (Hall et al., 1988). Significant post-Miocene uplift is represented by unconformity exposure at 1000 m above sea level. The western province is harder to determine given the large areas of cover by recent volcanics, however it is supposed that Pleistocene volcanics on the western coast of central Halmahera have been folded, commonly displaying dips of 40-60° (Hall et al., 1988). Conversely, the volcanics of the active and recently active arc in Tidore and Ternate are largely undeformed.

A major deformation event affected both the eastern and western provinces during the Pleistocene, causing tilting of major fault-bounded blocks, and intense folding and thrusting in the narrow 'neck' of the junction zone between the two, which is an important zone of intense deformation, with locally strongly deformed Neogene rocks. Some outcrops of the Subaim limestone (early Miocene-early Pliocene, reef and fore-reef to back reef and lagoon limestones) have been locally overturned and overthrust as flat sheets (Hall et al., 1988).

South of Ekor, sediments, volcaniclastics and volcanics have been folded into tight folds with steeply dipping limbs and axes (70-90°), with a general northward trend. Quater-

Fig. 2.5 Time-Space event stratigraphy for Halmahera Island Chart highlighting the relationship between the tectonic evolution of South East Asia and the structural and stratigraphic evolution of the different zones of Halmahera Island, including arc geometries, inversion tectonics, metallogeny, geochronology and stratigraphic contact information. From Global Ore Discovery, 2010

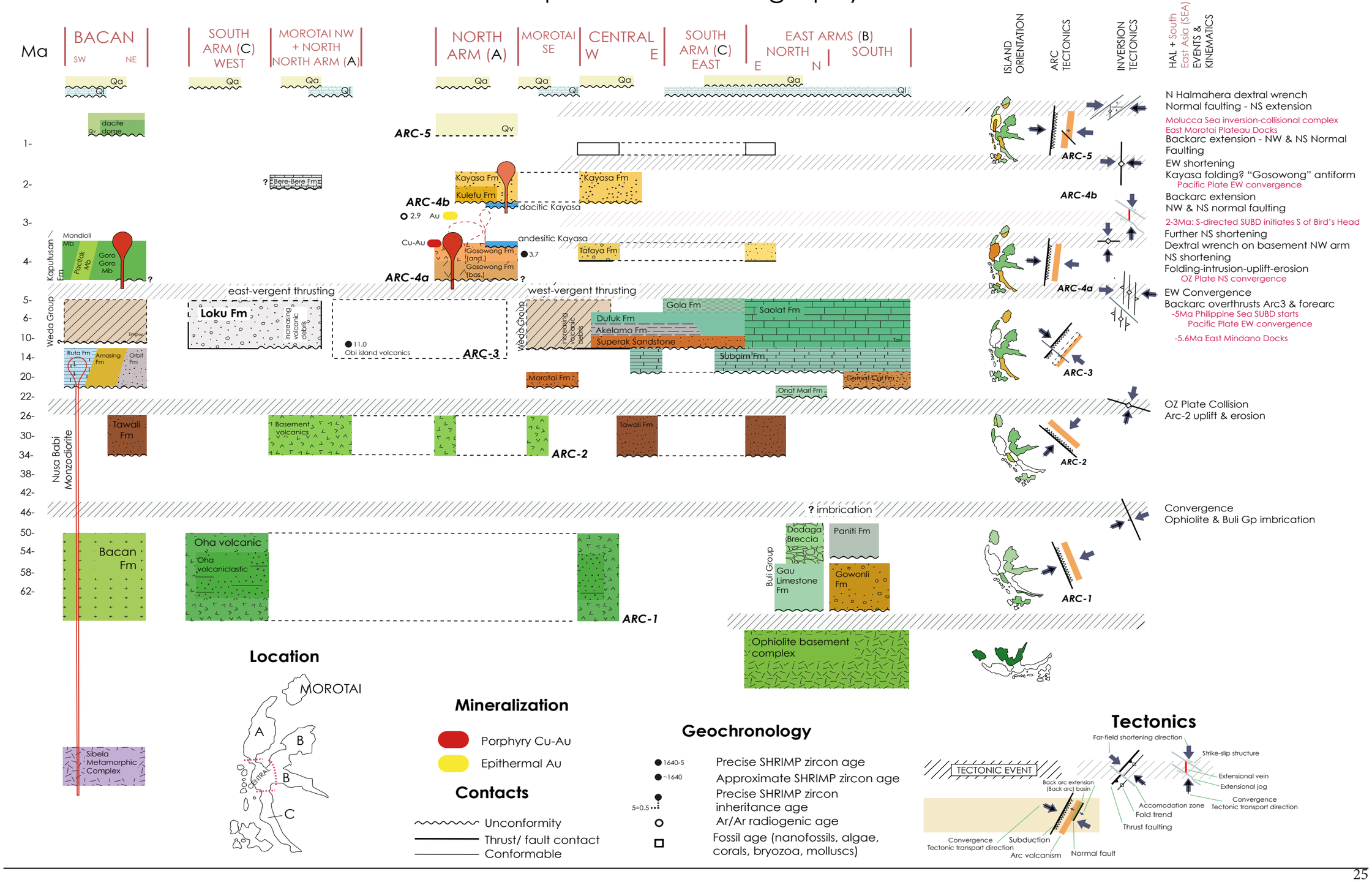

nary reef limestones are unconformable on older rocks, and since Pleistocene rocks are present in the deformed basement of the Quaternary volcanoes, it is supposed that deformation is no older than mid-Pleistocene (Hall et al., 1988). There are several plausible explanations for this deformation event but one is a tectonic event at one of the existing or developing plate margins in the region, for example, along the Sorong fault system to the south of Halmahera (Hall et al., 1988). Balanced cross-sections indicate that there has been at least 60 km east-west shortening between eastern and western Halmahera within this junction zone (Hall and Nichols, 1990). Major structures on Halmahera are displayed in Fig. 2.6. A number of important relationships and observations were determined by Global Ore Discovery (2010):

- A west-vergent fold-thrust belt of Miocene back-arc sediments in a suture zone between east and west Halmahera in central Halmahera (A) which is interpreted to be unconformably overlain by Pliocence arc sequences.
- A west-vergent thrust belt of Miocene back-Arc sediments overthrusting older arc volcanics and Miocene fore-Arc sediments extending the full length of the south arm of Halmahera (B)
- Major NW strike slip faults that compartmentalise the above thrust belt (C)
- Significant NW faults easily interpreted in the Pliocene sequences and partially re-activated up into the Quaternary volcanics in the north arm of Halmahera (Dark purple trend lines, D)
- Weakly developed NW fault zones in eastern Halmahera (e.g. within the ophiolite complex; E)
- Some coincidence of NW structure with NW bathymetric discontinuities in southern Halmahera (F)
- Preferential development of major NE faults in the north arm of Halmahera (see CoW structural interpretation)
- Well developed NE faulting in Pliocene and Quaternary volcanics in the north arm of Halmahera
- Approximately co-linearity of NE structures with significant bathymetric NE discontinuities (G)

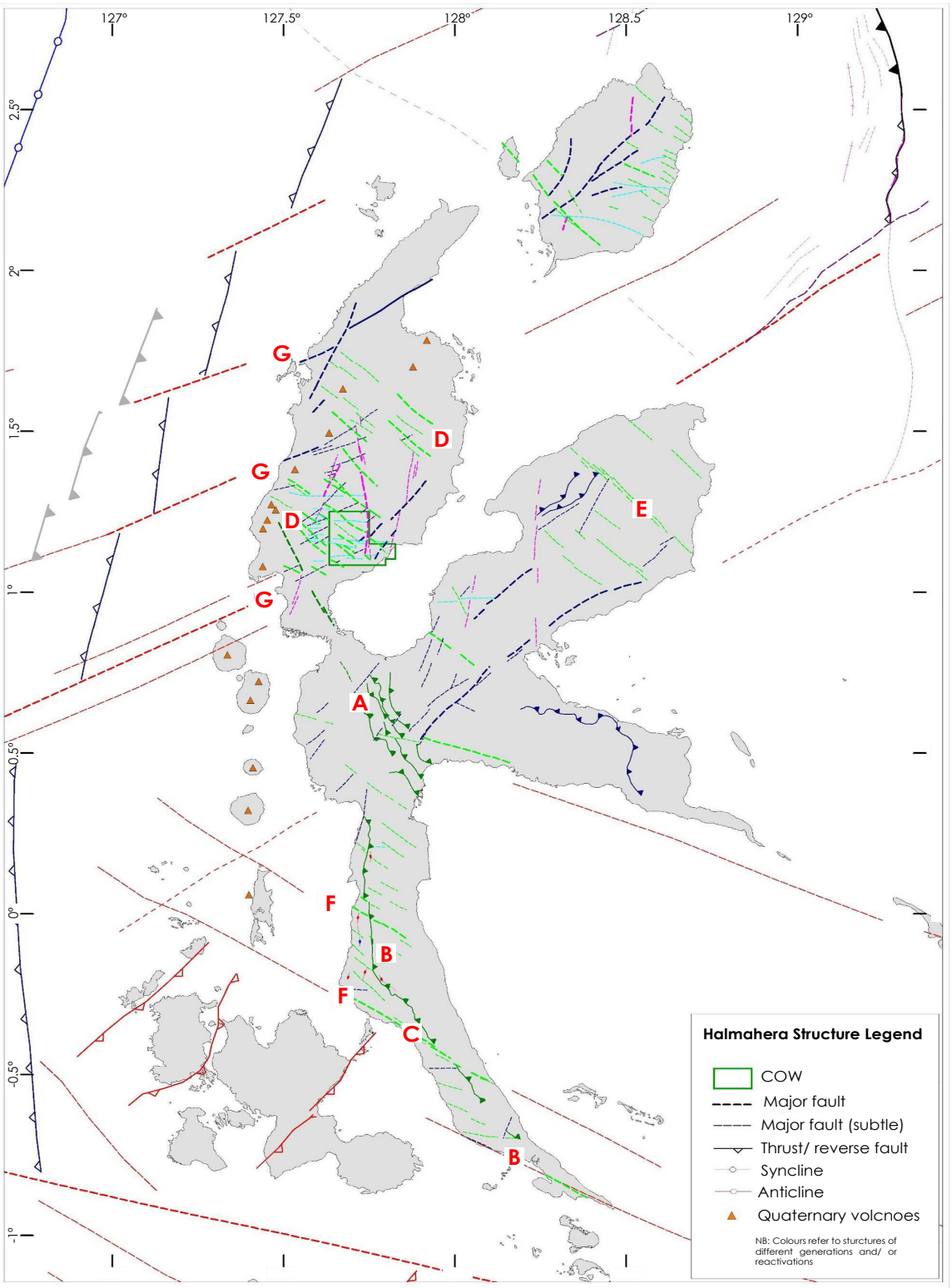

Fig. 2.6 Halmahera Structure Interpretation with south-east Asia (SEA) bathymetry interpretation backdrop highlighting important relationships and observations (A-G) as discussed in the text. From Global Ore Discovery, (2010).

2.6 Mineral Resources on Halmahera

Mineral resources are moderately scarce on Halmahera, with known economic deposits consisting of the Gosowong, Toguraci and Kencana epithermal Au-Ag deposits, the Weda bay nickel-cobalt laterite deposits, and the Kaputusan copper-gold porphyry deposit (Gemmell, 2007). Currently, only Kencana is in production, although Weda Bay Minerals (WBM; owned by Eramet, Mitsubishi Corporation and PT. Antam) are in the development process at Weda Bay (Santa Monica deposit), with indicated and inferred resources of 216 Mt at 1.37 % Ni and 0.12 % Co (Eramet, 2009). Production is due to commence in 2012.

Golden Peaks Resources Ltd. hold a 5000 Ha tenement to the north of the Gosowong contract of work (COW), targeting low sulfidation epithermal mineralization. The property is located in a similar geological setting as the Gosowong epithermal vein deposits and contains prospects where epithermal style veining and alteration has been mapped coincident with mineralization. Regional exploration discovered epithermal mineralization at the Pediwang Creek prospect within the current Kapa Kapa tenement (Golden Peaks Resources Ltd., 2010).

2.7 Gosowong Goldfield geology

This section describes the local geology in the Gosowong goldfield (Newcrest COW area) including structure, metallogeny, stratigraphy and geochronology. The Gosowong goldfield is situated on the eastern side of the NW arm of Halmahera, covering an area of approximately 30,000 Ha as part of the contract of work (COW) of PT. Nusa Halmahera Minerals. Currently, three economic Au-Ag epithermal deposits have been discovered in the region, namely the Gosowong, Toguraci and Kencana deposits. Geological mapping within the Newcrest COW is inhibited by the thick equatorial jungle and steep terrain.

The main focus area for mapping and stratigraphic determination has been the immediate area surrounding the existing epithermal veins. Information on the local geology has been principally determined from stream mapping and sampling, pit mapping, underground mapping (Kencana deposit) and exploration diamond drill core logging.

2.8 District stratigraphy

Four super-imposed volcano-sedimentary formations are present in the area, comprising the Bacan formation (Palaeogene), the Gosowong Formation (upper Miocene host to the Gosowong Goldfield mineralization), the Kayasa Formation (Pliocene), and the Quaternary Volcanic Formation (Fig. 2.7 A; Olberg et al., 1999). On a district scale, lithologies are dominated by upper Miocene to Pliocene andesite to basaltic andesite volcanic and volcaniclastic rocks and diorite intrusions (Fig. 2.7). There are two distinct mineralizing events in the goldfield: low grade, copper-gold porphyry style mineralization, and high-grade, gold-silver epithermal style mineralization (Gemmell, 2007).

Porphyry mineralization occurs predominantly in the central and northern areas, where four sub-economic porphyries (Matat, Ngoali, Bora and Tobobo, Fig. 2.8) are situated. The epithermal mineralization is generally concentrated toward the south of the district, hosted by the upper Miocene Gosowong Formation. Epithermal deposits or prospects in the goldfield include Gosowong, Toguraci, Kencana, Gosowong North, Anggrek, Ruwait, Batu Api, Tobobo and Langsat (Fig. 2.7 B).

The Gosowong formation is a series of interbedded volcaniclastic rocks, ignimbrites and coherent volcanic rocks, occurring as flows or intrusions. The components of the Gosowong Formation are considered below:

Basaltic to basaltic andesite volcanogenic mass flow units with grain sizes ranging from siltstone to boulder conglomerate are exposed to the north end of the Gosowong deposit (forming part of the pale orange volcaniclastic sandstones shown in Fig. 2.7 B). These are typically well bedded, competent and display normal grading, from a conglomeritic base fining upward to siltstone tops (Olberg, 2001). The sandstones have a minimum stratigraphic thickness of 350 m, with some individual beds exceeding 30 m, compared to a maximum thickness of 150 m for the Gosowong Volcaniclastics. This deposit type is symptomatic of a moderate to deep subaqueous setting, with a large influx of volcanic sediment from proximal volcanic edifices (McPhie et al., 1993).

Overlying the mass flow units are volcaniclastic rocks consisting of a range of lithologies, including andesite derived mudstone, siltstone, polymict fine to coarse-grained sandstones and conglomerates. Bedding in the volcaniclastic rocks strikes approximately

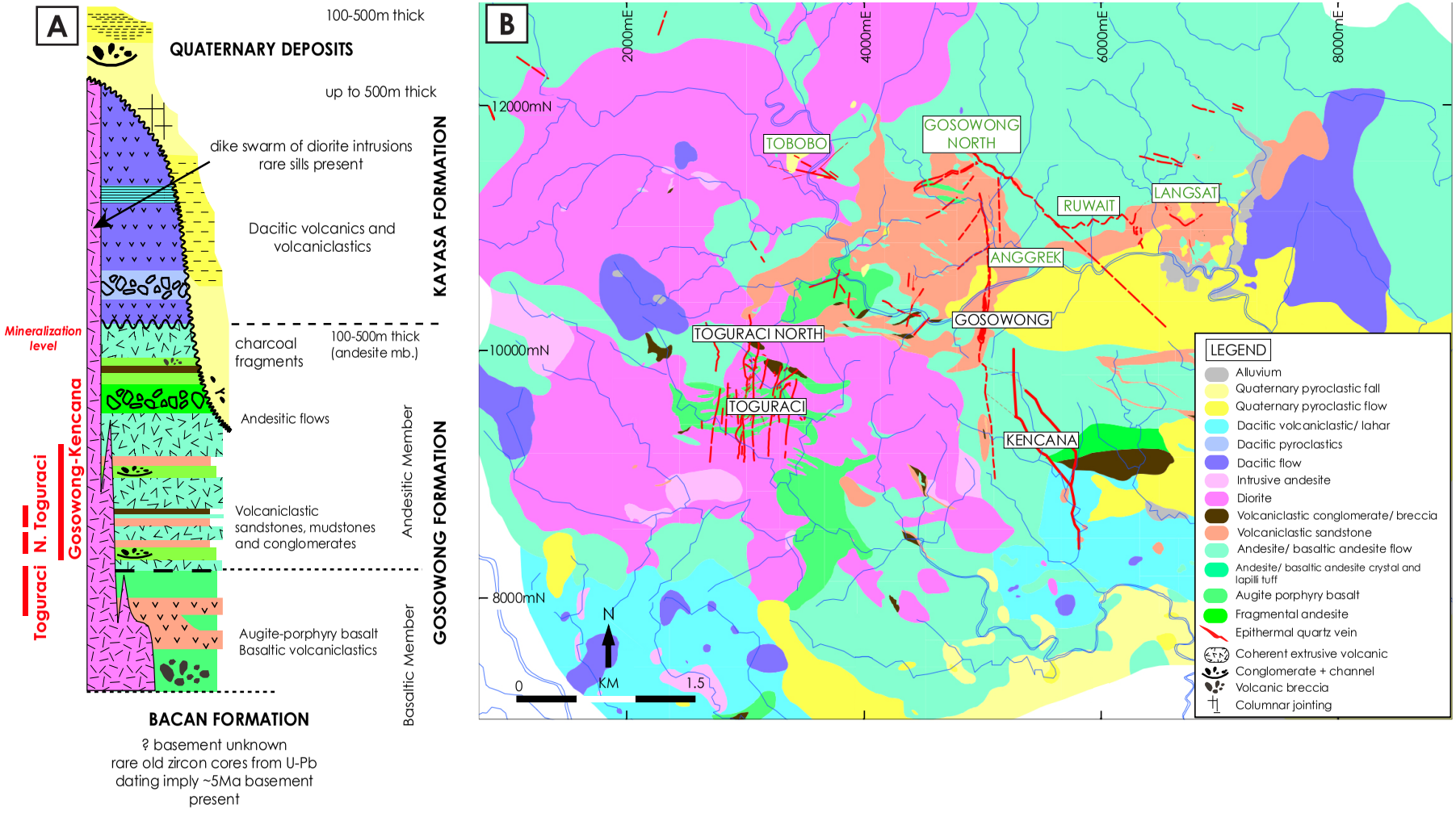

Fig. 2.7 Geology of the Gosowong Goldfield

A) Schematic stratigraphic column for the Gosowong goldfield (modified from Micklethwaite, 2010);

B) Simplified geology of the Gosowong goldfield showing distribution of the epithermal deposits and veins. Deposits labelled in black text, prospects labelled in green. After Newcrest 2010.

east with a moderate southerly dip. Bed thickness ranges from a few centimetres to tens of metres, and the formation has a total average thickness of 150 m. Several of the intrusive contacts display metamorphic contacts with the surrounding country rocks, and peperitic contacts can be observed particularly between the volcanics and the mudstone, which commonly has a hematite-rich matrix, interpreted as a mafic-rich airfall unit that has settled through a water column (see Chapter 3).

The hematitic ash is also present in other lithologies through the Gosowong Formation, where it forms the matrix of andesitic breccias, indicating redistribution and erosion of the original hematized ash beds. In some areas of the Gosowong pit, hematitic mudstone horizons were traceable along strike grading into a conglomerate with hematitic ash matrix support (Olberg, 2001).

The general depositional setting of the volcaniclastic rocks is thought to be a regressive, shallow sub-aqueous environment. It is not certain if the environment was shallow marine or lacustrine, although the lack of reef materials and limestones may be more suggestive of a lacustrine setting (Olberg, 2001). The differing depositional settings between the mass flow sandstones and the volcaniclastic rocks represent a shallowing of the sub-aqueous environment. This regression either represents a decreasing water level, uplift of the basin, or a combination of the two processes. Immediately overlying the volcaniclastic rocks are a series of coherent volcanic rocks, possibly deposited in the sub-aerial environment, indicating an almost complete regression (Olberg, 2001). These volcanic rocks are dominantly andesitic-dacitic with a marked lack of interbedded volcaniclastic material. Individual flows range up to 10 m in thickness, with a total thickness of 350 m. Flow margins are commonly autobrecciated. The lack of volcaniclastic material may indicate rapid effusive sub-aerial dome growth (Olberg, 2001).

The Pliocene Kayasa Formation has a similar composition to the Gosowong Formation. The Kayasa Formation is dominated by dark grey feldspar-porphyritic andesitic to basaltic lavas and breccias and autobreccias. The breccias have andesitic and basaltic components, are light to dark grey and aphanitic to phaneritic in texture, with a fine to medium-grained matrix.

To the east and North of the Gosowong deposit, the Tertiary volcanic rocks are overlain by a cover of Recent ignimbrites, locally known as the Dufadufa pyroclastics (Fig. 2.7 B). This sub-aerial, flow-deposited unit forms a blanket with a maximum (post-erosional) cover of 60 m on the ridges. The unit post-dates the epithermal and porphyry mineralization, displaying no ore mineralization or alteration.

2.9 District Structure

The Gosowong Formation occurs as an inlier within the Kayasa Formation. The Gosowong and Kayasa Formations were thought to be exposed in the core of a NNE-trending elongate dome, formed during strong upward magma intrusion, with arrays of north-south trending faults and joints formed as accommodation structures during uplift (Gemmell, 2007). In the late Pliocene, both formations were locally intruded by multiple phases of plagioclase-phyric basaltic-andesite (Richards and Basuki Dwi Priyono, 2004). Detailed descriptions of the lithologies hosting the Kencana deposit and their depositional environments are given in Chapter 3.

Several generations and orientation groups of structural features are identified in the Gosowong goldfield by Global Ore Discovery (2010), comprising N-, NW-, NE- and E-trending structures (Fig. 2.8). North and NW-trending structures are the most significant for low sulfidation epithermal mineralization and are discussed below.

There are two generations of N-trending structures in the goldfield (Fig. 2.8). The first are relatively early (2.9 Ma), short-length discontinuities that are interpreted to be extensional (purple structures shown on Fig. 2.8). The second are late, large scale discontinuities identified along the eastern edge of the COW, as well as more broadly throughout northern Halmahera (Dark purple structures shown on Figs. 2.6 and 2.8; Global Ore Discovery, 2010).

Important features and interpretation of the earlier, low sulfidation epithermal N-trending structures are:

- Steps are variable; both east-block-down and west-block-down
- Are compartmentalized between NW-trending structures (rather than offset by them)

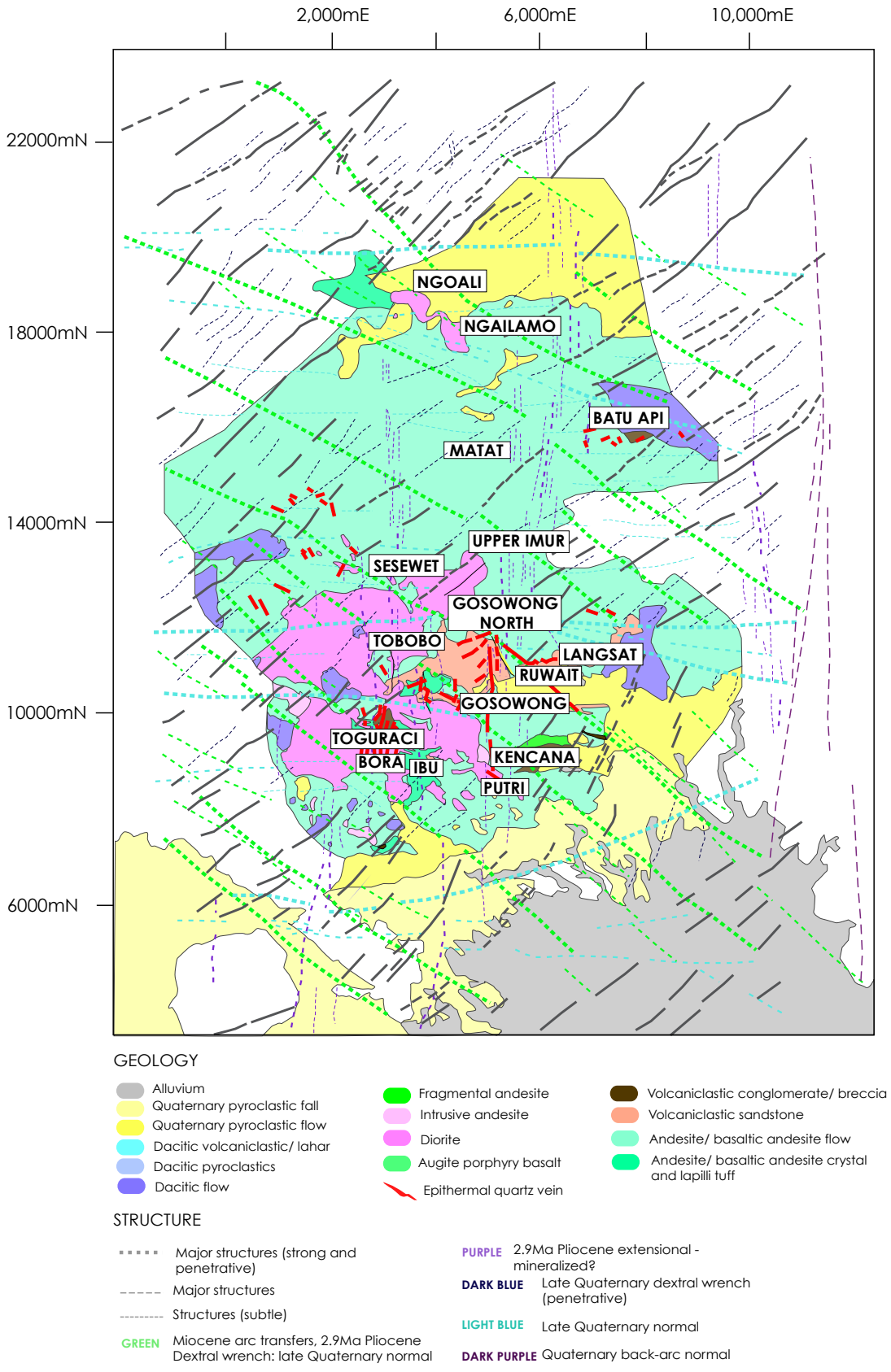

Fig. 2.8 Structural interpretation of Gosowong COW highlighting structures of different generations and their overprinting relationships. Regional geology shown (where mapped). Modified after Global Ore Discovery, 2010.

- Are offset by later NE- and E-trending structures
- Expressed in some mapped lithological contacts and zones of sediment rotation
- Interpretable through dacitic Kayasa and Quaternary in the south and east. May have later re-activation through the later sequences

Interpretation: Early N-trending structures are 2.9 Ma Pliocene extensional structures within the Gosowong Formation, formed between, and compartmentalized between, major NW-trending structures in the dextral wrench (Figs. 2.5 and 2.8). They are interpreted to reflect shallow reactivation of Miocene arc and arc-inversion, N- to NNE-trending, arc-parallel structures (Global Ore Discovery, 2010). These N-trending normal fault structures are inferred to have significant low sulfidation epithermal Au potential and may be steep, or dip variably to the east or west, depending on their geometry with respect to the extending Miocene N-trending structure (Global Ore Discovery, 2010). They may have undergone reverse reactivation in the late Pliocene to early Pleistocene, and again in the late Quaternary-Recent during eastward shortening (Fig. 2.5), associated respectively with Kayasa folding (-thrusting) and North Halmahera NE dextral wrench (Global Ore Discovery, 2010).

The later N-trending structures:

- Are major, long-length discontinuities faulting the Gosowong, Kayasa and Quaternary Formations
- Cut and displace NW- and E-trending structures
- Cut and truncate N-trending low sulfidation epithermal Au target structures
- Possibly compartmentalise very late E-trending normal faulting
- Do not appear to fault the Quaternary alluvium

Interpretation: Quaternary backarc normal faults with possible, late Quaternary reverse re-activation (Global Ore Discovery, 2010).

Northwest-trending structures are the most prominent structural feature within the Gosowong COW (green trend lines, Fig. 2.8) and have been previously highlighted, and variably implicated in low sulfidation epithermal Au mineralization in the Gosowong goldfield (Fitzgerald & Leonard, 1999; Olberg, 2001; Richards et al., 2005; Richards, 2006; Corbett, 2007; Micklethwaite, 2010; Global Ore Discovery, 2010; and other workers). Only the

more major NW-trending faults have been highlighted in Fig. 2.8. Important features and interpretation of the NW-trending structures include:

- Compartmentalize the development of the low sulfidation epithermal target N-trending structures
- Well developed and most easily mapped within the Gosowong Formation window
- Partially and/or weakly re-activated into the post-Gosowong Formation units
- Define apparent dextral, step-wise offsets of the central low sulfidation epithermal target zone
- Predominantly cut and offset by NE-trending structures (with some reverse overprinting relationships due to later NW re-activation)
- Cut and offset by E-trending structures (blue trend lines, Fig. 2.8).
- Compartmentalize contrasting Quaternary volcanic-volcaniclastic packages in the south
- Major NE-block-down faulting of Gosowong stratigraphy
- Define late fault offsets of Quaternary stratigraphy
- Do not appear to fault Quaternary alluvium

Interpretation: Miocene arc & arc-inversion transfer-accommodation zones reactivated as 2.9 Ma Pliocene dextral wrench structures at the end of the mid-Pliocene northward shortening episode (3.5-2.9 Ma, Fig. 2.5). They are interpreted to have compartmentalized the extensional reactivation of N- to NNE-trending, Miocene arc and arc-inversion, arc-parallel structures as low sulfidation epithermal, Au mineralized, extensional, N-trending normal faults at Gosowong Formation level (Fig. 2.8, Global Ore Discovery, 2010). They may have undergone transpressive reverse reactivation in the late Pliocene-early Pleistocene (at the time of Kayasa Formation folding and possible SW-thrusting of the Kayasa Formation, interpreted by Majoribanks, 1997). They were later reactivated (probably as normal faults) with significant block rotations in the Quaternary volcanic backarc, compartmentalizing contrasting Quaternary volcanic-volcaniclastic rock packages. Finally, they were possibly re-activated again, as late Quaternary-Recent transpressive-reverse structures during eastward shortening associated with the northern Halmahera NE dextral wrench episode (Global Ore Discovery, 2010).

Interpretations by Olberg (2001), Global Ore Discovery (2010) and other workers

suggest that there are significant large-scale block tilts and smaller-scale block rotations within the Gosowong COW with S- or SW-downward rotations. Complete reconstruction of the history of block tilting and rotation, mineralized system rotation and the pre-rotation intrusive geometries within the Gosowong COW was proved too complex to resolve in detail in these studies. However, a number of generalized and more specific observations have been made that support a block tilting and block rotation hypothesis. A number of important relationships with implications for block rotation are listed below:

- Predominant bedding orientations in the Gosowong goldfield region are highly clustered with moderate-steep (40-70°) southward dips
- Bases of mineralized horizons through the well-drilled portions of Gosowong and Toguraci have been previously interpreted to dip shallowly south at 10-15°
- The base of the high-temperature, advanced argillic cap in the northern COW dips regionally southward (at least in the southern three-quarters of the region)
- The Quaternary Volcanics dip south at 10-15°. The entire Gosowong low sulfidation system is interpreted to be tilted to the south at 20-30° and overprints a folded, 30° (on average) south-dipping sequence.

Olberg, (2001) proposed the 20-30° post-mineral, southward system rotation of the Gosowong Vein Zone based on interpretations as follows: (1) the south-dipping geometry of a remnant piece of low sulfidation epithermal related advanced argillic cap south of the Gosowong vein. In the Global Ore Discovery (2010) interpretation, it is truncated by a normally reactivated NW structure just south of the mine; (2) south-plunging ore shoots within a S-plunging alteration conduit, and a S-dipping thermal gradient which were all interpreted to have rotated from original sub-horizontal orientations consistent with dip-slip, gaping-formation on an east-dipping listric structure (Olberg, 2001); and (3) a southward deepening of interpreted low sulfidation epithermal textural and mineralogical zones in surface mapping.

2.10 District metallogeny

This section gives an overview of the three deposits in the Gosowong goldfield. The

deposits are situated in a small area (<4 km²), are thought to be kinematically coherent (Walsh and Watterson, 1991) and belong to a N-striking fault system (Fig. 2.8). Several studies indicate that the epithermal structures were, to a first order, dominated by normal dip-slip movement when active (Micklethwaite and Silitonga, 2011). There are large normal offsets of stratigraphy across the structures (Newcrest, 2011), abundant steep-plunging quartz slickenfibres preserved on the margins of veins, and the sub-vertical dip of wallrock extension veins found parallel to the epithermal lodes. This kinematic information reflects E-W extension of the North arm of Halmahera at 2.9-2.8 Ma (Micklethwaite and Silitonga, 2011).

Mining of the Gosowong deposit commenced in 1999 and by mid- 2006, two deposits (Gosowong and Toguraci) had been mined by open cut methods to yield around 1.40 Moz Au at an average grade of ~1oz Au per tonne (Sims and Benton, 2009).Three new veins were discovered in 2002 (Richards et al., 2005), and underground production from the first of these veins commenced in March 2006. These veins, jointly named Kencana – a Javanese term for 'gold' or 'expensive' – consist of the K1, K2 and K-Link (KL) orebodies, arranged in a network of sub-parallel and cross structures over a strike length of 800 m (Sims, 2008; Coupland et al., 2009). Hydrothermal alteration associated with epithermal mineralization in the Gosowong goldfield is reviewed in Chapter 5. The main geological features of the Gosowong goldfield deposits are reviewed below:

Gosowong Deposit: Gosowong is a low sulfidation epithermal gold quartz vein deposit. Au-mineralization is emplaced in two gently S-plunging ore shoots along an E-dipping normal fault, with a strike length of 400 m. The ore shoots are hosted within the volcanic and volcaniclastic rocks of the Gosowong formation. Mineralization is hosted within multiphase epithermal quartz-adularia and quartz-chlorite veins, breccias and peripheral stockworks (Olberg et al., 1999). Mineralization is divided into three domains: quartz-adularia (QA), quartz-chlorite (QC), and low-grade stockwork. The QA zone is characterized by massive to semi-massive banded adularia-quartz veins and breccias, covering a strike length of 150 m, from surface to ~50 m depth. The occurrence of the QA zone is approximately controlled by the locally steep dip of the Gosowong fault and the intersection of a low angle hanging-wall shear, producing a sub-horizontal zone of maximum dilation (Olberg et al., 1999). The

QC zone is characterized by semi-massive to stockwork style quartz-chlorite-illite veins and breccias that occur along the strike length of the deposit, but form a discreet zone outcropping at the northern end of the deposit, plunging gently south to ~135 m below the surface. QC mineralization is distinct as dark green, weakly developed, banded quartz veins with occasional very fine-grained visible gold. The QC zone contains the majority of the high-grade gold mineralization (5- >500 g/t Au) (Olberg et al., 1999). The low-grade stockwork zone is characterized by crystalline quartz to chalcedony vein stockworks peripheral to and overlapping the QA and QC zones, from surface to ~150 m depth. Barren quartz stockworks are also found at depth below the keel of ore-grade mineralization, visually indistinct from the mineralized stockwork veins (Olberg et al., 1999).

Gold in the Gosowong deposit occurs in native form (840 fineness), where grains are usually <20 μm in size, and is interstitial to and intergrown with quartz, adularia, pyrite and minor amounts of sphalerite, galena and chalcopyrite (Coote, 1996).

Gosowong mine produced 1.0 Mt @ 24 g/t Au for 0.77 Moz Au and production ceased in 2002, though the pit has recently re-opened to remove additional resources that now economic. The detailed geology of the Gosowong deposit is reviewed in Olberg et al. (1999).

Toguraci Deposit: Toguraci is a low sulfidation epithermal gold quartz vein deposit overprinting uneconomic copper-gold porphyry veining (known as the Bora porphyry), located 2 km WSW of the Gosowong deposit. Alteration associated with the porphyry Cu-Au event is biotite-magnetite±chlorite enveloped by chlorite±epidote±calcite±pyrite. Epithermal gold quartz veins clearly crosscut the porphyry style mineralization and the superimposed epithermal alteration is typical of the Gosowong goldfield: Quartz-adularia-illite-pyrite alteration in the epithermal vein zone, enveloped by illite-quartz-pyrite, which in turn is surrounded by a regional chlorite-epidote-albite-calcite-pyrite halo (Richards and Dwi Priyono, 2004). Most epithermal veins at Toguraci are controlled by a set of N-striking sub-vertical faults. High-grade gold shoots are confined to discrete dilation zones along these faults, preferentially developing in the diorite. NE cross-cutting faults also host lower grade gold-quartz mineralization with small high-grade shoots in some dilational jog positions (Richards and Dwi Priyono, 2004).

Toguraci veins display epithermal textures typical of the Gosowong goldfield. Mineralization is hosted within multiphase quartz-adularia vein breccias with clasts of both wallrock and earlier quartz veins, and chlorite and black sulfide bands or rims up to 5 mm thick, commonly with fine-grained visible gold which overprint the quartz adularia event and are present in bonanza gold grade zones. This quartz-chlorite-sulfide mineralization phase, although volumetrically minor, contributes significantly to the gold inventory, as at Gosowong. Early low-grade vuggy quartz veins and stockwork, and late stage crosscutting carbonate veinlets are common.

Toguraci produced 0.4 Mt at 27 g/t Au for 0.35 Moz Au between 2004 and 2006. Successful exploration targeting in the Gosowong goldfield lead to the discovery of further mineralization to the north of the Toguraci deposit (known as Toguraci North, Fig. 2.7 B). Currently, infrastructure is being developed to allow underground extraction of the new resource.

Kencana Deposit: Kencana is the third, and most recently discovered, low sulfidation epithermal Au-Ag deposit discovered in the Gosowong goldfield. The deposit, situated 1 km south of Gosowong, does not outcrop at surface, with mineralization occurring approximately 70 m below the current surface. Kencana is hosted in a mineralized normal-fault array, with two main sub-parallel, shallow eastward-dipping (40-46°) structures which flatten at depth (namely K1 and K2), connected by a conjugate structure (K-Link). Gold mineralization is present in complex multistage, banded quartz-adularia and quartz-chlorite veins, hydrothermal breccias and stockworks. The quartz-chlorite crustiform and cockade banded breccia events host the bulk of the bonanza grade Au-mineralization. Gold is present as electrum (Au-rich) and lesser native gold. Silver is more commonly present as selenide phases. Ag-, Pb- and lesser Au tellurides (with clausthalite) are accessory minerals in the vein. The youngest stage of mineralization at Kencana is represented by a dark, fine-grained black breccia and vein-fill material that is characterized by quartz, molybdenite and minor galena, Ag selenides, and pyrite. The detailed geology of the Kencana deposit will be discussed in the subsequent chapters. Kencana has a total endowment of approximately 4.4 Mt at 27.9 g/t Au, containing 4.0 Moz Au (Newcrest, 2010).

Porphyry mineralization: Porphyry intrusive bodies occur within the Gosowong For-

mation along a N to NNE-trending corridor from Bora and Tobobo in the south to Matat and Ngoali in the north. This trend is inferred to represent the emplacement of intrusive bodies along an arc-parallel accretionary structure (Fitzgerald and Leonard, 1999). However, no surface evidence for a major crustal discontinuity is observed, and thus the structure is believed to be deep-seated. A second control on porphyry emplacement may exist where prominent NW-trending structures intersect the N-trending corridor, with at least 3 major porphyry bodies in the district occurring at such intersections (Bora, Matat and Ngoali) (Fitzgerald and Leonard, 1999).

At the Bora porphyry, intrusive lithologies vary in texture from medium-grained sub-porphyritic to crowded, coarse-grained porphyritic rock types (Fitzgerald and Leonard, 1999). Crosscutting relationships and marked differences in style and intensity of alteration between intrusive lithologies indicate that several phases of intrusives occur at Bora. A characteristic of the Bora porphyry is the presence of wallrock fragments (augite-phyric basalt and early diorite) in a dioritic 'matrix', representing a primary magmatic intrusion breccia (Fitzgerald and Leonard, 1999). Other intrusive breccias recognized at Bora include pebble dykes characterized by narrow (few cm to >1 m), dyke-like bodies with sharp, sub-parallel contacts composed of sub-rounded, matrix-supported polymict clasts in a fine-grained matrix; and monomict diorite breccias (Fitzgerald and Leonard, 1999).

Diorite host rocks with basaltic dykes display intense potassic alteration, characterized by pervasive magnetite and strong K-feldspar flooding (which also occurs as local vein selvages). Laminated quartz-magnetite veins, described by Fitzgerald and Leonard (1999) as typical porphyry Cu-Au-style early M veins, contain local bornite, while magnetite dominates in the B style veins. Veins are commonly sheeted, though some stockwork B veins are recognized. The laminated quartz-magnetite veins are overprinted by parallel, milky-white epithermal quartz veins (Leach, 2005).

Primary ore minerals include chalcopyrite, bornite, molybdenite and tennantite/ tetrahedrite. Secondary copper sulfides include chalcocite and covellite, though there is little evidence for significant supergene enrichment of copper (Fitzgerald and Leonard, 1999).

2.11 District geochronology

Several studies have shown that hydrothermal mineral deposits are closely related both spatially and temporally with episodes of volcanism and plutonism, particularly in the later stages of such activity (McKee and Noble, 1989; Cathles et al., 1997). Geological evidence and modeling studies generally suggest that hydrothermal activity occurs either as short-lived pulses lasting less than 100,000 years or as long-lived systems of ~1 Ma (Cathles et al., 1997). In almost all cases, hydrothermal circulation, geothermal activity and magmatic events are closely related in time and space, and long-lived systems consist of a series of short-lived pulses of intrusion and hydrothermal circulation (Cathles et al., 1997).

Geochronological study of the host rock package and mineralization in the Gosowong goldfield is important in that the first-order geological evolution of the goldfield can be constrained, including determination of timing of intrusions, the relationship between stratigraphic units and the timing of epithermal and porphyry deposit formation in the goldfield. In this section, epithermal mineral ages from Gosowong, Toguraci and Kencana are compared to determine whether the systems can be considered coeval. $^{40}Ar/^{39}Ar$ data for the Gosowong deposit and U/Pb dating of igneous phases were determined in previous studies and are discussed.

This study reports new $^{40}Ar/^{39}Ar$ radiometric age dating to better constrain the ages of epithermal mineralization in the goldfield. Six samples were submitted during this study for $^{40}Ar/^{39}Ar$ age dating of adularia from the Gosowong, Toguraci and Kencana deposits (two samples from each), with the aim of providing a better age constraint on the timing of epithermal mineralization in the goldfield, and also determining the temporal relationship between the three deposits. In the Gosowong goldfield deposits, adularia is deposited directly with Au-bearing quartz within the hydrothermal veins. Dating adularia precipitation is therefore the best way to estimate the age of vein formation and hypogene mineralization.

2.11.1 Previous work

$^{40}Ar/^{39}Ar$ radiometric age determination of adularia and alunite in igneous rocks, hydrothermal alteration and mineralization at the Gosowong deposit was reported by Vasconcelos (1998). Epithermal alteration ages were determined by step-heating methods and

total fusion using both adularia vein material and alunite grains it was not made clear in this study whether the alunite was determined to be supergene, steam-heated or magmatic-hydrothermal in origin, and associated minerals or paragenesis were not described.

Lithologies selected for analysis included andesitic breccias, diorite, augite-phyric basalts (alteration analses), vein adularia and alunite alteration. Alunite analyses of 4 grains yielded ages of 2.85 ±0.01 Ma, 2.82 ±0.02 Ma, 2.83 ±0.02 Ma and 2.93 ±0.01 Ma. Individual growth bands in adularia samples were separately analysed and plateau ages were determined to be statistically indistinguishable (within 2σ) at 2.8-2.9 Ma (Vasconcelos, 1998). Magmatism in the Gosowong goldfield was determined to span a period from 4.1 Ma to 2.9 Ma, with an average age of 3.7 Ma. The study was inconclusive whether this represented sampling bias or the period of peak magmatism. The sample corresponding to 2.9 Ma was a propylitic altered andesite flow breccia taken from the hangingwall of the Gosowong vein. It was concluded that this young age may be a true representation of magmatic age, though it is possible that $^{40}Ar/^{39}Ar$ ages were reset during subsequent hydrothermal alteration (Vasconcelos, 1998).

K-feldspar and sericitized K-feldspar were analysed by total fusion and step-heating methods to obtain the age of porphyry alteration in the Gosowong Formation from the Toguraci region. Plateau ages provided poor constraint for the Gosowong Formation, with a total range from ~4 Ma to 2.6 Ma, but peak alteration ages clustered at 3.5 Ma, although hydrothermal alteration persisted until 2.9-2.6 Ma (Vasconcelos, 1998).

U/Pb zircon geochronology of the igneous phases in the Gosowong district was undertaken by Micklethwaite (2010). Samples selected for analysis included andesite from an outcrop of the Gosowong Formation, andesite-dacite volcanic breccia previously mapped as Kayasa Formation, samples confidently logged as Kayasa Formation from Kencana drill core, plus diorite samples from both Kencana drill core and Toguraci pit. Samples were also obtained from the Ngailamo area in the north CoW, and from adjacent outcropping epithermal veins in the Tiabo valley, North Halmahera. U/Pb analyses were carried out at the University of Tasmania by laser-ablation inductively coupled mass spectrometry (LA-ICPMS), and a summary of results is displayed in Fig. 2.9.

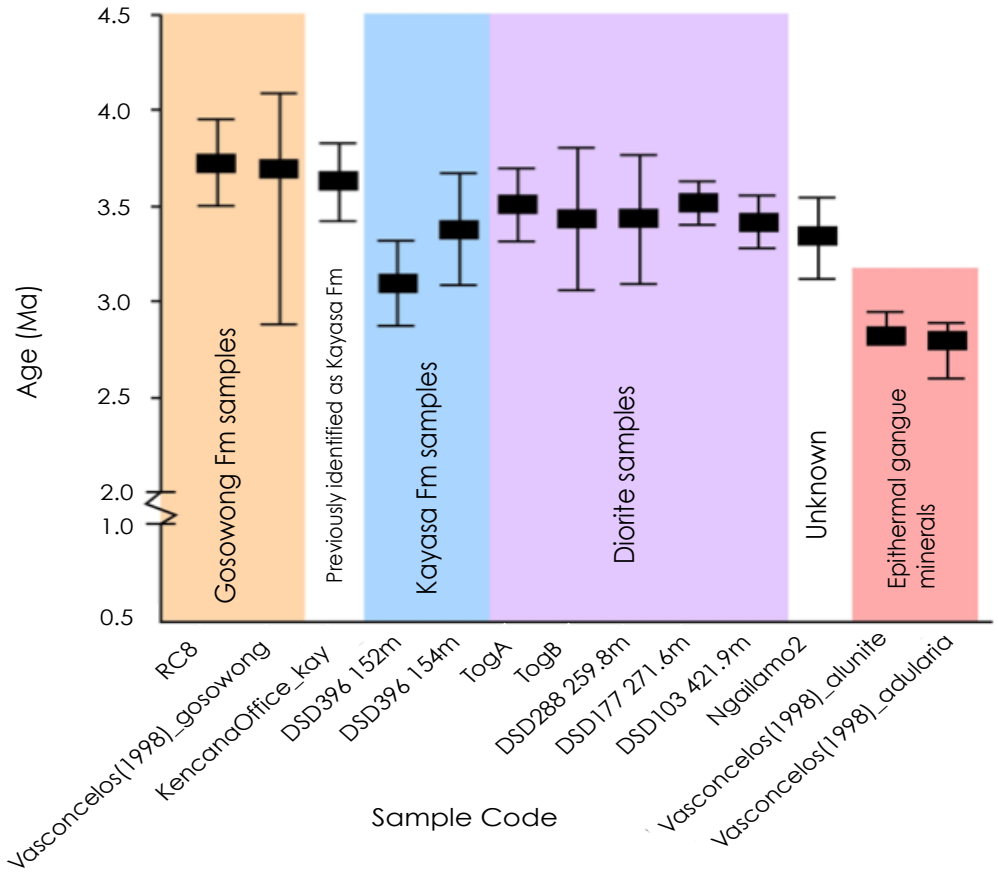

Fig. 2.9 U/Pb Geochronology Summary of U/Pb ages of different lithology samples from the Gosowong goldfield and CoW area, compared with $^{40}Ar/^{39}Ar$ ages obtained by Vasconcelos (1998) for adularia and alunite analyses on Gosowong lavas and epithermal mineralization. Micklethwaite, 2010.

Results suggest that andesites and diorites are closely temporally related, with andesite emplacement at 3.73 ± 0.22 Ma, followed by dioritic intrusions. Two diorite samples from Kencana drill cores and 1 sample from Toguraci pit yielded ages of 3.42 ± 0.13 Ma, 3.52 ± 0.10 Ma and 3.51 ± 0.18 Ma respectively, suggesting that the diorites can be considered as part of the same intrusive system based on the lack of resolvable time difference between the two locations (Micklethwaite, 2010).

2.11.2 Analytical methods

Sample preparation and irradiation

$^{40}Ar/^{39}Ar$ geochronology was undertaken at the University of Melbourne by Prof.

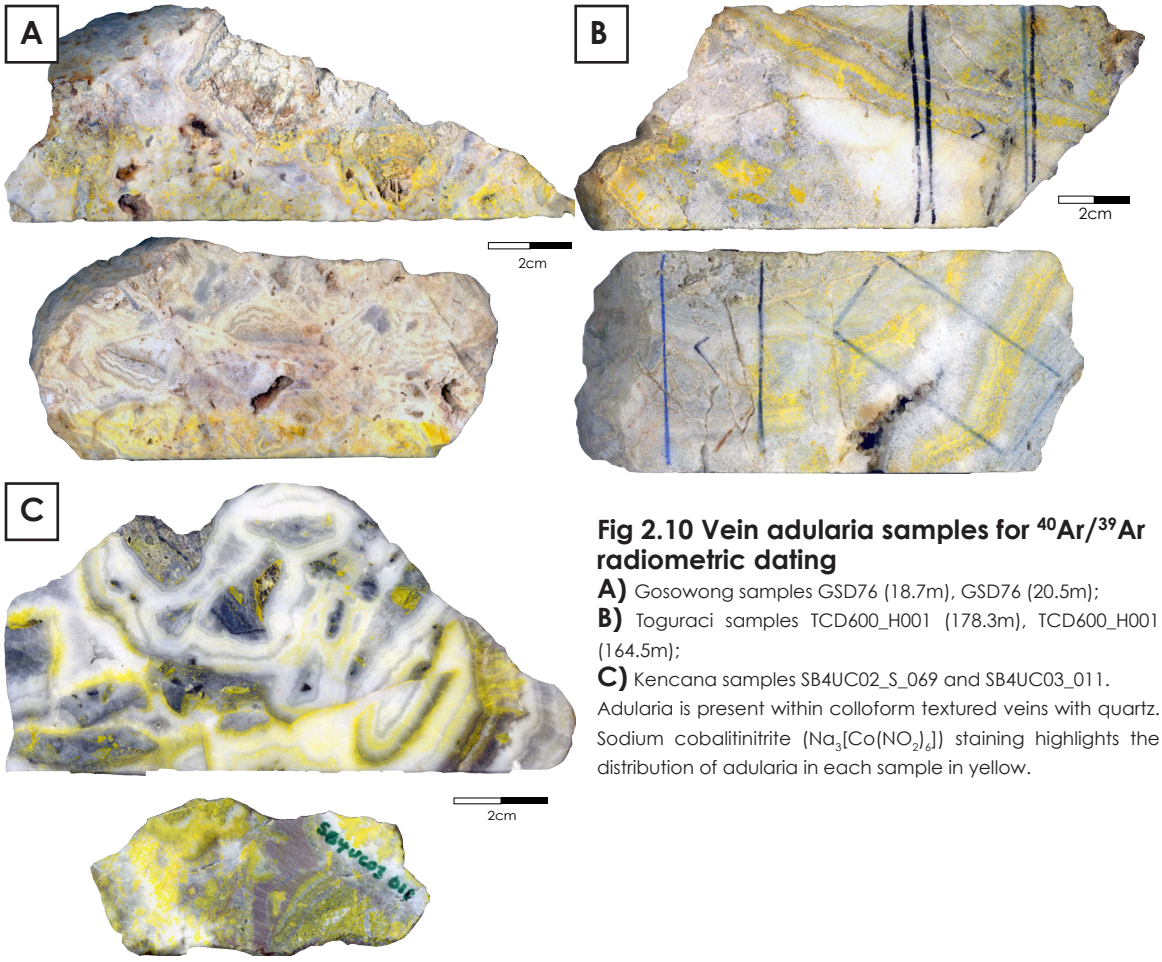

Fig 2.10 Vein adularia samples for $^{40}Ar/^{39}Ar$ radiometric dating
A) Gosowong samples GSD76 (18.7m), GSD76 (20.5m);
B) Toguraci samples TCD600_H001 (178.3m), TCD600_H001 (164.5m);
C) Kencana samples SB4UC02_S_069 and SB4UC03_011.
Adularia is present within colloform textured veins with quartz. Sodium cobalitinitrite ($Na_3[Co(NO_2)_6]$) staining highlights the distribution of adularia in each sample in yellow.

David Phillips. Adularia-rich veins were cut from core sections of samples GSD76 (18.7 m) and GSD76 (20.5 m) from the Gosowong deposit, TCD600_H001 (164.5 m) and TCD600_H001 (178.3m) from the Toguraci deposit, and underground hand samples SB4UC02_S_069 and SB4UC03_011 from the Kencana deposit (Fig. 2.10). Samples were stained with sodium cobalitnitrite (Na3[$Co(NO_2)_6$]) to determine the distribution of adularia within the samples (Fig. 2.10). The samples were crushed to ~2 cm chips using a jaw crusher. Individual chips were then screened for alteration and crushed manually using a steel piston crusher. Crushed samples were washed of dust and sieved to a 0.2-0.5 mm grainsize, with adularia grains handpicked under a binocular microscope. Adularia sample weights ranged from 11 to 35 mg.

Samples were loaded into aluminium foil packets and placed in quartz tubes (UM#23 and UM#25) along with the flux monitor GA1550 biotite (98.8 ± 0.5 Ma; Renne et al.,

1998) and irradiated in a cadmium-lined can (UM#40) in position 5c of the McMaster University reactor, Hamilton, Canada (Matchan and Phillips, 2011).

Gas extraction and analysis

$^{40}Ar/^{39}Ar$ laser step-heating analyses were conducted at the University of Melbourne. Irradiated samples were split into aliquots and loaded into a copper sample holder. The holder was then loaded into a vacuum sample chamber coupled to a MM5400 mass spectrometer equipped with a Daly detector. The extraction line and samples were baked overnight at ~200°C to remove low temperature contaminants. Aliquots were heated incrementally using a defocused 40W CO_2 laser. Released gases were admitted to the mass spectrometer following purification by two Zr-Al getters. Extraction line blanks were analysed prior to each analysis. Mass discrimination was monitored by measuring air aliquots from a Doerflinger pipette and averaged 1.0075 ± 0.19% (1σ) (Matchan and Phillips, 2011).

2.11.3 Results and Interpretation

Argon isotopic results are corrected for system blank, mass discrimination, radioactive decay, reactor-induced interference reactions and atmospheric argon. Decay constants used are those reported by Steiger and Jager (1977). Correction factors (± 1σ) for interfering isotopes were $(^{36}Ar/^{37}Ar)Ca = 0.000289 \pm 1.7\%$, $(^{39}Ar/^{37}Ar)Ca = 0.000680 \pm 2.79\%$, $(^{40}Ar/^{39}Ar)K = 0.000400 \pm 100\%$ and $(^{38}Ar/^{39}Ar)K = 0.0130 \pm 38.46\%$. Calculated uncertainties associated with mean and plateau ages include uncertainties in the J-values, but exclude errors associated with the age of the flux monitor and the decay constant.

Data are given in the appendix. Plateau ages are shown in Fig. 2.11. Errors are quoted in 1σ and are typically of the order of 1%. Plateau ages are defined as including at least 50% of the ^{39}Ar, distributed over a minimum of 3 contiguous steps with $^{40}Ar/^{39}Ar$ ratios within agreement of the mean at the 95% confidence level. Samples GSD5-1, S11-2, S69-1 and S69-4 did not conform to these requirements and were thus rejected from age calculations.

McDougall and Harrison (1999) and Love et al. (1998) caution that $^{40}Ar/^{39}Ar$ dates from alkali feldspar may be difficult to interpret. Adularia typically crystallizes in the ther-

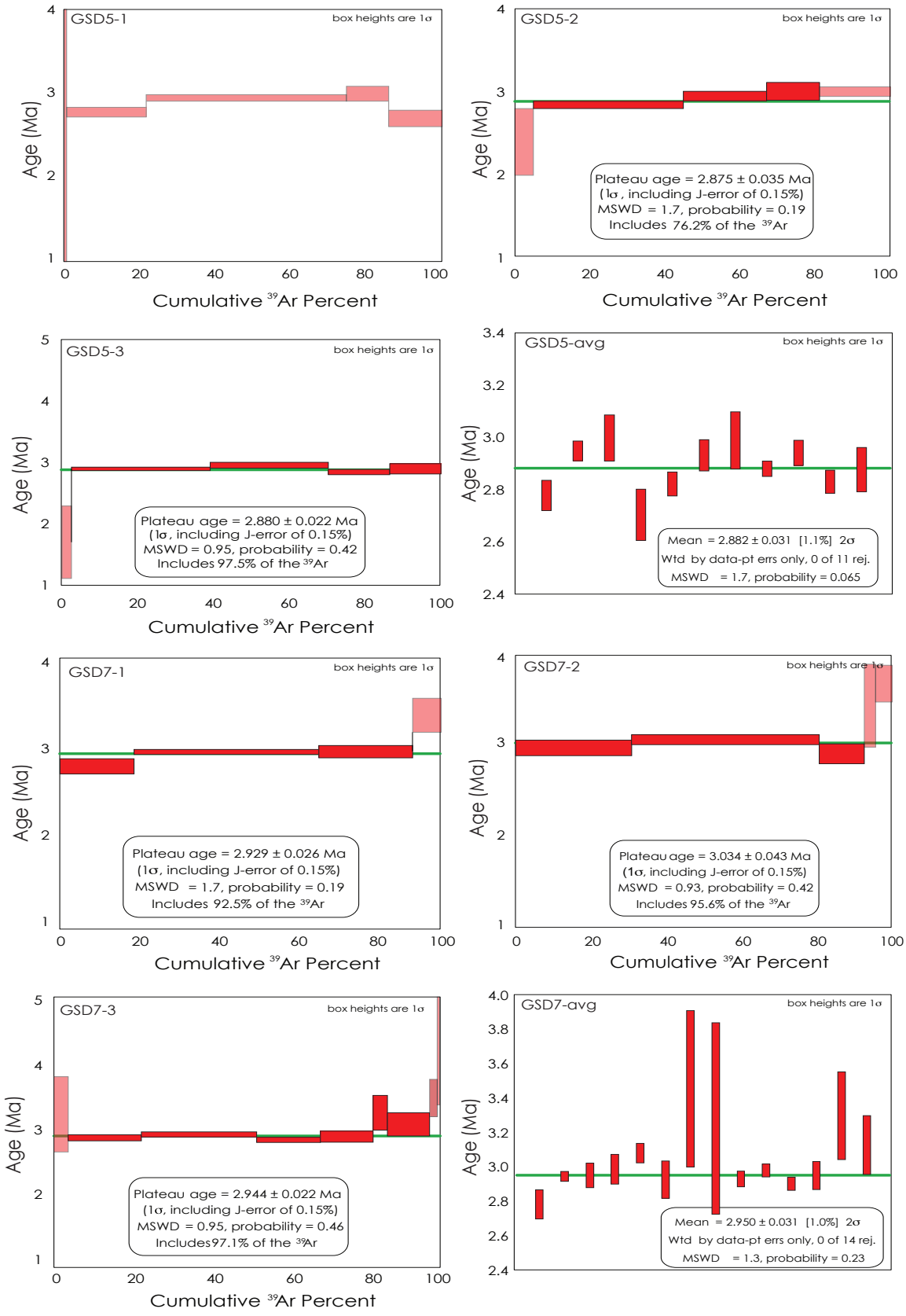

Fig. 2.11 Conventional $^{40}Ar/^{39}Ar$ age spectra of hydrothermal adularia samples from the Gosowong (GSD5, GSD7), Toguraci (TSD3, TSD5) and Kencana (S11, S69) deposits. Plateaus are defined by steps highlighted in red and average ages are shown as green lines. Pale red steps are excluded as these do not meet the criteria for defining plateaus.

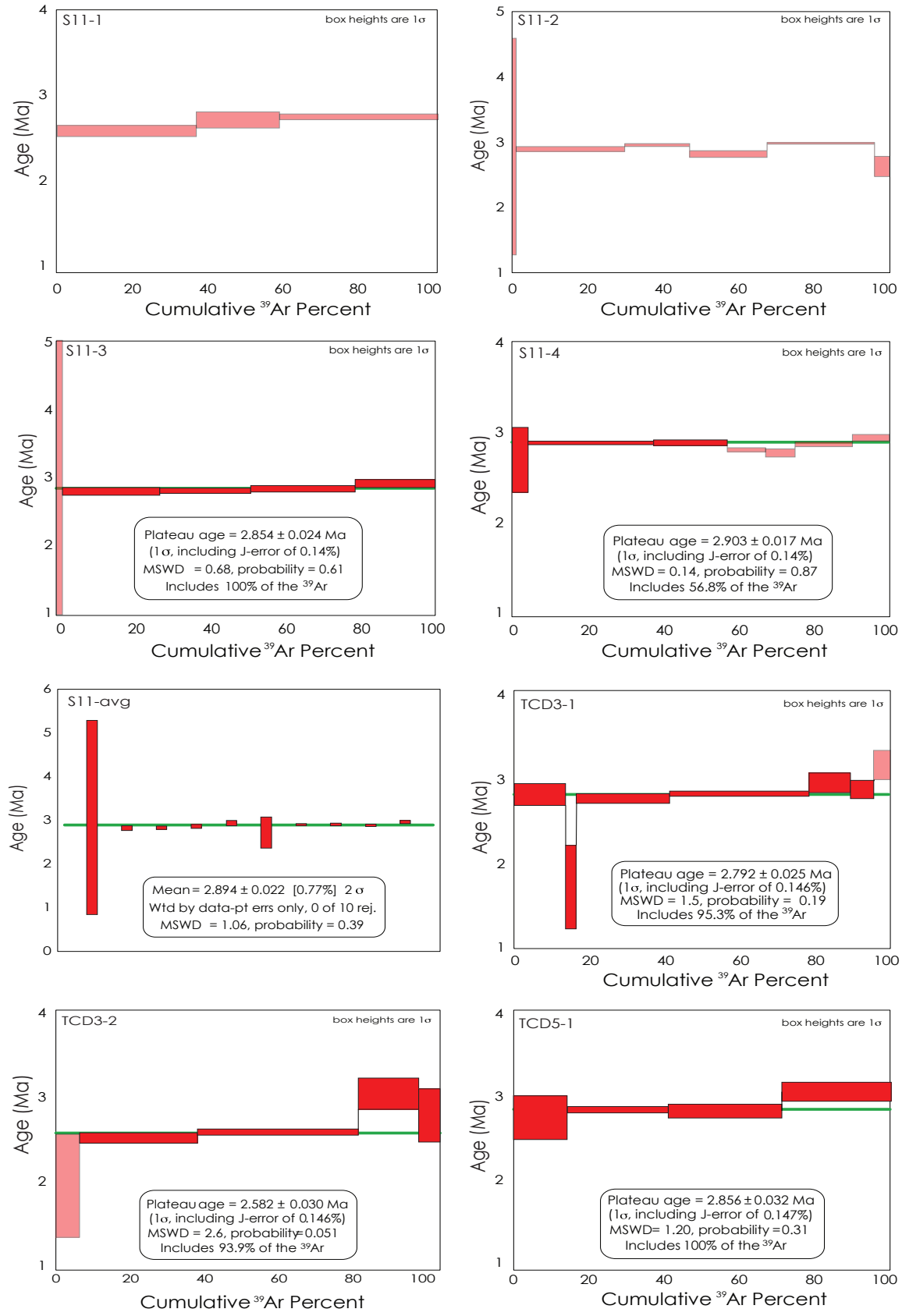
S11-1
box heights are 1σ
Age (Ma)
Cumulative ^{39}Ar Percent
S11-2
box heights are 1σ
Age (Ma)
Cumulative ^{39}Ar Percent
S11-3
box heights are 1σ
Plateau age = 2.854 ± 0.024 Ma
(1σ, including J-error of 0.14%)
MSWD = 0.68, probability = 0.61
Includes 100% of the ^{39}Ar
Age (Ma)
Cumulative ^{39}Ar Percent
S11-4
box heights are 1σ
Plateau age = 2.903 ± 0.017 Ma
(1σ, including J-error of 0.14%)
MSWD = 0.14, probability = 0.87
Includes 56.8% of the ^{39}Ar
Age (Ma)
Cumulative ^{39}Ar Percent
S11-avg
Mean = 2.894 ± 0.022 [0.77%] 2 σ
Wtd by data-pt errs only, 0 of 10 rej.
MSWD = 1.06, probability = 0.39
Age (Ma)
TCD3-1
box heights are 1σ
Plateau age = 2.792 ± 0.025 Ma
(1σ, including J-error of 0.146%)
MSWD = 1.5, probability = 0.19
Includes 95.3% of the ^{39}Ar
Age (Ma)
Cumulative ^{39}Ar Percent
TCD3-2
box heights are 1σ
Plateau age = 2.582 ± 0.030 Ma
(1σ, including J-error of 0.146%)
MSWD = 2.6, probability=0.051
Includes 93.9% of the ^{39}Ar
Age (Ma)
Cumulative ^{39}Ar Percent
TCD5-1
box heights are 1σ
Plateau age = 2.856 ± 0.032 Ma
(1σ, including J-error of 0.147%)
MSWD= 1.20, probability =0.31
Includes 100% of the ^{39}Ar
Age (Ma)
Cumulative ^{39}Ar Percent

Fig. 2.11 Cont.

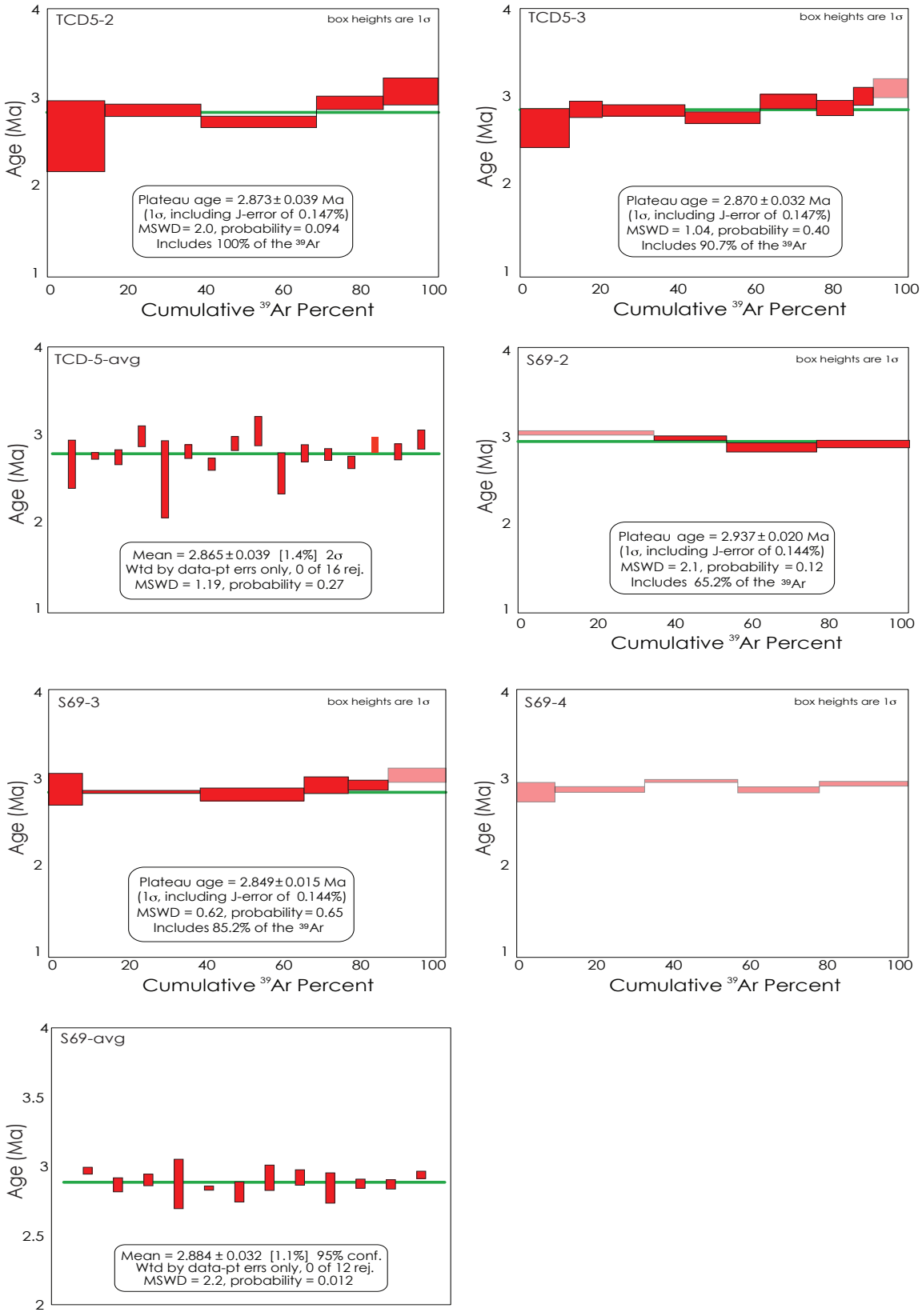
TCD5-2
box heights are 1σ
Plateau age = 2.873 ± 0.039 Ma
(1σ, including J-error of 0.147%)
MSWD = 2.0, probability = 0.094
Includes 100% of the 39Ar
TCD5-3
box heights are 1σ
Plateau age = 2.870 ± 0.032 Ma
(1σ, including J-error of 0.147%)
MSWD = 1.04, probability = 0.40
Includes 90.7% of the 39Ar
TCD-5-avg
Mean = 2.865 ± 0.039 [1.4%] 2σ
Wtd by data-pt errs only, 0 of 16 rej.
MSWD = 1.19, probability = 0.27
S69-2
box heights are 1σ
Plateau age = 2.937 ± 0.020 Ma
(1σ, including J-error of 0.144%)
MSWD = 2.1, probability = 0.12
Includes 65.2% of the 39Ar
S69-3
box heights are 1σ
Plateau age = 2.849 ± 0.015 Ma
(1σ, including J-error of 0.144%)
MSWD = 0.62, probability = 0.65
Includes 85.2% of the 39Ar
S69-4
box heights are 1σ
S69-avg
Mean = 2.884 ± 0.032 [1.1%] 95% conf.
Wtd by data-pt errs only, 0 of 12 rej.
MSWD = 2.2, probability = 0.012
Age (Ma)
Cumulative 39Ar Percent

Fig. 2.11 Cont.

mal stability field of triclinic microcline, but commonly has the metastable monoclinic structure because its rapid crystallization inhibits ordering of Si and Al (Arancibia et al., 2006). During slow cooling, Na- bearing K-feldspar may unmix and may also reorder to a more triclinic structure. Both unmixing and reordering may allow argon loss and result in a closure temperature as low as ~150°C (Love et al., 1998; McDougall and Harrison 1999; Arancibia et al., 2006). At Kencana, rapid cooling is inferred (and low temperature of formation) deduced from the habitat in which adularia crystallized (fine-grained adularia in veins and open spaces in association with cryptocrystalline quartz) and from fluid inclusion studies. In this case, unmixing and reordering, and consequent argon loss would be insignificant (Arancibia et al., 2006). Well-defined plateau ages obtained in this study show that overall argon loss was insignificant and that this analytical method can be successfully used for adularia formation in short-pulse epithermal veins (Groff et al., 1997; Love et al., 1998; Parsons et al., 1999; Sanematsu et al., 2004, Arancibia et al., 2006). Slight excess argon was detected in some of the analyzed samples.

Well-defined plateau ages beginning from the first or second step of the spectrum give mean ages of 2.882 ± 0.031 Ma (GSD5) and 2.950 ± 0.031 Ma (GSD7) for the Gosowong deposit, 2.865 ± 0.039 Ma (TCD5) for the Toguraci deposit, and 2.884 ± 0.032 Ma (S69) and 2.925 ± 0.026 Ma (S11) for the Kencana deposit (Fig. 2.11). The age of adularia precipitation in the deposits can be considered coeval as the dates are largely consistent within error. It is interpreted that the deposits are all related to the same hydrothermal event, over a time span of <100,000 years, in which periodic epithermal mineralization occurred. It is likely that several convecting cells were present in the region, though these most probably had the same underlying deep heat source.

New ages for mineralization in the Gosowong deposit (2.882 ± 0.031 Ma and 2.950 ± 0.031 Ma) show a hiatus of 10,000 years (inclusive of error) indicating an interval of periodic quartz-adularia precipitation in the vein for at least this length of time. Vein adularia precipitation post-dates igneous phases hosting the deposits by ~0.8 Ma, according to the dates obtained by Micklethwaite (2010).

Ages obtained in this study are similar to (to marginally older than) the $^{40}Ar/^{39}Ar$

(alunite) ages obtained by Vasconcelos (1998) for the Gosowong deposit (2.85 ±0.01 Ma, 2.82 ± 0.02 Ma, 2.83 ±0.02 Ma and 2.93 ±0.01 Ma). The clustering of ages around 2.9 Ma suggests that the magmatism age of 2.9 Ma obtained by Vasconcelos (1998) is most likely due to the resetting of $^{40}Ar/^{39}Ar$ dates during hydrothermal alteration related to quartz-adularia precipitation in the hangingwall of the Gosowong vein.

High Ca/K ratios occur in the first or last step of many samples (GSD5-1, GSD5-3, GSD7-3, S11-1, S11-2, S11-3, TCD3-1 [step 2], and TCD3-2). High Ca/K ratios are coincident with anomalously high or low ages, suggesting high Ca phases in inclusions within the adularia degassing during step heating (Berry, pers comm., 2012). These ages have been discounted from weighted mean age calculations. High Ar values in the last step (representing Ar loss) may also indicate degassing inclusions in the adularia.

2.12 Summary

- The Kencana deposit is situated on the island of Halmahera, which can be generally divided into two geologic domains (the eastern and western provinces), reflecting the separate geological histories of these two sections of the island.

- The Gosowong goldfield is situated on the eastern side of the NW arm of Halmahera, covering an area of approximately 30,000 Ha as part of the contract of work (CoW) of PT. Nusa Halmahera Minerals. The NW arm is composed of four superimposed volcanic arcs, produced as a result of subduction of the Maluku sea plate beneath Halmahera since the Palaeogene: the Bacan Formation (Palaeogene), the Gosowong Formation (Upper Miocene), the Kayasa Formation (Pliocene) and the Quaternary Volcanic Formation, currently being deposited by the stratiform calc-alkaline cones of the Halmahera arc). Lithologies are dominated by andesite to basaltic andesite volcanic and volcaniclastic rocks and diorite intrusions.

- There are two distinct mineralized events in the goldfield: low grade, copper-gold porphyry style mineralization, and high-grade, gold-silver epithermal style mineralization. Several epithermal prospects exist in the Gosowong goldfield, and currently three eco-

nomic Au-Ag epithermal deposits have been discovered in the region (Gosowong, Toguraci and Kencana deposits).

- Mineralization is hosted by the upper Miocene Gosowong Formation. The Gosowong Formation is a series of interbedded volcaniclastic rocks, ignimbrites and coherent volcanic rocks, occurring as flows or intrusions. The deposits are situated in a small area (<4 km^2), are thought to be kinematically coherent and belong to a N-striking fault system.

- The epithermal structures were dominated by normal dip-slip movement when active. There are large normal offsets of stratigraphy across the structures, abundant steep-plunging quartz slickenfibres preserved on the margins of veins, and sub-vertical dip of wallrock extension veins found parallel to the epithermal lodes.

- Andesites and diorites are closely temporally related, with andesite emplacement at 3.73 ± 0.22 Ma, followed by dioritic intrusions. Diorites from the Kencana and Toguraci deposits can be considered as part of the same intrusive system based on the lack of resolvable time difference between the two locations.

- Epithermal mineralization post-dates andesite and diorite emplacement. $^{40}Ar/^{39}Ar$ dating of hydrothermal adularia gives mean ages of 2.882 ± 0.031 Ma and 2.950 ± 0.031 Ma for the Gosowong deposit, 2.865 ± 0.039 Ma for the Toguraci deposit, and 2.884 ± 0.032 Ma and 2.925 ± 0.026 Ma for the Kencana deposit. The age of adularia precipitation in the deposits, and therefore the age of epithermal mineralization, can be considered coeval as these dates are consistent within error. The deposits are interpreted to be related to the same, long-lived (<100,000 years) hydrothermal event, during which pulses of epithermal mineralization resulted from the convection of hydrothermal fluids in several small cells, driven by one important underlying heat source.

CHAPTER 3

DEPOSIT GEOLOGY

3.1 Introduction

This chapter presents the mine-scale stratigraphy, petrology and volcanic facies of the Kencana gold deposit. The local geological setting is reviewed, with the major volcanic and volcaniclastic facies documented and plotted along 5 cross sections through the Kencana vein, and the conditions of deposition of the host rocks interpreted. Volcanic facies studies, descriptions and cross sections are derived from exploration diamond drill core logging of the Kencana deposit conducted over six months in three field seasons, complemented by hand specimen and thin section observations. Most volcanic facies show varying degrees of alteration (see Chapter 5), however the primary volcanic textures are generally preserved, allowing interpretations as to their depositional characteristics and genesis.

3.2 Geologic setting

Kencana is located 1 km south of the Gosowong deposit (see Chapter 2) and has a total endowment of approximately 4.4 Mt @ 27.9 g/t Au, containing 4 Moz Au (Newcrest, 2010). The deposit is associated with a NW-striking listric fault structure with an average dip of 40-46°NE, and normal fault movement as determined by bedding offset. The structure flattens at depth, marked by numerous splays and an increase in quartz stockworking. There is only a very weak surface expression of the Kencana structure represented by carbonate veining and clay-pyrite faulting. Stream sediment samples in the vicinity of Kencana all returned <0.1 g/t Au, and consequently the deposit is considered blind, with mineralization encountered approximately 70 m below the current surface.

The deposit is hosted by two main sub-parallel fault structures (namely K1 and K2), joined by link structures, such as K-link (KL) that exhibit a steeper dip than the main K1 and

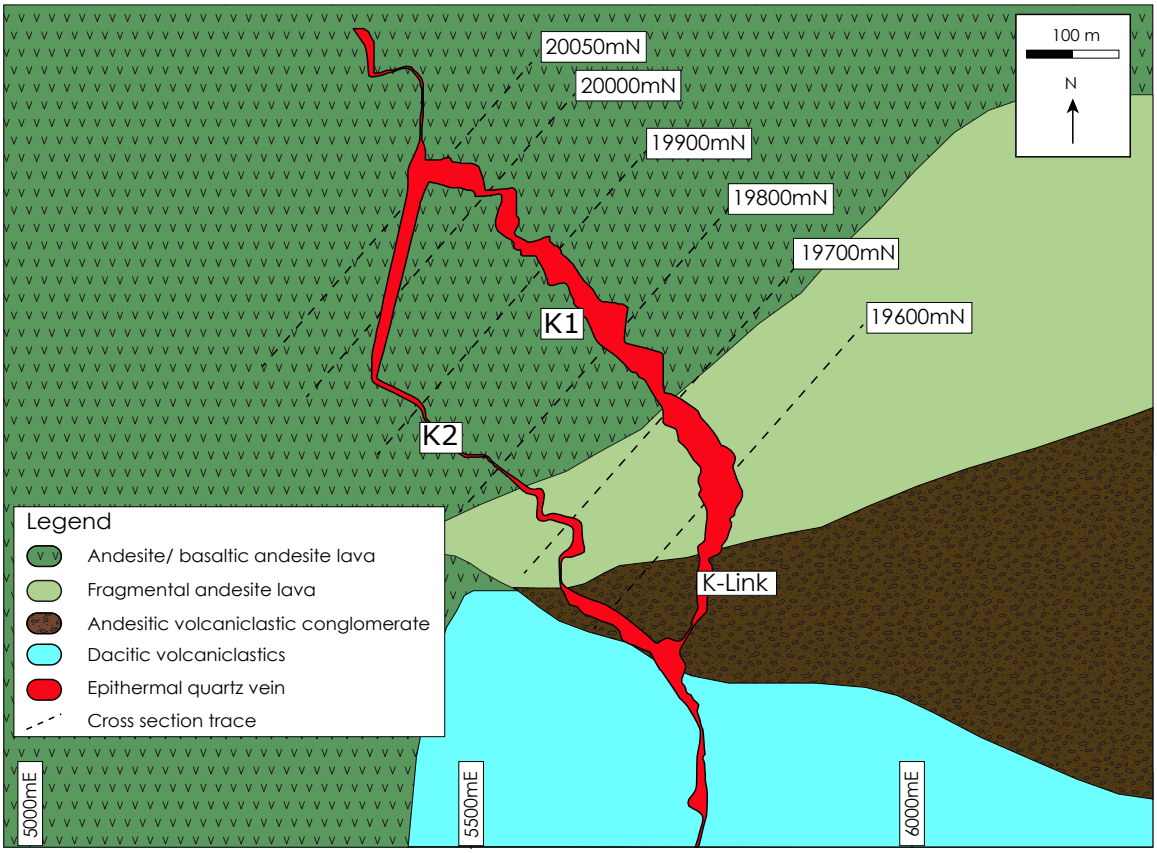

Fig. 3.1 Simplified plan view of the Kencana deposit depicting the major structures including the K1, K2 and K-Link epithermal veins and the associated host lithologies. Vein projected to surface (no outcrop), with dominant surface lithology units depicted. Modified from Newcrest, 2010.

K2 structures. Numerous minor structures have been identified forming a framework in the area. The K1 structure provided the focus for this study due to greater exposure in drill core and underground access.

3.3 Deposit stratigraphy

The Kencana deposit is hosted in a succession of upper Miocene to Pliocene basaltic to andesitic volcanic rocks, volcaniclastic rocks and diorite intrusions, forming part of two superimposed volcanic sequences: The Gosowong Formation (upper Miocene host to the Gosowong Goldfield mineralization), and the Kayasa Formation (Pliocene). An overview of the stratigraphic units hosting the Kencana deposit is given in Fig. 3.2, and the distribution of the volcano-sedimentary and intrusive facies hosting the Kencana deposit is summarized in Figs. 3.3-3.7. Descriptions of the primary lithofacies are given in section 3.3.1, and litho-

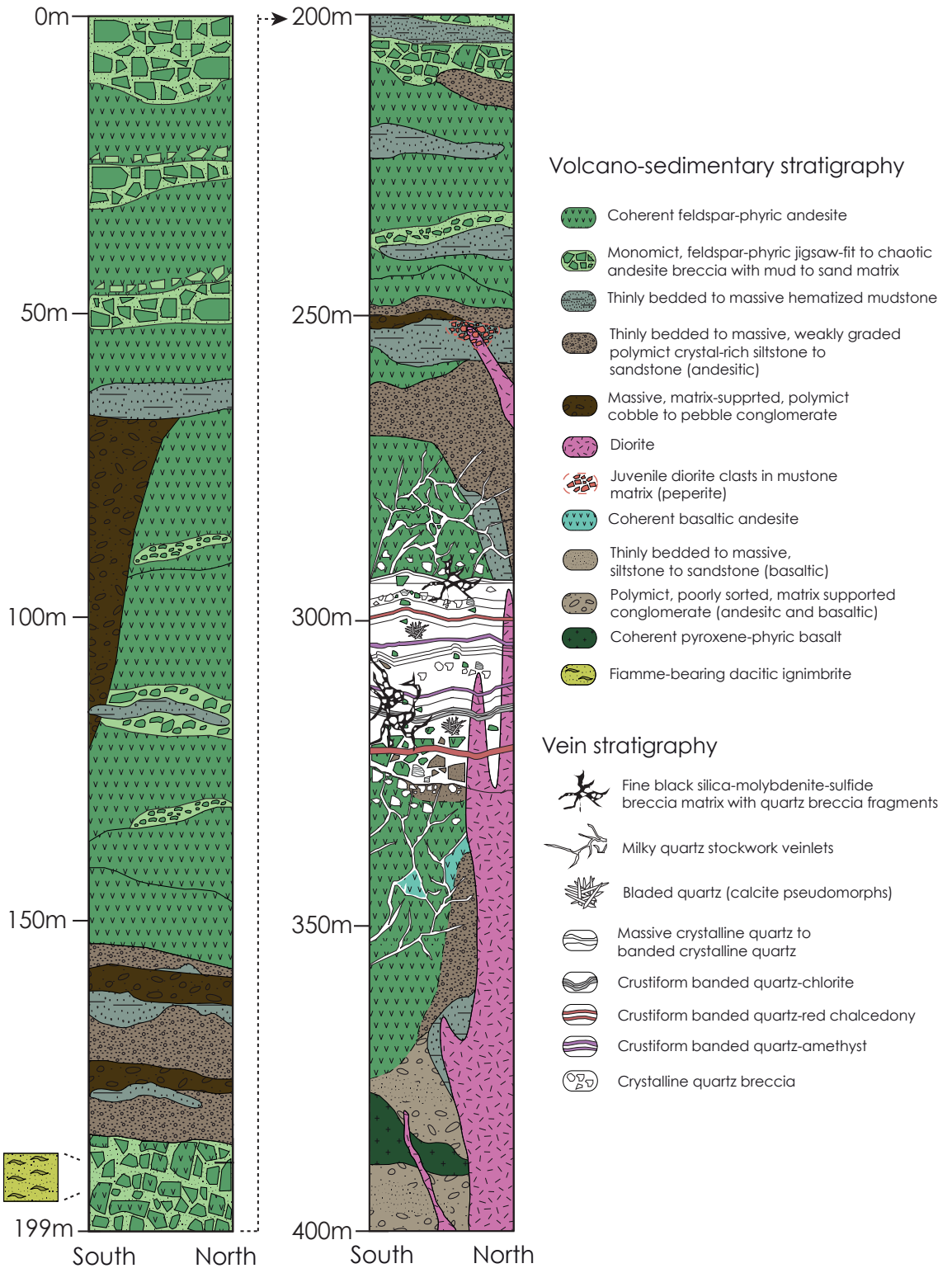

Fig. 3.2 Composite graphic log depicting the relationships among the major volcano-sedimentary and intrusive lithofacies hosting the Kencana deposit, and mineralization styles from the K1 vein. Note: Diorite intrusion pre-dates mineralization. Drawn from drill holes DSD047, DSD099, DSD103, DSD105 and DSD288. Depths in metres below current surface. All units upper Miocene to Pliocene. The fiamme-bearing facies was not present in the drillcores selected to create the composite log, however its relative position in the stratigraphy is shown.

facies are displayed in Figs. 3.8 and 3.9. Depositional environments for principal lithofacies at Kencana (and the Gosowong goldfield) are interpreted in Fig. 3.10. A summary of the volcano-sedimentary and intrusive lithofacies hosting the Kencana deposit is given in Table 3.1.

3.3.1 Kencana facies descriptions

Host rocks to the Kencana deposit include several coherent and volcaniclastic facies (Fig. 3.1) that define a moderately east-dipping stratigraphy with westward-rotated units offset by post-mineralization faulting (Figs. 3.3-3.7). The NW-trending structure dipping 46°E provides a host for epithermal mineralization, focused along lithological boundaries where rheologic differences are encountered (Figs. 3.3-3.7). Five principal lithofacies have been identified in the Kencana deposit: 1) Plagioclase-phyric coherent and clastic andesite facies; 2) Plagioclase-phyric coherent basalt facies; 3) Sedimentary facies; 4) Intrusive facies and 5) Fiamme-bearing facies. The facies descriptions, associations and distributions are described subsequently.

1) Plagioclase-phyric coherent and clastic andesite facies

This facies consists of the coherent andesite facies and the plagioclase-phyric monomict andesite breccia.

Coherent andesite facies

The coherent andesite facies is commonly plagioclase-phyric, though rare aphanitic units occur below the K1 orebody, interpreted as possible dykes. Phenocryst abundances range from 5 to 60 percent and are predominantly plagioclase with lesser amphibole, biotite and magnetite. Plagioclase phenocrysts are medium-grained (<5 mm) and display subhedral tabular habits (Fig. 3.8 A, B and F). Some flow alignment of feldspars is observed in the least altered flows toward the top of the stratigraphy. The coherent andesite facies is variably altered throughout the deposit to chlorite, epidote, silica, calcite and pyrite. Feldspar

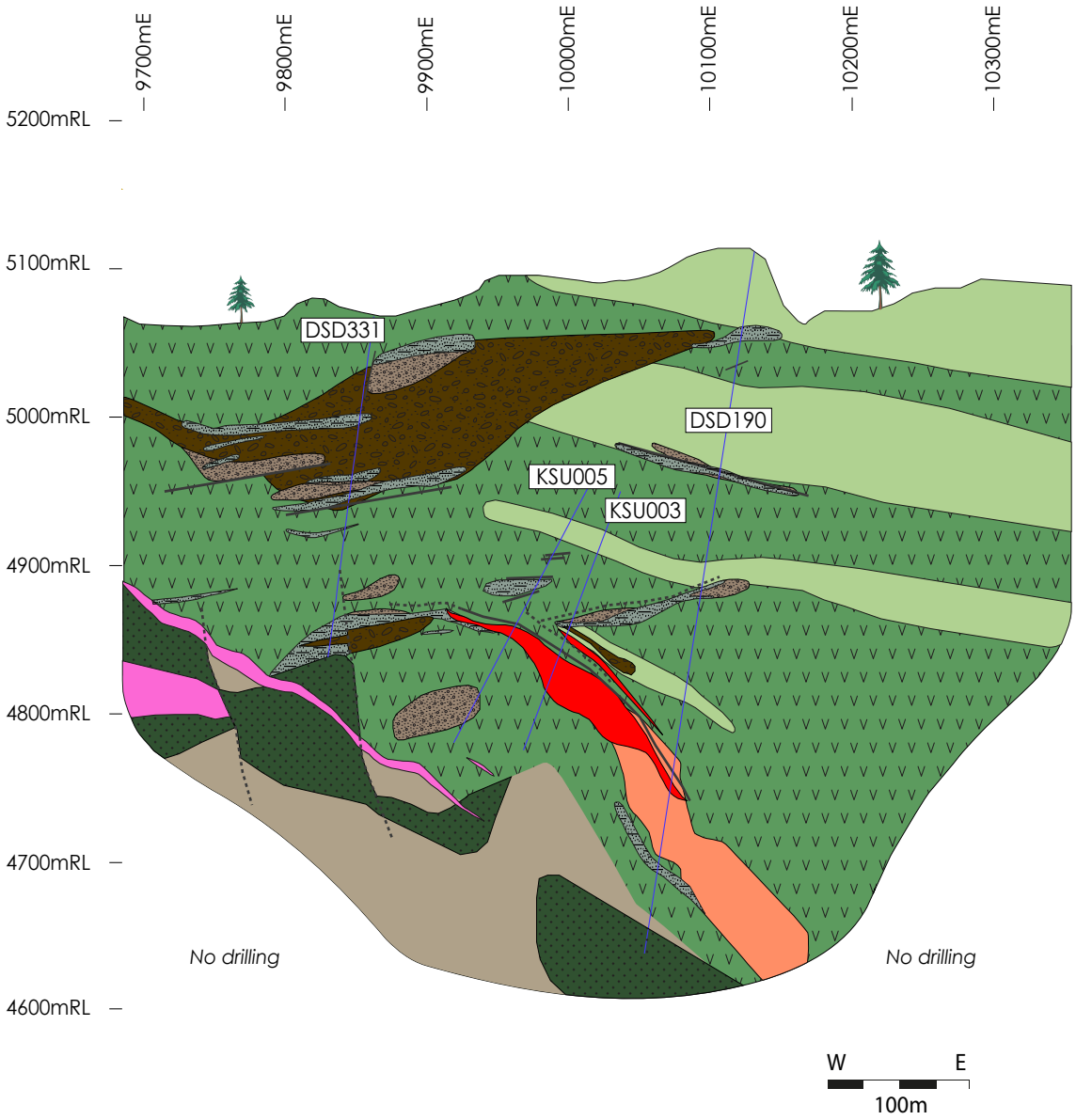

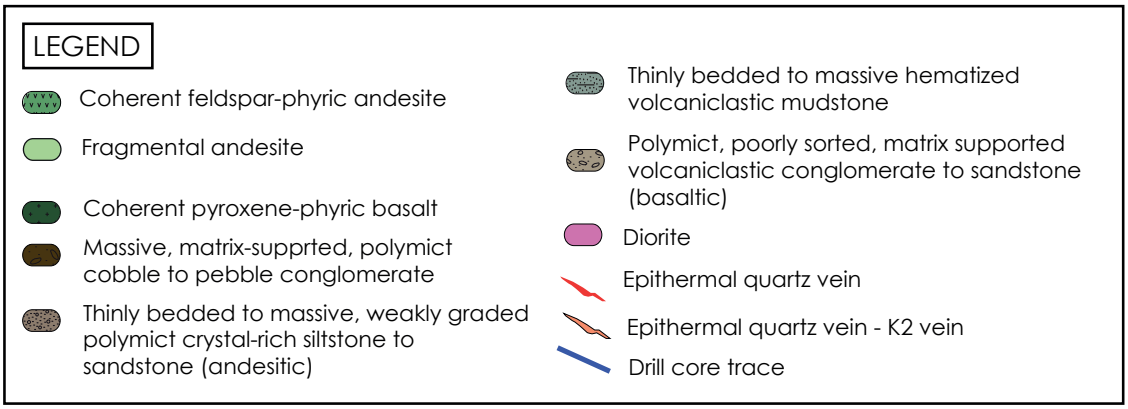

Fig. 3.3 Kencana section 19600mN geology showing the principal lithofacies and their associations. K2 ore-body is shown projected behind the K1 vein.

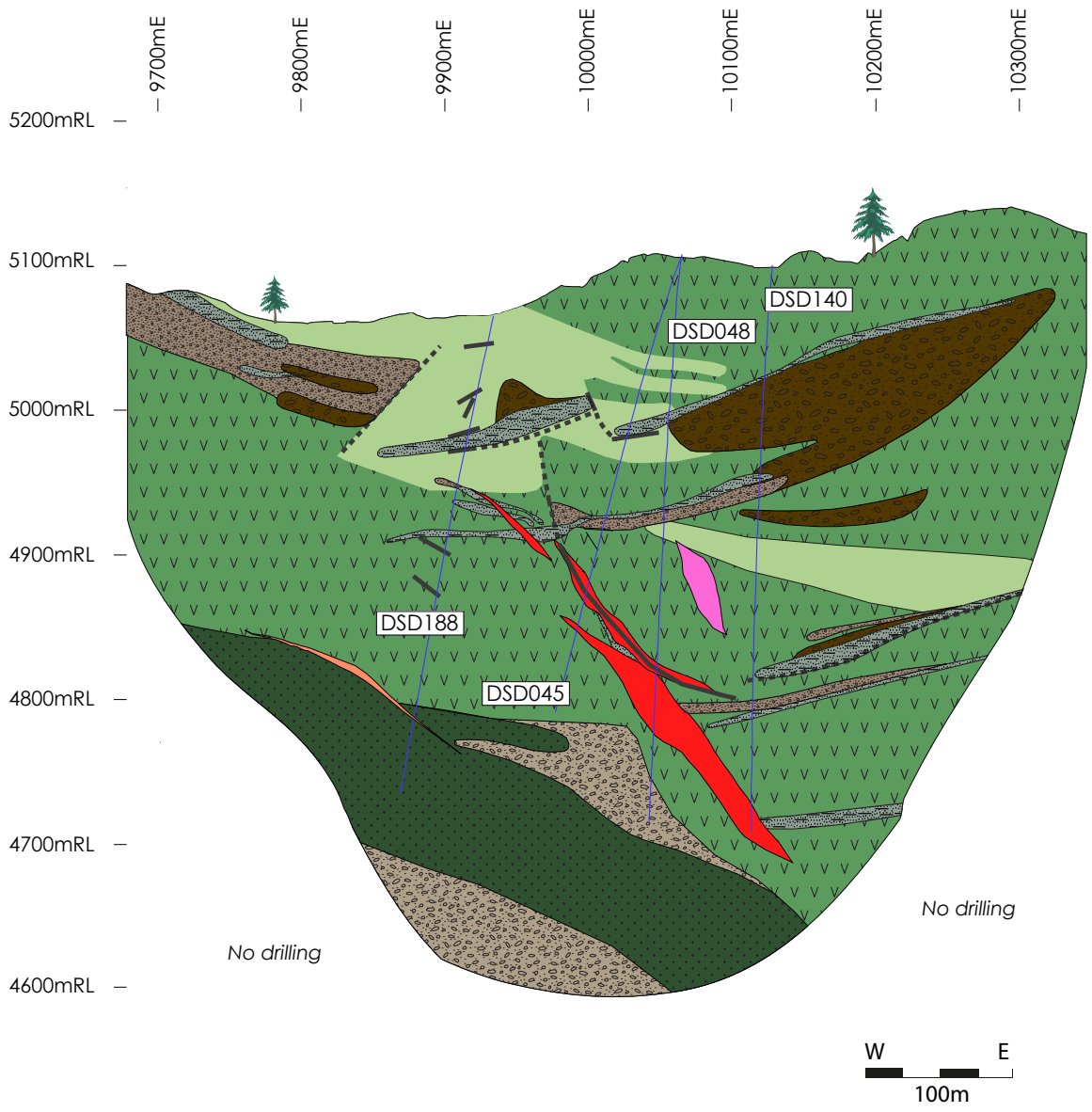

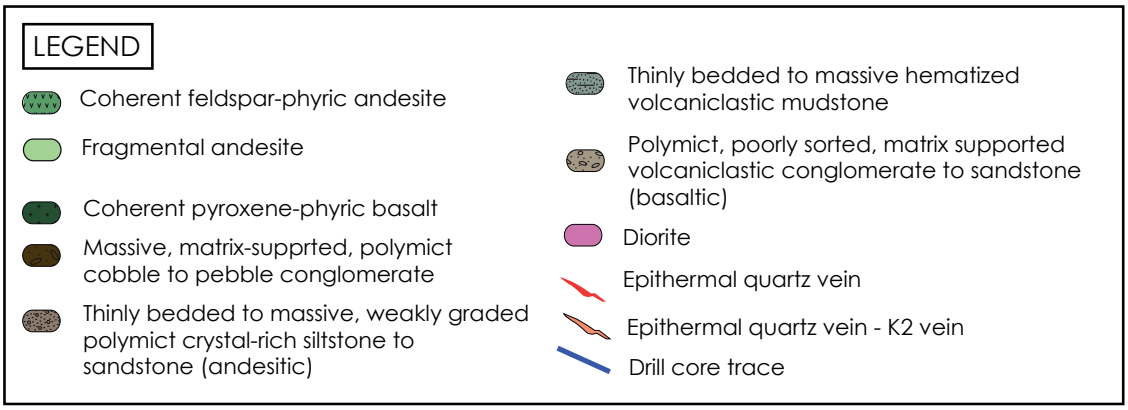

Fig. 3.4 Kencana section 19700mN geology showing the principal lithofacies and their associations.

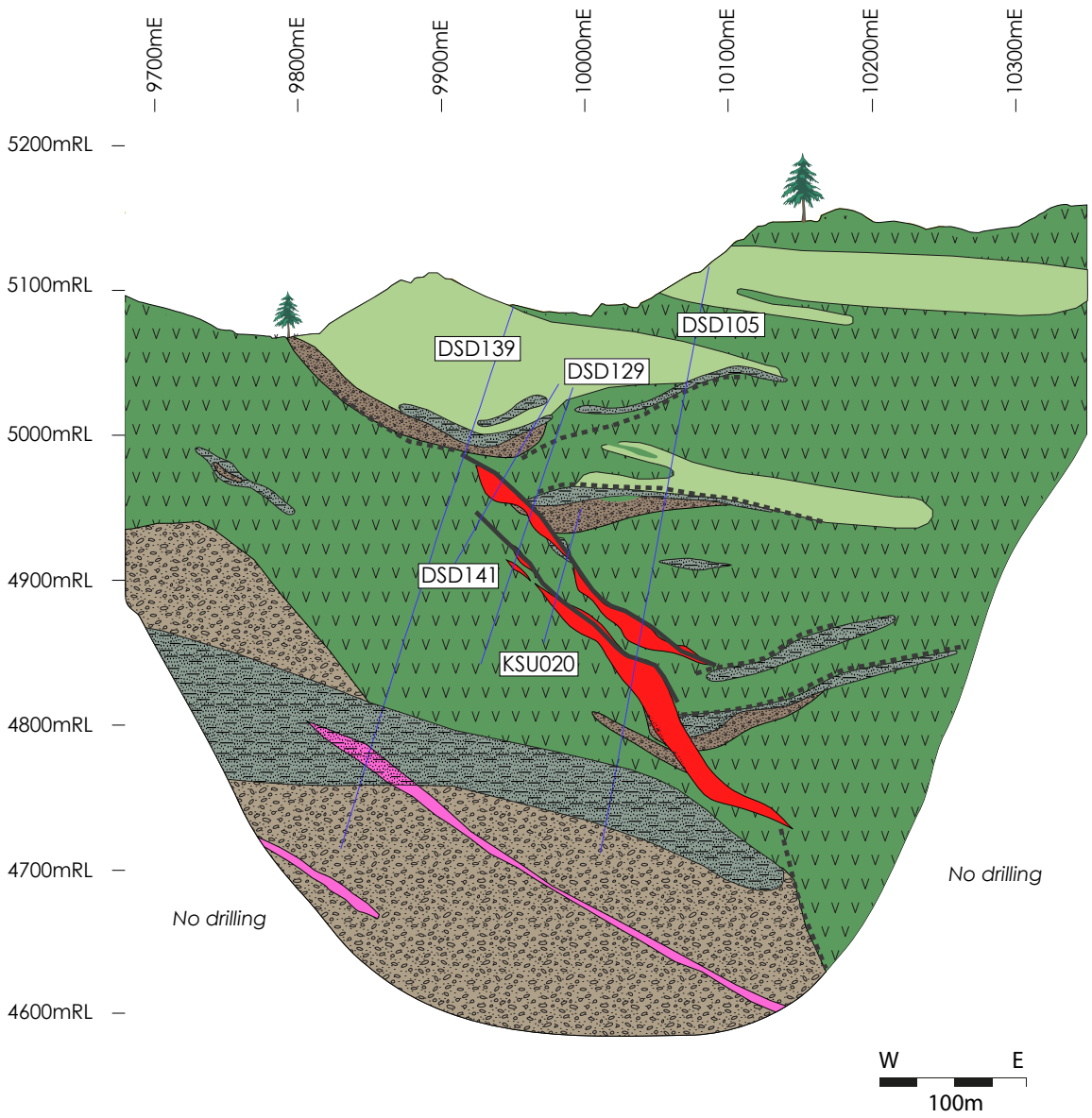

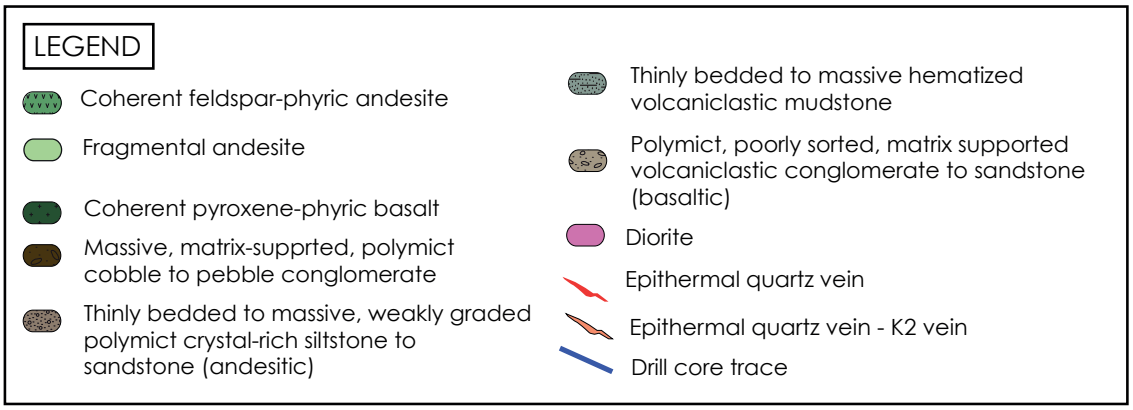

Fig. 3.5 Kencana section 19800mN geology showing the principal lithofacies and their associations.

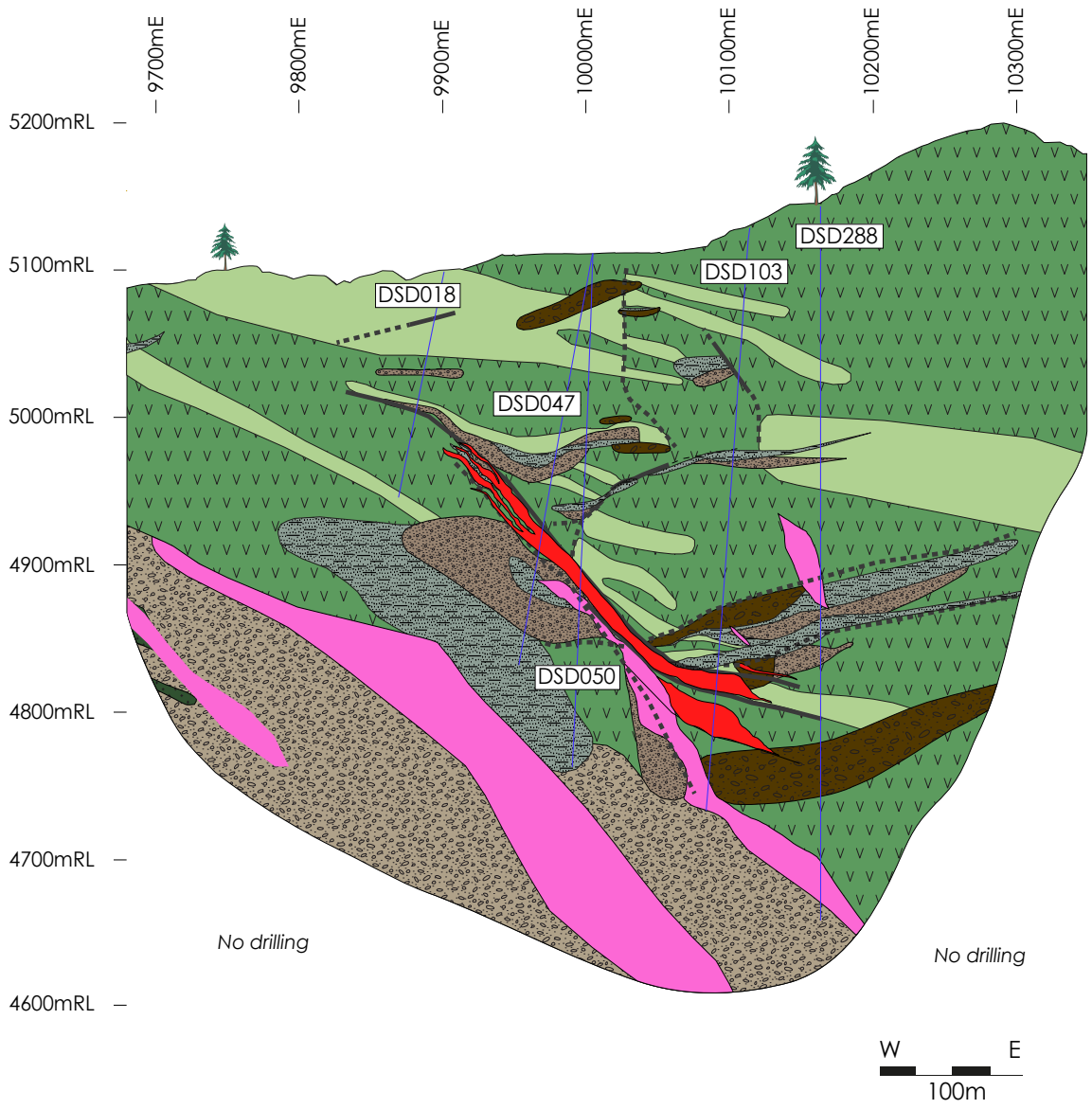

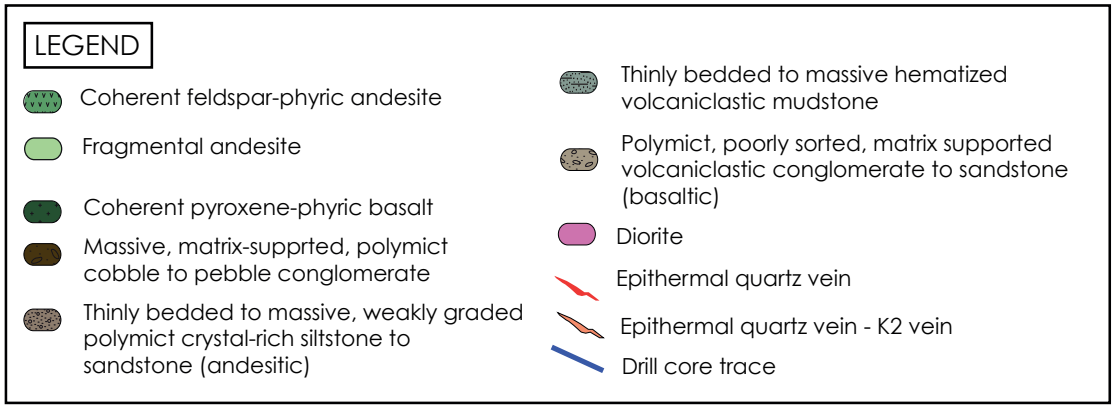

Fig. 3.6 Kencana section 19900mN geology showing the principal lithofacies and their associations.

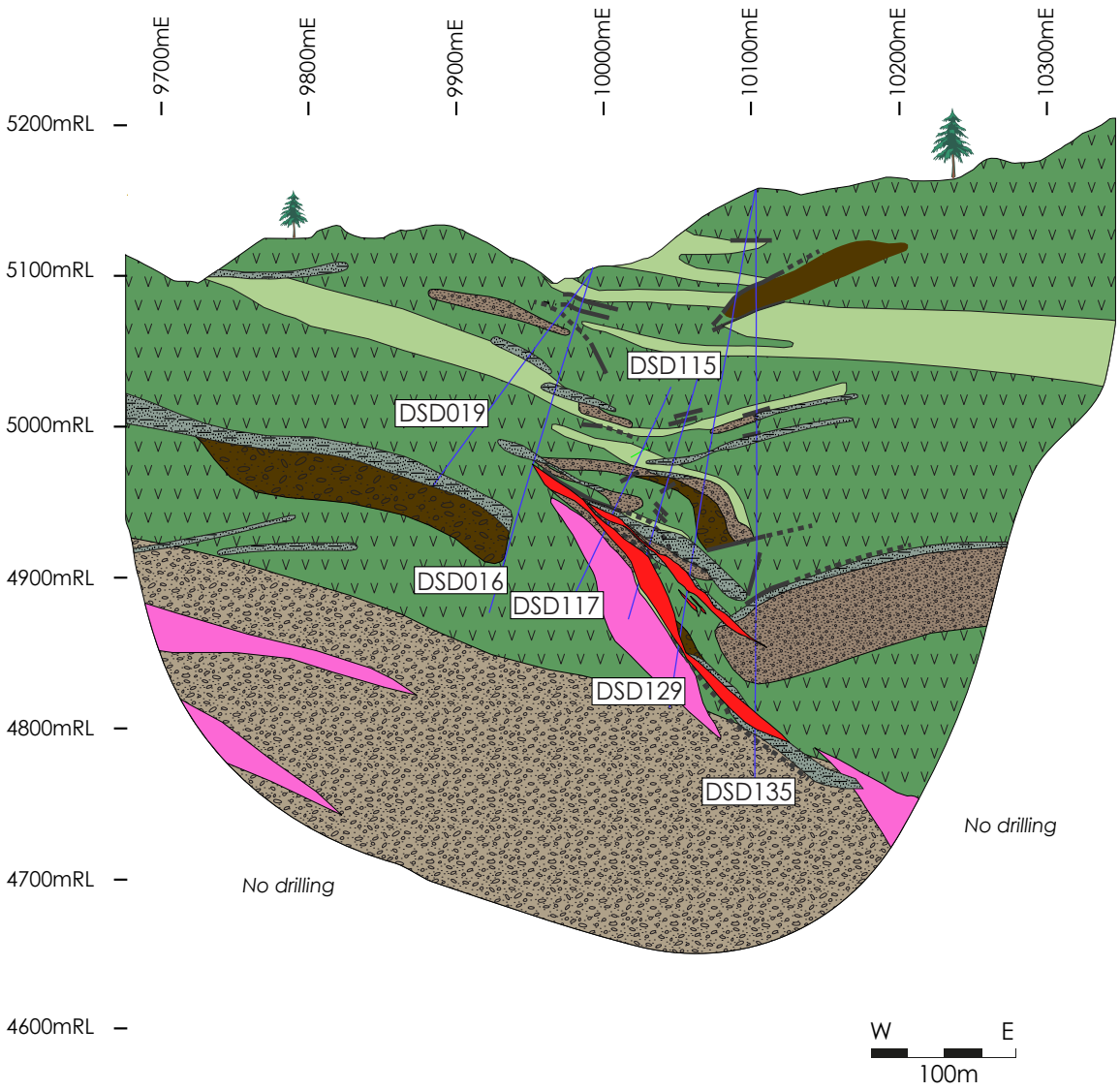

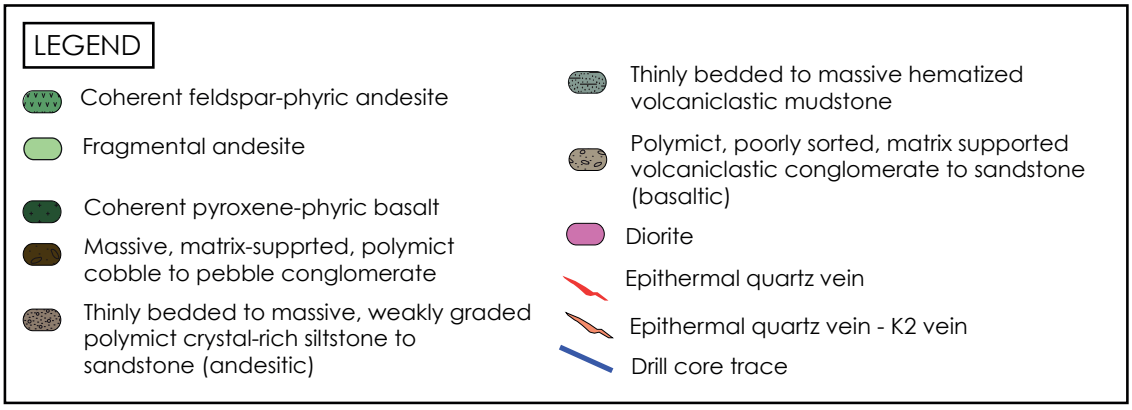

Fig. 3.7 Kencana section 20000mN geology showing the principal lithofacies and their associations.

phenocrysts are variably altered to smectite, illite, adularia or albite. The fine-grained matrix commonly displays a moderate to strong hematitic 'dusting' which is interpreted to be a pre-hydrothermal oxidation formed during lava emplacement.

The coherent andesite facies is observed throughout the Kencana deposit and is the dominant facies in the K1 hangingwall, though below the footwall it occurs predominantly toward the eastern deeps and is less common (Figs. 3.3-3.7). Lithologic contacts between distinct coherent andesitic flows are not always well defined and contacts are often gradational into andesite breccias. Phenocryst abundance is the best discriminator between unit boundaries where contacts cannot be defined. Coherent andesite units occasionally display pseudo-breccia textures where the groundmass has undergone propylitic alteration and hematite dusting. These pseudo-breccias are distinguishable from true andesitic breccias as the "matrix" displays the same abundance of phenocrysts as the "clasts" (Fig. 3.8 C).

Plagioclase-phyric monomict andesite breccia

The tops of plagioclase-phyric coherent andesite pass into zones of jigsaw-fit to chaotic fit clasts of plagioclase-phyric andesite of the same composition in a massive, hematized mud to sand matrix. Clasts are typically 2-30 cm and account for 40-90 percent volume of the rock, with angular to sub-rounded shapes and variable clay-chlorite alteration (Fig. 3.8 D, E and G). Units are laterally continuous and have a thickness 2-30 m. The breccia is matrix supported and is occasionally gradational into hematitic mudstone units (Fig. 3.5, 9900mE/ 5000mRL).

Fragmental andesite is predominant in the upper 200 m of stratigraphy at Kencana (above 4950mRL, Fig. 3.2), with minor discontinuous units around the vein structure (Figs. 3.3 and 3.6), and absent in the K1 footwall. Shear zones are often localized around the boundaries of the plagioclase-phyric monomict andesite breccia and hematitic mudstone units. The plagioclase-phyric monomict andesite breccia is interpreted as an autoclastic facies associated with a plagioclase-phyric lava, with mudstone sedimentation on top of irregular lava flows.

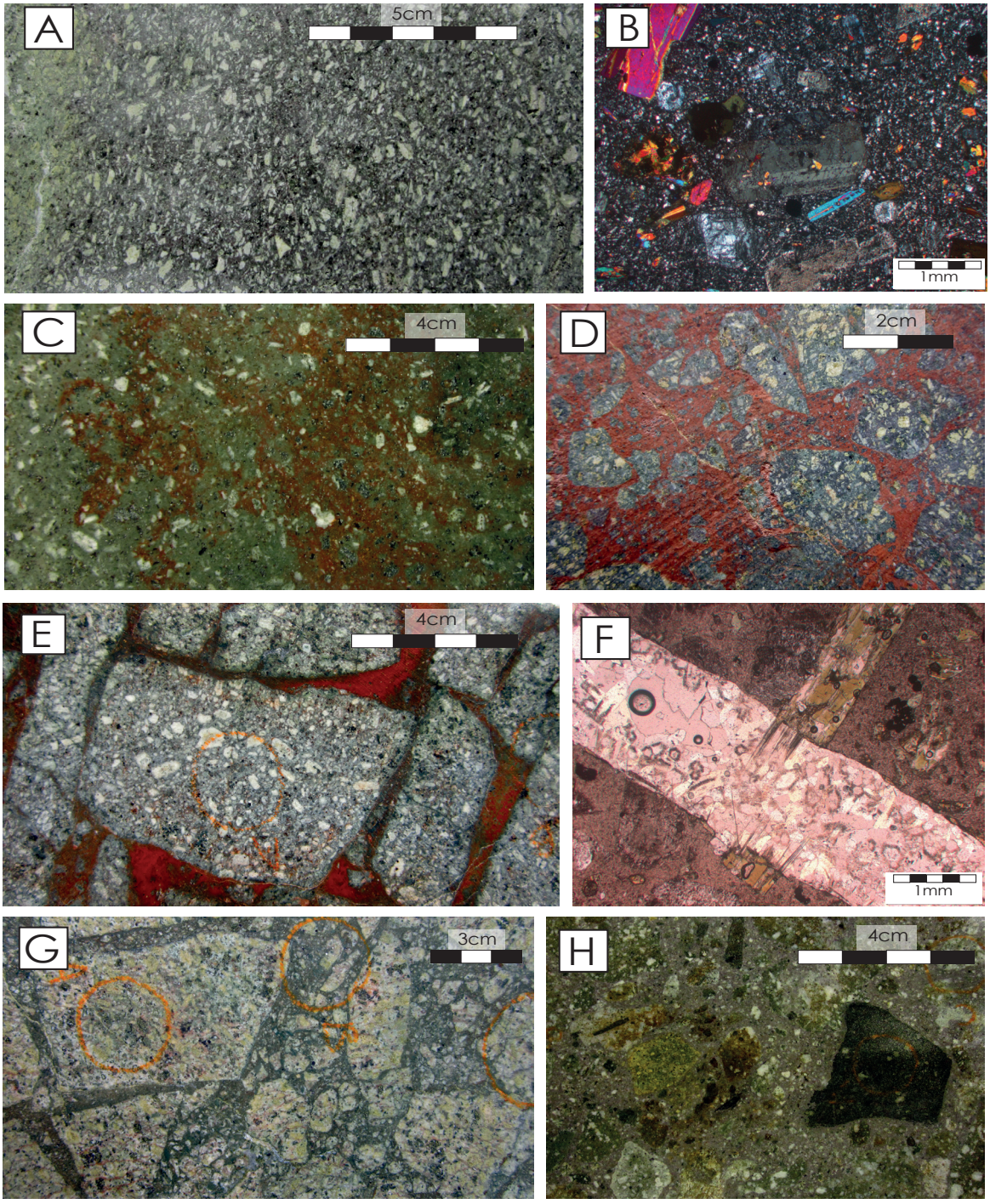

Fig. 3.8 Kencana lithofacies

A) Plagioclase-phyric coherent andesite from DSD099_159.0m; **B)** Plagioclase and amphibole phenocrysts in a fine-grianed plagioclase-rich matrix from plagioclase-phyric coherent andesite. Opaques are pyrite (cross polars) from DSD099_159.0m; **C)** Andesitic pseudo-breccia texture resulting from variable hematitic and proplylitic alteration (DSD099_91.5m); **D)** Rotated to chaotic fit plagioclase-phyric andesite breccia clasts in a hematitic mudstone matrix (DSD105_30m); **E)** Jigsaw-fit plagioclase-phyric andesite breccia clasts in a hematitic mudstone matrix (DSD105_157.5m); **F)** Elongate tabular amphibole phenocryst in diorite cross-cut by hydrothermal quartz vein (DSD117_270m); **G)** Amphibole-phyric andesite jigsaw fit to clast-rotated breccia with a sand matrix (chlorite altered) from DSD140_201.4m; **H)** Polymict, matrix-supported conglomerate with relict plagioclase phenocrysts in a sand matrix (DSD050_117.3m)

2) Plagioclase-phyric coherent basalt facies

Plagioclase-phyric coherent basalt

The plagioclase-phyric coherent basalt is a minor lithofacies in the Kencana deposit and is rarely encountered in drillcore. Laterally continuous units (offset by normal faults) 2-30 m thick occur below 4850mRL and are mainly observed south of 19700mN (Figs. 3.3 and 3.4) with very thin, discontinuous units around 9700mE/ 4850mRL on cross section 19900mN. The plagioclase-phyric basalt is characterised by euhedral plagioclase phenocrysts <3 mm and a groundmass of plagioclase, biotite, amphibole, and clinopyroxene. The units are intercalated with the polymict, basaltic matrix-supported conglomerate, in which it is the dominant clast component. The lithofacies is interpreted as the coherent component of basaltic lava flows, forming the lower section of the stratigraphy at the Kencana deposit.

3) Sedimentary facies

This facies association consists of hematitic mudstone; polymict, matrix-supported conglomerate; thinly bedded to massive sandstone; and polymict, basaltic matrix-supported conglomerate. The diffuse bedding and massive to weakly normally graded units are interpreted to reflect mass-flow transportation and deposition of volcanic-derived material within a decreasingly energetic sub-aerial to sub-lacustrine environment as reflected by grain size. This lithofacies occurs as discontinuous beds within the plagioclase-phyric coherent and clastic andesite facies.

Hematitic mudstone

The hematitic mudstone unit is characterized by dark-red to brown, friable to indurated variably feldspar crystal-rich mudstone, with a massive to thinly-bedded nature (Fig. 3.9 A). The unit is composed of euhedral to subhedral and fragmented euhedral phenocrysts of plagioclase <1 mm and magnetite.

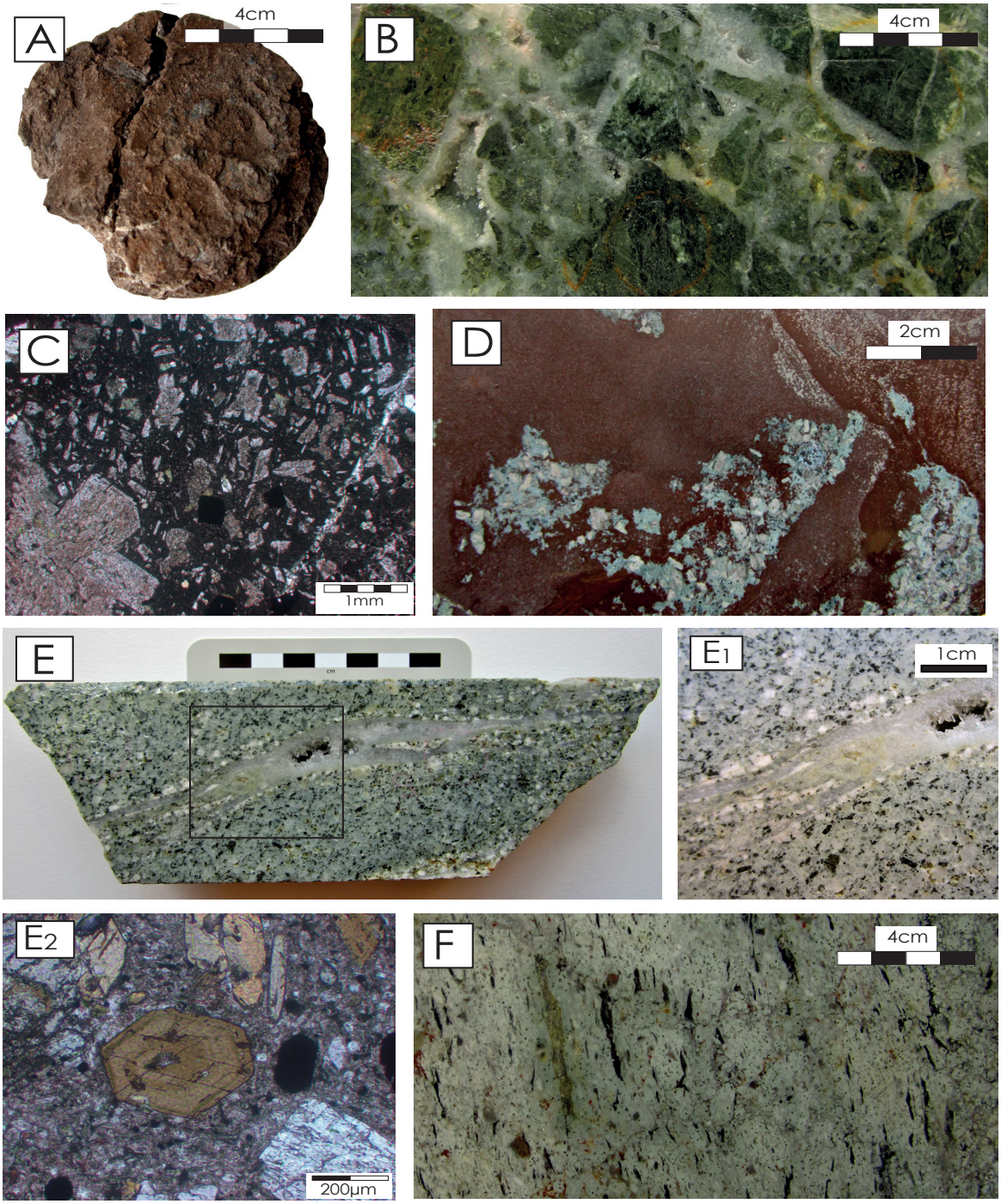

Fig. 3.9 Kencana lithofacies 2

A) Hematitic mudstone from DSD105_105.7m; **B)** Volcaniclastic sandstone breccia clasts (propylitic altered) cemented by hydrothermal quartz (DSD105_364.9m); **C)** Plagioclase-rich basalt in clasts of polymict, basaltic matrix-supported conglomerate (DSD103_377.7m) (plain polars); **D)** Peperitic texture (juvenile diorite fragments in hornfelsed hematitic mudstone) from DSD103_280.6m; **E)** and **E1)** Diorite (clay altered) with quartz veinlet from DSD115_285.4; (location of E1 represented by black box outline on E) **E2)** Sub-hexagonal biotite with amphibole and plagioclase in diorite. Opaques are pyrite and chalcopyrite (plain polars); **F)** Ignimbrite (argillic altered) with black fiamme, lithic fragments and glassy matrix with plagioclase phenocrysts (DSD099_183m). Far right of the sample shows autoclastic texture, indicating a transition from ductile to brittle deformation within the ignimbrite during deposition,

Mudstone units are common in the upper part of the stratigraphy (5100mRL-4800mRL) and are often gradational into thinly bedded to massive sandstone. Mudstone is commonly seen forming the matrix to the plagioclase-phyric monomict andesite breccia, which is often gradational into massive mudstone. Low-angle shears in the K1 footwall appear to localise along the mudstone contacts where there are rheologic differences. The mudstone is significant in controlling dilation of the host structure and thus gold grade at Kencana (see section 3.4).

The hematitic mudstone was interpreted by Coote (1996) as a mafic-rich airfall unit that has settled through a column of water, forming discontinuous sub-aqueous ash rich layers. Petrographic analysis indicates that the euhedral, fragmented crystals and dominantly ash-sized particles are of volcaniclastic rather than volcanogenic origin (Olberg, 2001). The ash source is thought to be fairly proximal, possibly from multiple phreatomagmatic eruptions, or from a nearby stratovolcano. The strong, pre-hydrothermal hematite alteration is most likely due to a thermal oxidation of the mafic ash on introduction to an oxidised environment.

Polymict, matrix-supported conglomerate

The conglomerate is composed of sub-rounded clasts of plagioclase-phyric andesite, hematitic mudstone and sandstone (30-70%) in a matrix of sand to mud sized particles, including local relict feldspar and amphibole phenocrysts (70-30%) (Fig. 3.8 H). The conglomerate units display massive bedding and moderate sorting, with local grading to sandstone. The polymict, matrix-supported conglomerate is interpreted as a debris-flow deposit forming channels in a sub-aerial to sub-lacustrine environment (Fig. 3.10).

This lithofacies typically occurs above 4950mRL and locally down to 4800mRL (in the K1 footwall, Fig. 3.6). The facies is most predominant toward the south of the deposit, where geological sections show a deepening channel structure, which cross cuts the plagioclase-phyric andesite facies, filled with the conglomerate which is gradational to sandstone within the channel structure, and interbedded with thin, discontinuous mudstone units (Figs.

Fig. 3.10 Summary of depositional environments interpreted for the Kencana deposit and Gosowong goldfield, showing the relationships and timing of extrusion and re-working of lavas, intrusion and pyroclastic activity from early to late stages (1-4)

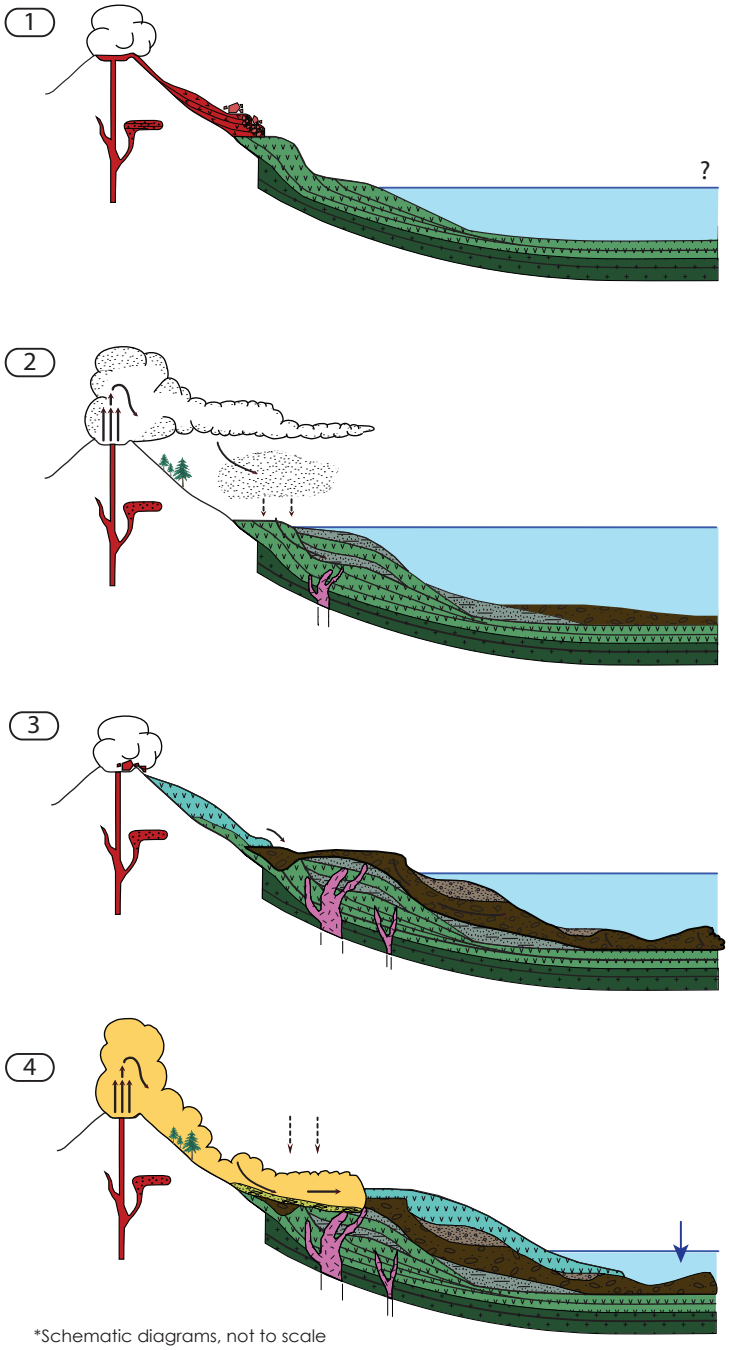

1) Basalt/ basaltic andesitic flows forming the lower section of the Gosowong Fm, reworked to form basaltic volcaniclastic conglomerates. Package overlain by andesitic flows, representing an evolving magma composition. Flow fronts are commonly autobrecciated. Minor intrusive intermediate aphanitic volcanics.

2) Ash from a proximal stratovolcano (or phreatomagmatic activitiy) is reworked to form hematized mudstone packages, settled through a column of water. Ash-sized particles forming the mudstone are of volcaniclastic, not volcanogenic origin. Pre-hydrothermal alteration of the mafic ash is a result of syn-eruptive thermal oxidation. Andesitic flows are reworked and deposited as breccias with a mudstone matrix; as well as deposition of mudstone on irregular flow tops. Diorite intrusion into the Gosowong Fm commences. Sub-aerial to lacustrine depositional environment.

3) Volcaniclastic conglomerates and sandstones form after erosion and transport of andesitic lavas, with some graded bedding evident. Conglomerates form channel structures with volcaniclastic material derived from the north. Dioritic intrusions continue and minor peperites are formed on contact with mudstones. Andesitic to dacitic lavas are extruded. Sub-aerial to regressive lacustrine depositional environment.

4) Continued extrusion of andesite-dacite lavas and fragmental lavas (Ridge Volcanics) over volcaniclastic and andesitic lava packages. Pyroclastic flow and fall deposits (welded and unwelded ignimbrites with charcoal fragments, such as the fiamme-bearing facies) with erosional bases overlie the sequence. Sub-aerial depositional environment.

3.3 and 3.4).

Thinly bedded to massive sandstone

This lithofacies is commonly associated with the polymict, matrix-supported conglomerate and hematitic mudstone facies with which the beds commonly show gradational contacts. Laterally discontinuous beds are common between 5050mRL and 4800mRl (Figs. 3.3-3.7) and the facies is significant in hosting epithermal mineralization along cross section 19900mN (Fig. 3.6). The facies is composed of relict plagioclase and amphibole phenocrysts with sand sized andesite-derived material. Beds are massive to thinly-bedded and have maximum apparent thicknesses of ~20 m, with local normal grading. The thinly-bedded to massive sandstone facies is interpreted to form as the distal parts of mass flow deposits and deposition of re-worked andesitic material in a medium-energy sub-aerial to sub-lacustrine environment (Fig. 3.10).

Polymict, basaltic matrix-supported conglomerate

The polymict, basaltic matrix supported conglomerate is the dominant facies in the lower part of the Kencana stratigraphy, occurring below 4925mRL in the west across the deposit region, and dipping and deepening to the east (Figs. 3.3-3.7). The facies has an irregular, unconformable relationship with the overlying plagioclase-phyric coherent andesite, although this contact is rarely seen due to high levels of quartz and chalcedony mineralization and alteration and hydrothermal brecciation within the lower section of the stratigraphy.

The facies is composed of sub-rounded to sub-angular clasts (50-70%) from gravel to pebble size, with moderate to poor sorting and chaotic to rotated clast organisation. Clasts are composed of plagioclase-phyric basalt (50%) (Fig. 3.9 C) and relict phenocrysts of plagioclase, amphibole and biotite in a matrix of relict fine grained phenocrysts and mud to sand sized particles. Pervasive propylitic alteration is common and many clasts display reaction rims.

The units are massive to diffusely bedded and intercalated with plagioclase-phyric coherent basalt flows. The diorite facies is known to crosscut the polymict, basaltic matrix supported conglomerate, though the contacts were not seen in this study. The facies is interpreted to represent mass flow deposition of material derived from basaltic flows.

4) Intrusive facies

Diorite

The feldspar-phyric intrusive body that underlies the central part of Kencana has an irregular distribution, suggesting it is either a sill or a slice within shallow east-dipping shears (Figs. 3.3-3.7; Morrison, 2007). This feldspar-phyric intrusive has been interpreted as diorite, characterized by abundant plagioclase phenocrysts (50%) up to 6 mm with a euhedral to subhedral tabular habit; subhedral to euhedral acicular amphibole (<30%) up to 3 mm, sub-hexagonal to tabular biotite (20%), and minor pyroxene and magnetite (Figs. 3.9 E, E1 and E2).

The distribution shown on the cross sections is not convincing for the diorite as a major intrusive body and the contacts, where seen, appear gradational between the crowded feldspar porphyry and apparently fine-grained dark-coloured volcanic rocks. The dark-coloured volcanic rocks are common near K1 and above the diorite. These have been interpreted as hornfelsed volcanic rocks in the aureole of the feldspar-phyric body (Morrison, 2007). Hornfelsed volcanics in the Kencana deposit are dark, fine-grained rocks with partial argillic bleaching (sericitization of biotite) causing brown patches. It has previously been interpreted that these hornfelsed volcanics may act as a hard part of the host sequence around which the ore-controlling structure may have been refracted (Morrison, 2007).

Fluidal juvenile feldspar-phyric clasts in hornfelsed hematitic mudstone are observed in drillhole DSD288 and DSD105 (in proximity with both coherent feldspar-phyric intrusives and hematitic mudstone), and these are interpreted as peperitic contact zones, where peperite is defined as forming where magma encounters unconsolidated, typically wet, sediments, in this case mudstone (Fig. 3.9 D). Magma includes any molten material, whether

Table 3.1 Summary of volcano-sedimentary stratigraphy

Lithofacies	Description	Distribution	Associated lithofacies	Interpretation
PLAGIOCLASE-PHYRIC ANDESITE				
Plagioclase-phyric coherent andesite	- plagioclase phenocrysts, up to 5mm (<60%) - euhedral to subhedral, tabular habit - minor amphibole (<10%), magnetite and pyroxene Fine grained to aphanitic groundmass, variably hematite altered (pre-hydrothermal stage) - variably altered - sharp contacts to gradational contacts with monomict andesite breccia	Dominant lithofacies at Kencana - laterally continuous to 4800mRL, deeper towards the east - significant in hosting epithermal vein structure along 19600mN, 19700mN, and19800mN - several units 10-100m thick (apparent thickness)	Plagioclase-phyric monomict andesite breccia	**VOLCANIC**: lava and shallow intrusion
Plagioclase-phyric monomict andesite breccia	*Clasts:* (40-90%) 2-30cm (but occasionally >50cm) Angular to sub-rounded - plagioclase phenocrysts, up to 5mm (<60%) - euhedral to subhedral, tabular habit - minor amphibole (<10%), magnetite and pyroxene - chlorite-clay altered *Matrix:* (10-60%) Mud to sand sized, hematite altered, massive - jigsaw fit to chaotic organisation, matrix supported, typically moderately sorted - gradational contacts with plagioclase-phyric coherent andesite and hematitic mudstone	- laterally continuous to 5000mRL, isolated zones around mudstone packages to 4900mRL - absent in K1 footwall - several units 2-30m thick (apparent thickness)	Plagioclase-phyric coherent andesite form the clasts of this breccia; gradational to hematitic mudstone (± incorporated andesite clasts) and polymict, matrix-supported conglomerate	**VOLCANIC**: Autoclastic facies
PLAGIOCLASE-PHYRIC BASALT				
Plagioclase-phyric coherent basalt	- plagioclase phenocrysts, up to 3mm (<50%) - euhedral to subhedral, tabular habit - biotite and amphibole (<30%), magnetite and pyroxene Fine grained to aphanitic groundmass	Rare lithofacies at Kencana (lack of exposure in drillcore) - laterallycontinuous (faulted) below 4850mRL in the south of the district (south of 19700mN); discontinous along 19900mN. - one to two units 3-20m thick (apparent thickness)	Intercalated with polymict, basaltic matrix-supported conglomerate	**VOLCANIC**: lava
SEDIMENTARY FACIES				
Thinly bedded to massive sandstone	- relict feldspar and lesser amphibole phenocrysts, sand sized particles. Andesite derived material. - massive to weakly bedded, locally normally graded - gradational contacts with polymict matrix supported conglomerate and hematitic mudstone facies	- laterally discontinuous beds <20m thick (apparent thickness) - Predominantly occur between 5050mRL and 4800mRL - significant in hosting epithermal vein structure along 19900mN.	Gradational contacts with polymict matrix supported conglomerate and hematitic mudstone facies	**VOLCANICLASTIC**: Sedimentary facies

Table 3.1 (cont.)

Lithofacies	Description	Distribution	Associated lithofacies	Interpretation
SEDIMENTARY FACIES cont.				
Hematitic mudstone	- relict plagioclase phenocrysts, mud sized particles. Andesite derived material. Occasional sub-rounded andesite fragments. - massive to weakly & thinly bedded - gradational contacts with polymict matrix supported conglomerate; massive to thinly bedded sandstone facies and plagioclase-phyric monomict andesite breccia - strongly hematite altered (pre-hydrothermal thermal oxidation)	- laterally discontinous though beds extended by shear deformation - significant in controlling dilation within the host structure - low-angle post-mineralization shears localized along mudstone contacts	Occurs as the matrix to the plagioclase-phyric monomict andesite breccia; polymict matrix supported conglomerate; massive to thinly bedded sandstone facies	**VOLCANICLASTIC**: Sedimentary facies/ reworked pyroclastic fall depsoit
Polymict, matrix-supported conglomerate	*Clasts:* (30-70%) Sub-rounded to sub-angular (gravel to cobble size) - Polymict (plagioclase-phyric andesite, hematitic mudstone and sandstone clasts) *Matrix:* (30-70%) - fine sand sized particles, relict feldspar and amphibole phenocrysts - moderately sorted - massive bedding to channel structures with weak grading	- laterally discontinuous beds <10m thick (apparent thickness) - fills one main channel structure towards the south (19600mN and 19700mN) <70m thick (apparent thickness) - Generally above 4950mRL, locally down to 4800mRL (19900mN) within shear zones	Thinly bedded to massive sandstone; hematitic mudstone facies; gradational to plagioclase-phyric monomict andesite breccia	**VOLCANICLASTIC**: Sedimentary facies/ debris flow deposit
Polymict, basaltic matrix-supported conglomerate	*Clasts:* (50-70%) Sub-rounded to sub-angular (gravel to pebble size) - polymict (plagioclase-phyric basalt, basaltic volcaniclastic sandstone) - relict crystals (plagioclase, amphibole, biotite) *Matrix:* (30-50%) - fine mud to sand sized particles, relict feldspar, biotite amphibole phenocrysts - poor to moderately sorted - massive to diffuse bedding	- laterally continuous beds of unknown thickness (no drillcore constraints) - occurs in the K1 footwall from 4925mRL in the west, dipping and deepening toward the east - intercalated coherent basalt units	Cross cut by diorite; intercalated with plagioclase-phyric coherent basalt.	**VOLCANICLASTIC**: Sedimentary facies/ debris flow deposit

Table 3.1 (cont.)

Lithofacies	Description	Distribution	Associated lithofacies	Interpretation
INTRUSIVE FACIES				
Diorite	- Plagioclase-phyric intrusive - porphyritic (<6mm) to equigranular - feldspar (50%) subhedral, <6mm - amphibole (~30%), acicular, subhedral to euhedral laths - biotite (20%), tabular to sub-hexagonal - minor magnetite, and pyroxene - variably altered to calcite, albite, illite and chlorite - contacts (where seen) gradational with fine grained dark volcanics (hornfelsed) to sharp and chilled with plagioclase-phyric coherent andesite; peperitic with hornfelsed hematitic mudstone.	- irregular distribution in the footwall of the K1 vein (except DSD288 ~280m) - series of sills or a slice within east-dipping shears - significant in hosting epithermal vein structure (footwall) along 19900mN and 20000mN	Hematitic mudstone; sharp, irregular and chilled (fine grained to aphanitic)contacts with plagioclase-phyric coherent andesite	**INTRUSIVE**: Minor sill complex
PYROCLASTIC FACIES				
Fiamme-bearing facies	- dark, plagioclase-bearing fiamme (5-30 mm; 15-20 percent volume) - eutaxitic texture in a matrix of flattened glass shards (<0.5 mm, partly devitrified, in places wrapping around the fiamme) and fine grained plagioclase (<2 mm). - Sub-angular lithic fragments (2-10 mm; <5 percent volume) - matrix is variably clay-silica-pyrite-chlorite altered	- irregular distribution in the hangingwall, not well constrained - apparent thickness of 2 m - possibly derived from elsewhere in the stratigraphy as part of a fault block	Plagioclase-phyric coherent andesite, plagioclase-phyric monomict andesite breccia	**EXTRUSIVE**: Dacitic ignimbrite

intruded, effused as lava, or fused from pyroclasts. Mingling accompanies fragmentation and occurs as a result of magma movement and/or sediment movement induced primarily by heat transfer (White et al., 2000).

Due to the abundance of plagioclase phenocrysts in the coherent andesite facies and lack of contacts observed between the diorite and country rock, it can be difficult to distinguish between the diorite and feldspar-phyric andesite. Amphibole abundance a distinguishing feature between the two lithologies, however this is only apparent in thin section analysis.

5) Fiamme-bearing facies

The fiamme-bearing facies occurs sporadically throughout the stratigraphy at Kencana but is not traceable between drill cores. The best example of the fiamme-bearing facies is taken from DSD099 along cross section 20500mN, at 183 m downhole (geology section not mapped in this study). The unit is massive with an apparent thickness of 2 m, though the unit is not constrained to the north or west through a lack of drilling.

The facies is composed of dark, plagioclase-bearing fiamme (5-30 mm) displaying eutaxitic texture in a matrix of flattened glass shards and fine grained plagioclase phenocrysts. Sub-angular lithic fragments (2-10 mm) are also present (Fig. 3.9 F). The presence of both fiamme and non-flattened lithic fragments suggest the fiamme were formed by plastic deformation, flattening and welding of hot, glassy pumice clasts, while lithic fragments resisted flattening due to their more competent nature and lack of vesicles (McPhie, pers. comm, 2012). Fiamme account for 15-20 percent volume of the facies, lithic fragments <5 percent and the matrix ~80 percent volume. The matrix is variably clay-silica-pyrite-chlorite altered, though fine plagioclase phenocrysts are identifiable. Glassy shards in the matrix are <0.5 mm, partly devitrified, and in places wrap around the fiamme.

The fiamme-bearing facies is interpreted as a probable ignimbrite of dacitic composition, based on the presence of fiamme and the welded matrix displaying flow alignment around the fiamme. However, the thin nature (2 metres) of the unit in drillcore DSD099 is not likely for an ignimbrite, suggesting that this example may have been derived from elsewhere in the stratigraphy as part of a fault block (e.g from the dacitic pyroclastic unit in the south east of the goldfield). Ignimbrites are typically continuous over distances of 100's to 1000's m with relatively flat topography (McPhie, pers. comm, 2012). Due to the uncertainty in the relative position of this facies in the stratigraphy at Kencana, it has not been included in the composite log (Fig. 3.10).

CHAPTER 3 DEPOSIT GEOLOGY

3.4 Deposit structure

The K1 structure was discovered in January 2003. Current known strike length is approximately 400 m with a vertical extent of 200 m, from 19600mN to 20500mN, although it has been indicated that mineralization continues to the south in an alternative orientation (Fig. 3.11). The structure appears to split towards the NW, although additional mineralized occurrences in this direction have not been discounted. The steeper sections of the K1 fault have a high tensional component and dilate, whilst the flatter segments deform principally by shear and remain tight (Benton, 2004; Morrison, 2007). Greater dilation in the steeper sections has lead to greater degrees of hydrothermal brecciation within the epithermal structure. Tectonic brecciation is apparent along the zones of the K1 hangingwall with a shear component (flatter segments), where foliated cataclasite to fault gouge often marks the structure. Shear zones are predominantly post-mineralization and disrupt rather than control the primary distribution of ore. Gold grade in the cataclasite shears is a result of incorporated mineralized clasts entrained from the main ore zone within the epithermal vein.

The fault structure hosting mineralization is generally continuous regardless of wallrock lithology. In the Gosowong goldfield flexures within the vein structures are generally related to competency contrast in the host rocks. At Kencana, the veins appear best developed along lithological boundaries, particularly where rheological differences exist (e.g. mudstone/ volcanic contact, andesitic volcaniclastic/ basalt contact; Figs. 3.3-3.7). In some instances the incompetent hematitic mudstone appears to have restricted structural dilation, impeding fluid flow and leading to displacement of mineralization and pinching of the structure. The structure is narrowest in the thicker mudstone packages; however, the structure above the mudstones has undergone strong dilation and mineralization, and forms the main part of the high-grade oreshoot. It is interpreted that the mudstone retards the fluid flow through the ‘pinch’ zone, with fluids rapidly depressurizing immediately above. This pressure release may cause gold precipitation and is likely to be the reason for the high grades observed. As there are multiple fluid events, this process appears to be repeated, creating

74

Fig. 3.11 Structural overview of the Kencana deposit in 3 dimensional cross section from LeapFrog models **(A)** looking North and **(B)** plan view showing the K1 (red), K2 (orange) and K-Link (blue) structures.

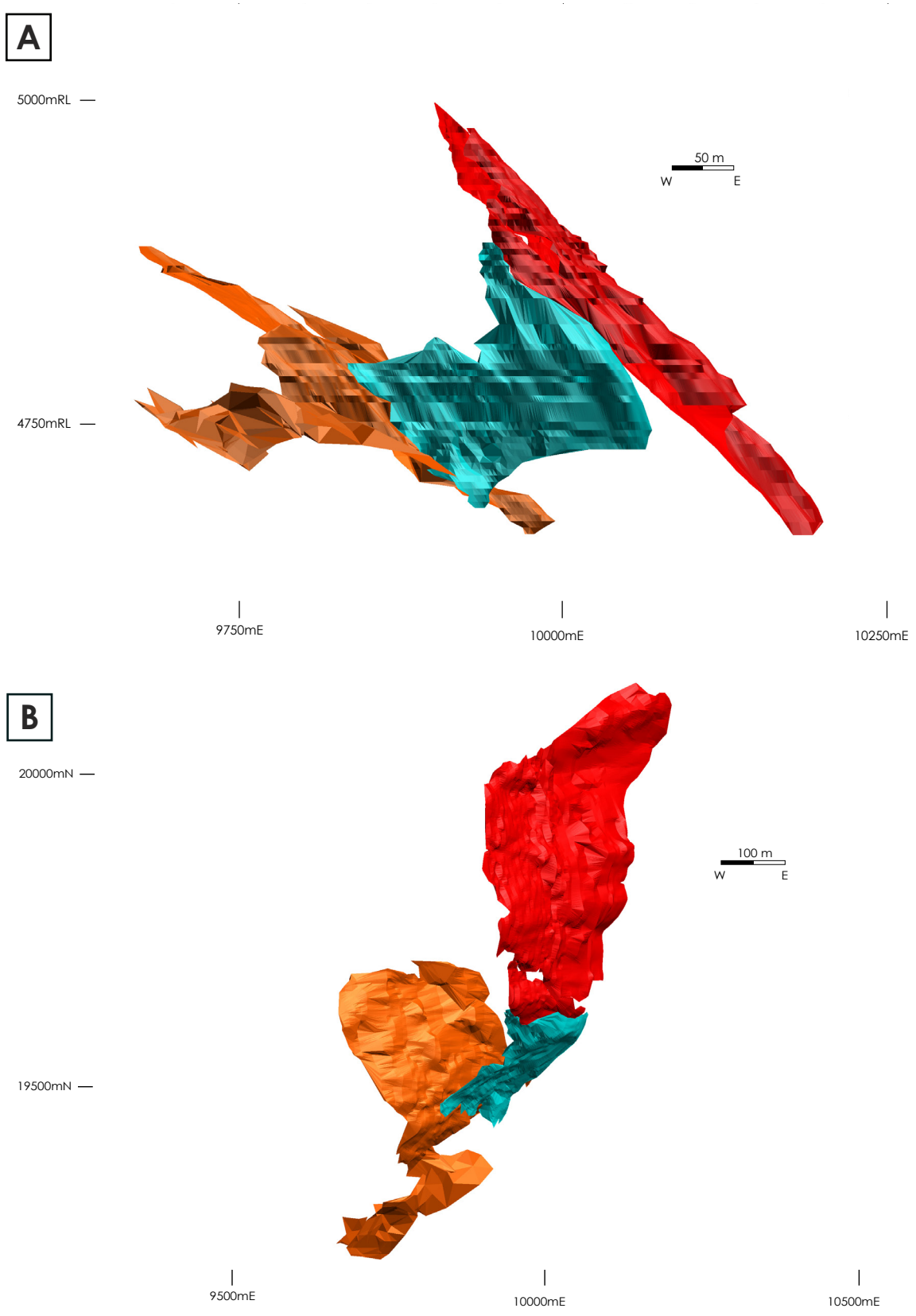

overprinted boiling zones and bonanza Au grades. Beneath the 'pinch' zone several of the intersections have a large component of hematitic material within the veins (see Chapter 4). This may be due to the proximity of the mudstones as well as shearing and fluid flow entraining fragments of wall rock and incorporating them into the lode zones. These mudstones can therefore be considered as significant in controlling the distribution and nature of mineralization. This cryptocrystalline hematitic vein material is silicified and hereafter referred to as red chalcedony.

A study into the kinematics and timing of the Kencana deposit (in comparison to Toguraci; Micklethwaite, 2010) compared the damage zone (stockwork) vein orientations from both deposits to investigate far-field stress conditions with regards to timing of formation of the deposits. Veins measured from the damage zone of the Kencana lode were compared to the orientation of the lode, for the first 5 undercut levels (Fig. 3.12). On each level, there is a large degree of scatter of vein orientations in both strike and dip. The study indicated no systematic patterns in vein orientation from level to level over the first 5 sublevels in the K1 structure, implying the vein measurements are universal for the whole system rather than biased by local-scale effects. However, damage zone veins are systematically sub-vertical and steeper than the lode. The majority of damage zone veins are parallel to slightly oblique to the lode, striking approximately eastward. This observation, as well as the sub-vertical dip, implies that the Kencana epithermal lode behaved as a dilational fault, and slip events generally had a normal dip-slip movement with a component of obliquity to the north (i.e. left-lateral) (Micklethwaite, 2010). However, there is a large scatter recorded in Kencana's damage zone vein population.

Results of the study indicate that epithermal veins from Toguraci (e.g. Bod, Kayu Manis and Wulan) also have normal dip-slip kinematics, as shown by both slickenfibre lineations and damage zone vein orientations (Micklethwaite, 2010). In both examples there is scatter in the orientations of wall rock veins, which is significant because it implies that although the systems were dominated by normal dip-slip movement, there were increments of failure where the kinematics changed, perhaps transiently (Micklethwaite, 2010).

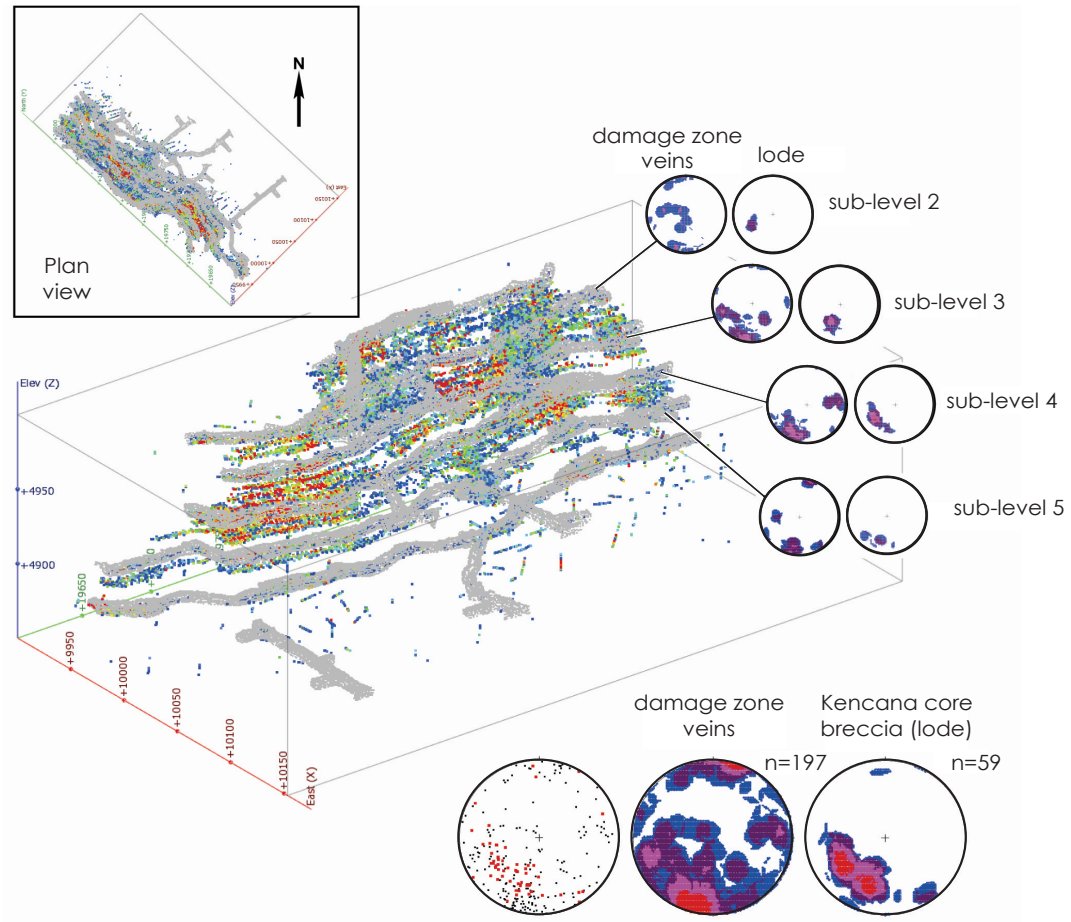

Fig. 3.12 Simplified LeapFrog model of the Kencana lode showing apparent corrugations of the structure relative to gold grade (warm colours), and stereonet orientation data of wall rock veins and lode, for each level (Micklethwaite, 2010).

3.5 Summary

- The Kencana deposit (located 1 km south of the Gosowong deposit) has a total endowment of ~4.4 Mt @ 27.9 g/t Au, containing 4 Moz Au (Newcrest, 2010). The deposit does not crop out, but displays a weak surface expression represented by carbonate veining and faults filled with clay and pyrite. Epithermal mineralization is intersected ~70 m below the current surface.

- Host rocks to the Kencana deposit include several upper Miocene to Pliocene coherent and volcaniclastic facies that define a moderately east-dipping stratigraphy with west-

ward-rotated units offset by post-mineralization faulting.

- Five principal lithofacies have been identified in the Kencana deposit: 1) Plagioclase-phyric coherent and clastic andesite facies; 2) Plagioclase-phyric coherent basalt facies; 3) Sedimentary facies; 4) Intrusive facies and 5) Fiamme-bearing facies.

- The general depositional setting of the volcaniclastic facies is thought to be a regressive, shallow sub-aqueous environment. Though it is uncertain if the environment was shallow marine or lacustrine, the lack of reef materials and limestones may be more suggestive of a lacustrine setting. The differing depositional settings between mass flow sandstones and conglomerates and the volcaniclastics represent a shallowing of the sub-aqueous environment. This regression either represents a decreasing water level, uplift of the basin, or a combination of the two processes. Coherent volcanic rocks overlying the volcaniclastics (Kayasa Fm) were probably deposited in the sub-aerial environment, indicating an almost complete regression.

- The deposit is hosted by two main sub-parallel NW-trending fault structures, (K1 and K2) dipping ~46°E, joined by numerous major and minor link structures, such as K-link (KL), that exhibit a steeper dip than the main K1 and K2 structures. The structures provide a host for epithermal mineralization, focused along lithological boundaries where rheologic differences are encountered.

- Current known strike length of the K1 vein is approximately 400 m with a vertical extent of 200 m. Steeper sections of the K1 fault have a high tensional component and dilate, whilst the flatter segments deform principally by shear and remain tight. Tectonic brecciation is apparent along the zones of the K1 hangingwall with a shear component (flatter segments), where foliated cataclasite to fault gouge marks the structure. Shear zones are predominantly post-mineralization and disrupt, rather than control, the pri-

mary distribution of ore.

- The fault structure hosting mineralization is generally continuous regardless of wallrock lithology; however, veins appear best developed along lithological boundaries, particularly where rheological differences exist (e.g. mudstone/ volcanic contact). Incompetent hematitic mudstone appears to have restricted structural dilation, impeding fluid flow and leading to displacement of mineralization and pinching of the structure. Bonanza Au grade zones are located in dilational zones above the thicker mudstone packages. Mudstones are inferred to retard fluid flow through the 'pinch' zone, with fluids rapidly depressurizing immediately above resulting in voluminous mineralization associated with pressure changes.

CHAPTER 4

VEIN GEOLOGY

4.1 Introduction

In low and intermediate sulfidation epithermal deposits, gangue and ore mineralization varies laterally and vertically along the host structure in response to variations in temperature, fluid composition, pressure, and wallrock interaction (Cooke and Simmons, 2000; Hedenquist et al., 2000; Sillitoe and Hedenquist, 2003; many other workers). Vein and breccia infill, as well as textural classification and ore mineral assemblages, can provide information on the physio-chemical environment of ore formation (Wurst, 2004).

This chapter documents the vein and breccia infill mineralogy for the K1 vein, including ore and gangue mineralogy, classification and distribution of epithermal vein textures. Paragenetic relationships were determined from careful observation of cross-cutting relationships, textural relationships and mineralogy. Representative samples of vein and breccia material were selected for characterization by microscopic and geochemical analysis. A textural classification was developed for the K1 vein using observations from underground mapping and SiroVision™ images of underground mine faces. Fluid inclusion data were collected from various textural types within the vein and were analysed in order to constrain the temperature and pressure conditions of entrapment and salinity of the ore-forming fluid. The metal zonation signature surrounding the K1 vein was contoured using data from diamond drill core assays to characterize the geochemical signature related to the vein.

4.2 Mineralization

Economic mineralization may occur over a 100 m up to ~1 km vertical interval, and may extend up to several kilometres along strike for a single vein. The vertical interval of low-sulfidation ore zones typically averages about 300 m (Buchanan, 1981), but may be as large as 600–1000 m for intermediate sulfidation deposits, or in the case of high-grade, low sulfidation deposits, may be as little as 100–150 m (Hedenquist et al., 2000).

Vein and breccia infill mineralogy and textural characteristics can provide information on the physiochemical environment of mineral deposition. At Kencana, identification of vein and breccia infill mineralogy and textures, and thus their distribution and paragenetic relationships, has provided insight into the evolution of the hydrothermal system over time and space.

The mineralized K1 structure at Kencana is a listric fault showing normal displacement with a strike length of ~400 m with a vertical extent of 200 m. The structure has an average thickness of 8 m wide, though locally dilates up to 20 m wide, and is composed of veins and breccias infilled with quartz, cryptocrystalline quartz, sulfide and sulfosalt minerals, electrum, amethyst and calcite.

4.2.1 Previous work

Prior to this study, infill stages for the Kencana deposit were documented in internal company and consultant reports (Coote, 2003; 2005). Coote (2003) recognized four Au-bearing petrologically distinct silica vein/ cement stages in the Kencana vein system from observations on a suite of exploration drill core samples. The four paragenetic stages were determined as:

1) Early massive to crustiform banded quartz + cryptocrystalline quartz + adularia + carbonate cement/vein assemblages, where electrum has a close spatial association with adularia, interstitial carbonate, and base metal sulfides.

2) Crustiform banded quartz + cryptocrystalline quartz + adularia in which interstitial chlorite (and some illite-smectite clays), electrum, silver selenides (naumannite), selenium-bearing galena and other base metal sulfides contribute significantly to the definition of crustiform banding.

3) Massive textured, ultra fine-grained cement composed mainly of quartz, enclosing fluidised and finely comminuted early vein/cement and wallrock fragments, including hematitic volcaniclastics, interstitial to which are grains of electrum and base metal sulfides.

4) Massive textured quartz and cryptocrystalline quartz interlocking with minor amounts of pyrite and interposed with voluminous amounts of interstitial, poorly crystalline, ultra fine-grained molybdenite, infilling cavities along late shears and fractures. Elec-

trum is interstitial to and intergrown with quartz, pyrite and molybdenite.

Coote (2003, 2005) determined mineralogy associated with these paragenetic stages by optical microscopy and microprobe analysis. Assemblages were found to be fairly typical of low-sulfidation epithermal deposits, with native gold, electrum, argentite, naummanite, with sulfide mineralogy dominated by chalcopyrite accompanied by (Se)-galena, sphalerite, pyrite and bornite, along with minor Au-Ag selenide and telluride species and latterly, molybdenite. The geochemical signature of the main ore stages was determined to be gold-silver-copper-lead-zinc-selenium.

4.3 Kencana infill types, gangue mineralogy and description

This section describes the gangue mineralogy at Kencana which is dominated by various silica polymorphs, with lesser adularia, carbonate and clay minerals. In this study, epithermal textural classification for silica polymorphs is based on the work of Dong et al. (1995). Bates and Jackson (1987) subdivided quartz into crystalline, microcrystalline and cryptocrystalline, based on individual grain size. In this study, chalcedony is included in the category of cryptocrystalline quartz.

Mineralization at Kencana shows a complex, multiphase history of formation with numerous brecciation and vein filling events, resulting in complex overprinting infill stages and crosscutting relationships, which record the multiple fissure opening events that provided a conduit for hydrothermal solutions. This study recognizes eleven vein and breccia infill types at Kencana which are described below and shown in Figs. 4.1-4.9. Refinement of the 4 breccia and vein infill types determined by Coote (2003) was possible based on collection of new data from underground mapping, hand sample analysis of both underground mine faces and diamond drill core, and examination of SiroVision™ images of underground mine faces.

The majority of the work in this study has concentrated on the K1 vein of the Kencana deposit and to a lesser extent, K-Link. Mining was active across many sub-levels at K1 during this study but the K-Link and K2 veins were only accessible during the last month of fieldwork. Due to these constraints, the infill vein and breccia types were determined based

on work at K1, but have been tested on drill core samples and underground observation at K-Link and K2 and are considered to be valid for the whole deposit.

A vein *type* is defined by compositional, textural and mineralogical relationships and is named for the most important or dominant gangue minerals and textures present. Vein types are described below disregarding chronological order. Distribution of vein types across the K1 orebody and infill paragenetic stages are discussed in sections 4.5 and 4.6. Interpretation of the paragenetic sequence at Kencana was based on the type of vein or breccia infill, the composition and degree of alteration of breccia fragments, fragments of pre-existing vein types in later veins or breccias, composition of breccia matrix, sequences of mineralization within crustiform banded packages, and crosscutting relationships (as at the Santo Niño vein, Fresnillo District, Mexico; Gemmell et al., 1988). Examples of typical vein textures and infill stage characteristics are displayed in Fig. 4.10. Ore mineralogy associated with vein types 1-11 is described in section 4.7.

4.3.1 Type 1: Wallrock

Type 1 is classified as coherent wallrock material > 50 cm within, or hosting, the vein. Wallrock material is relatively minor in volume and is represented as either 'in situ" attached lithologies marginal to vein/ cement assemblages or as angular to sub-rounded fragments enclosed by one or more vein types. Some finely comminuted wallrock material of fine sand to silt-sized particles occurs as highly concentrated fluidised material (together with vein/ cement material) entrained within one or more vein types. Wallrock lithology is variable and often shows strong illite + pyrite + chlorite ± epidote ± adularia alteration, making identification of the protolith difficult, though hematitic mudstone is easily identified and commonly restricts vein dilation (Chapter 3). The range of wallrock lithologies hosting the Kencana deposit are described and displayed in Chapter 3.

4.3.2 Type 2: Crystalline quartz stockwork

Crystalline to microcrystalline quartz stockwork is characterized by sheeted and crosscutting quartz veins and veinlets 2 to 80 mm thick, peripheral to the main mineral-

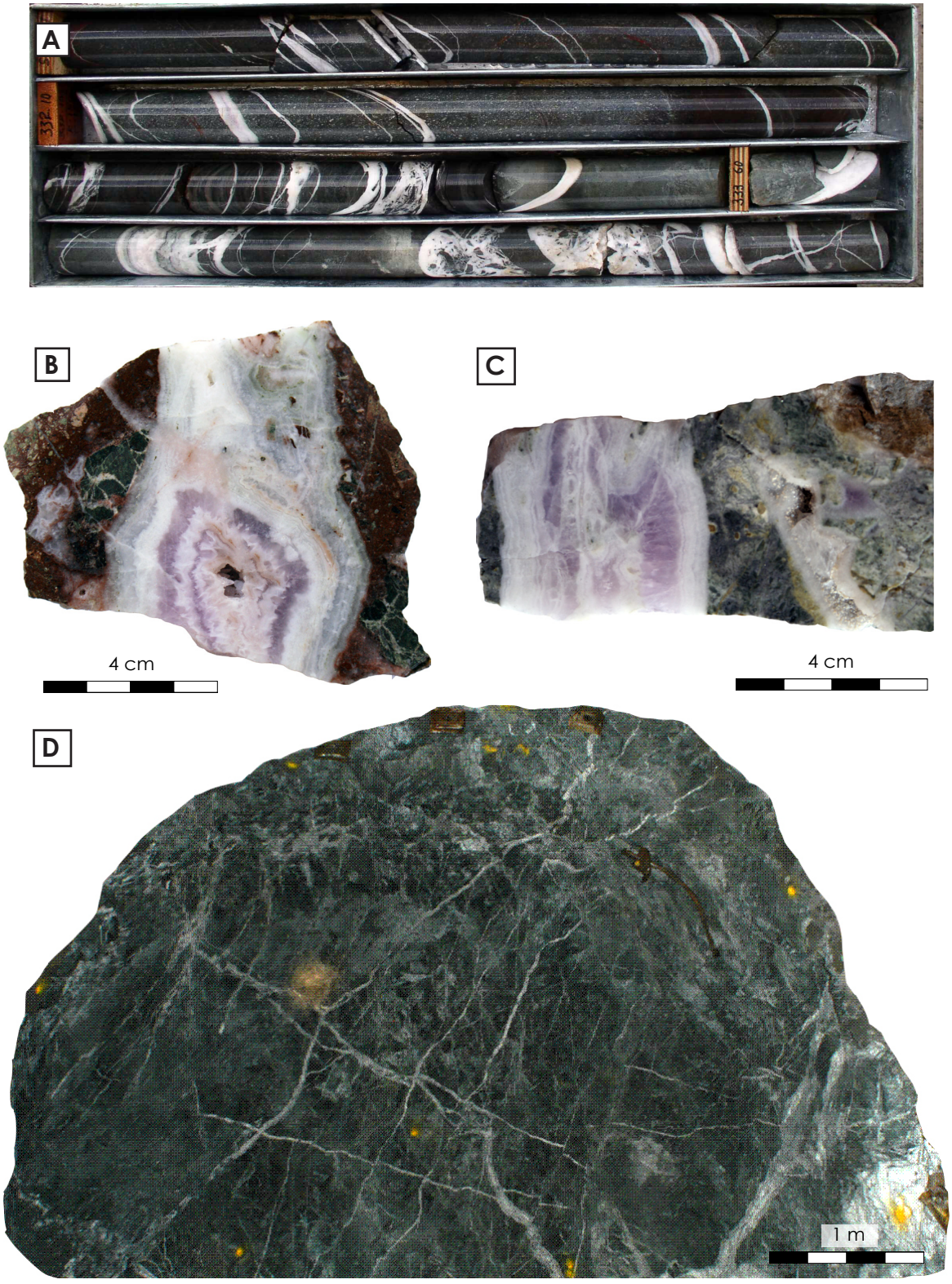

Fig. 4.1 Type 2 mineralization in the K1 vein. **A)** Sheeted crystalline quartz veins (type 2b) with weak crustiform banding and minor wallrock breccia fragments in altered andesite. Sample from drillcore DSD245 331-335 m; **B)** Crustiform banded crystalline quartz and microcrystalline quartz to amethyst infilling vein in hematite dusted volcaniclastic breccia, sample from Sub4UC2S069; **C)** Crustiform banded crystalline quartz and comb texture amethyst (top) with drusy crystalline quartz veinlet (bottom) crosscutting epidote-clay altered volcanic rock, sample from Sub4UC2S069; **D)** Underground face Sub6UA01N045 with crosscutting crystalline quartz stockwork veins (type 2a).

ized structures (Fig. 4.1). Quartz stockwork veining is found at all depths at Kencana but increases in intensity, crystallinity and vein thickness towards the K1 vein. Quartz textures are generally comb quartz to crustiform banded quartz in thicker veins, with zoned crystals. Late comb to vuggy amethyst is present in some veins and tends to occur <40 m from the K1 vein.

Crystalline quartz stockwork at Kencana is distinguished by the percentage of quartz stockwork present in host rock. Three sub-groups are identified: 2a) quartz stockwork 10%, 2b) quartz stockwork 25% and 2c) quartz stockwork 40%. Hangingwall and footwall host rocks generally display lower percentages of quartz stockwork (0-25% stockwork), and large (>1 m) wallrock fragments within the vein display higher percentages (25-40% stockwork). Smaller (<10 cm) wallrock breccia fragments within the vein typically show 40% quartz stockwork, often with complex overprinting relationships indicative of multiple phases of stockwork mineralization. Crystalline quartz stockwork contains no to low Au grade at Kencana, but can be considered prospective for Au mineralization, due to the increasing intensity in stockwork with proximity to the vein.

Crystalline quartz is a primary growth texture indicative of open space filling and slow cooling of hydrothermal fluids under stable conditions (Dong et al., 1995). It is typically formed from hydrothermal fluids that are slightly supersaturated with respect to quartz but undersaturated with respect to chalcedony (Olberg, 2001). Zoned crystals imply mildly fluctuating conditions during crystallization, with growth zones marked by primary fluid inclusion assemblages and impurities in the crystal.

4.3.3 Type 3: Crystalline quartz-cemented wallrock breccia

Type 3 is characterized by angular to sub-angular, jigsaw-fit to rotated clasts of types 1 and 2, ranging from 10 cm to 1 m, cemented by massive white crystalline and microcrystalline quartz (Fig. 4.2). Type 3 is sub-divided into two categories: 3a) wallrock breccia with <20% quartz cement, and 3b) wallrock breccia with 20-40% quartz cement.

Type 3 represents the earliest phases of brecciation at Kencana, and are characterized by jigsaw-fit or crackle breccia textures with large angular wallrock fragments and low volumes of quartz cement. Later phases are characterized by smaller, sub-angular rotated wallrock clasts in voluminous quartz cement, representing successive brecciation in type 3.

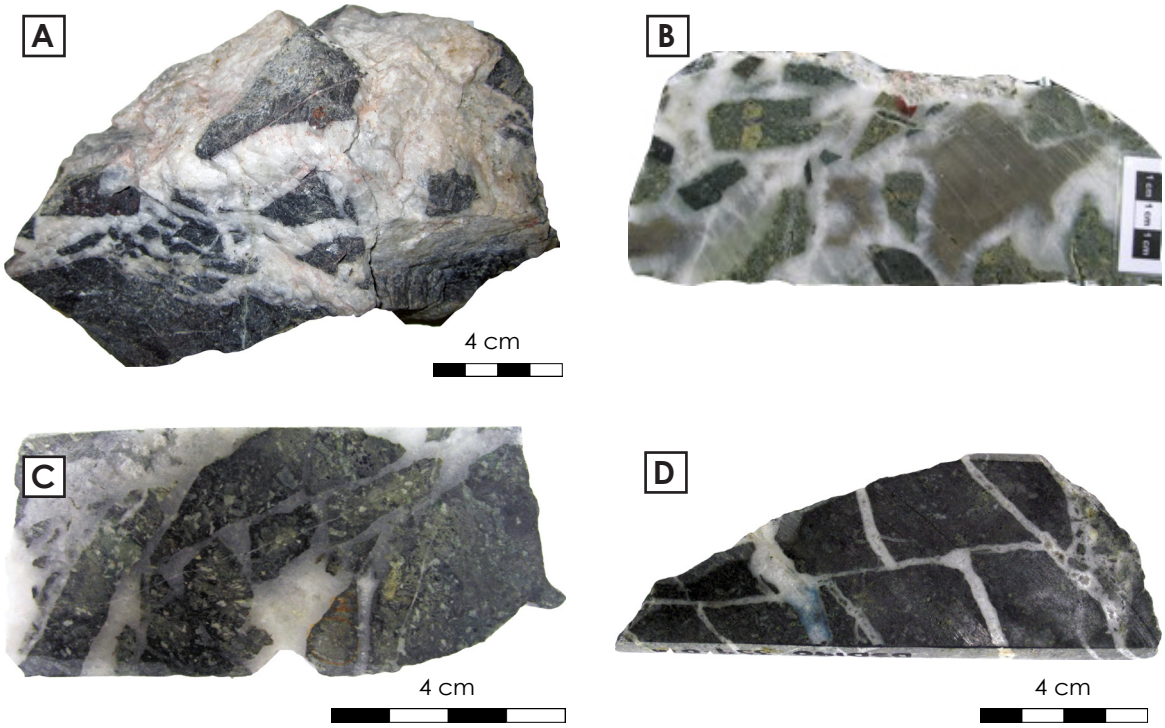

Fig. 4.2 Type 3 mineralization in the K1 vein. **A)** Angular wallrock fragments cemented by massive crystalline quartz (type 3b). Sample from Sub8SL01S006; **B)** Polymict altered wallrock breccia cemented by massive crystalline and microcrystalline quartz (type 3b). Sample from Sub3UC02N015; **C)** Epidote altered wallrock breccia with crystalline quartz cement (type 3a). Sample from drillcore DSD140_248.3m; **D)** Jigsaw-fit wallrock breccia with crystalline quartz cement (type 3a). Sample from drillcore DSD140_359m.

4.3.4 Type 4: Red chalcedony infill/ crustiform bands

The dark red to brown chalcedony infill and crustiform bands are characterized by ultra-fine grained hematitic rock fragments with fluidized silt to mud-sized wallrock fragments enclosed within cryptocrystalline silica. Red chalcedony is either present as thin, rhythmic crustiform bands, or forms the matrix to banded quartz + cryptocrystalline quartz breccias (Fig. 4.3).

Red chalcedony crustiform bands alternate on a millimetre to centimetre scale with clear to milky cryptocrystalline quartz, crystalline quartz, drusy quartz with minor open space and fine grained K-feldspar (inferred as adularia after staining), with ultra-fine grained sulfides (chalcopyrite and minor pyrite likely to have been re-mobilized from altered wallrock clasts). Red chalcedony bands are rarely continuous and multiple phases of brecciation are common. Breccia clasts are angular to sub-rounded, typically <4 cm and are composed of rhythmically banded red chalcedony + cryptocrystalline quartz ± adularia, supported in a matrix of later phases of red chalcedony mineralization or crustiform banded cryptocrys-

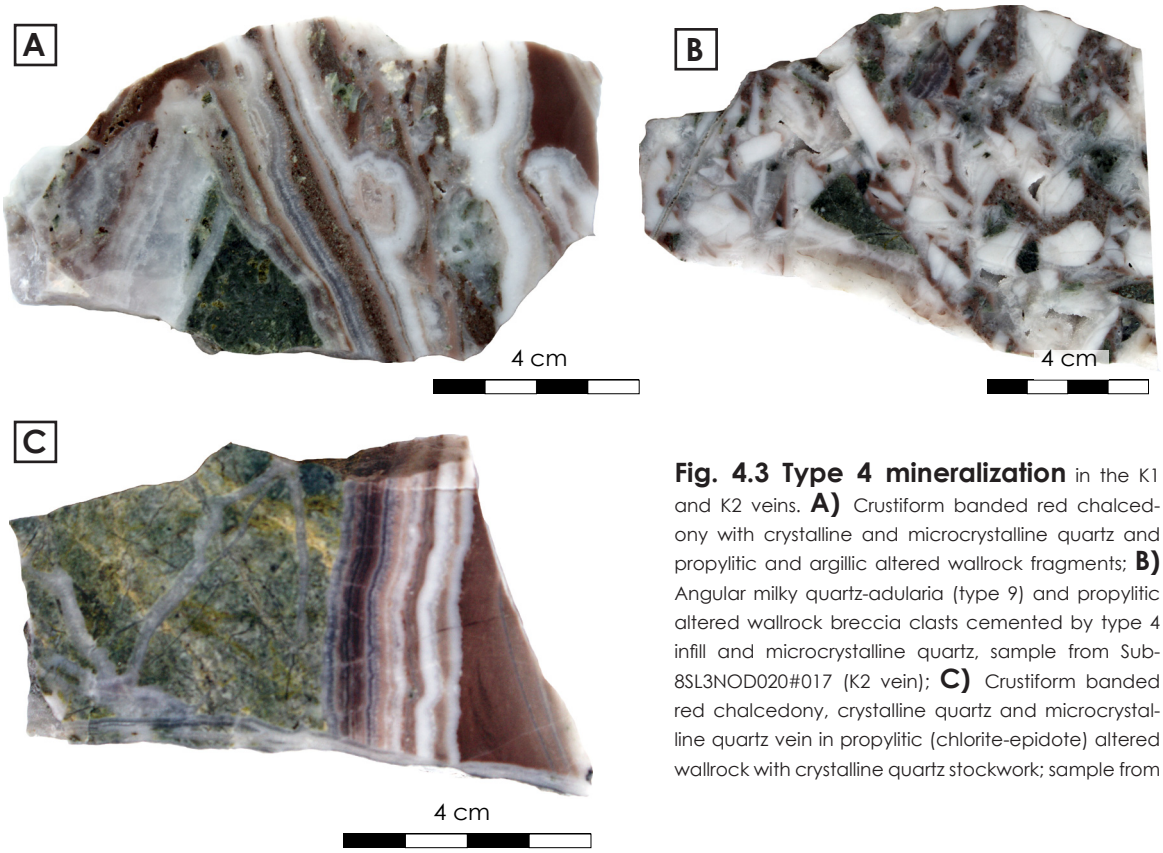

Fig. 4.3 Type 4 mineralization in the K1 and K2 veins. **A)** Crustiform banded red chalcedony with crystalline and microcrystalline quartz and propylitic and argillic altered wallrock fragments; **B)** Angular milky quartz-adularia (type 9) and propylitic altered wallrock breccia clasts cemented by type 4 infill and microcrystalline quartz, sample from Sub-8SL3NOD020#017 (K2 vein); **C)** Crustiform banded red chalcedony, crystalline quartz and microcrystalline quartz vein in propylitic (chlorite-epidote) altered wallrock with crystalline quartz stockwork; sample from

talline quartz. Angular and rotated illite + chlorite + pyrite ± epidote ± illite after adularia altered wallrock breccia clasts <4 cm are also common in type 4.

Massive red chalcedony infill cements angular to sub-angular banded milky quartz + cryptocrystalline quartz + adularia breccia clasts. Red chalcedony infill is the first stage of infill in these breccias, with later cryptocrystalline quartz followed by minor drusy quartz infilling vug space.

4.3.5 Types 5 and 6: Massive crystalline quartz infill (5) and massive crystalline quartz breccia (6)

Type 5 is characterized by crystalline and microcrystalline quartz infill of veins and breccias, with rare sub-angular wallrock fragments 2 mm - 10 cm. Fragments of type 5 occasionally occur as angular to sub-angular and rotated breccia clasts in types 9 and 11. Type 6 consists of fractured, brittle fragments of type 5 material with angular jigsaw-fit to rotated clasts <50 cm, cemented by subsequent type 5 mineralization (Fig. 4.4).

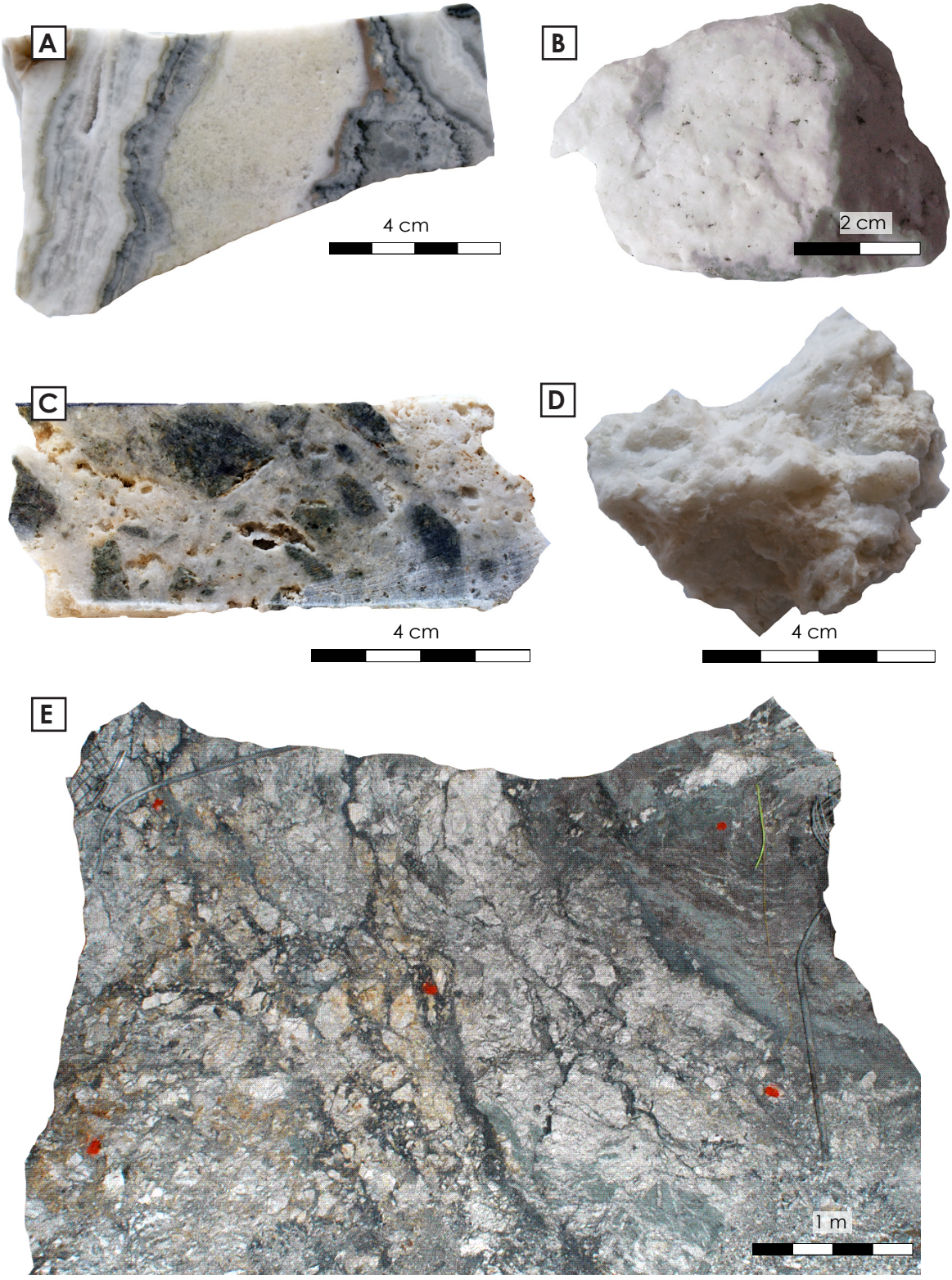

Fig. 4.4 Types 5 and 6 mineralization in the K1 vein. **A)** Type 5 vuggy crystalline quartz vein (centre of sample) with minor quartz-chlorite crustiform bands and banded quartz-adularia infill; **B)** Massive type 5 quartz with saccharoidal texture; **C)** Type 5 bladed quartz after calcite pseudomorphs and microcrystalline milky quartz cementing propylitic altered wallrock breccia clasts, from drillcore DSD139 231.4 m; **D)** Type 6 milky crystalline quartz breccia from Sub4UC3S011; **E)** Underground face Sub3UA07N006 (K1 vein) with type 6b massive crystalline quartz breccia (white) cemented by type 11 infill (black) and type 1 propylitic altered and hematized wallrock to the top right (footwall).

Quartz in type 5 is typically massive and ranges from microcrystalline, anhedral and equigranular to coarser crystals 0.5 - 4 cm; is milky white to pale grey, hard, and breaks with a conchoidal fracture. Rare crude crustiform banding can be observed. The last phase of mineralization in each isolated depositional sequence is generally fine-grained (<3 mm) drusy quartz crystals infilling microvugs. Staining of type 5 shows that fine-grained disseminations of K-feldspar (inferred to be adularia) are present. Occasional calcite crystals <7 mm are also present and bladed quartz after calcite pseudomorphs. Quartz is occasionally vuggy or pitted in appearance, in places inferred to represent incomplete replacement of calcite crystals.

Massive crystalline quartz veins are typically 50 cm to 4 m, with gold grades typically ~5 g/t Au. Multiple phases of massive crystalline quartz mineralization are inferred, based on the relationship of massive crystalline quartz breccia fragments with later massive crystalline quartz, and the association with both early wallrock and crystalline quartz stockwork mineralization (types 1 and 2), and later type 11 mineralization.

4.3.6 Type 7 and 8: Cockade banded quartz-chlorite breccia (7) and crustiform banded quartz-chlorite infill (8)

Types 7 (Fig. 4.5) and 8 (Fig. 4.6) are characterized by banded microcrystalline to cryptocrystalline quartz, adularia and very fine-grained dark green chlorite with sulfides and significant gold mineralization. Mineralization (sulfides, sulfosalts, electrum + chlorite) forms crustiform to colloform banded veins and cockade banded breccias. Breccia clasts are composed of types 1, 2, 5, 7 and 9, and cemented by type 8 with later massive crystalline quartz infill. Type 7 and 8 mineralization is volumetrically minor in the Kencana deposit, though it contains the bulk of the Au mineralization (average grades of >50 g/t to several thousand g/t Au).

The first phase of mineralization within each depositional sequence in types 7 and 8 contains a concentration of thin (<1 cm), dark green to black chlorite bands interposed with cryptocrystalline quartz and milky microcrystalline quartz, followed by banded cryptocrystalline quartz and adularia. The latest phase of mineralization in each depositional sequence (more common in type 7) is white massive microcrystalline to crystalline quartz.

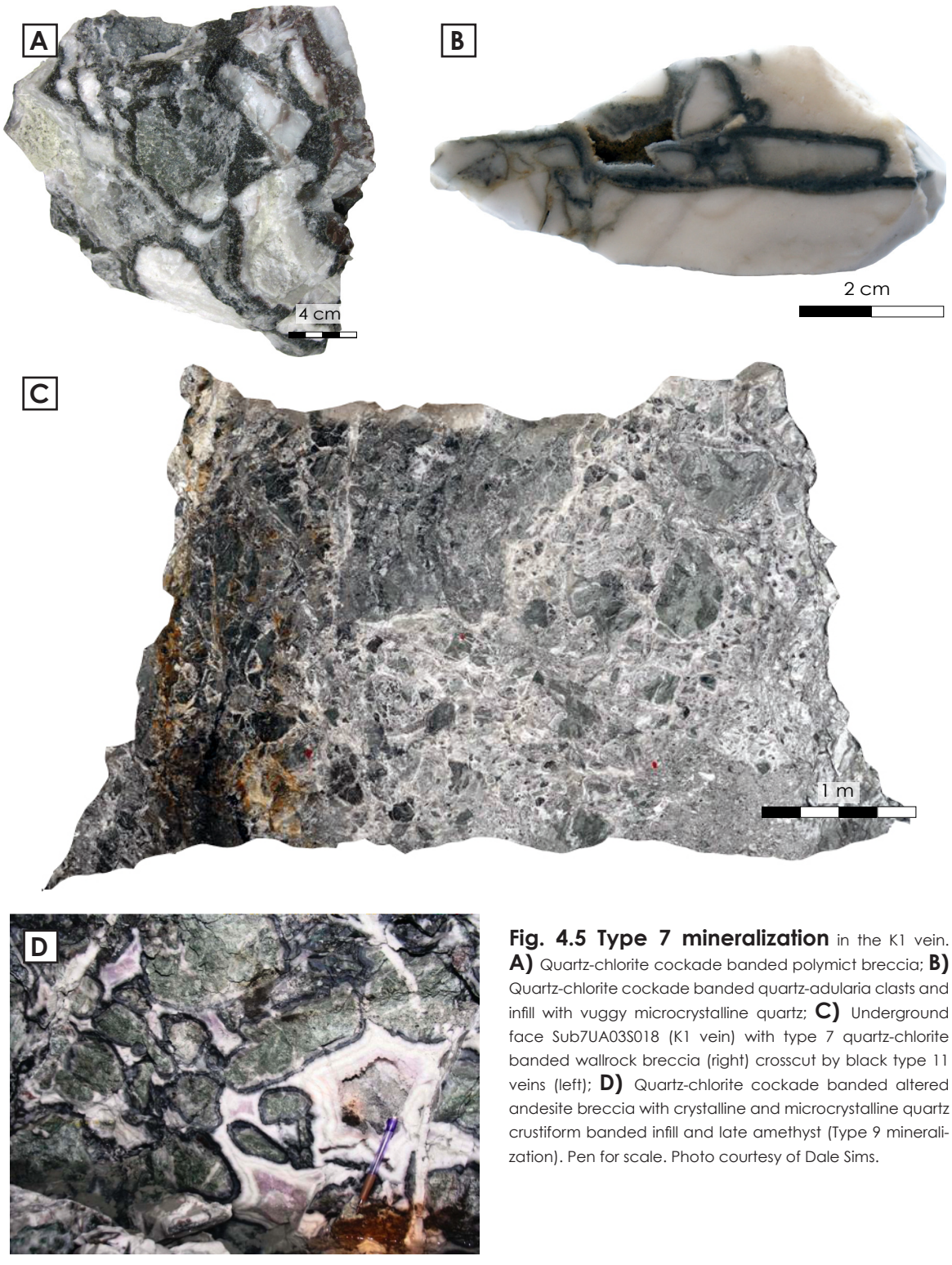

Fig. 4.5 Type 7 mineralization in the K1 vein. **A)** Quartz-chlorite cockade banded polymict breccia; **B)** Quartz-chlorite cockade banded quartz-adularia clasts and infill with vuggy microcrystalline quartz; **C)** Underground face Sub7UA03S018 (K1 vein) with type 7 quartz-chlorite banded wallrock breccia (right) crosscut by black type 11 veins (left); **D)** Quartz-chlorite cockade banded altered andesite breccia with crystalline and microcrystalline quartz crustiform banded infill and late amethyst (Type 9 mineralization). Pen for scale. Photo courtesy of Dale Sims.

4.3.7 Type 9: Banded cryptocrystalline quartz + quartz + adularia breccias and infill

Type 9 is characterized by fine to medium-grained, white to greenish-grey crystalline

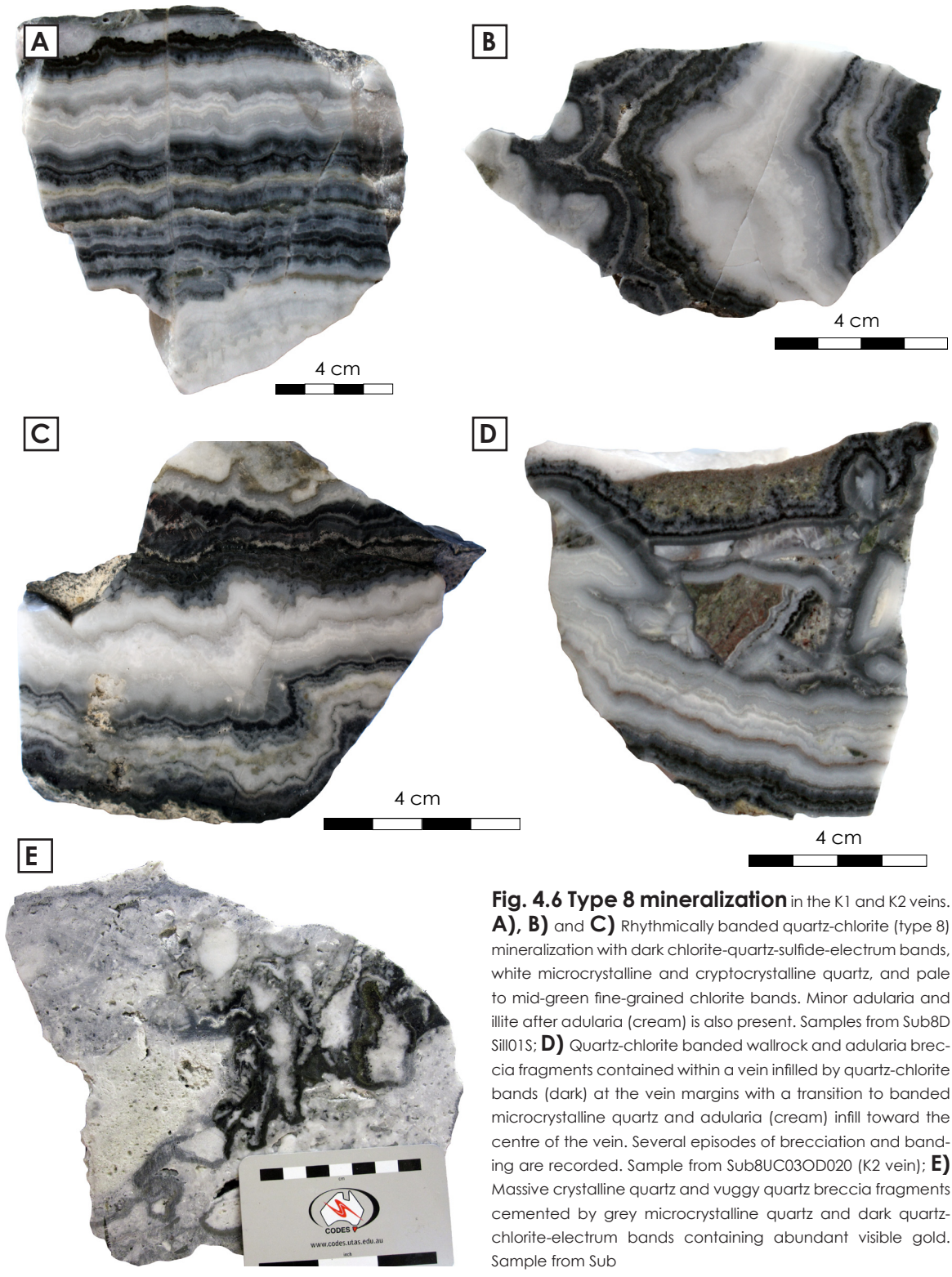

Fig. 4.6 Type 8 mineralization in the K1 and K2 veins. **A), B)** and **C)** Rhythmically banded quartz-chlorite (type 8) mineralization with dark chlorite-quartz-sulfide-electrum bands, white microcrystalline and cryptocrystalline quartz, and pale to mid-green fine-grained chlorite bands. Minor adularia and illite after adularia (cream) is also present. Samples from Sub8D Sill01S; **D)** Quartz-chlorite banded wallrock and adularia breccia fragments contained within a vein infilled by quartz-chlorite bands (dark) at the vein margins with a transition to banded microcrystalline quartz and adularia (cream) infill toward the centre of the vein. Several episodes of brecciation and banding are recorded. Sample from Sub8UC03OD020 (K2 vein); **E)** Massive crystalline quartz and vuggy quartz breccia fragments cemented by grey microcrystalline quartz and dark quartz-chlorite-electrum bands containing abundant visible gold. Sample from Sub

quartz, microcrystalline quartz, cryptocrystalline quartz, and adularia, with illite after adularia, calcite, late amethyst and sulfides. Well-developed, repeated, symmetric to asymmetric crustiform and cockade banding is defined mainly by the grain-size and colour variation of

cryptocrystalline, microcrystalline and comb texture quartz, the distribution of medium-grained to ultra fine-grained adularia, and dark grey sulfide-rich bands (Fig. 4.7). Type 9 is volumetrically the most significant style of mineralization within the Kencana deposit, with a moderate to high average gold grade (10-50 g/t Au).

Multiple phases of type 9 mineralization are evident in the Kencana deposit, where early phases of type 9 are brecciated and cemented by subsequently formed bands of the same mineralogy. Earlier type 9 mineralization often exhibits darker grey cryptocrystal-

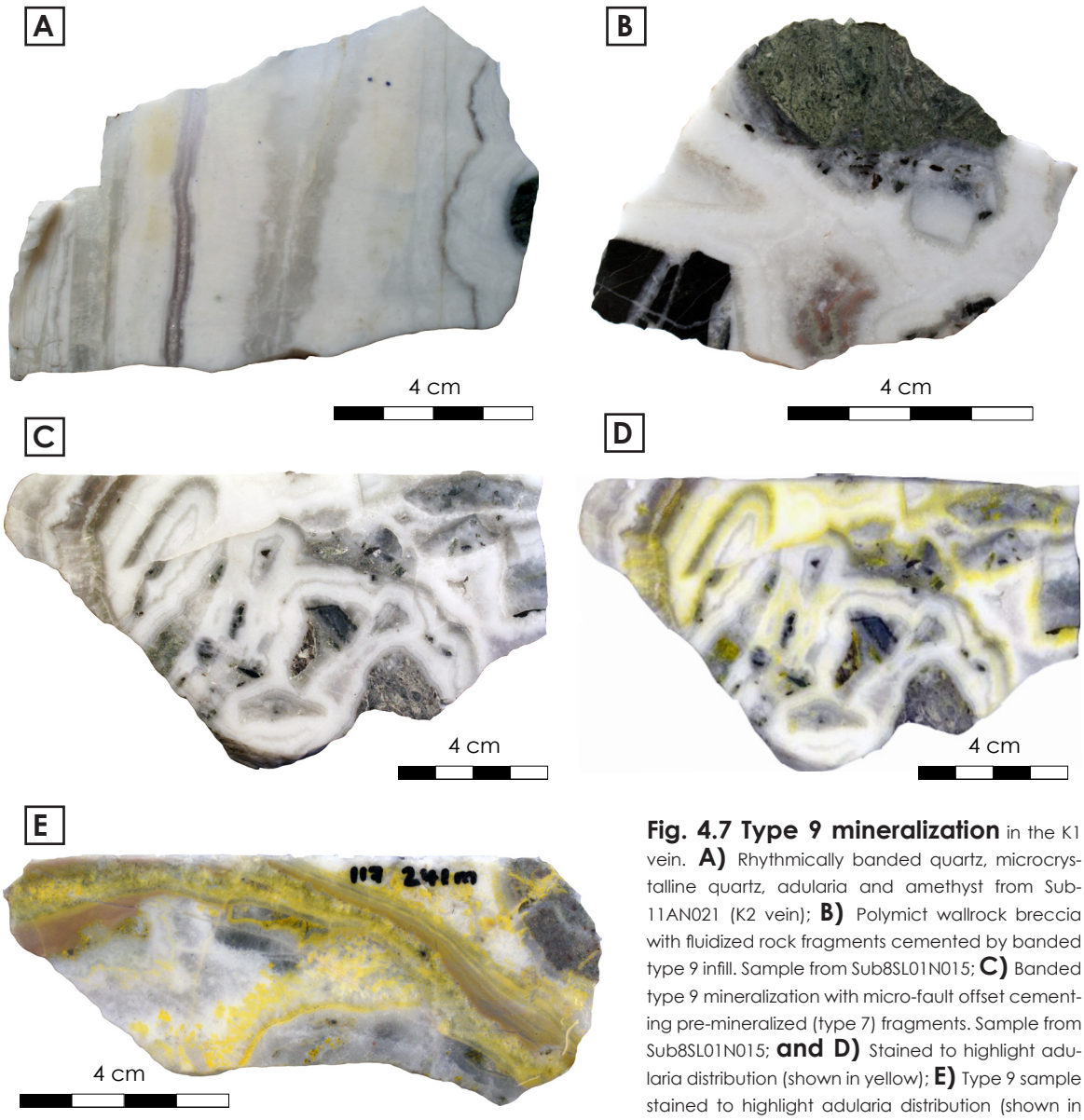

Fig. 4.7 Type 9 mineralization in the K1 vein. **A)** Rhythmically banded quartz, microcrystalline quartz, adularia and amethyst from Sub-11AN021 (K2 vein); **B)** Polymict wallrock breccia with fluidized rock fragments cemented by banded type 9 infill. Sample from Sub8SL01N015; **C)** Banded type 9 mineralization with micro-fault offset cementing pre-mineralized (type 7) fragments. Sample from Sub8SL01N015; **and D)** Stained to highlight adularia distribution (shown in yellow); **E)** Type 9 sample stained to highlight adularia distribution (shown in yellow) with associated type 4 red chalcedony vein. Sample from drillcore DSD117_241 m.

line quartz, thinner crustiform banding and sporadic type 4 material. Subsequent type 9 mineralization cementing these earlier mineralized breccia fragments is dominated by white microcrystalline quartz and adularia, with adularia commonly occurring as the first phase of mineralization within each individual depositional sequence (i.e. forming rims to pre-mineralized breccia clasts), through microcrystalline and cryptocrystalline to crystalline quartz, with drusy amethyst infilling vugs as the last phase in each sequence.

Adularia is most abundant in bands of very fine to ultra fine-grained quartz and is sporadically replaced by illite. Due to the fine grained nature of adularia, morphologies are difficult to ascertain, however rhombic and rare tabular adularia were identified. Blades of fine to medium-grained carbonate are dispersed through the vein assemblage. Bladed quartz after carbonate textures are also observed, where bladed carbonate is replaced by very fine to ultra fine-grained quartz. The presence of bladed carbonate and quartz after bladed carbonate suggests that the bladed carbonate present is metastably preserved (i.e. not in equilibrium with a rapid cooling hydrothermal fluid; Coote, 2003). Contained within some bands of very fine-grained quartz are concentrations of fluidized and sorted, mainly silt-sized silicified wallrock fragments. Angular to sub-angular, rotated wallrock breccia clasts <7 cm cemented by cockade banded crystalline quartz, cryptocrystalline quartz and adularia are common through veins filled by type 9.

4.3.8 Type 10: Grey cryptocrystalline quartz stringer veins

Type 10 is characterized by hard, grey cryptocrystalline quartz stringer veins (2-30 cm thick) crosscutting types 3-9, though most commonly crosscutting types 4 and 9 (Fig. 4.8). Type 10 is the least common vein type in the Kencana deposit. The majority of type 10 veins are sub-vertical and are generally not laterally continuous. Type 10 veins are not associated with any Au mineralization.

4.3.9 Type 11: Molybdenite + black quartz matrix infill/ veins

Type 11 is characterized by friable and sooty to silicified black quartz, very fine-grained milky quartz, microcrystalline quartz and cryptocrystalline quartz, interstitial to poorly crystalline, ultra fine-grained molybdenite (Fig. 4.9). Type 11 crosscuts all other vein types and commonly occurs as a breccia matrix containing clasts of types 1, 4, 5 8 and 9.

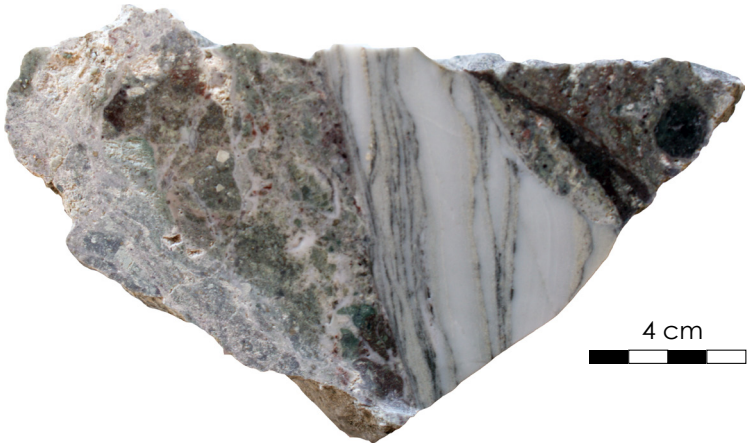

Fig. 4.8 Type 10 mineralization in the K1 vein. Grey, cryptocrystalline quartz veins with minor sulfide banding in intensely illite-chlorite altered volcanic rock.

Breccia clasts are angular to sub-angular and <5 cm. Type 11 infill is also localized along shears and fills fractures particularly within types 5 and 6. Type 11 infill is associated with a bright to dark blue stain, discolouring black quartz and occasionally massive crystalline quartz in contact with fractures filled by type 11.

4.4 Discussion of Kencana gangue mineralogy and infill types

The range of silica polymorphs indicate different depositional environments and physiochemical characteristics of the hydrothermal fluid during different mineralization stages (Wurst, 2004). As quartz is the only phase deposited over the entire life of the system, it records vein growth and evolution pre-, syn- and post- precious metal deposition (Dowling and Morrison, 1989; Wurst, 2004).

Deposition of silica minerals is a function of variations in temperature and to a lesser extent, pressure, salinity, pH, rate of deposition and the presence of complexing agents (Fournier, 1985). Microcrystalline and cryptocrystalline quartz are common features of many epithermal deposits and are recognized in many vein types at Kencana. Microcrystalline and cryptocrystalline quartz are associated with vein types hosting high grade Au, and electrum is often found as inclusions within or interstitial to cryptocrystalline and microcrystalline quartz (See section 4.7). In many epithermal deposits, microcrystalline quartz occurs in proximity to high grade ore zones but does not host significant ore mineralization (e.g. Cracow, Queensland, Dong et al., 1995, Braund, 2006; and Golden Cross, New Zealand, Faure and Braithwaite, 2002). However, the PBH and Kerikil veins at the Mt. Muro

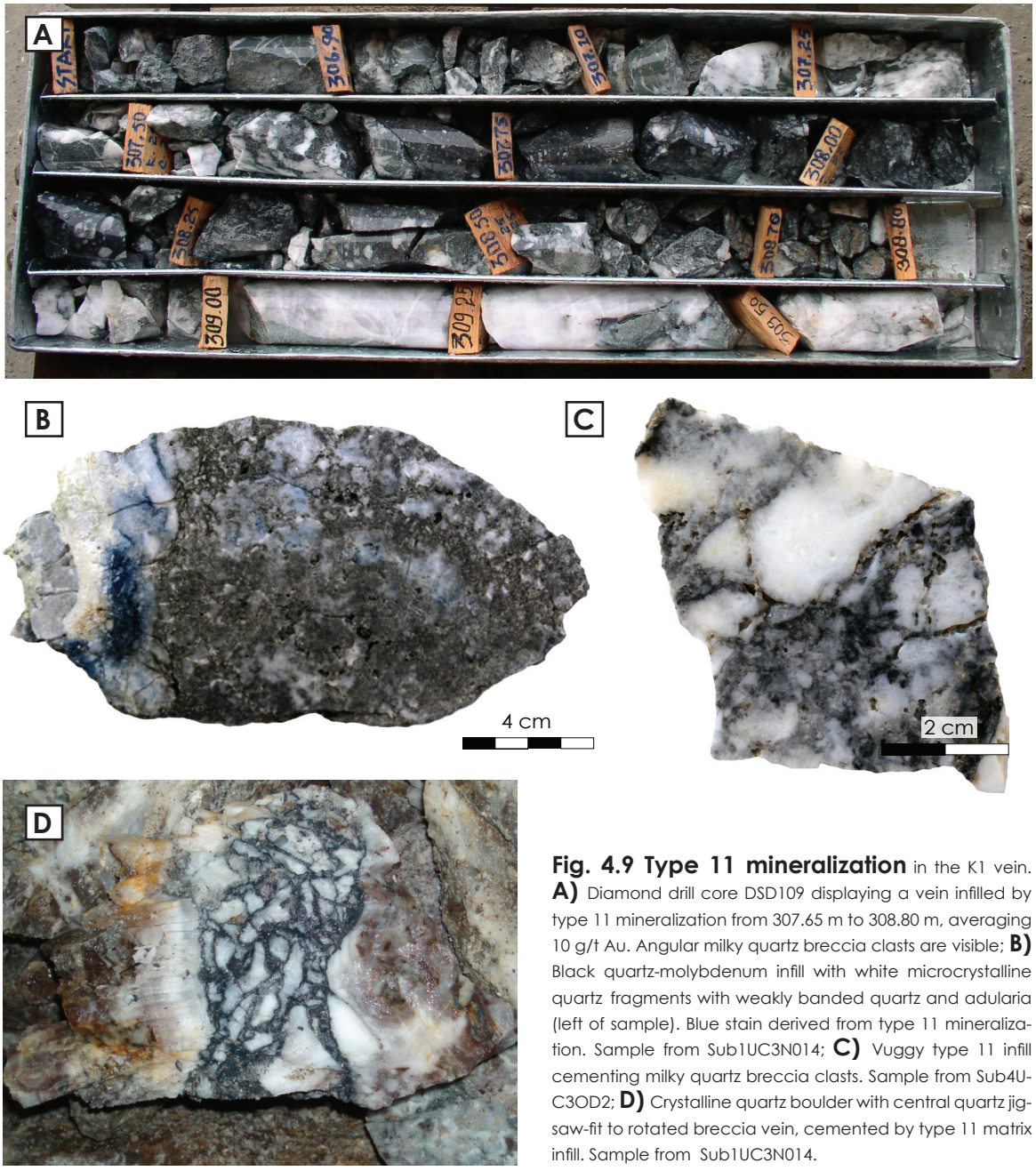

Fig. 4.9 Type 11 mineralization in the K1 vein. **A)** Diamond drill core DSD109 displaying a vein infilled by type 11 mineralization from 307.65 m to 308.80 m, averaging 10 g/t Au. Angular milky quartz breccia clasts are visible; **B)** Black quartz-molybdenum infill with white microcrystalline quartz fragments with weakly banded quartz and adularia (left of sample). Blue stain derived from type 11 mineralization. Sample from Sub1UC3N014; **C)** Vuggy type 11 infill cementing milky quartz breccia clasts. Sample from Sub4UC3OD2; **D)** Crystalline quartz boulder with central quartz jigsaw-fit to rotated breccia vein, cemented by type 11 matrix infill. Sample from Sub1UC3N014.

deposit show a spatial association between microcrystalline quartz and areas of high grade ore (Wurst, 2004).

Geothermal wells provide a modern analogue of the low sulfidation epithermal environment (Henley and Ellis, 1983; Simmons and Browne, 2000). Processes occurring in wells and the products formed within are often recognized in low sulfidation epithermal veins; for example, colloform and crustiform banded microcrystalline and cryptocrystalline

quartz deposited on pipe walls in modern geothermal wells is directly analogous to the fine-grained, banded textures observed in epithermal deposits. These textures were recognized in geothermal pipes forming from rapidly cooling hydrothermal solutions supersaturated in amorphous silica at <180°C (Simmons and Browne, 2000). Evidence from geothermal wells also suggests that microcrystalline quartz forms in areas of high fluid flux; therefore, the recognition and distribution of microcrystalline quartz in epithermal deposits may indicate upflow zones and areas of high fluid flow (Wurst, 2004).

Microcrystalline and cryptocrystalline quartz show a variety of textures in the infill types at Kencana including abundant colloform and crustiform banding, which are inferred to represent primary growth textures formed during crystal growth or from the deposition of amorphous silica (Dong et al., 1995). At Kencana, cryptocrystalline and microcrystalline quartz are most abundant in type 9 veins. These veins show an overall increase in quartz grain size from microcrystalline and cryptocrystalline quartz to crystalline quartz towards the centre of the veins, representing the latest stages of infill. Coarse-grained comb and crustiform textures in quartz require relatively slow changing conditions in open space during crystal growth. This transition in grain size may reflect a decrease in the rate of cooling and/or a decrease in the overall flow rate. Decreasing fluid flux rates can occur as a result of vein dilation, as an increase in vein width would result in a drop in pressure and lower flow rates (Wurst, 2004). Sealing of the vein by deposition of microcrystalline and cryptocrystalline quartz may also decrease flow rates. Complex crustiform bands with numerous repetitive changes in mineral composition as observed at Kencana are inferred by Buchanan (1981) to form by episodic pressure release, where drops in total confining pressure allow fluids to boil, resulting in loss of volatiles, cooling, increase in pH and deposition of gangue (and ore) minerals. As mineralization progresses, fractures are filled thus reducing fluid flow rate. Once sealed, pressure increases and boiling at depth ceases (Dong et al., 1995). New mineral deposition can only occur after the development of new veins or re-opening of the conduit by brecciation, a process that is widely recognized at Kencana. This process of constriction and sealing is known from modern geothermal wells (Simmons and Browne, 2000). Alternatively, waning of the hydrothermal system can cause both flow rate and pressure decreases.

Recrystallization and replacement textures are evident in crystalline quartz, includ-

ing feathery, mosaic, parallel bladed and pseudo-acicular textures (defined by Dong et al., 1995). Replacement textures in the K1 vein represent partial or complete pseudomorphs of other minerals (principally calcite) by silica minerals within veins.

Amethyst formation is a result of substitution of Fe^{3+} ions into quartz, with darker varieties containing more Fe^{3+} ions (Dennen and Puckett, 1972). Amethyst formation can occur under a variety of conditions applicable to epithermal veins (Dennen and Puckett, 1972) including: Formation from a Fe-rich/ Al-poor solution; oxidizing conditions (with respect to ferrous-ferric iron species); moderate temperatures (incorporation of Fe^{3+} for Si^{4+} or Al^{3+} increases at higher temperature); and low pressures (permitting an increase in cell size and therefore the incorporation of the larger Fe^{3+} ion). Zoned crystals exhibiting a colour change from clear to purple from base to termination have most likely formed during a change from reduced to oxidized conditions, a change in solution composition from Fe-poor to rich (± Al-rich to poor), and/ or a rise in temperature and drop in pressure (Dennen and Puckett, 1972; Wurst, 2004).

Amethyst is a relatively common mineral that occurs as a late stage product in the vein paragenesis of many low sulfidation epithermal deposits (e.g. Santo Niño, Fresnillo, Mexico, Gemmell et al., 1988; Waihi, New Zealand, Braithwaite and Faure, 2002; Comstock, Nevada, USA, Hudson, 2003; Mt. Muro, Indonesia, Wurst, 2004; Cracow, Queensland, Braund, 2006), as observed at Kencana. The formation of amethyst late in the life of these epithermal systems is consistent with a hydrothermal fluid that has previously boiled and deposited $Al(OH)^{-}$ as sericite, illite or adularia, as amethyst formation is possibly promoted by a change from Al-rich to poor conditions (Dennen and Puckett, 1972). At Kencana, amethyst is most common in the late bands and infill of type 9 veins, forming coarse crystalline comb texture crystals and occasionally infilling vug spaces, after mineral assemblages inferred to form as a result of boiling processes and not directly associated with precious metal deposition. The development of coarse comb texture amethyst crystals suggests slow rates of deposition in open space (Dong et al., 1995).

Minor carbonate is recognized at Kencana as euhedral calcite crystals ranging from 1 - 40 mm and bladed calcite aggregates. Bladed calcite is most common on the margins of the vein, in particular along cross section 19600mN. In the main ore zone, bladed calcite is

often replaced by silica polymorphs and remaining calcite is present as small, disseminated crystals through vein types 5, 6 and 9.

Carbonate forms from reheating fluids sufficiently saturated with respect to CO_2 (Simmons and Christenson, 1994). CO_2-rich fluids can be produced by deep boiling of CO_2-rich chloride waters, which partitions CO_2 into steam, a process recognized at the Broadlands-Ohaaki geothermal field (Hedenquist, 1999; Simmons et al., 2000). Condensation and absorption of steam into cool meteoric waters at shallow levels in the system produces a CO_2 saturated fluid, from which calcite precipitates (Hedenquist, 1999). Simmons et al. (2000) suggested that high-density CO_2-rich fluids were excluded from the active upflow zone at the Empire Vein (New Zealand) due to buoyancy effects created by upwelling fluids and the thermal plume. The CO_2-rich fluids then migrated downward into the Empire Vein after cessation of the upwelling of chloride waters, depositing late-stage carbonates (e.g. calcite and rhodochrosite) in vugs and crosscutting veins. The general paucity of calcite and absence of other carbonates (e.g. rhodochrosite, manganoan calcite) at Kencana suggests a low-CO_2 (and manganese) source fluid, inferring H_2O as the dominant vapour phase in the system, an observation verified by the lack of clathrates in fluid inclusions from Kencana (section 4.10).

Adularia is an indicator of boiling in the epithermal environment (Browne and Ellis, 1970; Henley, 1985; Hedenquist, 1990; Dong and Morrison, 1995), where boiling promotes an increase in fluid pH and causes precipitation of adularia (Browne, 1978). Thermodynamic research by Reed and Spycher (1985) also showed that silicates such as adularia (and sericite) precipitate in response to cooling of hydrothermal fluids, as a result of boiling and destabilization of $Al(OH)^-$.

Adularia crystal morphology can also be used to determine modes of deposition. Tabular and rhombic adularia (as defined by Dong and Morrison, 1995) are both recognized at Kencana, though tabular adularia is less common. Rhombic crystal morphologies indicate rapid crystallization (as a result of boiling), whereas tabular adularia mineralization results from violent boiling (Dong and Morrison, 1995). The association of adularia with microcrystalline quartz in type 9 veins provides further evidence for cyclic boiling events in the main ore stages at Kencana.

4.5 Distribution and timing relationships of Kencana infill types

Determination of vein stratigraphy is important in establishing the time-space relationships of individual mineralizing pulses. Distribution of vein and breccia infill types at Kencana was determined for the K1 vein using underground mapping observations and interpretation of SiroVision™ images of underground mine faces (Fig. 4.10). Sirovision™ is a photogrammetric data acquisition tool originally developed by CSIRO, which generates highly accurate and scaled 3D images of rock faces in open pit and underground mines. Structural information can be digitally mapped directly on to the surface of the 3D models. As the system can generate 3D mosaics of entire rock walls, it is possible to map large scale structures that may traverse an entire wall as opposed to trying to collate many pieces of paper. Mapping in 3D reduces mapping bias, in that all orientations of structures can be seen, as opposed to 2D manual mapping which produces a bias towards perpendicular oriented structures (CAE Mining, 2013).

SiroVision™ simultaneously utilises two off-the-shelf digital SLR cameras. As different fixed focal length lenses can easily be interchanged, the system is extremely flexible in terms of what resolution can be achieved at ranges between 3 to 2000 meters. The SiroVision™ unit used in underground mines contains two cameras and a flash, as well as its own ambient light system, targeting lasers and an integrated touch screen computer. It is designed to take left and right photographs in synchronisation with a flash gun. This means an entire heading can be captured in only a few minutes. In order to create accurately scaled 3D images, 3 basic rules apply:

1. A left and right photograph of the same rock face must be taken to produce a stereopair.
2. The left and right photographs must have a baseline (distance between camera positions) at very roughly a ratio of 1:7 to the distance to the rock face.
3. In order to mosaic 3D images together, adjacent stereopairs must overlap by around 30%. (CAE Mining, 2013).

Sirovision™ delivers an angular accuracy in terms of dip angle and dip direction of structures of less than 0.5 degrees at any distance up to 2000 meters. Angular measurements are calculated by mathematical algorithms which eliminate the human errors introduced by manual mapping.

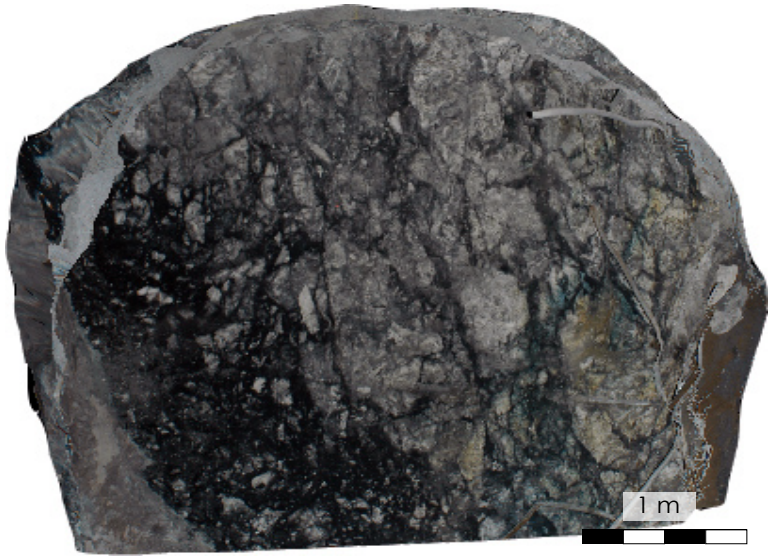

Sub6 SL03 N018

A) Massive crystalline quartz breccia (type 6b) cemented by black quartz-molybdenite infill (type 11).

Sub5 UA06 N009

B) Massive crystalline and weakly crustiform banded quartz veins with angular wall-rock breccia fragments, cross-cutting early crystalline quartz stockwork in altered wallrock.

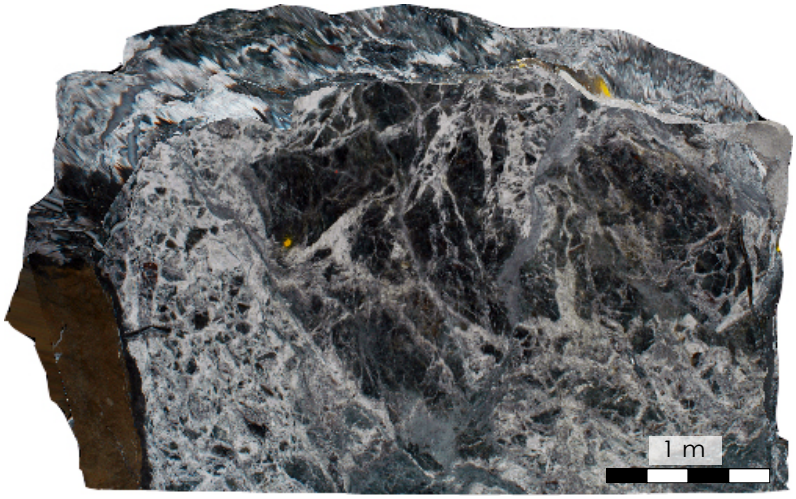

Sub5 SL04 S005

C) Altered wallrock jigsaw breccia (centre) cemented by massive crystalline quartz, with subsequent quartz-cemented breccia with smaller, rotated wallrock fragments (left).

Fig. 4.10 K1 vein textures SiroVision™ images displaying typical textures and infill type characteristics in the K1 vein.

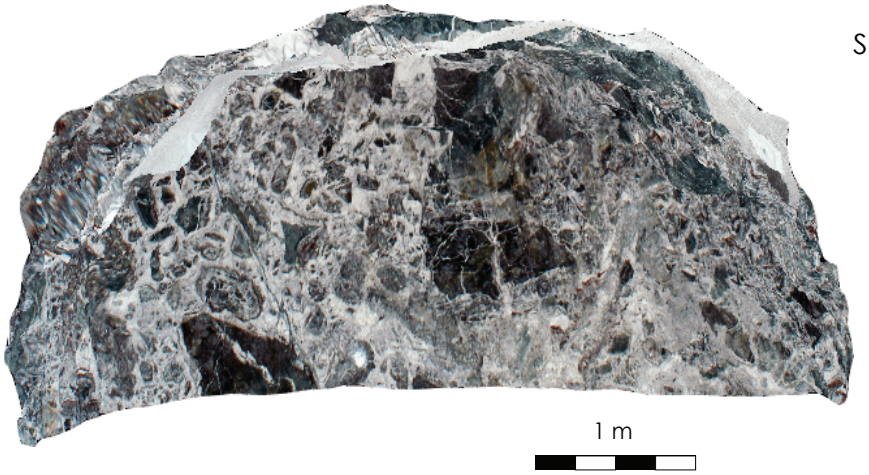

Sub5 SL03 S010

D) Multiple brecciation phases: Quartz-cemented altered andesite breccia (type 3b) centre right) with cockade banded quartz-chlorite wallrock breccia (type 8, left), crosscut by later crustiform banded type 7 quartz-chlorite mineralization located along fractures.

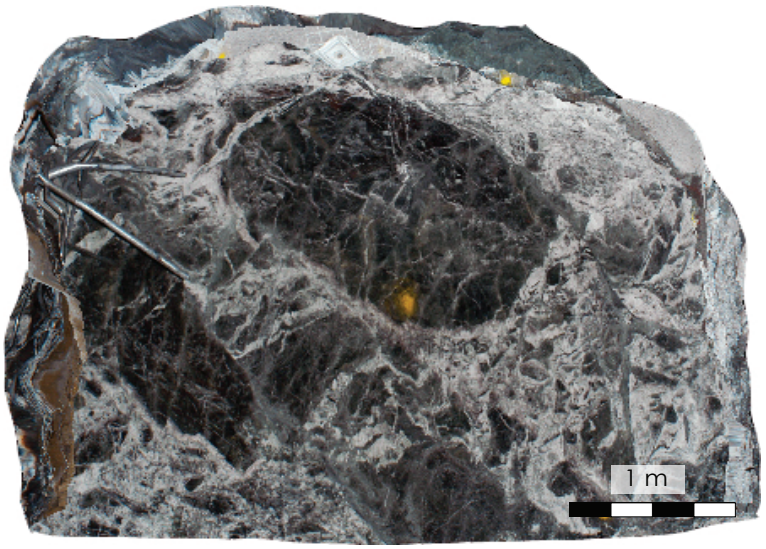

Sub5 SL04 S003

E) Massive to banded quartz-cemented, jigsaw-fit to rotated altered andesite breccia (large clasts with quartz stockwork).

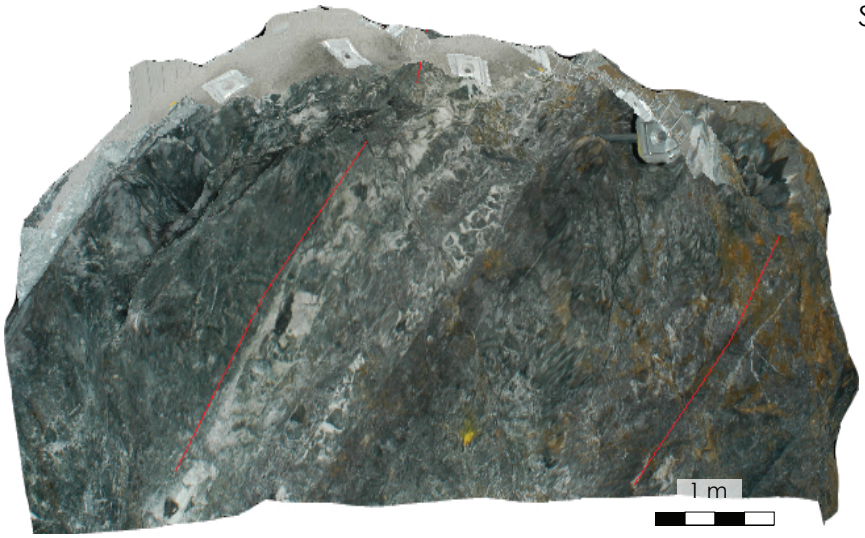

Sub3 UB01 S008

F) Multiple brecciation phases: Parallel veins displaying quartz-cemented wallrock breccias (types 3a and 3b), crystalline quartz stockwork in altered wallrock (type 2) and cockade banded quartz-chlorite wallrock breccia (type 8) with late type 11 stringer veins (left).

Fig. 4.10 cont. K1 vein textures SiroVision™ images displaying typical textures and infill type characteristics in the K1 vein.

Fig. 4.11 A Examples of vein type interpretation and textural distribution in the K1 vein, highlighting the various breccia and vein types and crosscutting relationships observed from SiroVision™ images and underground mapping of the K1 vein.

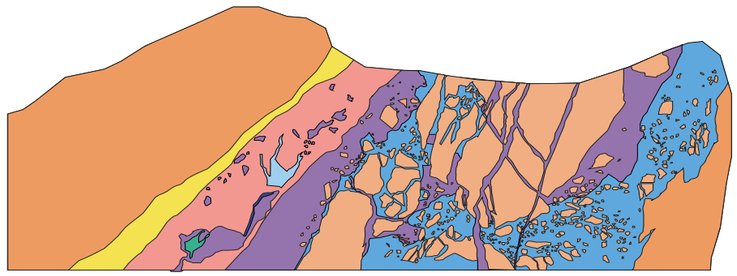

Sub6 UC3S OD01 033 Jigsaw-fit quartz-stockworked breccia fragments (top centre) cemented by massive crystalline quartz infill and later cockade banded quartz-chlorite breccia with quartz-stockworked rotated breccia fragments. Minor discontinous banded quartz-chlorite, quartz-adularia and black quartz-molybdenite veins are present croscutting wallrock breccia to the left of the face.

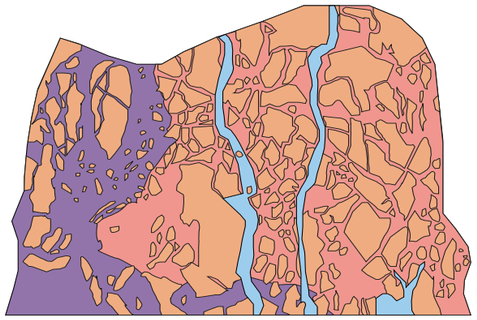

Sub7 UA02 N 017 Jigsaw-fit wallrock breccia (clasts with quartz stockwork 25%) cemented by crystalline quartz. All breccias crosscut by sub-vertical quartz-adularia veins.

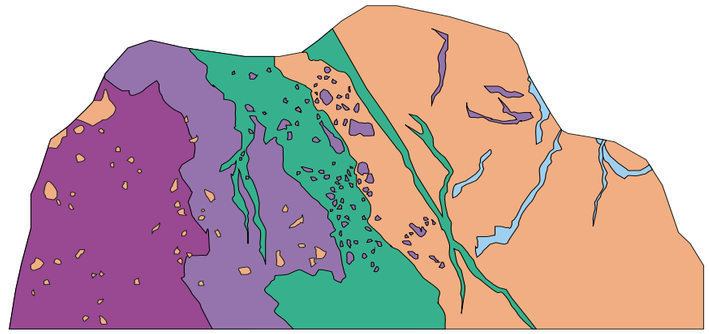

Sub5 UC3 N OD2 029 Sub-parallel red chalcedony, crystalline quartz and black quartz-molybdenum (type 11) veins and breccias (left) with thin veins and veinlets of type 9 and 11 infill in quartz-stockworked wallrock (right).

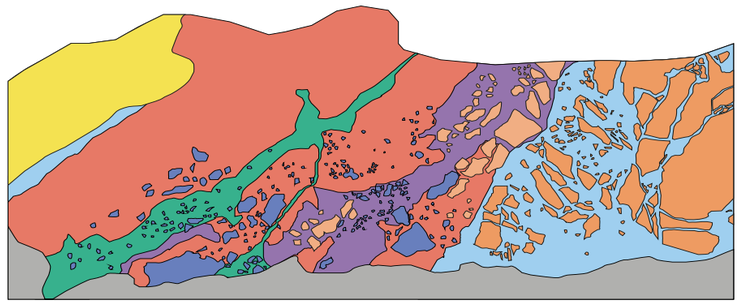

Sub6 UC3S OD01 024 Sub-parallel veins and wallrock and crystalline quartz breccias (cemented by crystalline quartz and quartz-adularia infill), crosscut by type 11 mineralization.

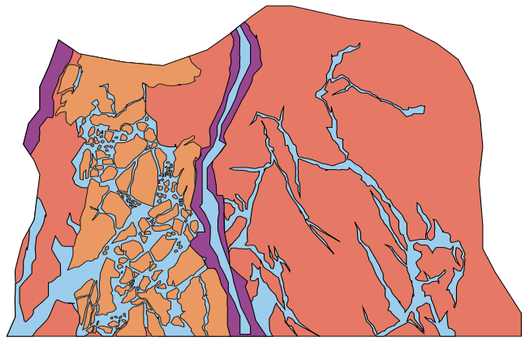

Sub6 UC3S OD01 005 Jigsaw-fit to rotated wallrock breccia cemented by quartz-adularia infill (left) with crystalline quartz cemented wallrock breccia (right) crosscut by quartz-adularia stockwork veins. Central vein filled with type 4 red chalcedony and quartz-adularia.

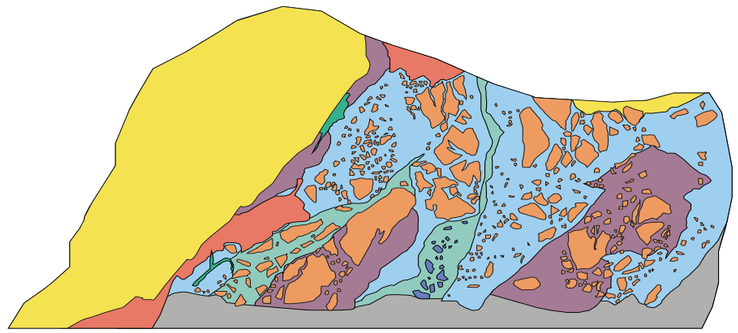

Sub6 UC3S OD01 027 Voluminous bended quartz-adularia infill with quartz-stockworked wallrock breccia fragments, with minor crystalline quartz and quartz-cemented wallrock breccia. Quartz-adularia mineralization is crosscut by type 10 veins, and the latest stage of infill is represented by thin, discontinuous type 11 veins. Footwall contact between wallrock and crystalline quartz phases (left).

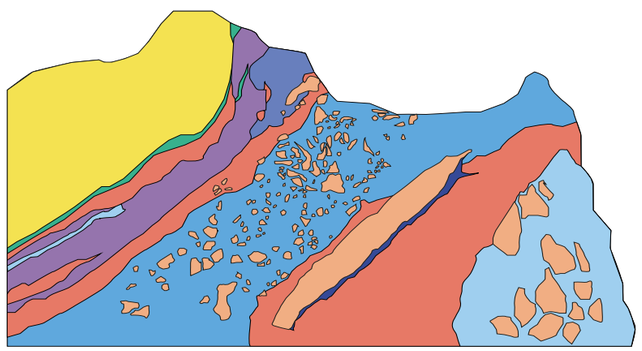

Sub5 UA01 S 048 Sub-parallel veins and quartz-chlorite breccia with subangular wallrock clasts (with 25% quartz stockwork).

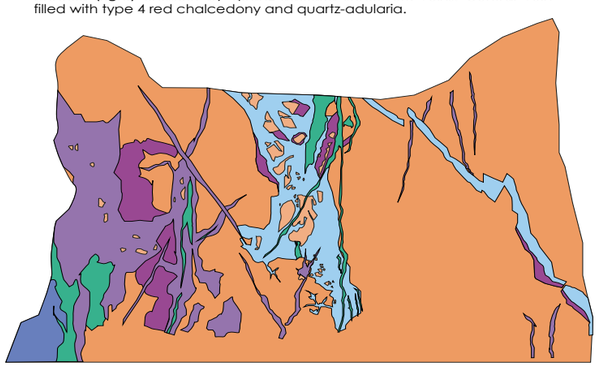

Sub7 UA02 N 005 Wallrock breccia with 40% quartz stockwork, crosscut by multiple phases of crystalline quartz veins (type 5), red chalcedony veins (type 4), quartz-adularia veins (type 9) and black-quartz molybdenite (type 11) veins.

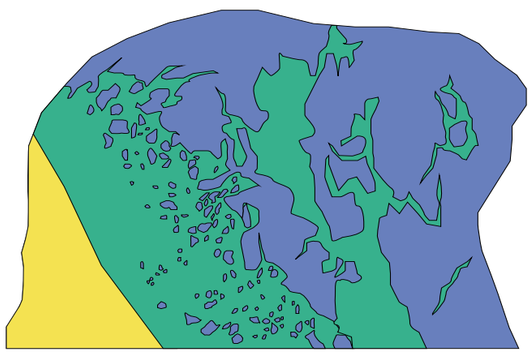

Sub6 UC3S N018 Massive crystalline quartz breccia (type 6b) cemented by type 11 infill. Hangingwall contact between wallrock (type 1) and type 11 infill.

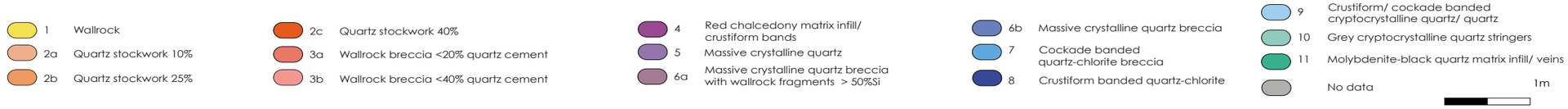

Data were collected for one undercut each to the north and south for sub-levels 2-8 in the K1 vein. SiroVision™ images were collected from the Newcrest database. Where possible, the faces were mapped underground by the author. Where mine faces could not be accessed, or for those cuts that had been mined previous to the author's fieldwork, underground maps by on site geologists were obtained for comparison with the SiroVision™ images. Due to the high resolution of the images, detailed textural and mineralogical information could be determined. Quartz percentages and cross cutting relationships were determined visually as no quantitative measurement is given by the SiroVision™ technology. Where possible, vein types and textures were mapped every 1-3 faces along each underground cut; however, inability to access several areas of the mine and lack of suitable images for textural analysis (lower resolution images, or images affected by difficult underground conditions such as high temperature and humidity) are reflected by gaps in the data. Successive faces along an underground cut are typically laterally separated by 3-5 m. Interpretation of the distribution of vein textures between successive faces has not been made due to the highly variable nature of vein types and the abundance of small faults offsetting the structure. Examples of vein type interpretation face maps are displayed in Fig. 4.11 A, and all face maps are in the appendix.

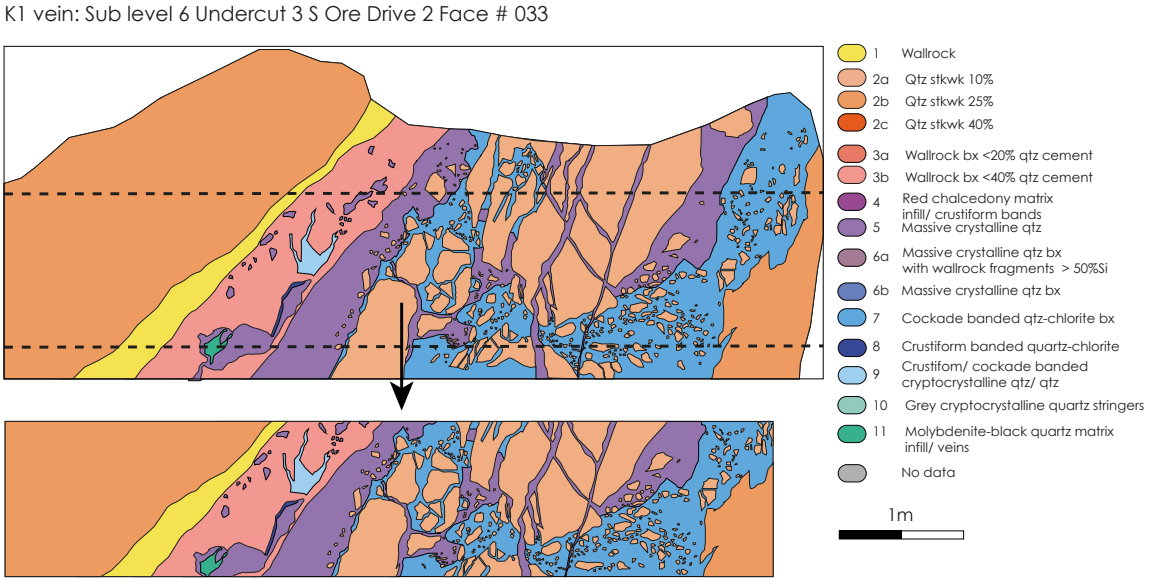

Fig. 4.11 B Examples of face map 'slice' construction derived from mapped faces in the K1 vein. Representative slices were selected for each face between 1-3 metres from the floor of the cut, and where all vein types and textural variations present in the face are included. The area between the dashed lines on the face map was used for Sub level 6 undercut 3 S Ore Drive 2 face #033, and edges trimmed to produce the slice used in the face map plans.

K1 vein: Sub level 2 Undercut 1 N

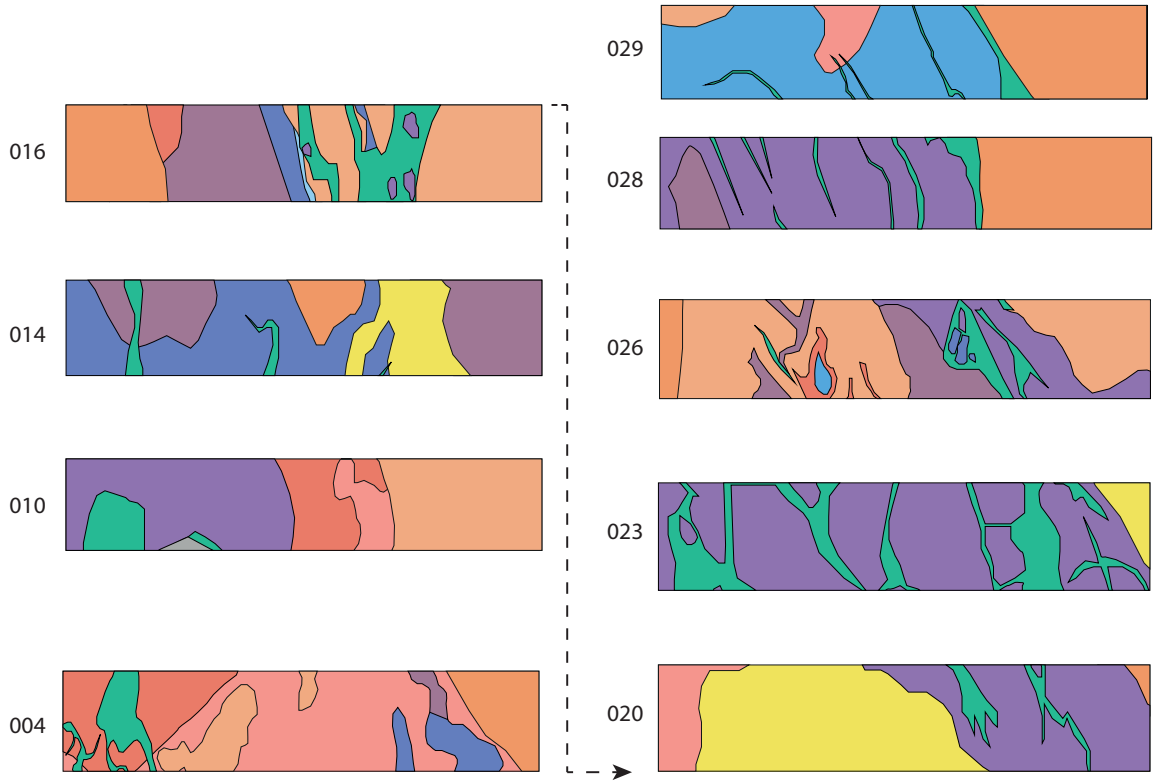

1 Wallrock
2a Quartz stockwork 10%
2b Quartz stockwork 25%
2c Quartz stockwork 40%
3a Wallrock breccia <20% quartz cement
3b Wallrock breccia <40% quartz cement
4 Red chalcedony matrix infill/ crustiform bands
5 Massive crystalline quartz
6a Massive crystalline quartz breccia with wallrock fragments > 50%Si
6b Massive crystalline quartz breccia
7 Cockade banded quartz -chlorite breccia
8 Crustiform banded quartz-chlorite infill
9 Crustifom/ cockade banded cryptocrystalline quartz / quartz infill
10 Grey cryptocrystalline quartz stringers
11 Molybdenite-black quartz matrix infill/ veins
No data

Fig. 4.12 Vein type interpretation floor map Sub2 UC01 N highlighting the various breccia and vein types and crosscutting relationships. The cut is dominated by crystalline quartz and quartz-stockworked wallrock, with numerous cross-cutting type 11 veins and stringers in crystalline quartz.

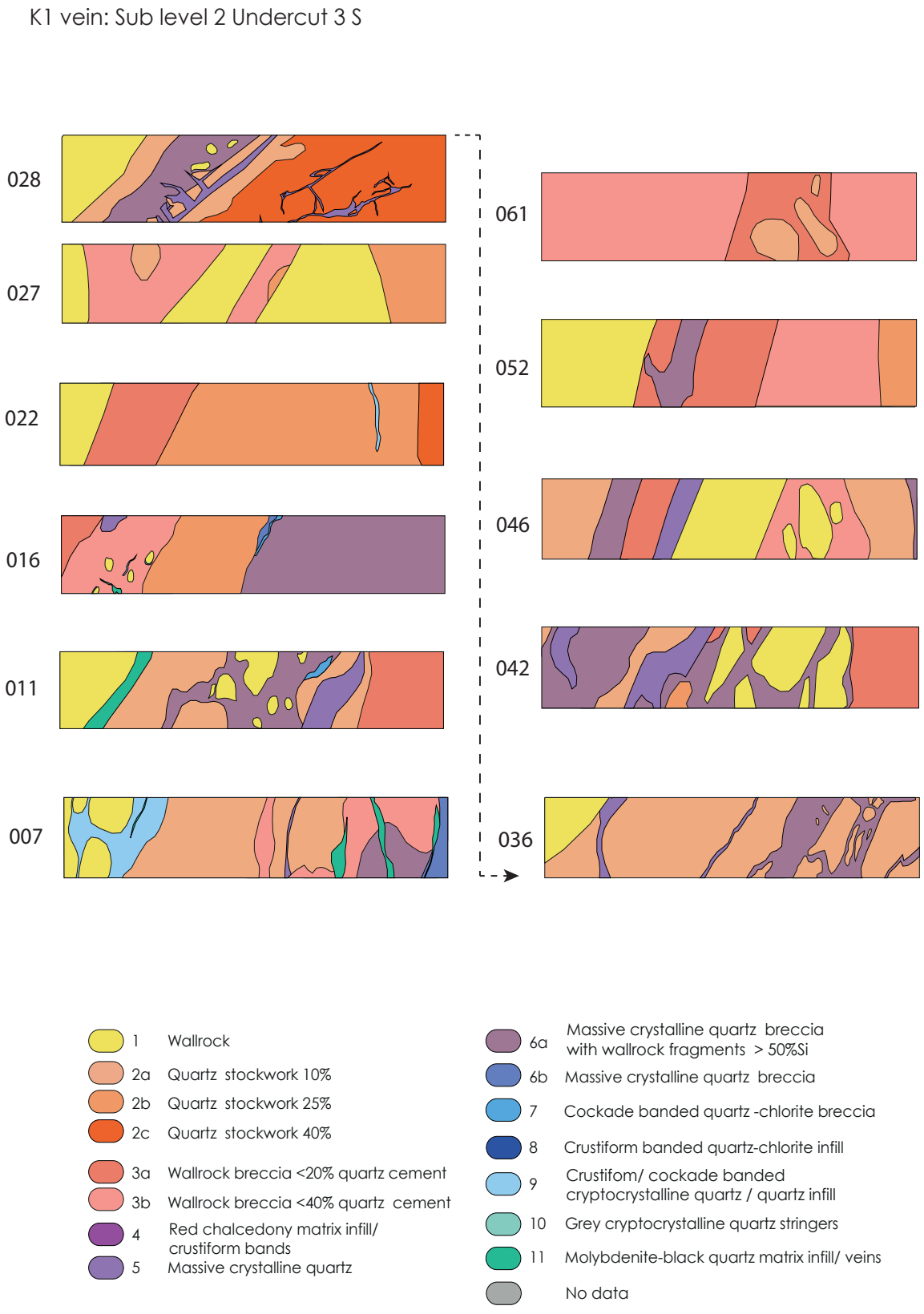

Fig. 4.13 Vein type interpretation floor map Sub2 UC03 S highlighting the various breccia and vein types and crosscutting relationships. The cut is dominated by quartz-stockworked wallrock and quartz-cemented wallrock breccias (types 2 and 3) crosscut by multiple phases of crystalline quartz veins (types 5 and 6) and minor banded quartz-adularia veins (type 9). Brecciation is limited and textures typically represent incremental vein opening.

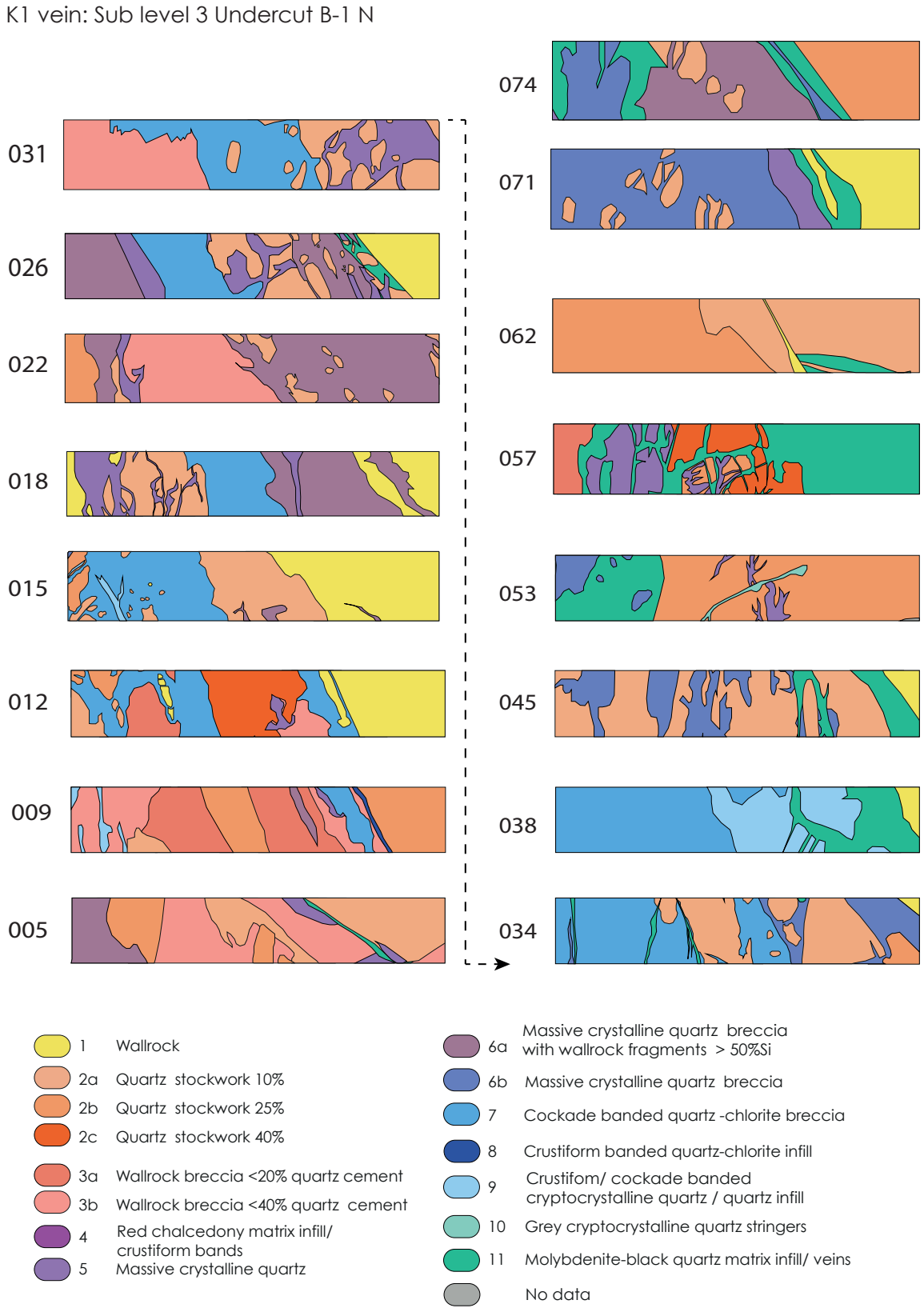

Fig. 4.14 Vein type interpretation floor map Sub3 UCB-1 N highlighting the various breccia and vein types and crosscutting relationships. The cut shows a complex sequence of vein types with sequential opening of thick cockade banded quartz-chlorite breccia veins (type 7) toward the centre of the vein. Type 11 veins and stockworking are common from face #053 to the end of the cut, with increased abundance of type 8 infill from face #034.

K1 vein: Sub level 3 Undercut B-1 S

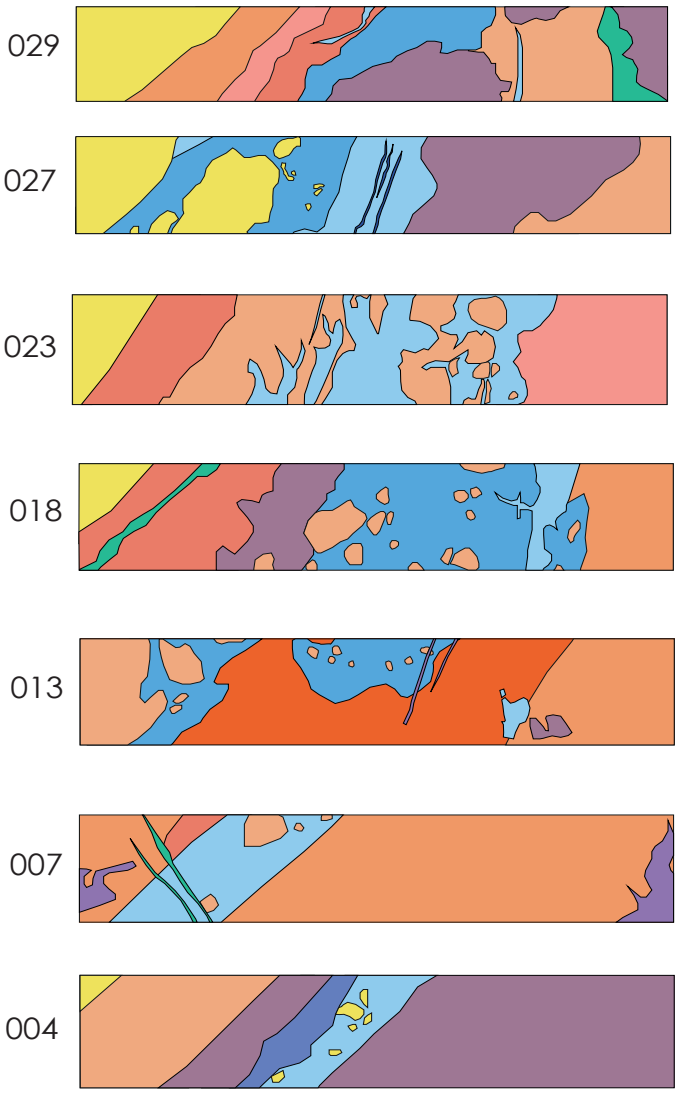

1 Wallrock
2a Quartz stockwork 10%
2b Quartz stockwork 25%
2c Quartz stockwork 40%
3a Wallrock breccia <20% quartz cement
3b Wallrock breccia <40% quartz cement
4 Red chalcedony matrix infill/ crustiform bands
5 Massive crystalline quartz
6a Massive crystalline quartz breccia with wallrock fragments > 50%Si
6b Massive crystalline quartz breccia
7 Cockade banded quartz -chlorite breccia
8 Crustiform banded quartz-chlorite infill
9 Crustifom/ cockade banded cryptocrystalline quartz / quartz infill
10 Grey cryptocrystalline quartz stringers
11 Molybdenite-black quartz matrix infill/ veins
No data

Fig. 4.15 Vein type interpretation floor map Sub3 UCB-1 S highlighting the various breccia and vein types and crosscutting relationships. A clear opening sequence of sub-parallel veins and breccias from stockwork - wallrock breccia - crystalline quartz - cockade banded quartz-chlorite breccia - quartz-adularia infill - black quartz-molybdenite can be observed along the cut.

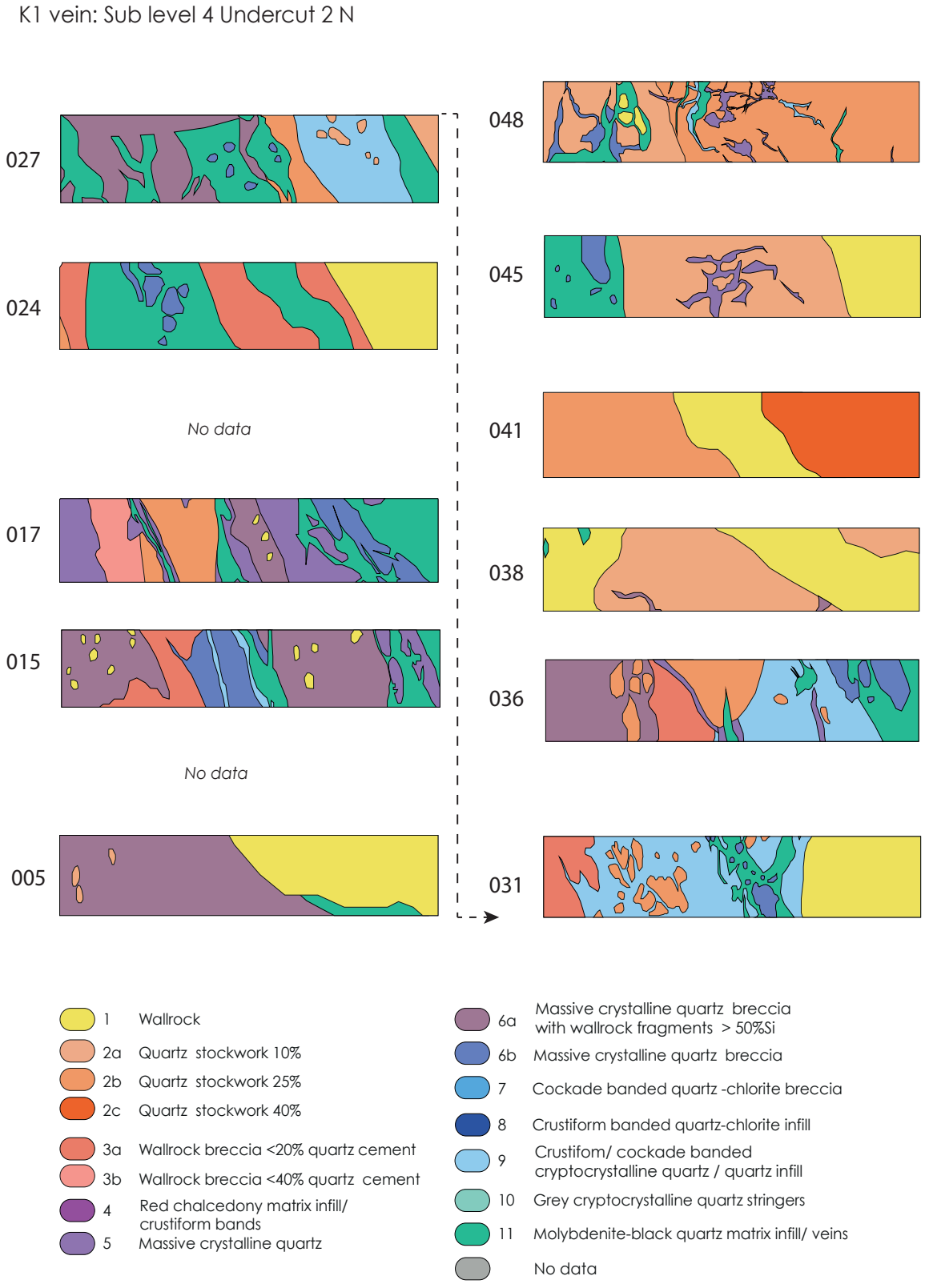

Fig. 4.16 Vein type interpretation floor map Sub4 UC02 N highlighting the various breccia and vein types and crosscutting relationships. The southern end of the cut is marked by voluminous, laterally continuous type 6a breccias and type 11 veins, with an increase in type 9 infill toward the central section of the cut (faces #027-#036). Quartz veins become thinner and more discontinuous to the north, with an increase in abundance of wallrock and quartz stockwork.

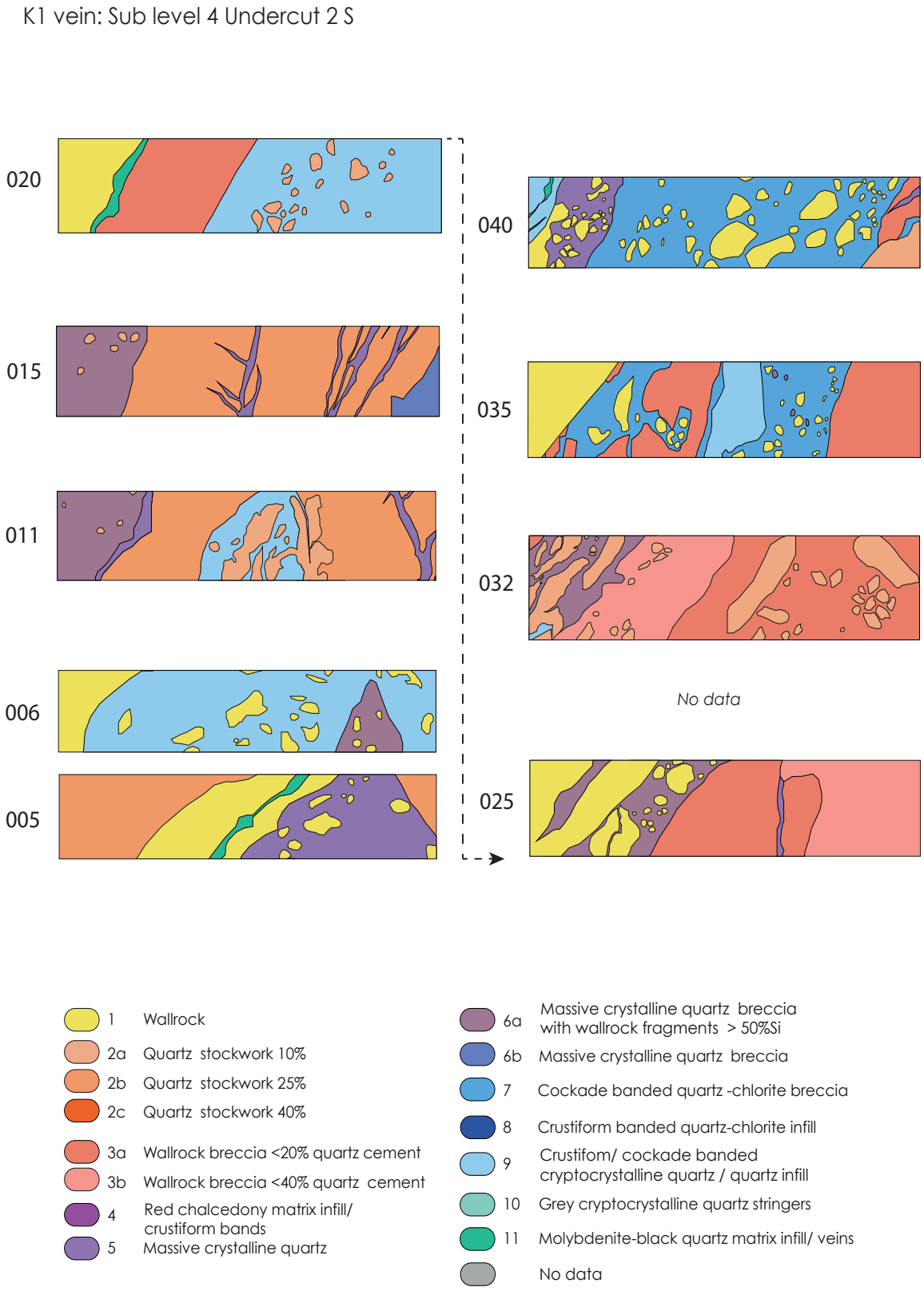

Fig. 4.17 Vein type interpretation floor map Sub4 UC02 S highlighting the various breccia and vein types and crosscutting relationships. A wide range in textural variation is present, with a general transition from simple-vein dominated textures to more complex breccias along the cut. Type 7 mineralization hosted in type 3a wallrock breccia becomes volumetrically significant from face #035. Distribution of type 9 infill is sporadic but is most significant in faces #006 and #020.

K1 vein: Sub level 5 Undercut 3 N Ore Drive 2

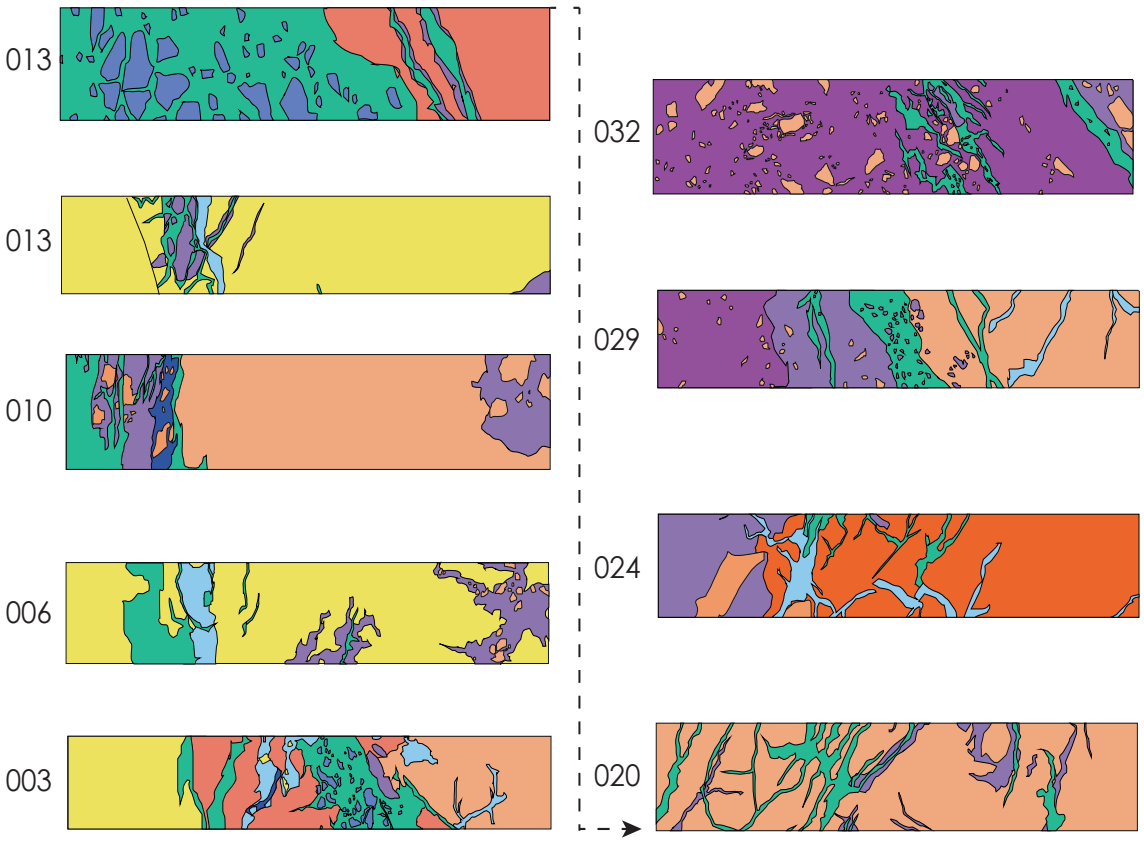

1 Wallrock
2a Quartz stockwork 10%
2b Quartz stockwork 25%
2c Quartz stockwork 40%
3a Wallrock breccia <20% quartz cement
3b Wallrock breccia <40% quartz cement
4 Red chalcedony matrix infill/ crustiform bands
5 Massive crystalline quartz
6a Massive crystalline quartz breccia with wallrock fragments > 50%Si
6b Massive crystalline quartz breccia
7 Cockade banded quartz -chlorite breccia
8 Crustiform banded quartz-chlorite infill
9 Crustifom/ cockade banded cryptocrystalline quartz / quartz infill
10 Grey cryptocrystalline quartz stringers
11 Molybdenite-black quartz matrix infill/ veins
No data

Fig. 4.18 Vein type interpretation floor map Sub5 UC03 N OD02 highlighting the various breccia and vein types and crosscutting relationships. Complex crosscutting veins and veinlets infilled with types 5, 8, 9 and 11 hosted in wallrock and quartz-stockworked wallrock are common, with volumetrically significant type 4 infill dominating the northern end of the cut.

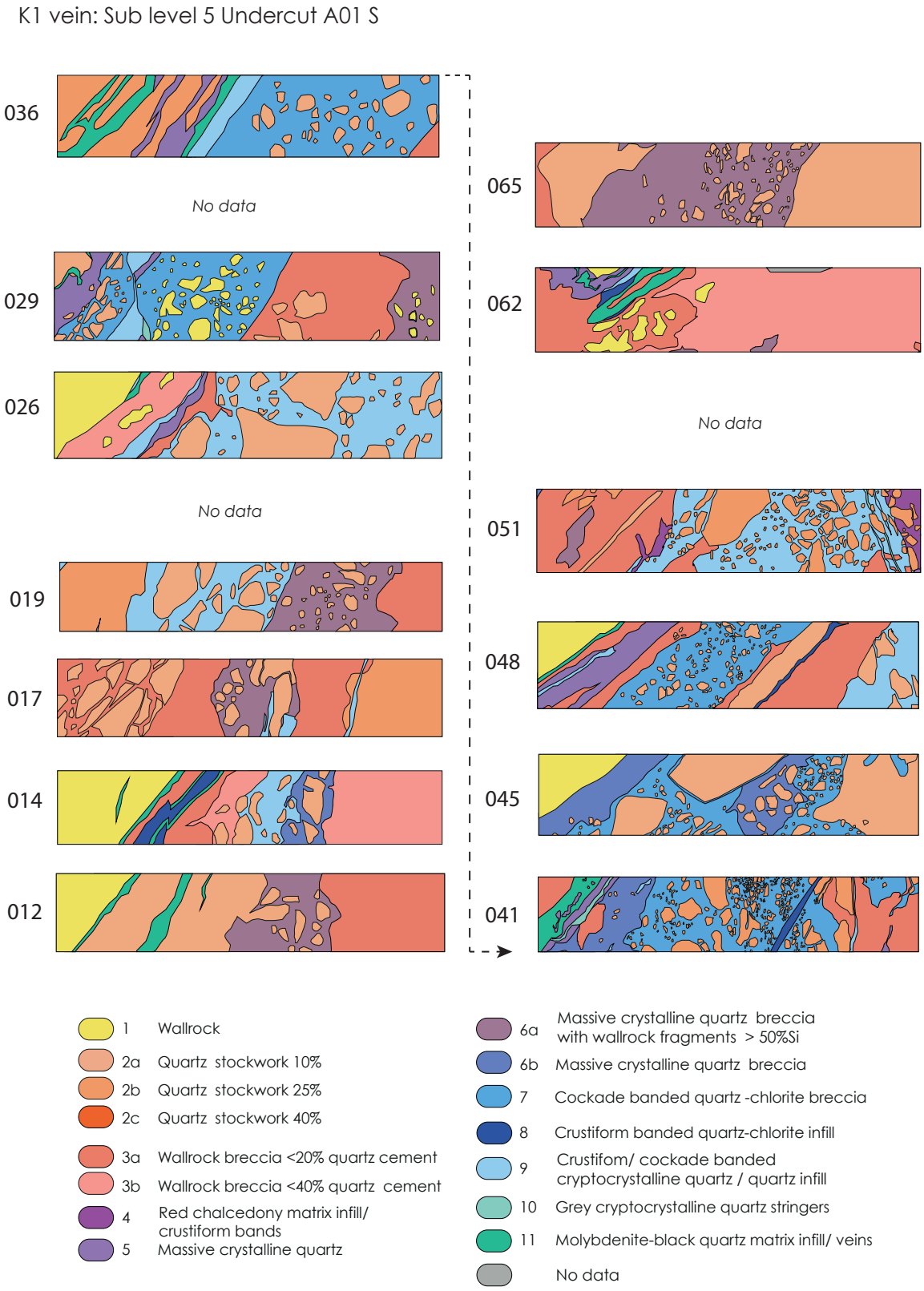

Fig. 4.19 Vein type interpretation floor map Sub5 UCA-01 S highlighting the various breccia and vein types and crosscutting relationships. A wide variety of crosscutting veins and complex breccias are present. All 11 vein types are represented along the cut, with volumetrically significant type 3, 7 and 9 mineralization. Thin type 11 veins are common along the footwall margin.

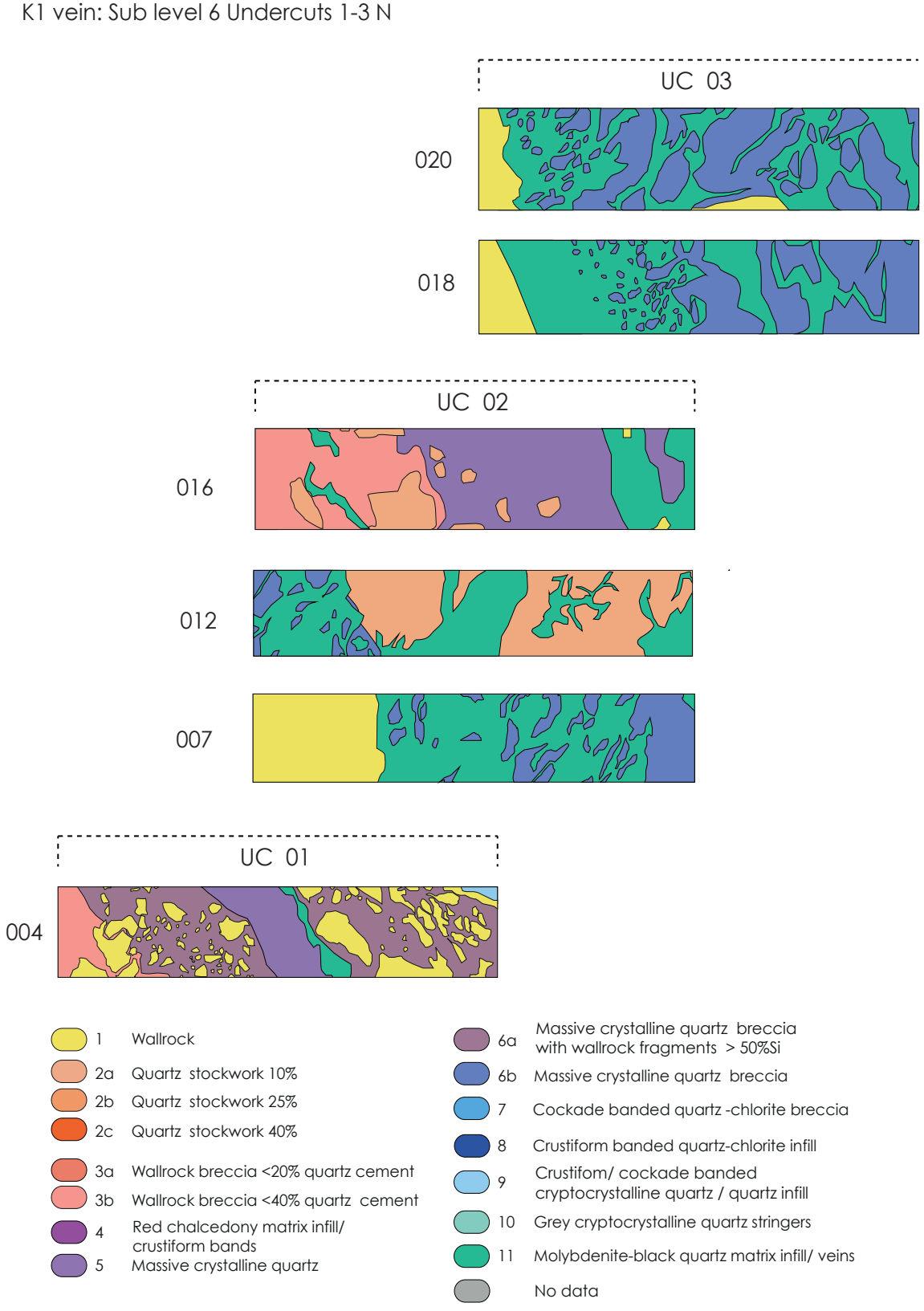

Fig. 4.20 Vein type interpretation floor map Sub6 UC1-3 N highlighting the various breccia and vein types and crosscutting relationships. Undercut 1 displays abundant massive crystalline quartz and crystalline quartz breccia with wall-rock fragments, and minor veins infilled with type 9 and 11 mineralization. Undercuts 2 and 3 are dominated by late-stage type 11 breccia infill with massive crystalline quartz fragments.

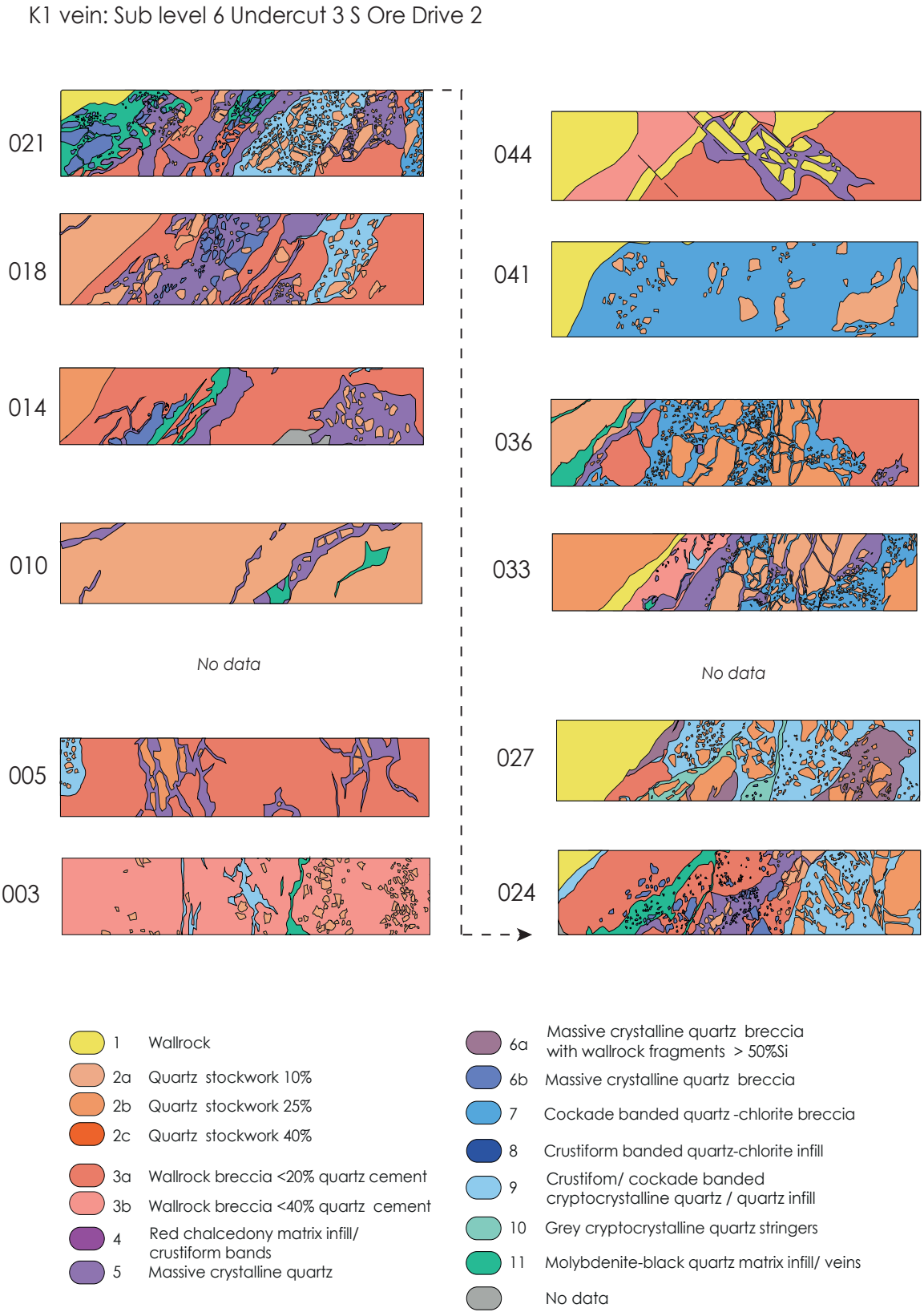

Fig. 4.21 Vein type interpretation floor map Sub6 UC3 S OD02 highlighting the various breccia and vein types and crosscutting relationships. A complex sequence of veins and breccias is present along the cut, with all vein types represented (excluding type 4). Wallrock breccia and quartz-stockworked wallrock with minor crystalline quartz veins dominate between faces #003 to #014, with a transition to voluminous type 7 and 9 cemented jigsaw-fit breccias (faces #018 to #041).

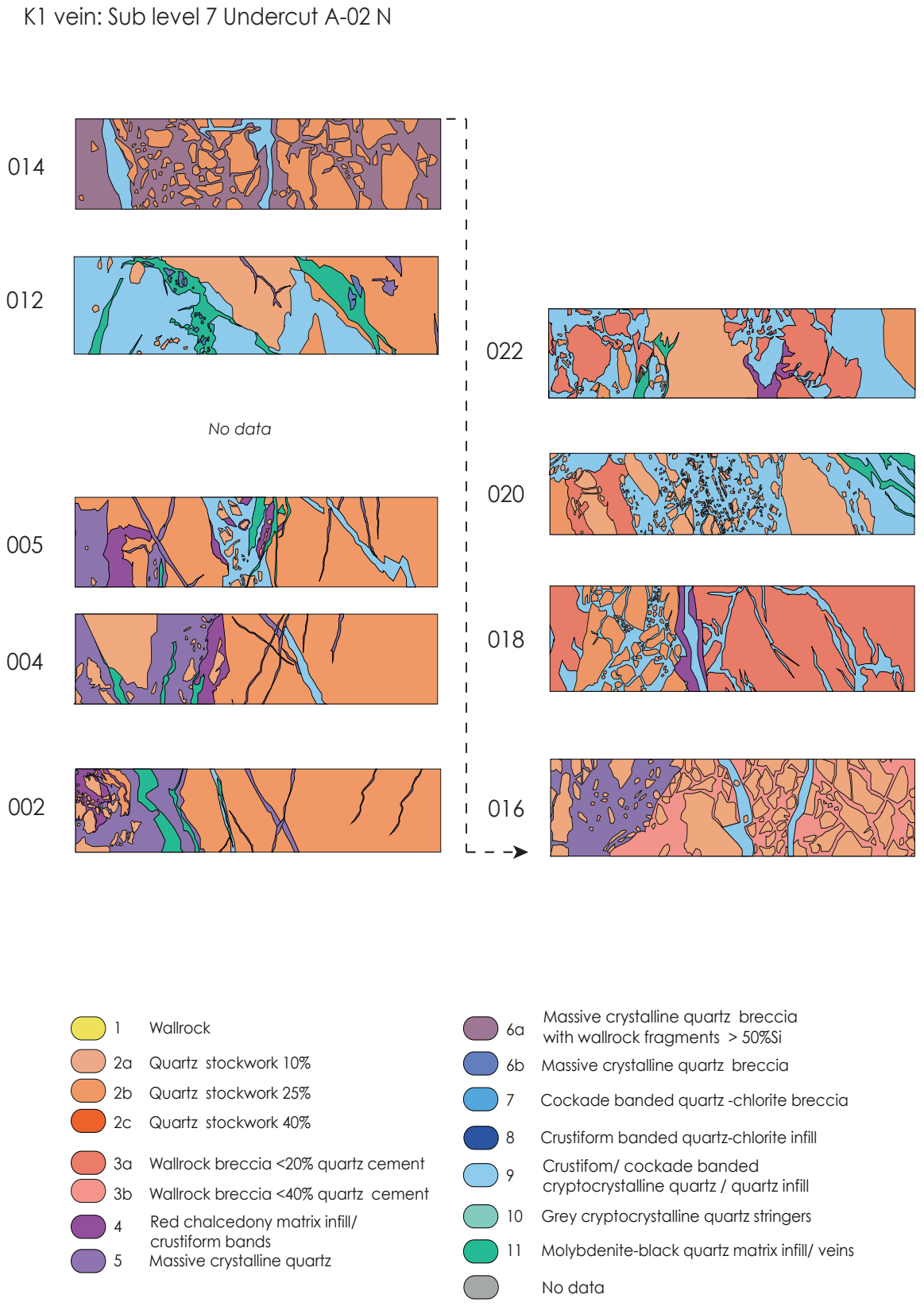

Fig. 4.22 Vein type interpretation floor map Sub7 UCA02 N highlighting the various breccia and vein types and crosscutting relationships. Progressive dilation of type 9 veins hosted in wallrock breccias and crosscutting red chalcedony and massive crystalline quartz phases (type 5 and 6a) is evident along the cut. Some late type 11 veins crosscut type 5 and 9 infill and occasionally contain type 8 fragments.

K1 vein: Sub level 7 Undercut A-A S Sill 3

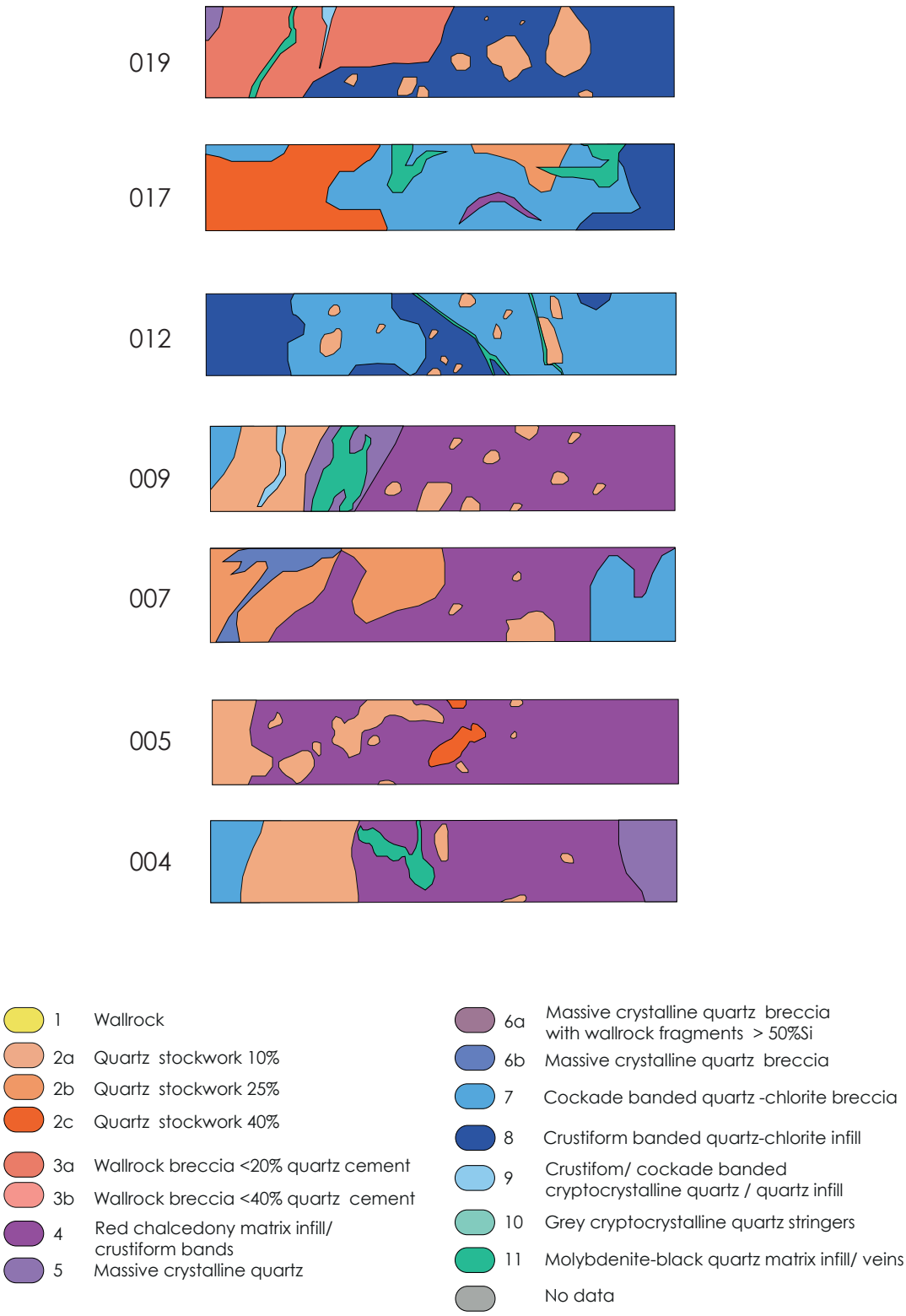

Fig. 4.23 Vein type interpretation floor map Sub7 UCA02 N highlighting the various breccia and vein types and crosscutting relationships. The northern section of the cut (faces #004 to #009) are dominated by type 4 infill cementing quartz-stockworked breccia fragments. Type 4 infill is largely absent south of face #009, with voluminous quartz-chlorite mineralization (type 7 and 8) and thin,crosscutting type 11 veins.

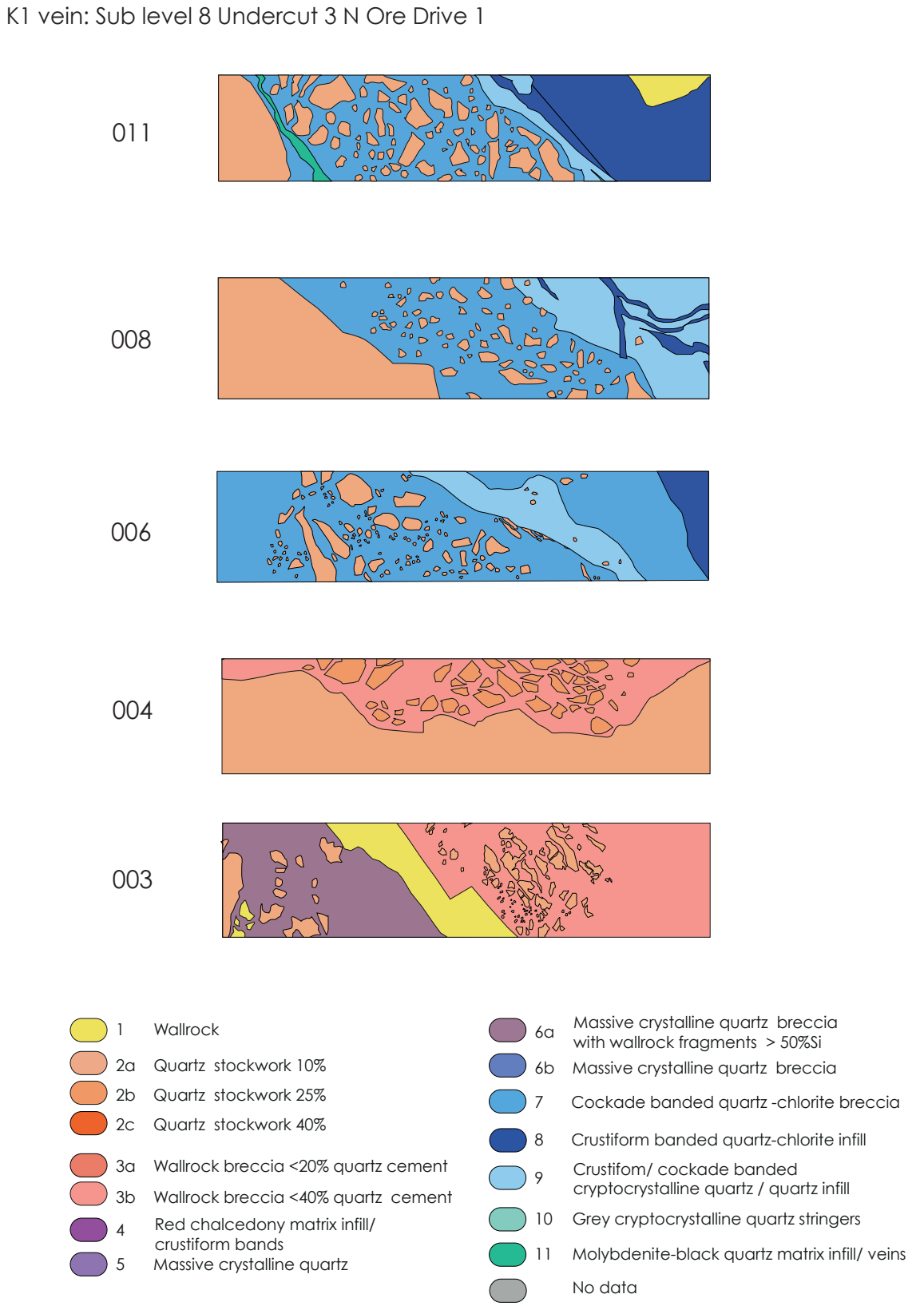

Fig. 4.24 Vein type interpretation floor map Sub7 UCA02 N highlighting the various breccia and vein types and crosscutting relationships. Faces #003 and #004 are dominated by wallrock breccias and quartz stockwork, with minor crystalline quartz. Faces #006-#011 are characterized by abundant quartz-chlorite infill and breccias (type 7 and 8) with type 9 veins. Mnor type 11 infill occurs near the hangingwall contact on face #011.

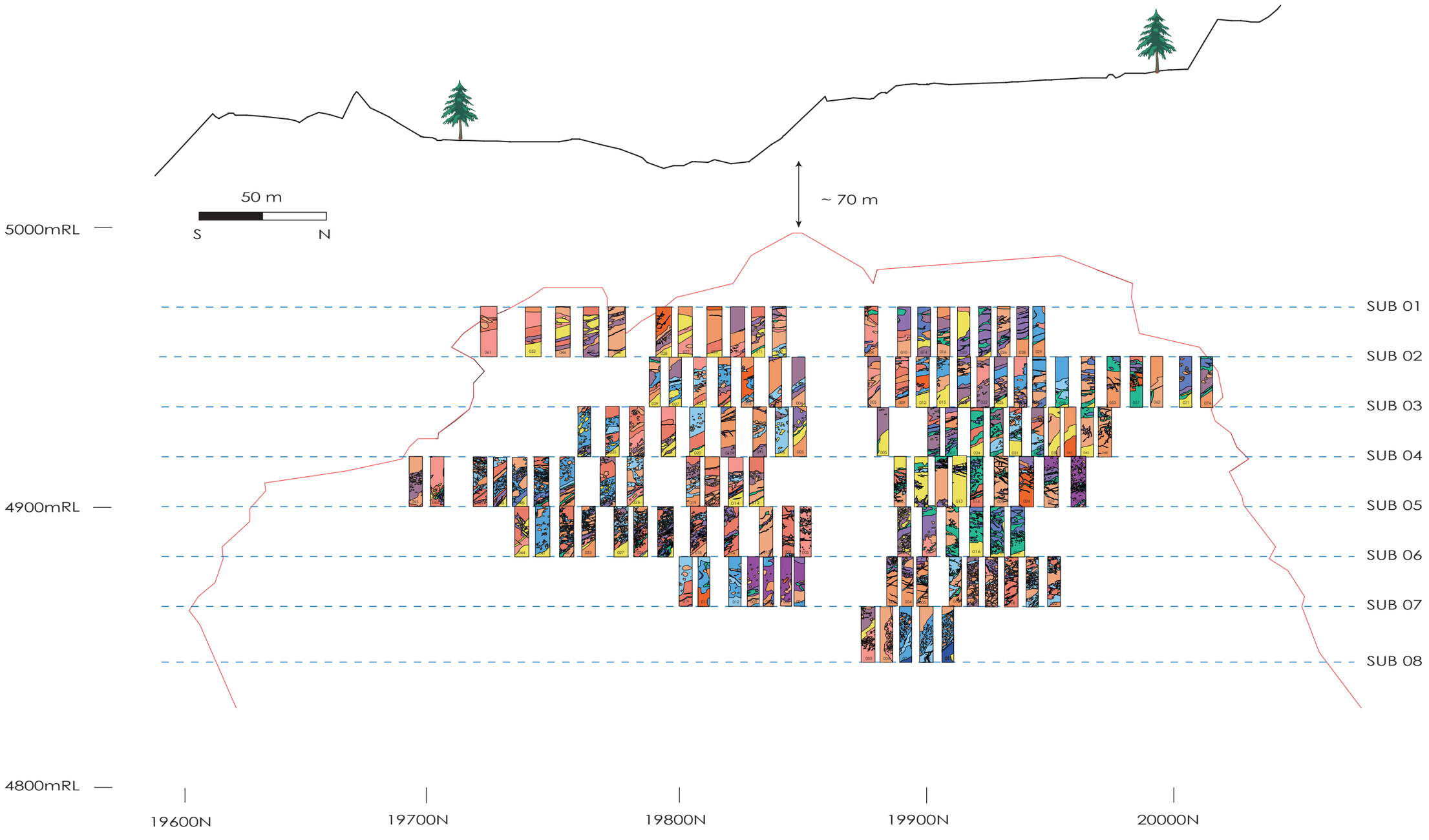

Fig. 4.25 Distribution of infill types in the K1 vein highlighting the distribution of infill types and textures across the structure. Simple veining and sequential opening sequences are observed towards the margins of the vein, with increasingly complex crosscutting relationships and intense brecciation with depth. Red outline = vein boundary; blue dashed lines = sub-level traces.

Face map plans displaying the lateral variation in vein textures and types along each undercut were constructed by selecting a representative "slice" (Fig. 4.11 B) from each mapped face (between 1-3 metres from the floor of the cut, and containing all vein types and textural variations present in the selected face) and placing these in sequence along the cut (Figs. 4.12-4.24). These plans are used to infer a paragenetic sequence for mineralization in the K1 vein based on the type of vein or breccia infill, the composition and degree of alteration of breccia fragments, fragments of pre-existing vein types in later veins or breccias, composition of breccia matrix, sequences of mineralization within crustiform banded packages, and crosscutting relationships (Gemmell et al., 1988). Face maps were plotted along the long section for the K1 orebody to show the vertical and lateral vein type distribution (Fig. 4.25), where the maps for individual faces are displayed rotated to the vertical for ease of presentation.

4.6 Discussion of distribution and timing relationships of Kencana infill types

The distribution and timing relationships of Kencana vein types are summarized in Table 4.1. The horizontal and vertical extent of distribution for each vein type is variable. Infill types may persist over distances of up to 300 m or may change significantly over distances of <5 m. Generally, the shallow levels of the system show a simpler dilation and infill sequence, becoming increasingly complex with depth, where greater dilation and multiple phases of intense brecciation produce complex textures and relationships between vein types.

The K1 vein shows a broad textural zonation from north to south. Types 1, 2 and 3 are distributed throughout the deposit and are particularly prevalent on the margins of the vein. Types 7, 8 and 9 are the main ore-bearing stages and form the bulk of the central section of the vein, particularly below 4950mRL (Fig. 4.25). These infill types are rarely visible above sub-level 2. Type 11 infill is most prevalent to the north of 19900mN, between 4950mRL and 4880mRL (Fig. 4.25). Types 4, 5, 6 and 10 are variably and sporadically distributed across the vein.

Brecciation is greatest below 4900mRL, as determined by the greatest abundance of

Vein type	Description	Distribution	Paragenesis	Interpretation
TYPE 1 (WALLROCK)	- Coherent wallrock material >50 cm (within vein) or in situ marginal lithologies hosting epithermal structure - Some highly concentrated fluidised material (finely comminuted sand/silt paricles) - Variable lithology, often strongly illite + pyrite + chlorite ± epidote ± adularia altered	- Vertically and laterally present (hangingwall and footwall) - Hosts epithermal vein - Commonly forms breccia clasts	- Pre-dates epithermal mineralization	
TYPE 2 (CRYSTALLINE QUARTZ STOCKWORK)	- Crystalline to microcrystalline quartz - Sheeted and crosscutting veins and veinlets (2 - 80 mm thick) peripheral to main epithermal lode, increasing in intensity, crystallinity and vein thickness towards (K1) vein - Comb quartz to crustiform banded veins (zoned crystals), - Some vuggy amethyst Three sub-groups identified: a) quartz stockwork 10% b) quartz stockwork 25% c) quartz stockwork 25-40% Occurs as both in situ, attached lithologies marginal to vein/ cement assemblages and as breccia clasts, (angular crackle breccias to sub-rounded and rotated clast breccias within several other vein types). No to low Au content. Fluid temperatures range from 203.0 to 248.8°C and salinities range from 0.1 to 0.5 wt% NaCl (equiv.)	- Vertically and laterally widespread across the Kencana system, increasing in intensity towards the main epithermal structures - Most common between sub-levels 1-4, and breccia fragments between sub-levels 8-5 (particularly sub-levels 5 and 6 Southand sub-level 7 North	- Represents first phase of epithermal mineralization at Kencana, - Multiple phases of type 2 mineralization (complex crosscutting relationships)	**Crystalline quartz: Primary growth texture (open space filling and slow cooling of fluids) under stable conditions.** **Fluids slightly supersatured with respect to quartz, undersaturated with respect to chalcedony** **Abundant type 2 material represents zones of constriction within the structure**
TYPE 3 (CRYSTALLINE QUARTZ-CEMENTED WALLROCK BRECCIA	- Sub-angular to angular, jigsaw fit, crackle breccia or rotated clasts of types 1 + 2 (10 cm - 1 m) - White crystalline + micocrystalline quartz cement Two sub-categories identified: a) wallrock breccia <20% quartz cement b) wallrock breccia 20-40% quartz cement	- Vertically and laterally variable - Most commonly associated with type 2 material, most abundant at shallow levels peripheral to the bulk of quartz mineralization (Sub-level 2)	- Deposited during and after deposition of type 2, but prior to types 4-11.	**Type 3a: Represents zones of restricted dilation within the structure; more commonly forms the hangingwall and/ or footwall margins of the vein** **Type 3b has undergone further dilation; also occurs as detached blocks within the vein cemented by later vein types.**

Table 4.1 Summary of vein geology(K1 vein) highlighting vein types, their distribution, paragenesis and implications for conditions of formation

Vein type	Description	Distribution	Paragenesis	Interpretation
TYPE 4 (RED CHALCEDONY INFILL/ CRUSTIFORM BANDS)	- Ultra-fine grained hematitic rock fragments, fluidised mud to silt sized particles, with cryptocrystalline quartz cement - Thin, rhythmic crustiform bands OR forms matrix to banded quartz + cryptocrystalline quartz breccias - Banded type 4: (mm's scale) Associated with clear to milky cryptocrystalline quartz, crystalline quartz, drusy quartz with minor open space and adularia + remobilized, ultra fine grained sulfides - Breccia clasts: Angular to sub-rounded, typically <4 cm, rhythmically banded red chalcedony + cryptocrystalline quartz ± adularia, supported in a matrix of red chalcedony or crustiform banded cryptocrystalline quartz Angular and rotated illite + chlorite + pyrite ± epidote ± illite after adularia altered wallrock breccia clasts <4 cm are also common in type 4.	- Main ore zone below 4900mRL and northward from 19830mN; isolated occurrences known from face #051 Sub-level 5 Undercut A01 South.	- Multiple phases of deposition - Often occurs in association with type 6a and typically contains fragments of type 2 material. - Deposited after type 2 and 3, but episodes of type 4 mineralization occurred both before and after type 5 and 9 infill - Crosscut by types 7 and 11 - Timing relationship with types 6, 8 and 10 undetermined	**Fluidised mud to silt sized particles, remobilized hematitic mudstone material.** **Tectonic brecciation and rhythmic quatz banding reflect variations in structural dynamics**
TYPE 5 (MASSIVE CRYSTALLINE QUARTZ INFILL)	- Crystalline + microcrystalline quartz infill of veins and breccias - Rare sub-angular wallrock fragments (2 - 100 mm) - Rarely present as angular to sub-angular rotated breccia fragments in types 9 and 11 - Massive, mycrocrystalline, andhedral and equigranular quartz to coarser crystals (5 - 40 mm) - Occasionally vuggy or pitted appearance (incomplete replacement of calcite crystals) - Milky white to pale grey, some crude crustiform banding, disseminated adularia - Occasional calcite crystals (<7 mm), some bladed calcite pseudomorphs Forms veins 50 cm to 4 m wide; Au grades ~5 g/T	- One of the most common mineralization stages - Occurs along all sub-levels over the vertical and lateral extent of the deposit.	- Multiple stages of type 5 mineralization - Main stage of deposition occurred after types 2 and 3, during deposition of vein types 4 and 6, and before all other types.	**Increasing rate of crystal nucleation, stable conditions in a rapidly dilating structure** **Adularia and bladed calcite provide evidence for boiling processes** **Au-bearing fluids**
TYPE 6 (MASSIVE CRYSTALLINE QUARTZ BRECCIA)	- Fractured, brittle fragments of type 5 material with angular jigsaw-fit to rotated clasts <50 cm, cemented by subsequent type 5 mineralization	- Type 6a: Most prevalent northward of 19850mN between 4900mRL and 4925mRL, and above 4950mRL Type 6b: Most commonly present as fragmental blocks cemented by vein type 11; spatially most prevalent between 4880mRL and 4960mRL, particularly to the north of 19900mN	- Main stage of deposition occurred after types 2 and 3, during deposition of vein types 4 and 5, and before all other types.	**Multiple phases of brecciation** **Rapid pressure release and rock fragmentation; unloading of the hydrothermal system by tectonic movement or hydraulic release**

Table 4.1 cont.

Vein type	Description	Distribution	Paragenesis	Interpretation
TYPE 7 (COCKADE BANDED QUARTZ-CHLORITE BRECCIA)	- Banded microcrystalline to cryptocrystalline quartz , adularia and very fine-grained dark green chlorite, with sulfide and gold mineralization - Ore minerals form crustiform to colloform bands around breccia clasts - Breccia clasts are composed of types 1, 2, 5, 7 and 9, and cemented by type 8 with later massive crystalline quartz infill - Average grades of >50 g/t to several thousand g/t Au) First phase of mineralization within each depositional sequence contains a concentration of thin (<1 cm), dark green to black chlorite bands interposed with cryptocrystalline quartz and milky microcrystalline quartz, followed by banded cryptocrystalline quartz and adularia. The latest phase of mineralization in each depositional sequence is white massive microcrystalline to crystalline quartz.	- Observed over the full vertical and lateral extent of the deposit from 4950mRL to 4850mRL - Mineralization is laterally continuous over distances of >30 m - Common at the widest parts of the structure, in particular along sections of the structure with low-angle displacement (e.g. Sub-level 8 North) - Fills the central part of the vein and often contains angular and splintery fragments of types 1 and 2 that appear to have been spalled from the vein wall contacts where these types are contiguous	- Deposited after types 1-6. Mineralization occurs both pre- and post-deposition of type 9 infill, though the bulk of type 7 infill is deposited after type 9. Occasional type 7 breccia clasts are included in later phases of type 9 mineralization.	**Cockade bands reflect primary growth textures formed during crystal growth or from the deposition of amorphous silica** **Coarse(r) grained electrum and sulfides than other vein types suggests a slower formation, gradual decrease in temperature.** **Tectonic breciation formed by rapid pressure release in a dilating conduit** **Very effetive mechanism of Au deposition, mixing an important process**
TYPE 8 (CRUSTIFORM BANDED QUARTZ-CHLORITE INFILL)	- Banded microcrystalline to cryptocrystalline quartz , adularia and very fine-grained dark green chlorite, with sulfide and gold mineralization - Ore minerals form crustiform to colloform banded veins (sulfides, sulfosalts, electrum + chlorite) - Average grades of >50 g/t to several thousand g/t Au) First phase of mineralization within each depositional sequence contains a concentration of thin (<1 cm), dark green to black chlorite bands interposed with cryptocrystalline quartz and milky microcrystalline quartz, followed by banded cryptocrystalline quartz and adularia Homogenisation temperatures indicate fluid temperatures 202.7 to 306.9°C and salinities range from 0.0 to 1.0 wt% NaCl (equiv.)	- Common at the widest parts of the structure, in particular along sections of the structure with low-angle displacement (e.g. Sub-level 8 North) - Restricted below 4900mRL, with greatest abundance in the lowest mapped levels of the system (Sub-level 8 North)	- Deposited after types 1-6. Mineralization occurs both pre- and post-deposition of type 9 infill, though the bulk of type 8 infill is deposited after type 9.	**Cockade bands reflect primary growth textures formed during crystal growth or from the deposition of amorphous silica** **Coarse(r) grained electrum and sulfides than other vein types suggests a slower formation, gradual decrease in temperature.** **Very effetive mechanism of Au deposition, mixing an important process**

Table 4.1 cont.

Vein type	Description	Distribution	Paragenesis	Interpretation
TYPE 9 (BANDED CRYPTOCRYSTALLINE QUARTZ + QUARTZ + ADULARIA BRECCIAS AND INFILL)	- Fine to medium-grained, white to greenish-grey crystalline quartz, microcrystalline quartz, cryptocrystalline quartz, and adularia, with illite after adularia, calcite, late amethyst and sulfides - Well-developed, repeated, symmetric to asymmetric crustiform and cockade banding defined mainly by the grain-size and colour variation of cryptocrystalline, microcrystalline and comb texture quartz, the distribution of medium-grained to ultra fine-grained adularia, and dark grey sulfide-rich bands - Angular to sub-angular, rotated wallrock breccia clasts <7 cm cemented by cockade banded crystalline quartz, cryptocrystalline quartz and adularia are common Average Au grade 10-50 g/t Bladed carbonate and bladed carbonate pseudomorphs noted Homogenization temperatures range from 195.8 to 258.7°C and salinities range from 0.0 to 0.8 wt% NaCl (equiv.)	- Vertically and laterally widespread between 4940mRL to 4850mRL - Up to 5 m wide and up to 100 m in the centre of the vein along sub-levels 6 and 7.	- Crosscuts types 1-6 and angular to sub-angular breccia clasts of type 2 from a few cm's to >1 m in diameter. - Majority of type 9 mineralization occurs before types 7 and 8, though some thinner (<70 cm) type 9 veins crosscut type 8 infill. - Type 9 is crosscut by type 10 and 11 veins.	**Voluminous mineralization, high volumes of fluid with effective mechanisms of depositon** **Drops in total confining pressure allow fluids to boil, resulting in loss of volatiles, cooling, increase in pH and deposition of gangue in rhythmic crustiform bands of different mineral compositions** **Boiling inferred as an important process - adularia precipitates in response to cooling of hydrothermal fluids, as a result of boiling and destabilization of Al(OH)-.**
TYPE 10 (GREY CRYPTOCRYSTALLINE QUARTZ STRINGERS)	- Hard, grey cryptocrystalline quartz stringer veins (2-30 cm thick) - Sub-vertical, laterally discontinous veins	- Vertical and lateral distribution of type 10 veins inferred from SiroVisio™ images. - Type 10 is restricted to the south of 19775mN along sub-levels 5 and 6, filling thin (<30 cm) fractures in type 5 and 9 infill	- Post stages 1-9 - Crosscuts types 3-9 (observed).	**Waning hydrothermal activity, rapid crystallization of cryptocrystalline quartz from amorphous silica gels.**
TYPE 11 (MOLYBDENITE + BLACK QUARTZ MATRIX INFILL/ VEINS)	- Friable and sooty to silicified black quartz, very fine-grained milky quartz, microcrystalline quartz and cryptocrystalline quartz, interstitial to poorly crystalline, ultra fine-grained molybdenite - Commonly occurs as a breccia matrix containing clasts of types 1, 4, 5 8 and 9 - Breccia clasts are angular to sub-angular and <5 cm - Associated with a bright to dark blue stain, discolouring black quartz and occasionally massive crystalline quartz in contact with fractures filled by type 11.	- Most prevalent between 4940mRL and 4880mRL - At shallow levels in the system, type 11 infill is contained within thin stockwork veins (e.g. Fig. 4.12, Sub-level 2 North, faces #016 to #029) in association with type 5 infill - With increasing depth, type 11 is more commonly present as the matrix to breccias cementing clasts of type 6b; and as stringer veins in type 2 and 9 infill.	- Last phase of mineralization at Kencana, crosscutting all other vein types	**Possible input from magmatically derived fluids, higher temperatures.** **Gold may be remoblized from earlier infill stages.**

Table 4.1 cont.

breccia clasts and the most complex sequence of vein types, textures and crosscutting relationships (Fig. 4.25). The detailed distribution and timing of each vein type are described below.

Type 1: Wallrock material (predominantly andesite) hosts the vein and pre-dates mineralization. Altered wallrock breccia clasts occur through many vein types and typically display angular, crackle-breccia and jigsaw-fit textures, with a transition to sub-rounded, rotated textures with time and successive brecciation events. Type 1 is most common as in situ, attached lithologies marginal to vein/ cement assemblages, though coherent blocks of wallrock also occur in the centre of the vein, most commonly along sub-levels 5 and 6 North (Fig. 4.25).

Type 2: Type 2 is one of the most common vein types in the K1 vein and occurs as both in situ, attached lithologies marginal to vein/ cement assemblages and as breccia clasts, which range from angular crackle breccias to sub-rounded and rotated clast breccias within several other vein types. Type 2 material is recognized across the vertical and lateral extent of the deposit. In situ type 2 material is more common between sub-levels 1-4, and breccia fragments between sub-levels 8-5 (particularly sub-levels 5 and 6 South, and sub-level 7 North; Fig. 4.25)

Areas of the vein with abundant type 2 material represent zones of constriction within the structure, where only minor fractures have opened and provided a locus for epithermal mineralization. Type 2 is interpreted to represent the first phase of epithermal mineralization at Kencana, though multiple phases of type 2 mineralization have occurred, based on complex crosscutting relationships of quartz stringer veins within this vein type.

Type 3: The distribution of type 3 is variable across the vertical and lateral extent of the K1 vein. Type 3 is most commonly associated with type 2 material and is most abundant at shallow levels peripheral to the bulk of quartz mineralization (e.g. Sub-level 2, Figs. 4.12 and 4.13). Individual faces that are dominantly composed of type 3 generally only host thin veins infilled with later quartz mineralization (Types 4-11; e.g. Fig. 4.21 faces #003 to #014). Type 3a is inferred to represent zones of restricted dilation within the structure and

more commonly forms the hangingwall and/ or footwall margins of the vein. Type 3b has undergone further dilation and also occurs as detached blocks within the vein cemented by later vein types, and as anhedral to sub-angular and rotated breccia fragments, typically cemented by type 9 (Fig. 4.22 face #022). Type 3 was deposited during and after deposition of type 2, but prior to types 4-11.

Type 4: Type 4 is recognized in the main ore zone below 4900mRL and northward from 19830mN, though isolated occurrences are known from face #051 Sub-level 5 Undercut A01 South (Fig. 4.19). Type 4 often occurs in association with type 6a and typically contains fragments of type 2 material.

Multiple phases of type 4 deposition have occurred through the life of the system. Type 4 is deposited after type 2 and 3, but episodes of type 4 mineralization occurred both before and after type 5 and 9 infill. Types 7 and 11 crosscut type 4 mineralization. Timing relationships with type 6, 8 and 10 veins are undetermined as associations between these phases were not observed in this study.

Types 5 and 6: Type 5 is one of the most common mineralization stages in the K1 vein, and occurs along all sub-levels over the vertical and lateral extent of the deposit (Fig. 4.25). Type 5 commonly fills wide (>1 m) fractures or thin stockwork veins hosted in vein type 2 and 3 material. Type 6a is less common, but shows an association with vein type 4 material and often hosts veins infilled with type 11. Type 6a is most prevalent northward of 19850mN between 4900mRL and 4925mRL, and above 4950mRL (Fig. 4.25). Type 6b is most commonly present as fragmental blocks cemented by vein type 11, and spatially is most prevalent between 4880mRL and 4960mRL, particularly to the north of 19900mN (Fig. 4.25).

Type 5 is the first major phase of quartz mineralization associated with significant gold grades at Kencana. Multiple stages of type 5 mineralization have occurred, though the main stage of deposition occurred after types 2 and 3, during deposition of vein types 4 and 6, and before all other types.

Types 7 and 8: Types 7 and 8 are closely spatially related, though type 7 is much

more abundant in the K1 vein. Types 7 and 8 are common at the widest parts of the structure, in particular along sections of the structure with low-angle displacement (e.g. Sub-level 8 North, Fig. 4.24). Type 7 is observed over the full mapped vertical and lateral extent of the deposit from 4950mRL to 4850mRL, and mineralization is laterally continuous over distances of >30 m (Fig. 4.25). Type 7 infill often fills the central part of the vein and often contains angular and splintery fragments of types 1 and 2 that appear to have been spalled from the vein wall contacts where these types are contiguous. Type 8 mineralization is restricted below 4900mRL, with greatest abundance in the lowest mapped levels of the system (Sub-level 8 North).

Type 7 and 8 mineralization occurred after types 1-6. Mineralization occurs both pre- and post-deposition of type 9 infill, though the bulk of type 7 and 8 infill is deposited after type 9. Occasional type 7 breccia clasts are included in later phases of type 9 mineralization.

Type 9: Type 9 infill is recognized across a wide lateral extent between 4940mRL to 4850mRL in the K1 vein. Zones up to 5 m wide and up to 100 m containing type 9 infill occur in the centre of the vein along sub-levels 6 and 7.

Type 9 crosscuts types 1-6 and angular to sub-angular breccia clasts of type 2 ranging from a few centimetres to over a metre in diameter are common. The majority of type 9 mineralization occurs before types 7 and 8, though some thinner (<70 cm) type 9 veins crosscut type 8 infill. Type 9 is crosscut by type 10 and 11 veins.

Type 10: Complete veins infilled with type 10 mineralization are rare in the Kencana deposit. The vertical and lateral distribution of type 10 veins in this study was inferred from SiroVision™ images. Type 10 is restricted to the south of 19775mN along sub-levels 5 and 6, filling thin (<30 cm) fractures in type 5 and 9 infill, and often containing angular to sub-angular clasts of type 2 material. Type 10 is a late stage in the paragenesis of the system, occurring post stages 1-9.

Type 11: Type 11 infill and veins occur sporadically through the K1 vein. Type 11 is recognized across the full mapped vertical and lateral extent of the deposit, though is most

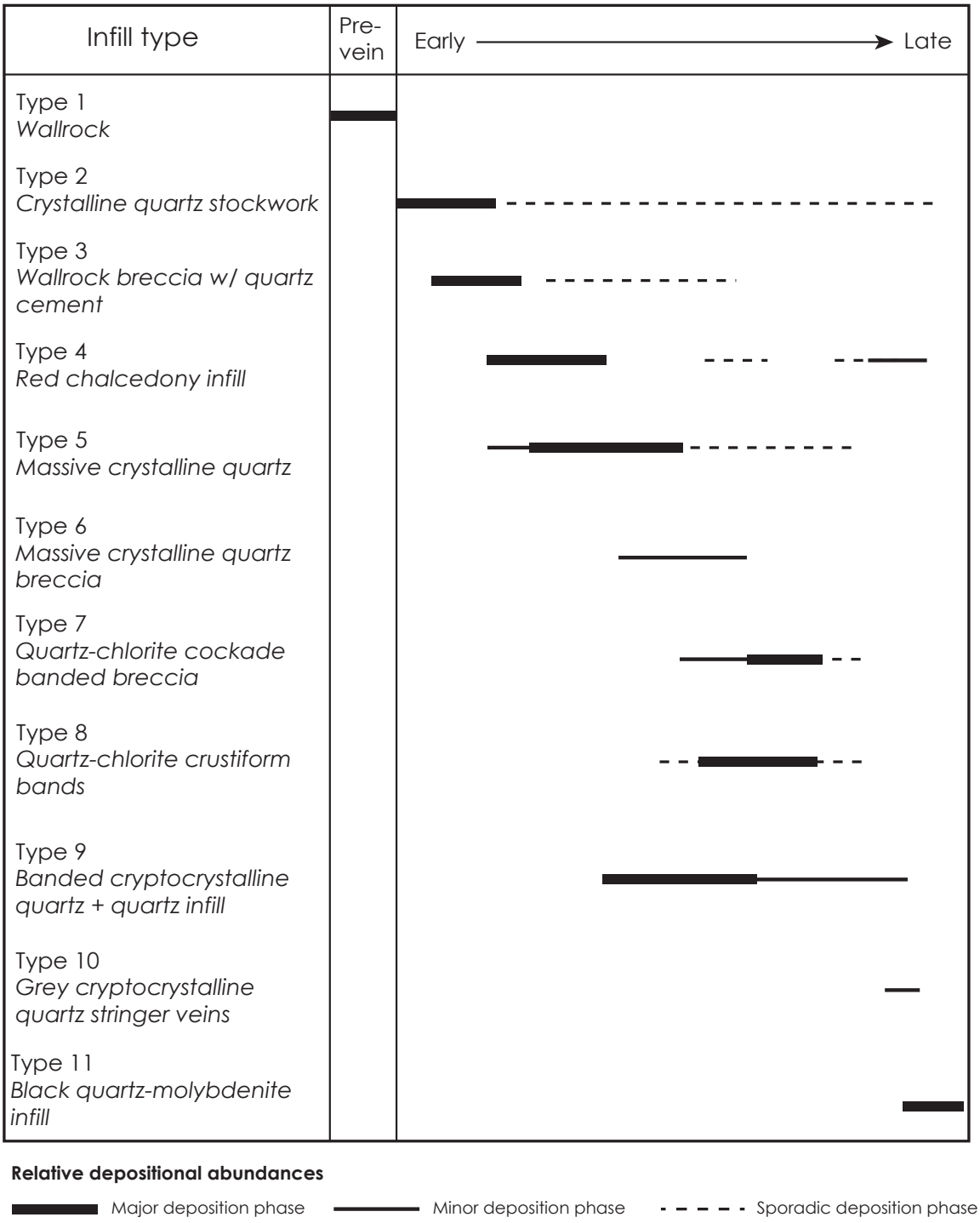

Fig. 4.26 Kencana infill stage paragenesis detailing gangue mineral assemblages and relative abundances for deposition volume of each infill type.

prevalent between 4940mRL and 4880mRL. At shallow levels in the system, type 11 infill is contained within thin stockwork veins (e.g. Fig. 4.12, Sub-level 2 North, faces #016 to #029) in association with type 5 infill. With increasing depth, type 11 is more commonly present as

the matrix to breccias cementing clasts of type 6b; and as stringer veins in type 2 and 9 infill.

Type 11 is the last phase of mineralization at Kencana, crosscutting all other vein types. Attempts were made at Re/Os dating of molybdenite from type 11 infill during this study to complement $^{39}Ar/^{40}Ar$ dating of adularia from earlier vein types; however, no suitable samples could be identified due to the ultra fine-grained nature of the molybdenite.

Paragenetic relationships in the K1 vein are complex and this study identifies at least 11 main opening events. These events are primarily brecciation episodes and not simple banding events. The majority of vein types occur at more than one stage through the life of the system and many complex crosscutting relationships are observed. A paragenetic sequence for gangue and ore mineralogy in the K1 vein at Kencana has been established and is shown in Fig. 4.26.

Early stage mineralization and opening events are dominated by thin veins and veinlets to jigsaw fit brecciation of host rocks (coherent andesite, basalt and volcaniclastic rocks) with low volume deposition of silica polymorphs (predominantly crystalline quartz), with increasing volumes of gangue mineralization (predominantly cryptocrystalline and microcrystalline quartz ± adularia ± chlorite) and a transition from vein-dominated infill to rotated breccia dominated infill over time. Jigsaw breccia textures commonly associated with types 1-3 suggest rapid pressure release and rock fragmentation, possibly due to unloading of the hydrothermal system by tectonic movement or hydraulic release. Identification of type 1 and 2 clasts in later stages suggests that sealing and re-brecciation was common. Initial opening of veins infilled with types 3, 7, 8, and to a lesser extent, type 9 is represented by jigsaw and crackle breccias, indicative of rapid pressure release. These breccias are often cockade banded and contain high Au grade (particularly type 7 infill) where Au- and sulfide-rich bands are deposited as the first phase surrounding the wallrock or previously mineralized breccia clasts, forming in response to the associated pressure release and change in physiochemical conditions. Observations from K-Link suggest that steeper sections of the vein have undergone greater and more complex episodes of brecciation, and shallow sections of the structure display more continuous, symmetric crustiform banding within veins, particularly in type 7 and 8 infill.

The transition from coarse crystalline quartz with zoned crystals in type 2 infill to

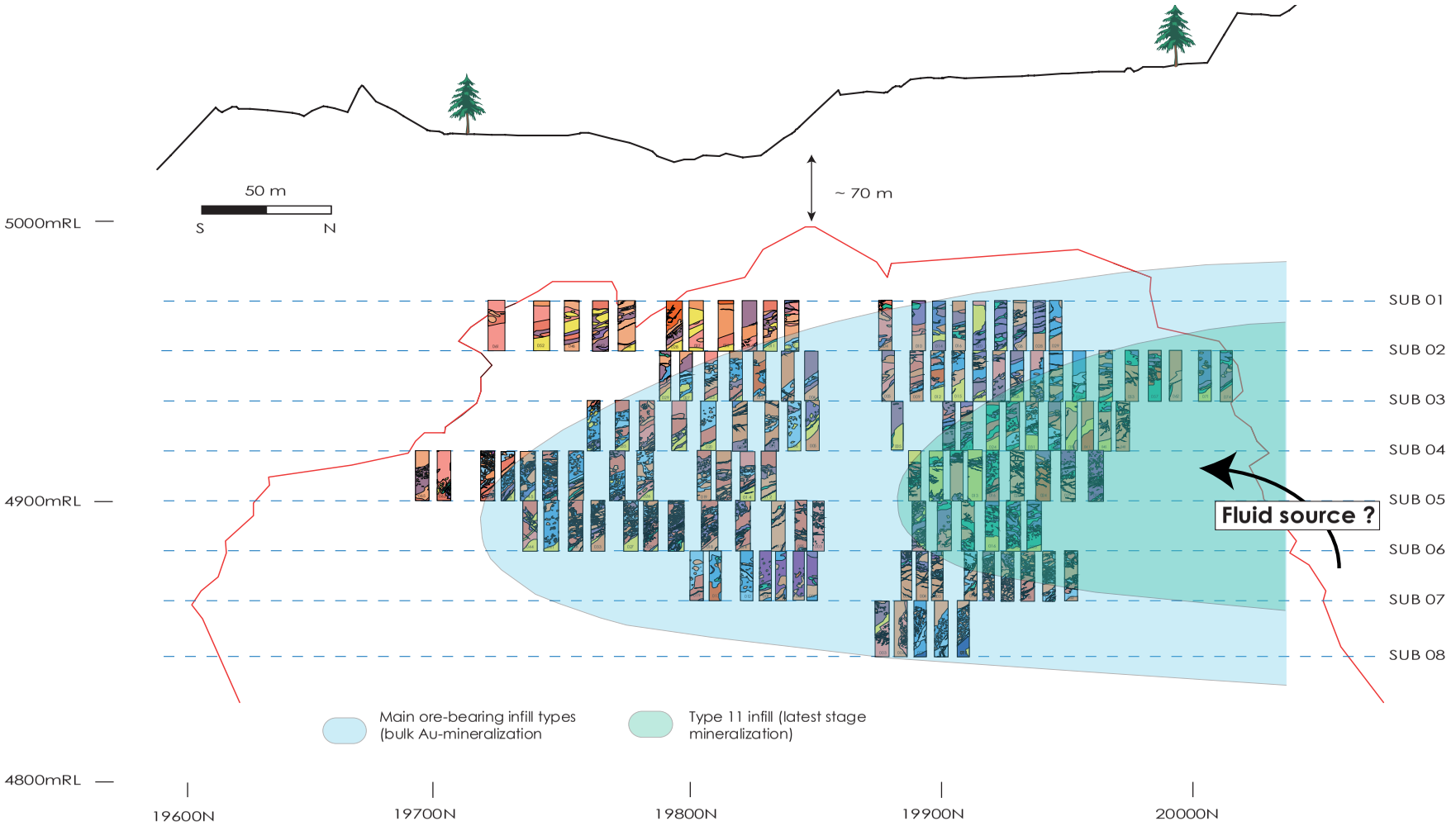

Fig. 4.27 Interpretation of infill type zonation in the K1 vein highlighting the distribution of infill types 7, 8 and 9 in the central and northern section of the structure, and the northern distribution of late-stage type 11 infill. Other vein types show a sporadic distribution. A fluid source from the north may be responsible for the zonation pattern.

banded finer-grained crystals and microcrystalline quartz in stages 3-10 indicates a change from slow rates of crystallization to an increase in the rate of crystal nucleation with more rapidly fluctuating conditions in a dilating structure. Mineralogical evidence for boiling is not observed until deposition of type 5 infill (adularia and bladed calcite pseudomorphs; minor evidence for adularia in type 4), corresponding with formation of wider veins, larger volumes of gangue mineralization and increased Au grade.

The bulk of economic mineralization is deposited later in the life of the system and is contained within stages 7, 8 and 9, and to a lesser extent, stage 11, though it is not clear whether the majority of gold contained within stage 11 mineralization is primary or remobilized from earlier mineralized stages. The broad north-south textural zonation observed in this study, with the bulk of ore-bearing infill types located in the centre of the deposit and the latest mineralization stage (type 11 infill) toward the north may indicate a fluid source from the north (Fig. 4.27).

4.7 Kencana ore mineralogy

This section describes in detail the ore mineralogy of the Kencana deposit, focusing on the K1 vein, which is dominated by electrum and sulfides with selenides and lesser tellurides and sulfosalts. Chalcopyrite is the most common sulfide mineral, with selenian-galena, sphalerite, bornite and pyrite in order of decreasing abundance. Other common accessory minerals include aguilarite and molybdenite (in type 11 infill), with trace tennantite, arsenian-pyrite, silver and lead tellurides, naummanite and bismuth minerals. Ore microscopy, electron microprobe and SEM-EDS analyses were used to determine mineral assemblages due to the fine-grained nature (typically 1-20 μm, though can be up to 200 μm for base metal sulfides) of the mineralization. Ore mineralization is present in multistage, banded quartz-adularia, crystalline quartz, cryptocrystalline quartz and quartz-chlorite veins, hydrothermal breccias and stockworks. Overall opaque minerals are a minor component by volume of the vein material, but concentrations of electrum with sulfide and selenide minerals contribute significantly to the crustiform banded structure in many samples. A summary of gangue and ore mineralogy for each infill type at Kencana is given in Fig. 4.28. Descriptions of ore mineral occurrences and associations are given below.

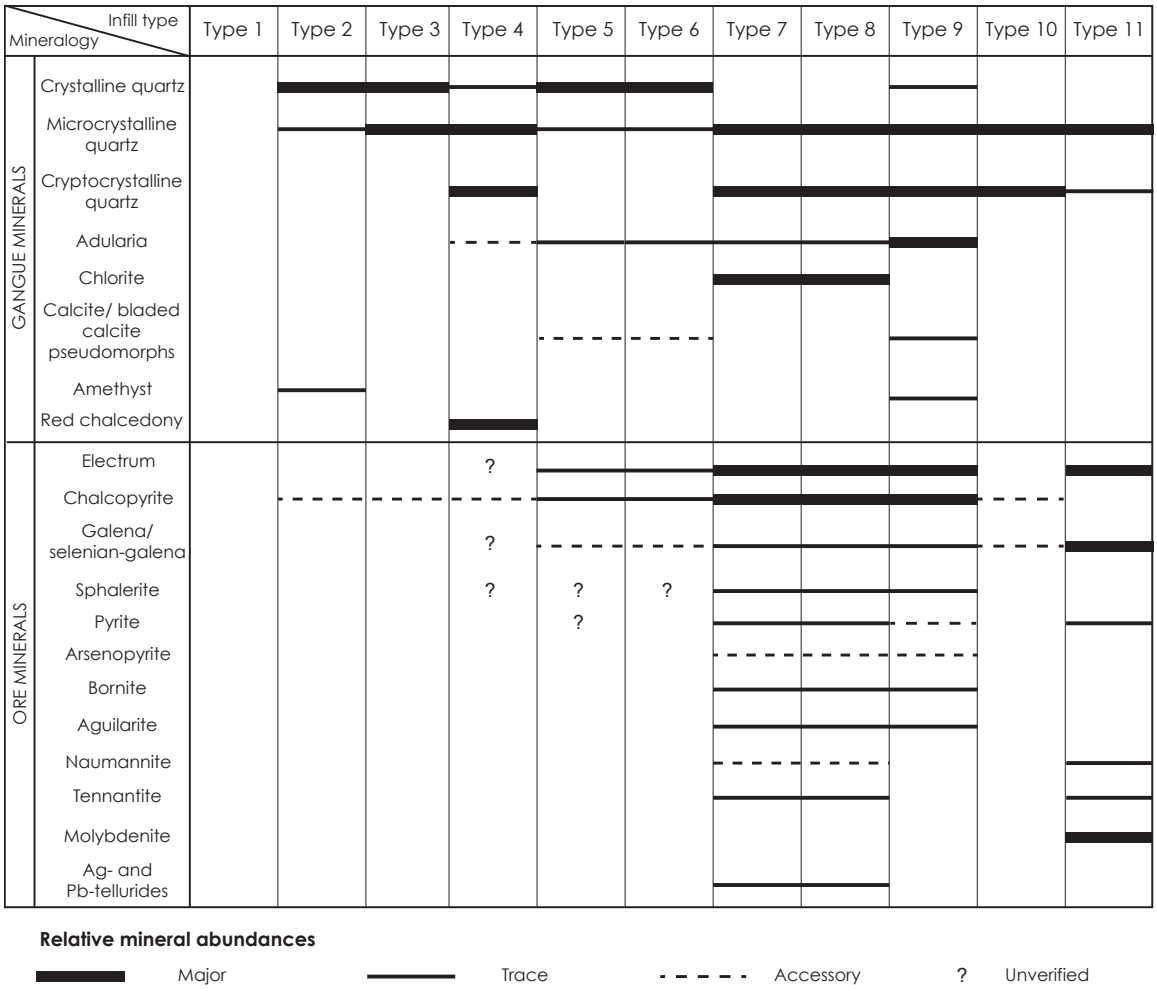

Fig. 4.28 Summary of Kencana ore and gangue mineral occurrences. Relative mineral abundances for each infill type based on microscope, SEM-EDS and microprobe analyses of K1 and K2 vein samples.

Electrum: Electrum is the primary ore mineral in the K1 deposit. Gold is present within the vein as free gold and electrum (61-82 wt% Au or fineness ~600-850, as determined by electron microprobe analysis). Grains are between 1-40 μm, anhedral with irregular boundaries to sub-rounded and range from bright yellow to very pale yellow under reflected light, where colour variations are related to Ag content of the electrum, with paler grains containing more Ag. Visible gold is contained within thin dark bands composed of electrum + chlorite + chalcopyrite ± sulfides ± selenides ± tellurides ± sulfosalts in vein types 7 and 8 (Fig. 4.29).

Electrum occurs in association with several minerals:

1) As grains interstitial to or as inclusions within quartz, cryptocrystalline quartz and

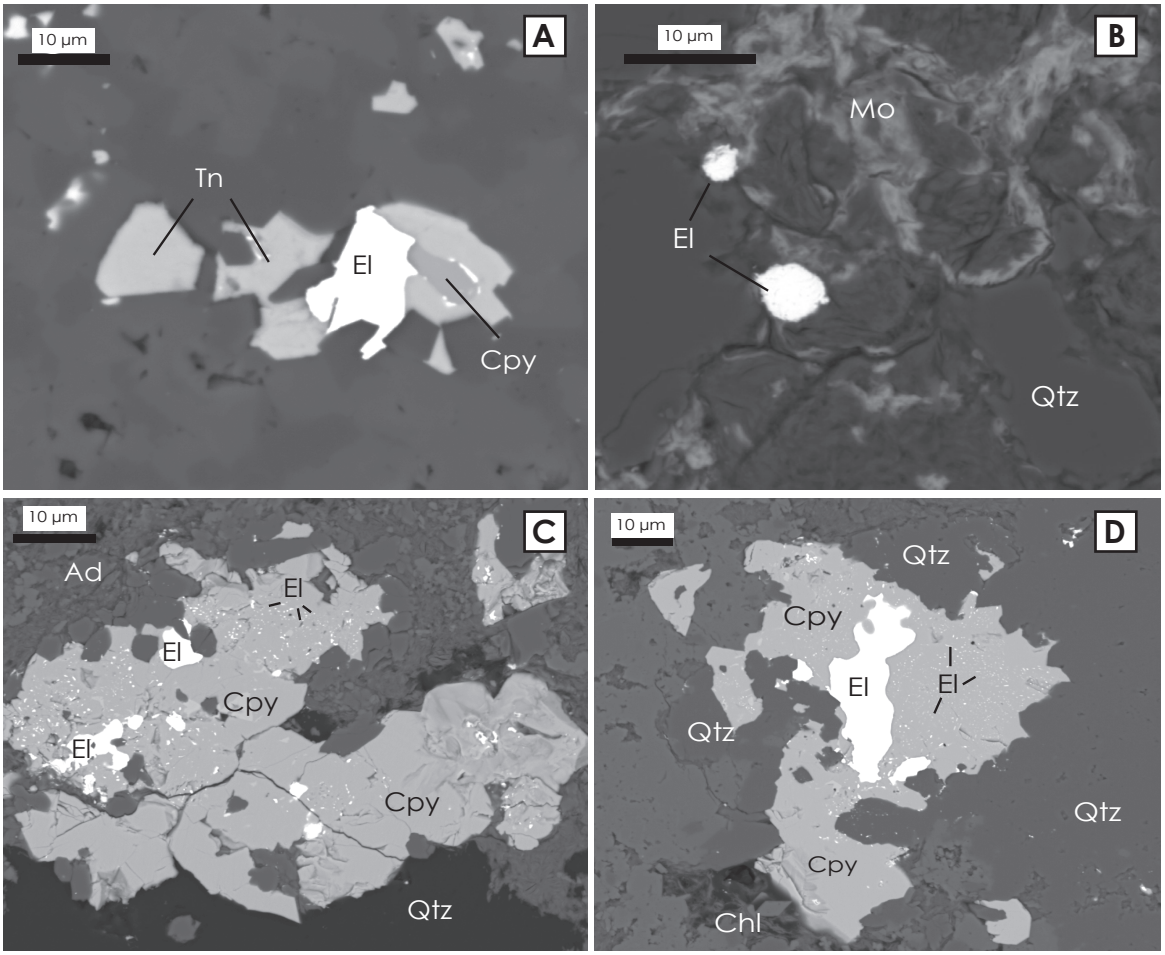

Fig. 4.29 SEM photomicrographs of electrum mineralization in the K1 vein A) Electrum (white) intergrown with chalcopyrite (dark grey, with electrum rim) and tennantite (pale grey), sample from Sub11UC3a; **B)** Sub-rounded electrum grains (white) in fine grained, poorly crystalline molybdenite (pale grey) and quartz (dark grey) from vein stage 11, sample from Sub1UC3N014b; **C)** Electrum (white) exsolution in chalcopyrite(pale grey), intergrown with quartz (dark grey) and adularia(mid grey), sample from Sub1UC3N014a; **D)** Electrum (white) intergrown with (and exsolution in) chalcopyrite (pale grey) intergrown with quartz (dark grey) and chlorite (weakly bladed texture), sample from Sub11UC3c. Mineral abbreviations: El = electrum, Cpy = chalcopyrite, Qtz = quartz/ cryptocrystalline quartz, Ad = adularia, Mo = molybdenum, Chl = Chlorite, Tn = tennantite.

adularia

2) As intergrowths with chlorite and calcite

3) As apparent intergrowths with illite-smectite (after adularia)

4) As complex intergrowths with base metal sulfide, selenide, sulfosalt and telluride species.

5) Very locally as intergrowths with, or as inclusions within pyrite.

6) Very locally as intergrowths with poorly crystalline molybdenite.

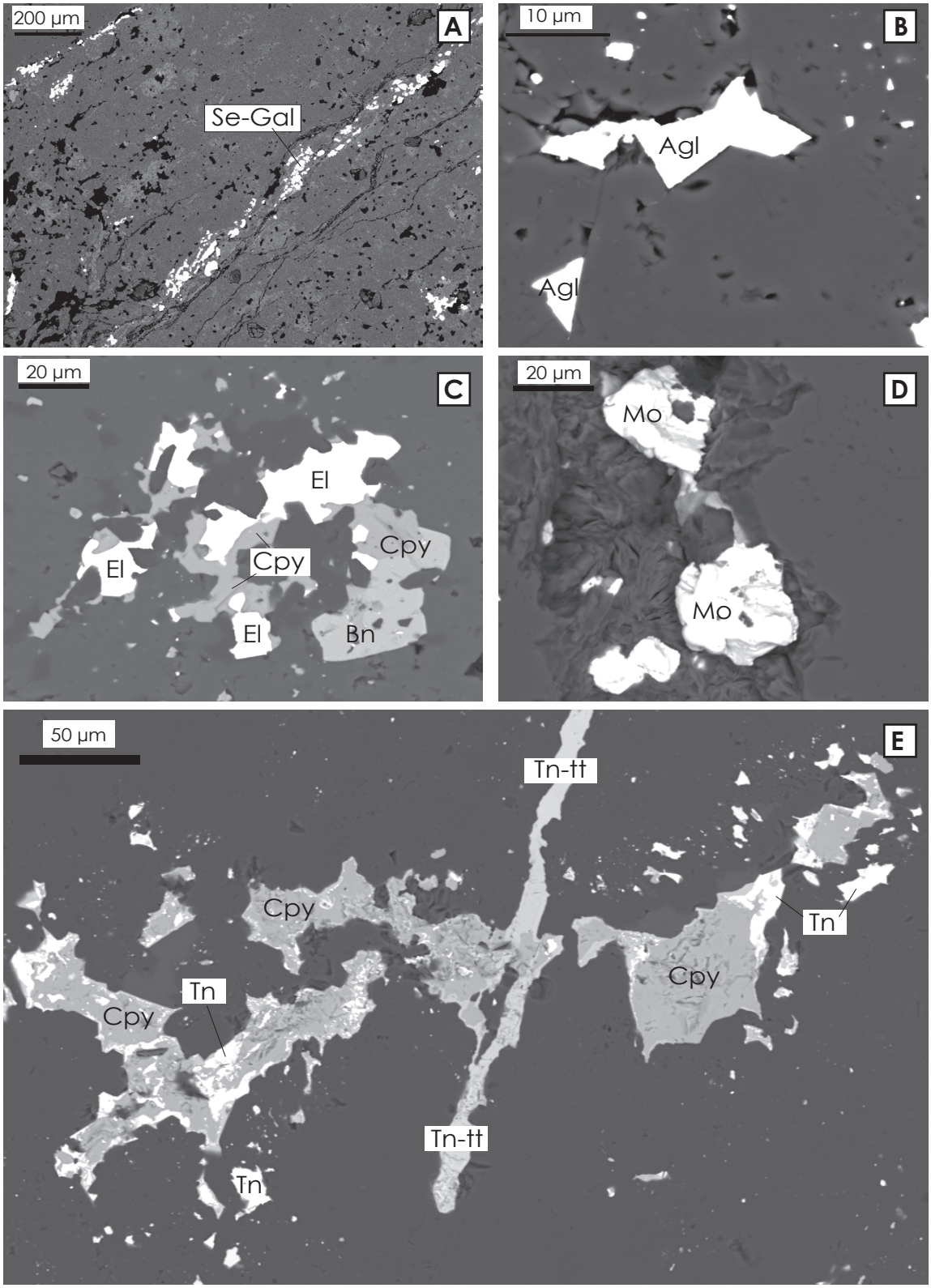

Fig. 4.30 SEM photomicrographs of ore mineralization in the Kencana deposit. A) Selenian-galena veins. Sample from Sub113C (K2 vein); **B)** Angular aguilarite grains from Sub1UC03N014; **C)** Anhedral electrum intergrown with chalcopyrite and bornite. Sample from K113 (K2 vein); **D)** Sub-rounded, flaky molybdenite grains from Sub1UC03N014; **E)** Tenantite-tetrahedrite vein with complex tennantite-chalcopyrite intergrowths. Sample from Sub1UC03N014. Mineral abbreviations: Agl = aguilarite, Bn = bornite, El = electrum, Cpy = chalcopyrite, Mo = molybdenum, Se-gal = selenian-galena, Tn = tennantite, Tn-Tt = tennantite-tetrahedrite

Chalcopyrite: Chalcopyrite is the most abundant sulfide phase in the Kencana vein. It is ubiquitous through all ore-bearing vein types and is in equilibrium with electrum. Gold also occurs as exsolution textures in chalcopyrite. Grains are very fine to medium-grained (5-200 μm), subhedral to anhedral and often occur as complex intergrowths with electrum, silver selenides, bornite, selenian galena and locally tennantite. Chalcopyrite is either contained in discreet bands with electrum and other sulfide and selenide species, or disseminated in massive crystalline or cryptocrystalline quartz. Chalcopyrite grains <1 mm are also common as an alteration mineral in clay-chlorite altered wallrock fragments within the vein.

Bornite: Bornite (approx. 1 vol.% in the K1 vein) is one of the least common sulfides in the Kencana deposit. Bornite appears pale to mid-purple in reflected light and occurs in association with chalcopyrite, sphalerite, galena and very minor pyrite. Bornite mineralization is restricted to crustiform bands rich in opaque minerals in quartz-adularia and quartz-chlorite veins (type 7, 8 and 9 veins).

Pyrite: Pyrite is the least common sulfide in the mineralization assemblage at Kencana, and is often overgrown by other sulfide minerals (and molybdenite in the later stages of mineralization in the system). Pyrite crystals are subhedral to euhedral, <1 mm and appear pale yellow to buff in reflected light. Very rare arsenopyrite has been identified in the K1 vein though its distribution is not well constrained. Pyrite is present as single crystals or agglomerates, some with evidence of dissolution. Pyrite mineralization within the Kencana vein is rare but typically constrained to banded quartz-chlorite (types 7 and 8) and type 11 infill, forming bands dominated by pyrite with few other sulfides. Some minor Pb-telluride overgrowths have been observed on euhedral pyrite crystals from type 8 infill.

Galena: Galena in the Kencana system, in particular where a close spatial association with electrum and/or naumannite is observed, contains significant amounts of selenium in solid solution (up to 18 wt% Se, but not enough for the mineral to take on the stoichiometry of clausthalite). Galena in close spatial association with electrum in places also contains some gold, but it is not known whether this is as colloidal form or solid solution within the galena. Selenian galena occurs as anhedral to subhedral crystals typically <100 μm in association with chalcopyrite, sphalerite and bornite; and as complex intergrowths with other sulfide and selenide minerals in thin sulfide-dominated bands in type 7, 8 and 9 veins, and

rarely as disseminated grains in crystalline quartz in type 5 and 6b infill. Galena also occurs in association with poorly crystalline molybdenite interstitial to quartz in type 11 infill.

Silver: Silver is commonly present in selenide and locally, telluride minerals. Selenide mineralization is more prevalent than telluride mineralization in the Kencana deposit. Ag-selenides are anhedral to subhedral and typically <20 μm. The geochemistry of the silver selenide minerals indicates the best stoichiometric approximation to be naumannite (Ag_2Se) and aguilarite (Ag_4SeS). As well as the selenium substitution for sulfur, there is also gold substitution for silver. Gold-bearing naumannite typically occurs as overgrowths to or intergrowths with electrum (Coote, 2003).

Molybdenite: The latest stage of mineralization in the Kencana deposit is represented by a poorly crystalline, dark, fine-grained black breccia matrix and vein infill, characterized by quartz and molybdenite with minor galena, Ag-selenides and pyrite. Molybdenite is poorly crystalline and ultra fine-grained to flaky crystals rarely up to 40 μm.

Tellurides: Minor amounts of unidentified Ag-, Au- and Pb-tellurides have been identified at Kencana. Tellurides are typically fine grained (<5 μm) and exhibit irregular to subhedral morphologies. Telluride mineralization is currently constrained to type 7 and 8 infill in the Kencana vein, although further study is needed to verify the presence of tellurides in other vein types. Ag- and Au-Ag tellurides occur in cryptocrystalline quartz bands in association with chalcopyrite and electrum, and Pb-tellurides occur in cryptocrystalline quartz bands in association with Se-galena and pyrite.

4.8 Discussion of Kencana ore mineralogy

Kencana ore mineralogy is generally typical of low sulfidation epithermal deposits, though several features of the mineral assemblages are less common and may reflect on the metal transport and depositional processes in the Kencana vein.

Electrum at Kencana is deposited with a variety of sulfides, selenides and sulfosalts. Studies have shown that gold is preferentially transported as bisulfide complexes in low temperature epithermal environments and under near-neutral, dilute conditions (Seward, 1991; Cooke and Simmons, 2000). The fact that gold is deposited with silver as electrum and Au-bearing naummanite suggests that gold precipitated from bisulfide complexes under

similar conditions to silver. Spycher and Reed (1989) indicated that electrum fineness can be indicative of depositional mechanisms in epithermal systems. They calculated that a typical Broadlands geothermal water will deposit Ag-rich electrum (fineness ~300) during boiling, but that Au-rich electrum (fineness ~700) forms by mixing with acid waters. Electrum fineness at Kencana is typically in the range 600-850 which may suggest that mixing was an important mechanism for Au deposition where electrum is not associated with common indicators of boiling, (such as adularia), in particular the electrum-chlorite association in type 7 and 8 mineralization. It is interpreted that a combination of mixing and boiling processes were responsible for ore deposition at Kencana, though it is likely that quartz-adularia (type 9) mineralization was formed predominantly by boiling processes, and types 7 and 8 (quartz-chlorite) by mixing.

The local and regional controls on Se-rich mineral associations in epithermal deposits are not well understood, though many Se-rich epithermal deposits contain bonanza gold grades, such as Midas (USA), Hishikari (Japan), and Broken Hills (New Zealand) (Cocker et al., 2012). Selenium substitution in sulfide minerals was noted at the Mt. Muro deposit (Wurst, 2004), and a positive correlation between gold, silver and selenium was recognized at the Pongkor low sulfidation epithermal deposit (Warmada et al., 2003).

Simon et al. (1997) suggest that selenium substitution in sulfide minerals has important implications for fluid composition and oxidation state. They demonstrated that hydrothermal fluids with high fSe_2 (g)/fS_2 (g) ratios, and the presence of sulfide assemblages that buffer fSe_2 (g) and fS_2 (g), prevent the enrichment of selenium in the hydrothermal fluid and deposition of selenide minerals (except for silver selenides). A highly oxidizing environment is needed for selenium deposition (Simon et al., 1997), conditions not commonly associated with low sulfidation epithermal systems, which are known to form under reduced conditions. However, it is interpreted at Kencana that rising reduced fluids in the system mixing with large volumes of oxidised meteoric water (which is the dominant component in the mineralizing fluid in the system, as determined by fluid inclusion study, section 4.9) could contribute to a less reduced environment than typically encountered in low-sulfidation epithermal systems. The host rock package at Kencana also contains hematitic mudstones, which may buffer the mineralizing fluids to more oxidised conditions. Such an environment also

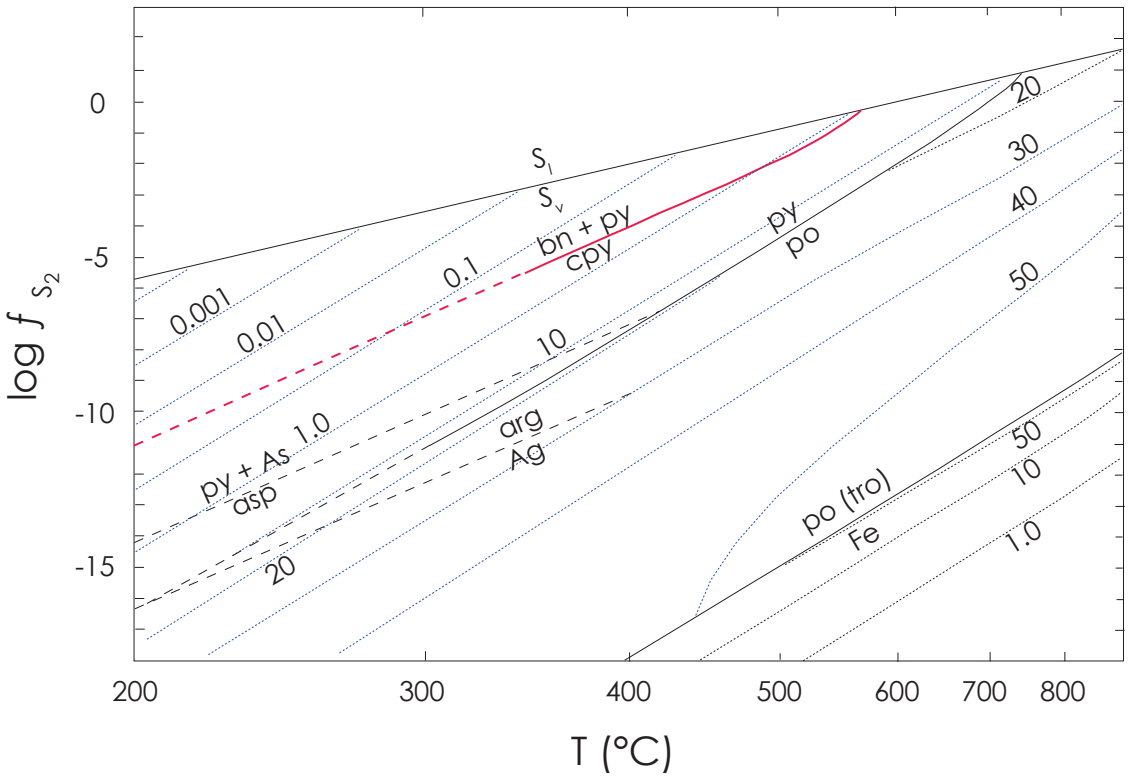

Fig. 4.31 Sphalerite composition (blue dashed lines) in the assemblage sphalerite + pyrite + pyrrhotite as a function of fugacity of S_2 and temperature with chalcopyrite + bornite + pyrite curve (red line) from Barton and Toulmin (1964). At Kencana, temperatures of ore formation peak at 200-225°C as determined by fluid inclusion study, consistent with Fe contents in sphalerite <0.1 wt%. After Barton and Skinner, 1979.

favours gold deposition (Hannington and Scott, 1989) and may contribute to explaining the high gold grade in the Kencana deposit and other Se-rich bonanza Au deposits.

Substantial boiling of hydrothermal fluids promotes cooling and loss of H_2S to the vapour phase, which lowers fS_2 and promotes formation of selenium-bearing minerals (Simon et al., 1997; Cocker et al., 2012). However, evidence for high levels of boiling is not present at Kencana, suggesting mixing may have been a more important process in the formation of Se-bearing minerals. Reyes (2002) demonstrated that copper, silver, tellurium, zinc, lead and gold were deposited by boiling in geothermal pipes in the Rotokawa goldfield, whereas mercury, boron, arsenic, antimony and selenium were deposited a distance from the wellhead, due to cooling and mixing (Reyes, 2002; Wurst, 2004).

Regional controls on Se-rich epithermal deposits are currently poorly constrained; however, epithermal deposits containing silver selenides have been associated with bimodal volcanism (andesite-rhyolite, Great Western Basin, USA and Hauraki Goldfield, New Zea-

land; andesite-dacite, Hishikari, Japan; Christie et al., 2007; Cocker et al., 2012), concurrent with bimodal andesite-dacite volcanism in the Gosowong goldfield. Andesite-only volcanism in the Hauraki goldfield is associated with epithermal deposits lacking Ag-selenides (Cocker et al., 2012).

Tellurium is precipitated as Au-, Ag- and Pb- tellurides, particularly in type 7 and 8 infill. Cooke and Bloom (1990) suggest tellurium may be preferentially transported in the gas phase in boiling epithermal systems, but that throttling of the conduit may be an effective mechanism to keep tellurium in the fluid. Tellurium deposition can occur subsequently during cooling, mixing or condensation (Cooke and Bloom, 1990). The presence of coarser-grained electrum and sulfide minerals in type 7 and 8 infill compared to other vein types also suggests a slower, gradual decrease in temperature.

The lack of pyrite and abundance of chalcopyrite in the Kencana system implies a Fe-poor/ Cu-rich source fluid. Low Fe contents in sphalerite as determined by microprobe analysis (<0.2 wt%) also confirm a Fe-poor mineralizing fluid. Fe-rich fluid pulses later in the life of the system are inferred based on the presence of banded chlorite (± pyrite) intergrown with quartz in type 7 and 8 infill.

Bornite is an uncommon mineral in low sulfidation epithermal deposits, though has been reported at the Royal, Crown and Roses Pride veins, Cracow goldfield, Australia (Braund, 2006). Thermodynamic calculations by Barton and Skinner (1979) demonstrate that the presence of bornite and chalcopyrite in equilibrium determines a position on the reaction boundary between bornite and chalcopyrite on Fig. 4.31. The model predicts chalcopyrite and bornite in equilibrium at temperatures predicted for the Kencana system (~200-225°C, section 4.10) at a sulfur fugacity ~ -11 fS_2 and Fe contents <0.1 wt%, which is consistent with microprobe analysis of Fe in sphalerite.

Numerical modeling experiments performed for the Acupan deposit in the Baguio District, Philippines (Cooke and McPhail, 2001) predict that bornite and chalcopyrite can form in low sulfidation deposits at low temperatures (100-130°C) during boiling in a closed epithermal system, or to a lesser extent, multistage boiling. Precipitation of copper minerals was not predicted in cooling models (Cooke and McPhail, 2001). Although such conditions are unlikely to have prevailed for the duration of ore formation in Kencana, and fluid inclu-

sion analysis indicates temperatures of ore formation at 200-225°C, the modeling results give insight into the possible constraints on the occurrence of chalcopyrite and bornite in the system, and it is interpreted that boiling processes may contribute to explaining the high gold grades present at Kencana. Boiling as a mechanism for Au deposition is suggested from pressure of entrapment calculations for fluid inclusions (section 4.11), though fluid inclusion boiling assemblages were not observed during this study. Bladed calcite, quartz after bladed calcite and adularia within the vein also provide evidence for boiling at Kencana, and have been reported in higher abundances in exploration drill holes to the south of the Kencana deposit (Coote, 2005).

4.9 Fluid inclusion study

Fluid inclusion studies of epithermal systems can provide significant insights into the character and chemistry of hydrothermal fluids, and of processes responsible for ore formation (Braxton, 2007). In this section, microthermometric studies of fluid inclusions constrain the temperature and pressure conditions of entrapment, and the salinity of the mineralizing fluids.

Prior to this study, preliminary fluid inclusion data for the Kencana deposit were determined by Coote (2003). The study included 18 samples reflecting the different depositional stages described by Coote (2003). Data for the high-grade, quartz chlorite mineralization event (equivalent to type 7 and 8 infill) were not obtainable due to the fine-grained nature of the silica minerals in the samples (Coote, 2003; this study). The lack of suitable fluid inclusion-bearing material (given the very small size of fluid inclusions and difficulty of access to suitable underground sampling sites) disallowed a spatial study of fluid evolution. Summary fluid inclusion (homogenization and salinity) data from this study are presented in the appendix. Across the different depositional stages, primary fluid inclusions homogenized within the range 175 to 270°C, whereas secondary fluid inclusions homogenized within the range 72 to 126°C. Primary fluid inclusions in early stage crystalline quartz homogenized with a mean temperature of 210 to 220°C, as did inclusions in adularia from later stage quartz-adularia mineralization. No significant variation was observed in calculated fluid salinities between the different mineralization stages, and all calculated salinities were deter-

mined as <1 wt% NaCl (equiv.) (Coote, 2003). The precision of measured temperatures are ±1.0°C and 0.3°C for heating and freezing respectively.

4.9.1 Methodology

The current fluid inclusion study was undertaken to supplement the existing fluid inclusion data, and to provide information for paragenetic stages and vein types not previously recognised or analyzed.

Microthermometric analyses were conducted at Imperial College, London under the supervision of Dr. Jamie Wilkinson, and CODES, University of Tasmania, in both cases using a Linkam MDS600 heating and freezing stage. Calibration was performed using 5 different synthetic fluid inclusions from Synflinc Inc. (detailed calibration in the appendix). 14 doubly polished thick sections (150 μm) from the early stage crystalline quartz, quartz-adularia and quartz-chlorite mineralization stages (vein type 2c, 9 and 8 respectively) were prepared at UTAS. First ice melting (Te), freezing point depression (Tm) and liquid-vapour homogenization (Th) were measured in 99 primary quartz inclusions from 10 assemblages in 7 chips. Primary inclusion assemblages (FIAs) were defined according to the method described in Goldstein and Reynolds (1994). Inclusions in a FIA are inferred to have been trapped simultaneously from the same fluid, representing a population of inclusions representative of that fluid event. Relating the timing of entrapment of FIAs to the relative growth history of the host quartz was critical to making correct interpretation of results (Goldstein and Reynolds, 1994; Braxton, 2007). The method classifies FIAs as primary (entrapped at the fluid-mineral surface during quartz growth), secondary (entrapped in a healed fracture subsequent to quartz growth) or uncertain.

At Kencana, FIAs were classified as primary only where they defined lines of inclusions parallel to quartz growth banding (Fig. 4.32). Secondary fluid inclusions were also measured from arrays defining growth zones in quartz crystals, though these were discordant to those fluid inclusions confidently established as primary (Fig. 4.32).

Salinity was determined as NaCl equivalent weight percent (wt% NaCl equiv.) and calculated according to the equation: $S = -1.78 \times T - 0.0442 \times T^2 - 0.000557 \times T^3$ (Bodnar, 1993), where S = salinity in NaCl-H_2O system, T = freezing point depression (corrected after stage

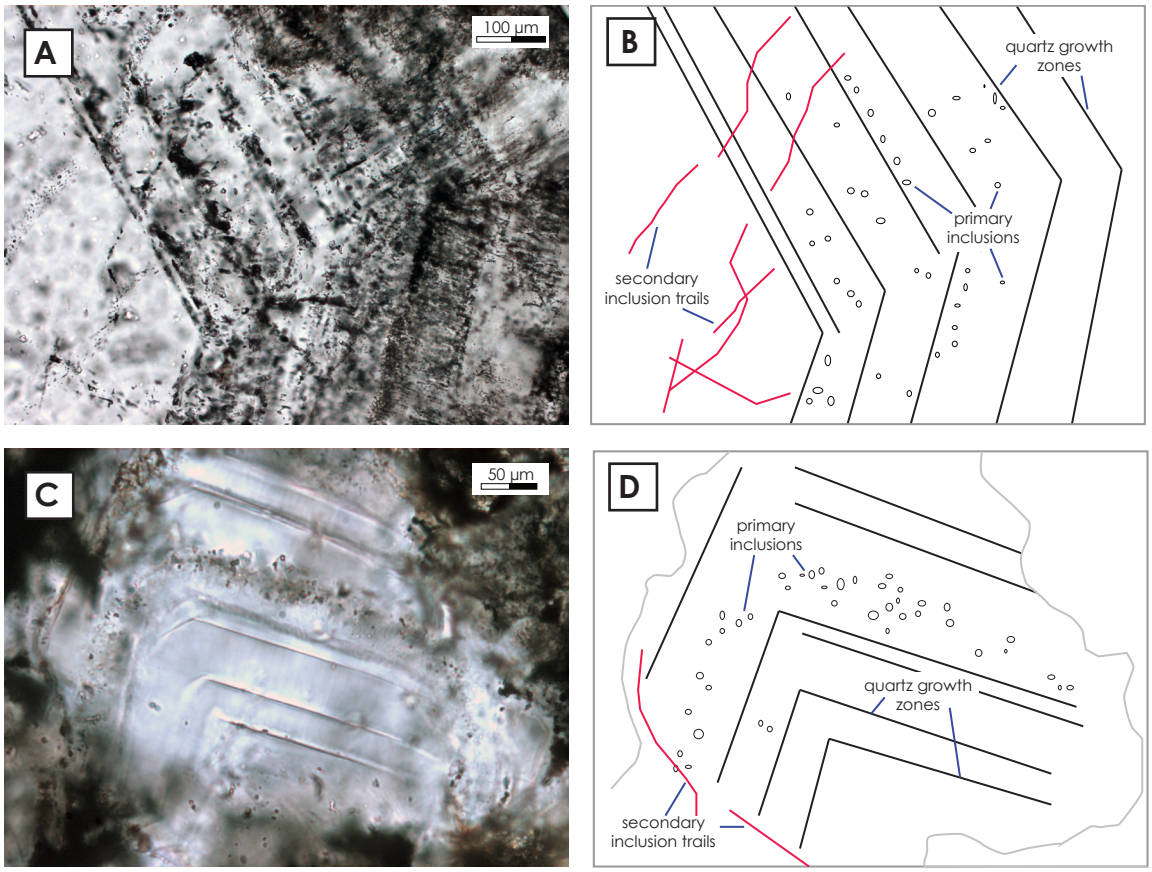

Fig. 4.32 Examples of timing relationships between fluid inclusions and quartz crystal growth. A) and B) Photomicrograph and sketch of primary fluid inclusions in type 9 (quartz-adularia stage) quartz. The fluid inclusion array is parallel to the growth surfaces of the quartz crystal. Secondary fluid inclusion trails cross-cut growth zones and overprint primary fluid inclusions. Sample Sb801N015C; **C) and D)** Photomicrograph and sketch depicting fine primary fluid inclusions parallel to concentric growth surfaces in a crystal from type 9 (quartz-adularia) quartz. Sample DSD105_332.6 m.

calibration). An error of ±0.05 wt% NaCl at temperatures between 0 and -21.21°C (the eutectic temperature for H_2O-NaCl) is quoted for the H_2O-NaCl system algorithm (Bodnar, 1993).

4.10 Discussion of microthermometry

The majority of fluid inclusions from the Kencana deposit are sub-angular to sub-spherical two-phase liquid-vapour (LV) inclusions with an average size of <10 µm (very rarely up to 60 µm) and a vapour proportion between 5-10% (rarely up to 20%; Fig 4.33).

One liquid-vapour-daughter inclusion was noted from sample K11 sub 3 (assemblage 2), though the mineral was too small (<1 µm) for further analysis leading to identification of

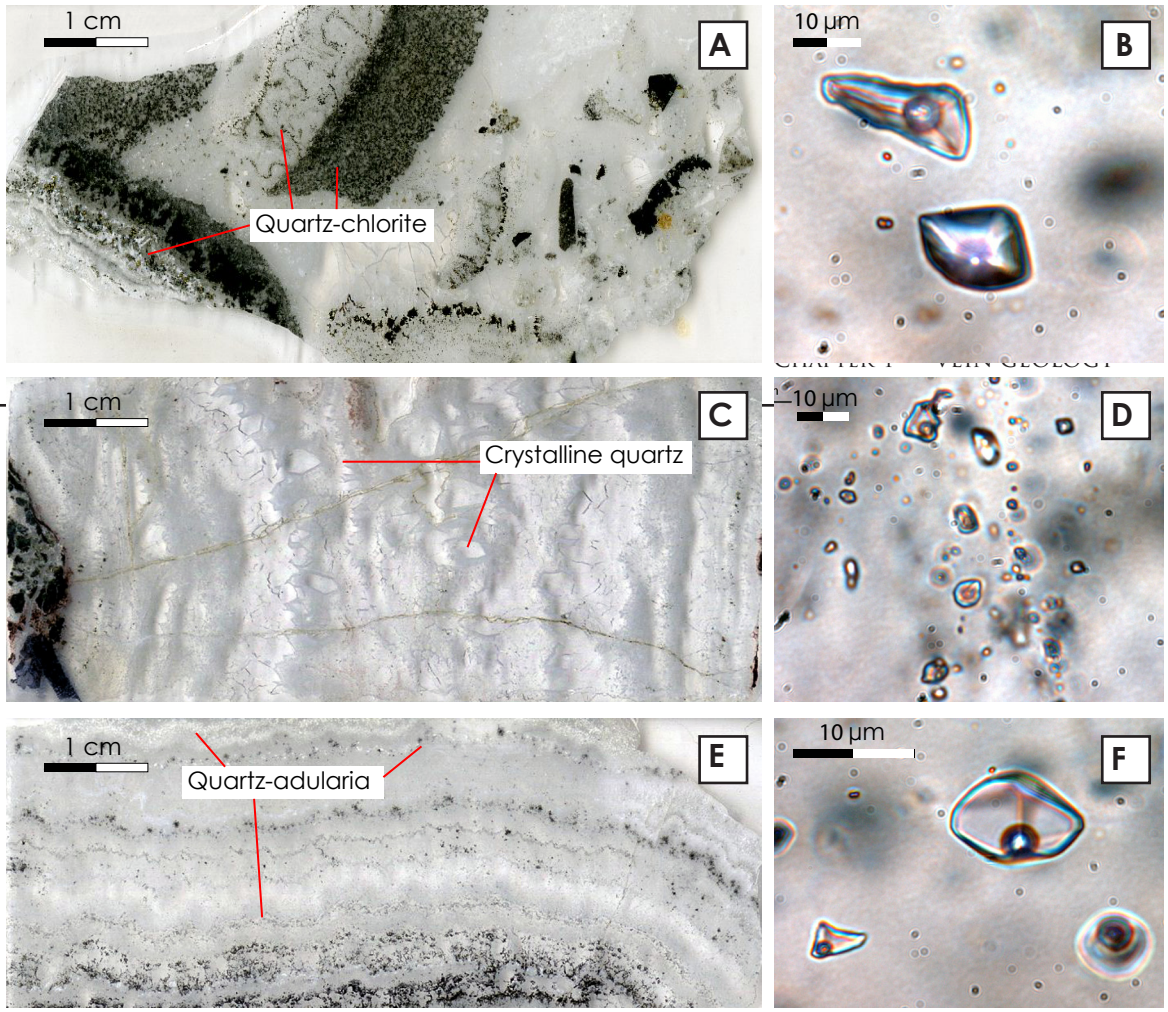

Fig. 4.33 Examples of fluid inclusions in the Kencana deposit
A) Crustiform banded quartz-chlorite breccia (vein type 8) inclusion wafer. Sample K11 sub3 B. Quartz chlorite material is present in rhythmic bands with crystalline quartz and minor adularia; **B)** Sub-angular liquid-vapour (LV) fluid inclusions from sample DSD105_332.6 m (QX vein type); **C)** Banded crystalline quartz (vein type 2c) inclusion wafer. Sample DSD105_332.6 m; **D)** Primary LV fluid inclusion trail within a quartz crystal from sample Sub801N015C; **E)** Crustiform banded quartz-adularia (vein type 9) inclusion wafer. Sample Sub8WA01. Quartz-adularia is banded with crystalline quartz and sulfide/ selenides and electrum; F) Sub-angluar and sub-rounded LV fluid inclusions from Sub801N015C.

the daughter crystal. Based on salinity measurements obtained from inclusions in the same FIA, the daughter mineral is unlikely to be halite or other salts. This inclusion returned the highest homogenization temperature (306°C) measured in this study. Boiling assemblages (co-existing liquid-rich and vapour-rich fluid inclusions) were not observed in this study.

Microthemometry involved measuring the temperatures at which the phase transformations occurred during heating and freezing of fluid inclusions. Data from Coote (2003) is shown with data collected during this study due to the statistical similarities in the results.

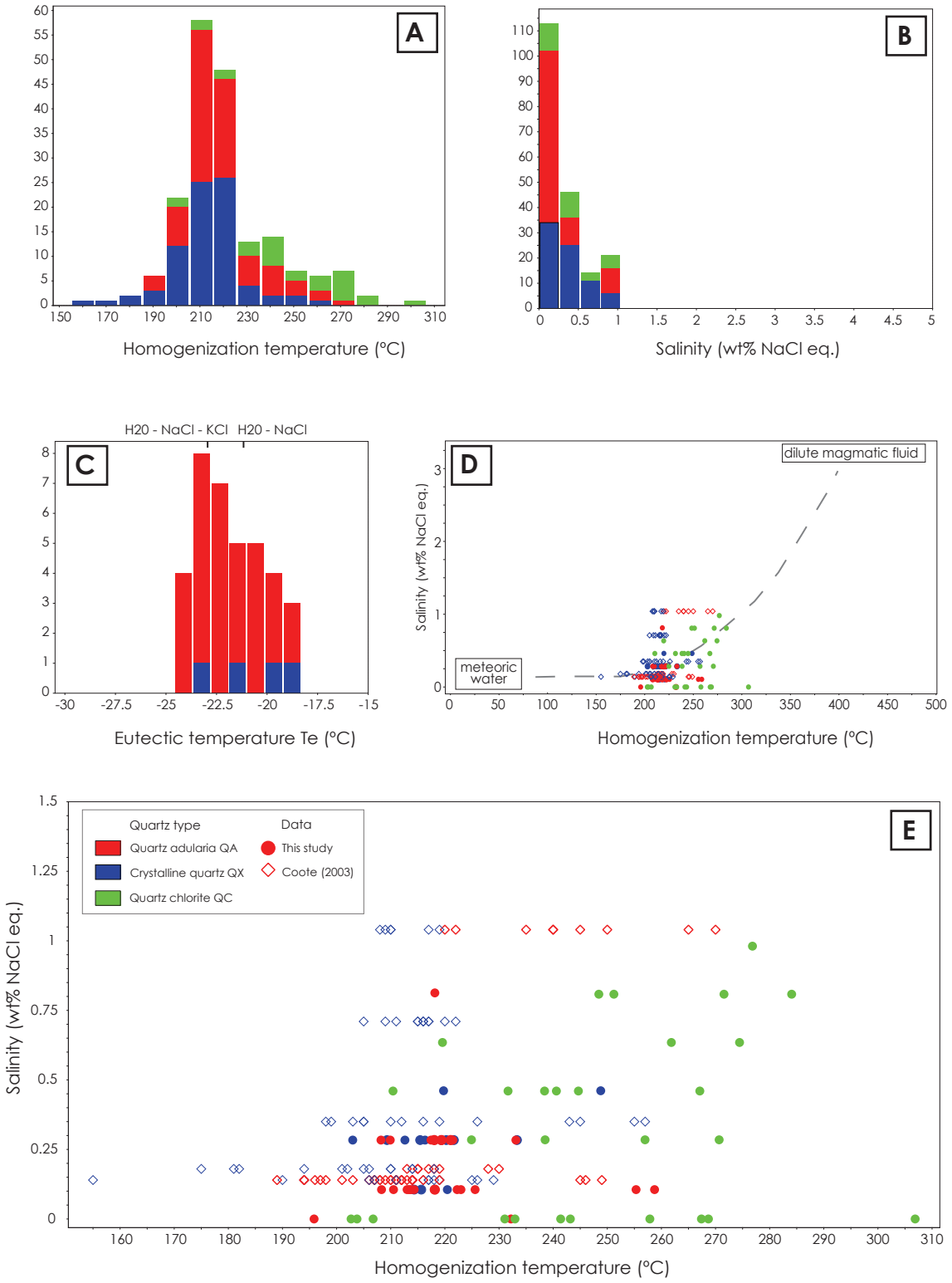

Fig. 4.34 Summary of microthermometric data from Kencana fluid inclusions

A) Summary of homogenization temperature data from different vein types of the Kencana deposit; **B)** Summary of salinity data from the different vein types of the Kencana deposit; **C)** Eutectic temperatures plotted relative to salt solutions; **D)** Homogenization temperature versus salinity plot for fluid inclusions from QX (type 2c), QA (type 9) and QC (type 8) vein types at Kencana plotted relative to reservoirs for fluid mixing processes; **E)** Homogenization temperature versus salinity plot for fluid inclusions from QX, QA and QC vein types at Kencana. Data from this study shown in filled circles, data from Coote (2003) shown in hollow diamonds.

A total of 138 temperatures were measured, including H_2O freezing (Tf), 1st ice melting or eutectic temperature (Te), final ice melting temperature (Tm), and homogenization to liquid (Th). The presence of CO_2 in the fluid inclusion can lead to a shift (toward 0°C) of the final ice melting temperature and consequently a significant underestimation of the salinity (Hedenquist and Henley, 1985). No clathrates were observed in Kencana fluid inclusions. The lack of clathrate implies that if dissolved CO_2 is present in inclusions, its concentration has to be less than 0.015 m CO_2 (Diamond, 2001). Based on this observation, no correction was applied to the final ice melting temperature.

Eutectic or first ice melting temperatures (Te) range from -24.6 to -18.3°C (Fig. 4.34 C; data in the appendix). Based on the eutectic temperatures of various salt solutions (e.g. H2O-NaCl-KCl: -23°C; Brown, 1998), it is concluded that the fluid inclusions of the Kencana deposit are formed from fluids dominated by NaCl with minor KCl contribution (Fig 4.34 C).

Homogenization temperatures were variable depending on quartz type. Homogenization temperatures for inclusions in crystalline quartz (QX, type 2c) veins range from 203.0 to 248.8°C (155.0 to 257.0°C including data from Coote, (2003); 79 inclusions) and salinities range from 0.1 to 0.5 wt% NaCl (equiv.) (0.1 to 0.7 wt% NaCl (equiv.) including data from Coote, (2003)) (Fig. 4.34 A and B). Homogenization temperatures for inclusions in quartz-adularia (QA, type 9) veins range from 195.8 to 258.7°C (189.0 to 270.0°C including data from Coote, (2003); 102 inclusions) and salinities range from 0.0 to 0.8 wt% NaCl (equiv.) (0.0 to 1.0 wt% NaCl (equiv.) including data from Coote, 2003) (Fig 4.34 A and B). Homogenization temperatures for inclusions in quartz-chlorite (QC, type 8) veins range from 202.7 to 306.9°C and salinities range from 0.0 to 1.0 wt% NaCl (equiv.) (29 inclusions; Fig 4.34 A and B).

A peak in the homogenization temperature range for both QA and QX fluid inclusions is apparent between 200 and 225°C. QC fluid inclusions record slightly higher homogenization temperatures than QA and QX inclusions (Fig 4.34 A and B), inferring a pulse of higher temperature fluid at the same low salinity during this stage of vein formation.

Fig. 4.34 D shows the data relative to salinity and homogenization temperature. Data fall along a trend defined by mixing between meteoric water and a very dilute magmat-

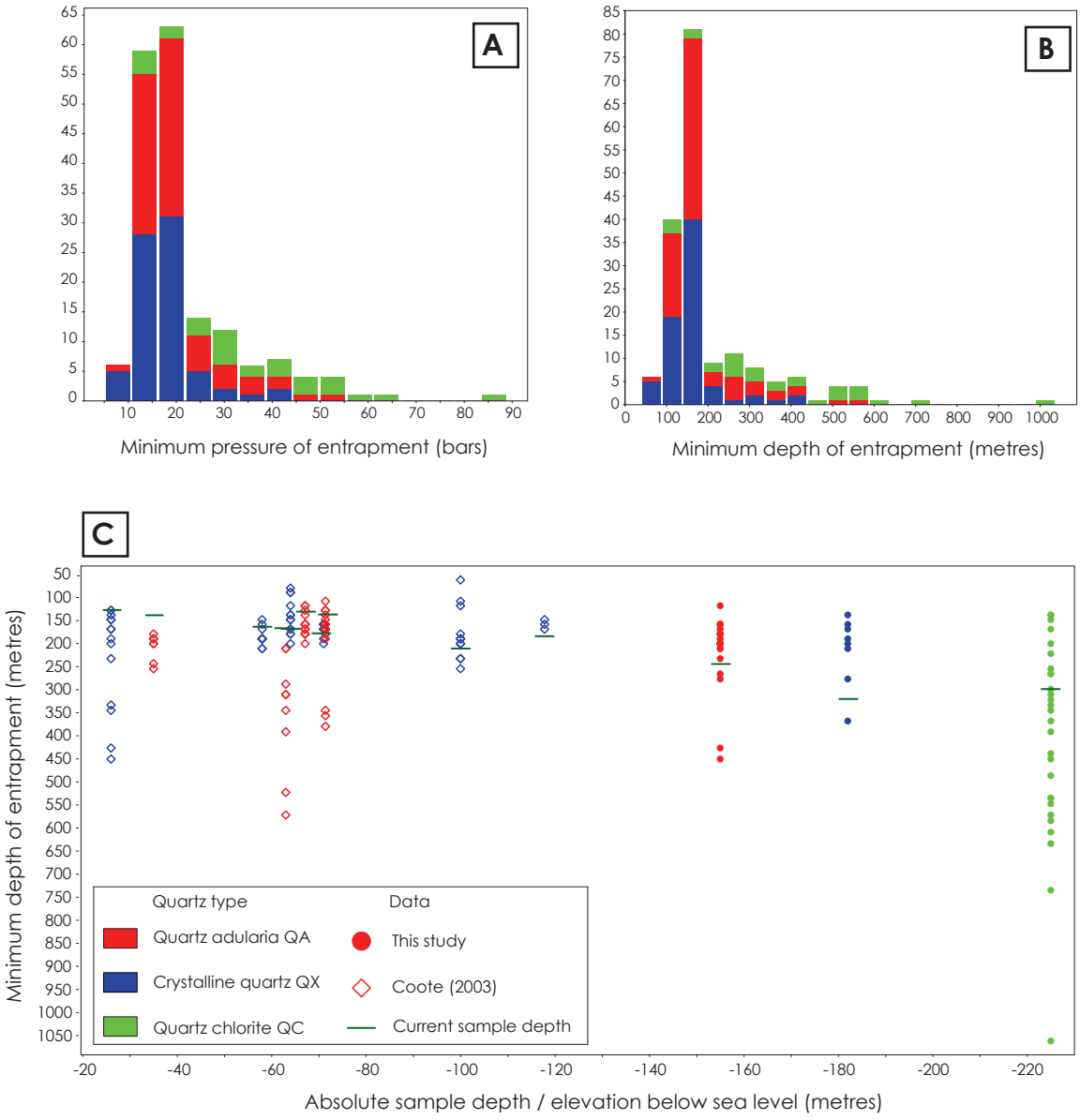

Fig. 4.35 Summary of pressure data from Kencana fluid inclusions
A) and B) Summary of minimum pressure of entrapment and minimum depth of entrapment. Minimum pressure of entrapment was calculated using Flincor™ and using the equation of Zhang and Frantz (2007). Minimum depth of entrapment was calculated using the equation from Hedenquist and Henley (1985) and based on hydrodynamic pressure; **C)** Summary plot of the minimum depth of entrapment against each current sample elevation location. Current location downhole of each sample is also displayed. Data from this study shown in filled circles, data from Coote (2003) shown in hollow diamonds.

ic fluid. The magmatic fluid reservoir is defined by a moderate to high salinity (5-10 wt% NaCl eq.) and by high temperature (T > 350°C; Hedenquist et al., 1998). Fluid inclusions from QA and QX vein types are strongly dominated by meteoric water composition, and fluid inclusions from the QC vein types have a slightly increased dilute magmatic component

(Fig. 4.34 D).

Microthermometry data can be used to infer processes of gold transportation within the hydrothermal system. Cooke and Simmons (2000) suggested that gold chloride is unlikely to be important as a transporting agent at temperatures below 300°C, due to its strongly temperature dependent stability. It is proposed that gold hydrosulfides (in particular, $Au(HS)_2^-$; Cooke and Simmons, 2000) are most significant in terms of gold transport in a reduced, dilute magmatic-derived fluid. It is possible that Au in a hydrothermal fluid undergoing temperature (and/ or salinity) decrease can switch from chloride to hydrosulfide complexes without resulting in gold deposition (Cooke and Simmons, 2000)

Boiling is a process in the Kencana deposit that does not affect the stability of gold chloride (Cooke and Simmons, 2000) but will affect the stability of gold hydrosulfide and trigger gold precipitation due to H_2S loss. Evidence for boiling is supported by pressure of entrapment calculations (Fig. 4.35 C) and the presence of bladed quartz pseudomorphs within the vein, though no boiling assemblages were observed in fluid inclusions. Mixing is also an important process in gold deposition. If it is assumed that most of the gold was transported as hydrosulfide complexes in a reduced, dilute magmatic-derived fluid, any mixing with a more oxidised fluid such as meteoric water could destabilize the gold hydrosulfide and trigger gold precipitation.

4.11 Discussion of pressure estimates

Pressures of entrapment were calculated using the equation of Zhang and Frantz (2007, H_20-NaCl system) and Flincor™ software (Brown, 1989). Boiling assemblages (vapour-rich coexisting with liquid-rich fluid inclusions) were not observed, so consequently the calculated pressure is not absolute but should be considered the minimum pressure of entrapment. Minimum depth of entrapment was calculated based on hydrodynamic pressure using the equation: $P_h = 0.2087*h0.8719$ or $h = 0.8719\sqrt{(P_h/0.2087)}$, where P_h = hydrodynamic pressure in bars and h = the minimum depth of entrapment in metres (Hedenquist and Henley, 1985). A detailed database of the minimum pressure and minimum depth of entrapment for each fluid inclusion can be found in the appendix.

The majority of fluid inclusions from QX and QA vein types recorded a pressure of entrapment between 10-20 bars. All QX fluid inclusions were trapped between 5 to 40 bars, and all QA fluid inclusions were trapped between 5 to 50 bars (Fig. 4.35 A). Fluid inclusions from QC type veins show a range of entrapment pressures, with the majority falling in the range 30-50 bars. The highest estimate of pressure entrapment was recorded in the LVD fluid inclusion (89 bars).

Minimum depth of entrapment for each fluid inclusion from crystalline quartz, quartz-adularia and quartz-chlorite veins based on data from this study and from Coote (2003) was plotted against their absolute (based on actual sea level) elevation (Fig. 4.35 C). Specific depth downhole (below surface, marked by a green line) of each fluid inclusion is also displayed and is assumed to represent the current hydrologic column sitting respectively on top of each sample, assuming the water table is near-surface. Most of the fluid inclusions were trapped between 50 m shallower and 200 m deeper than their current depth. Anomalously deep inclusions can be explained by the fact that calculation of the minimum depth of entrapment is extremely sensitive to homogenization temperature; consequently fluid inclusions from the QC veins located just below the QX and QA veins exhibit higher minimum depth of entrapment compared to the others. Minimum depths of entrapment higher than their current location (depth) can explained by the fact the water table elevation is not well constrained, which can shift the green line toward shallower depth if the water table wasn't located near the surface at the time of the formation. In summary, if the uncertainty in the position of the water table is taken into account, most of the fluid inclusions were trapped 50 to 200 m deeper than their current location which implies that Kencana was uplifted up to 200 m between the time of its formation and the present, or that the water table was at least 200 m higher than the current erosion surface.

4.12 Metal Distribution, Zonation and Ratios

Vertical and lateral metal zonation is a common feature of epithermal deposits. The distribution and zonation of metals in ore deposits can aid in the determination fluid pathways and the physio-chemical conditions of metal transport and precipitation (e.g. Julcani Mining District, Peru, Goodell and Petersen, 1974; Fresnillo, Mexico, Gemmell et al., 1988;

Mt Muro District, Indonesia, Wurst, 2004). Precious metal mineralization in low sulfidation systems is more prevalent at shallow levels, with a transition to higher base metal values with increasing depth in response to changing physiochemical conditions.

Geochemical data for the K1 vein of the Kencana deposit were obtained from exploration and mine metal assays. Exploration drill cores are routinely assayed at 1 m intervals through mineralized zones for Ag, As, Au, Cu, Mo, Pb, Sb and Zn by conventional methods using an Indonesian commercial laboratory. Only sparse data for sulfur and selenium were available, and were not used in this study. This study includes assays obtained from diamond drill cores on 6 east-west cross-sections that span the vertical and lateral extent of the K1 structure (19600mn, 19700mN, 19800mN, 19900mN, 20000mN and 20050mN; Fig. 4.36), comprising a total of 58,790 sample points. Assay methods and detection limits (LOD) are displayed in Table 4.2. Metal assays returning values below LOD were not in-

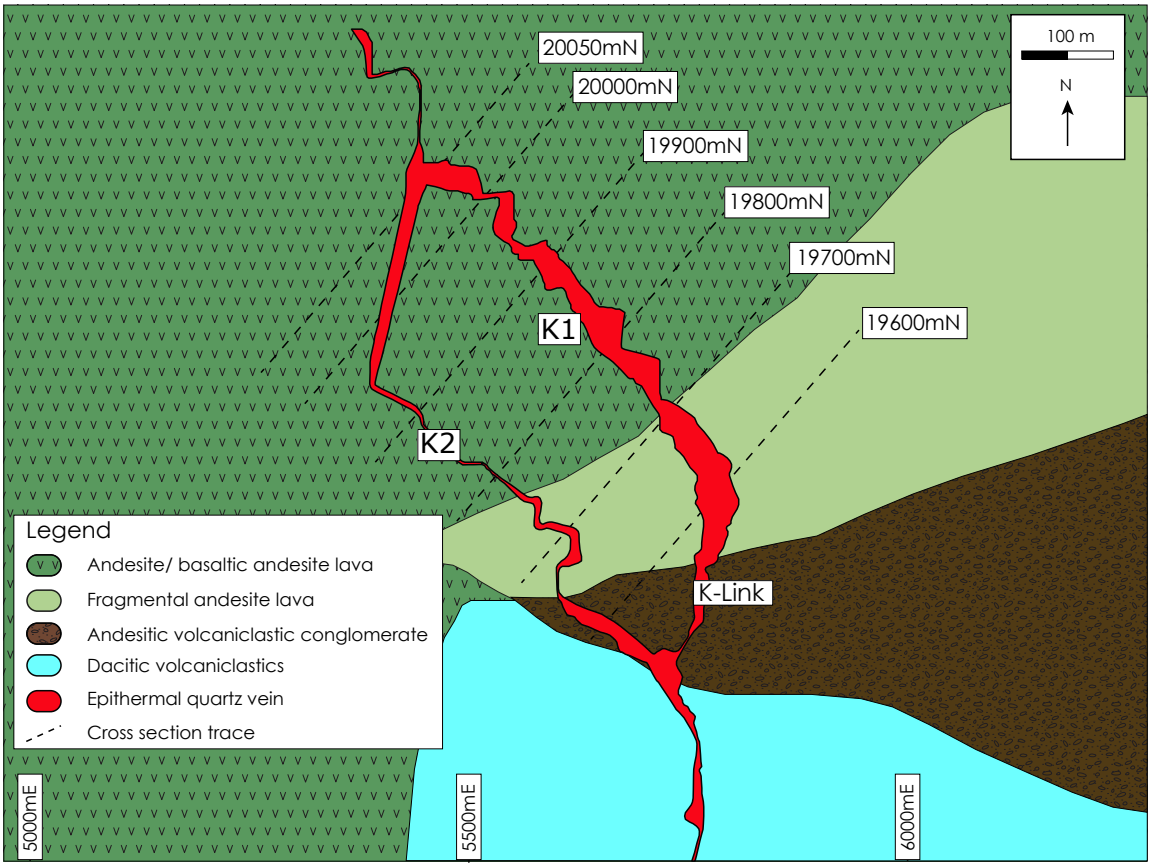

Fig. 4.36 Representative cross sections for metal zonation contouring 6 east-west cross-sections covering the vertical and lateral extent of the K1 structure: 19600mn, 19700mN, 19800mN, 19900mN, 20000mN and 20050mN.

cluded in the study. Detailed metal contouring along the 6 cross sections was undertaken using Surfer® by natural neighbour method with an anisotropy ratio of 1, and 3 m line spacing.

Assay data were plotted relative to elevation (*relative level*, RL) in the Kencana deposit to determine the major trends in vertical metal zonation. The deposit was divided into 4 RL

Element	Au	Ag	As	Cu	Mo	Pb	Sb	Zn
Assay method	FAAS	AAS	AAS	AAS	XRF	ICP	XRF	AAS
LOD (ppm)	0.1	0.1	1.0	1.0	1.0	1.0	0.4	1.0

Table 4.2 Assay methods and limits of detection (LOD) by element for Kencana drill core. FAAS = Fire Assay, AAS = Atomic Absorption Spectrometry, XRF = X-Ray Fractionation, ICP = Inductively Coupled Plasma Mass Spectrometry.

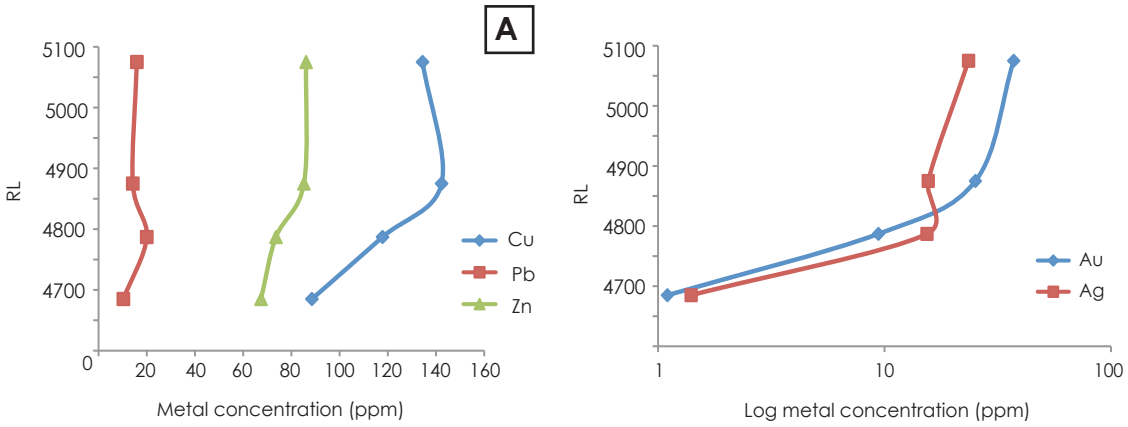

Fig. 4.37 Kencana mean metal values vs. relative level (RL). A) Base metals vs. RL **B)** Precious metals vs. RL

RL (mRL)	N	Au (ppm)				Ag (ppm)				Cu (ppm)			
		Max	*Min*	*Mean*	*S.D*	*Max*	*Min*	*Mean*	*S.D*	*Max*	*Min*	*Mean*	*S.D*
4670-4800RL	1141	52.3	0.02	1.1	0.9	19.7	0.1	1.4	2.9	351	4	88.5	61.2
4800-4875RL	2291	134	0.02	9.4	23.4	650	0.1	15.4	58.4	966	6	117.8	96.7
4875-4950RL	2136	1960	0.02	25.2	124.4	640	0.1	15.6	59.8	966	6	142.3	37.9
4950-5100RL	1764	1720	0.02	37.2	214	649	0.1	23.51	92.5	3740	12	134.4	108
	N	**Pb (ppm)**				**Zn (ppm)**							
		Max	*Min*	*Mean*	*S.D*	*Max*	*Min*	*Mean*	*S.D*				
4670-4800RL	1141	78	4	10.3	10.9	214	10	67.4	34.6				
4800-4875RL	2291	272	4	20	33.5	419	9	73.6	48.4				
4875-4950RL	2136	225	4	14.2	22.7	679	17	85.2	54.2				
4950-5100RL	1764	407	3	15.9	31.8	455	25	86.1	44.6				

Table 4.3 Summary of Kencana metal values vs. relative level (RL)

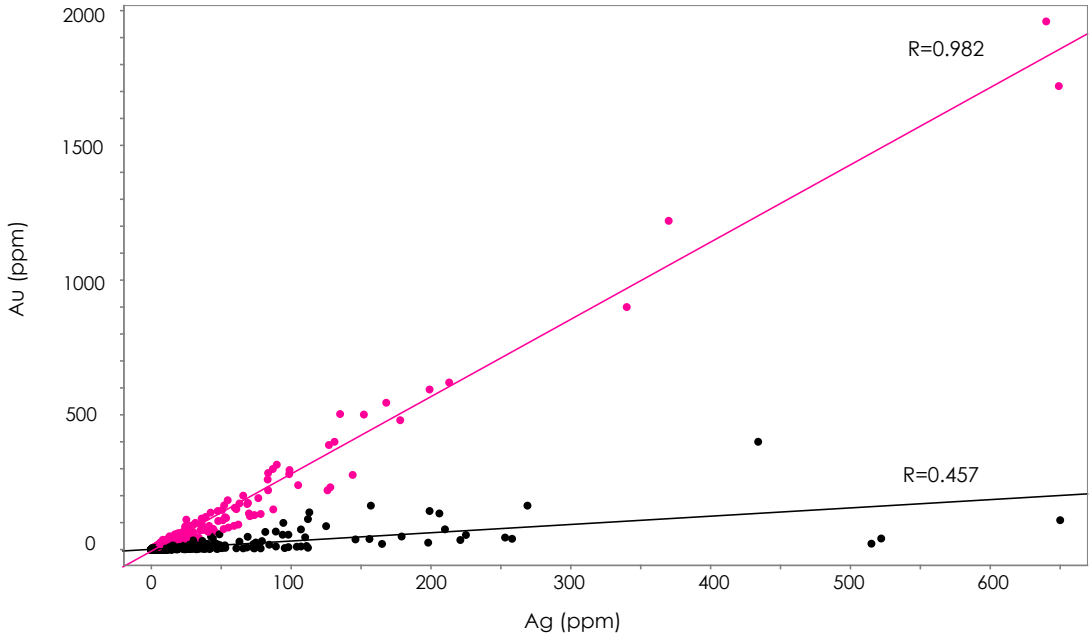

Fig. 4.38 Au (ppm) vs. Ag (ppm) plot for metal values from the K1 vein, showing multiple regression and two separate populations. Pink population represents a good correlation (R=0.982) between Au and Ag, reflecting electrum mineralization. Black population represents a trend to high Ag values with low Au (R=0.457), reflecting silver-rich species such as aguilarite and naumannite.

intervals (4670-4800mRL, 4800-4875RL, 4875-4950mRL, and 4950-5100mRL) and mean values for precious and base metals were plotted for these intervals. Summary results are shown in Table 4.3 and major trends are shown in Fig. 4.37.

Summary data show that the Kencana deposit is vertically zoned with respect to Au, Ag, Cu, Pb and Zn. Fig. 4.37 shows the distribution of precious metals vs. relative level. Both Au and Ag grades increase towards shallower RLs, with highest mean grades at the top of the deposit. Base metal distribution (Fig. 4.37 A) shows the vertical distribution of highest mean Cu, Pb and Zn grades. Zn is enriched in the higher to mid levels of the deposit (5150-4900mRL), followed by a peak in Cu values at 4875RL and Pb values at 4800mRL. This zonation is a result of metals preferentially precipitating at different temperatures across the system. Overall, Cu is the most enriched base metal in the system, with mean grades from 88.5-142.3 ppm compared to 67.4-86.1 ppm and 10.3-20 ppm for Zn and Pb respectively. Data for single element (Au, Ag, Cu, Pb, Zn, As, Sb, Mo) assays are plotted in Figs. 4.39-4.44, showing the composite elemental values for each vein intercept on the 6 cross sections.

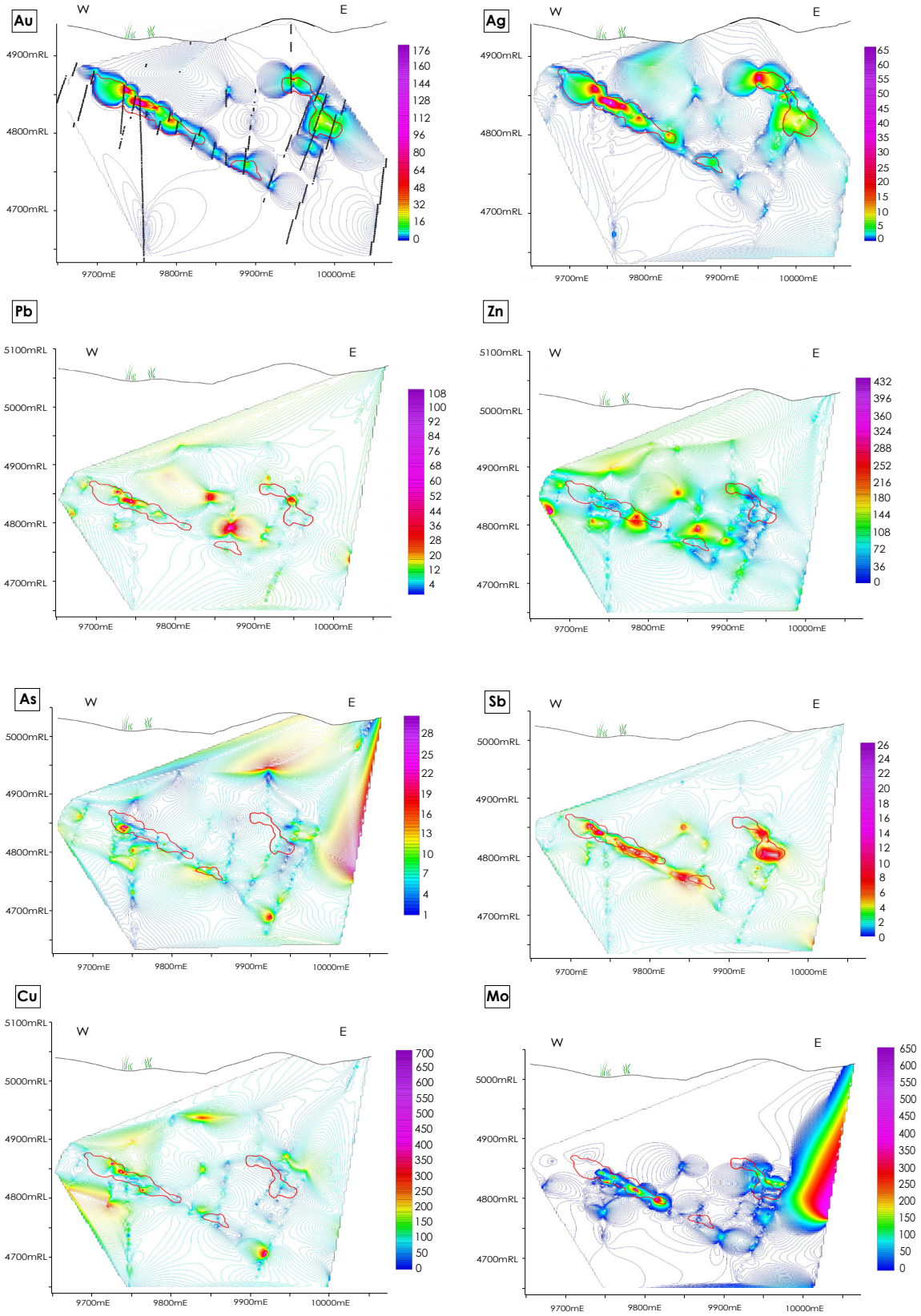

Fig. 4.39 Metal zonation section 19600mN Metal values obtained from diamond drill core assays on section 19600mN. Assay locations shown as black dot points (sample locations are consistent for all figures on this cross section). Red outlines depict Au anomaly. Au zonation; Ag zonation; Pb zonation; Zn zonation; As zonation; Sb zonation; Cu zonation; Mo zonation

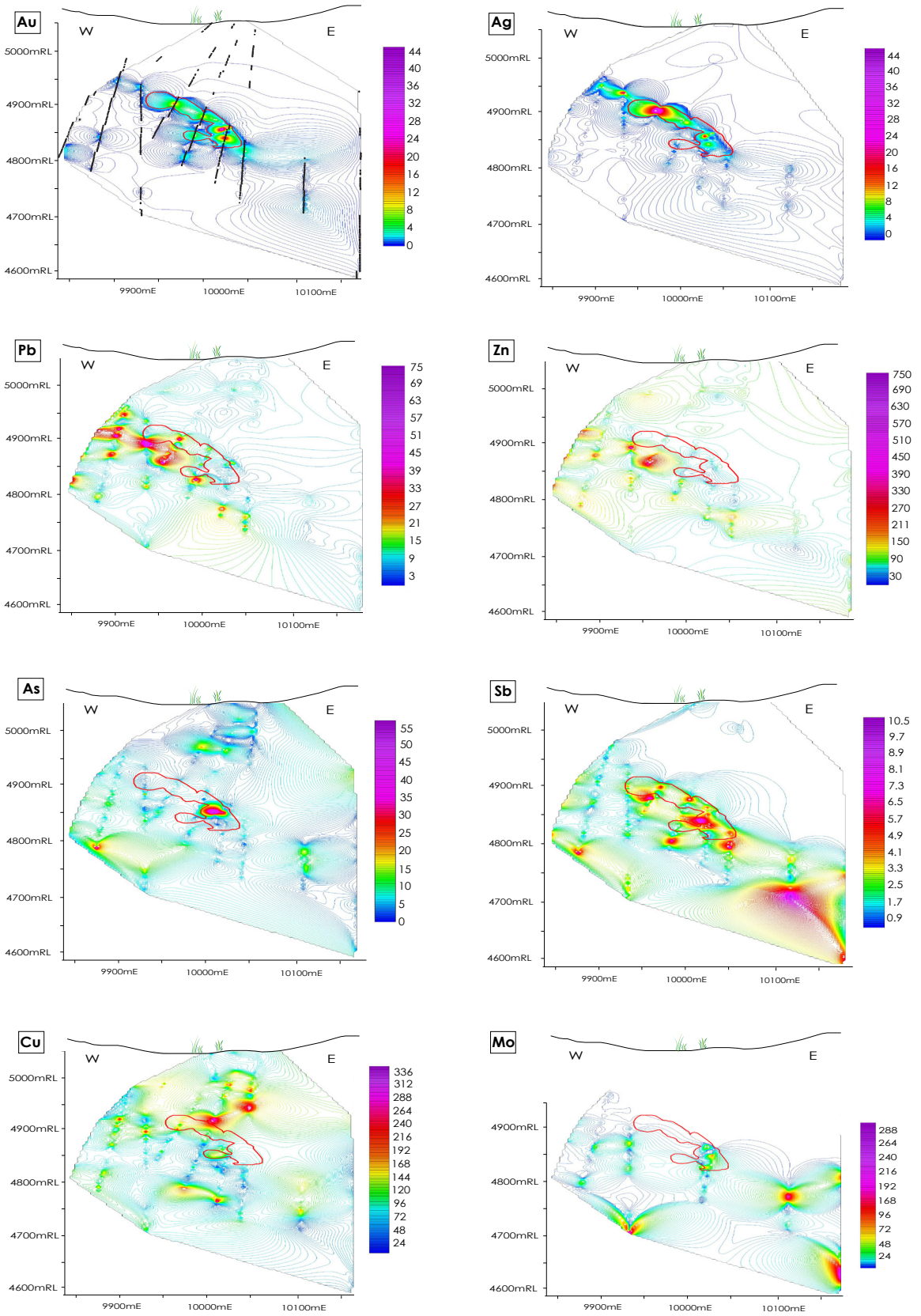

Fig. 4.40 Metal zonation section 19700mN Metal values obtained from diamond drill core assays on section 19700mN. Assay locations shown as black dot points (sample locations are consistent for all figures on this cross section). Red outlines depict Au anomaly. Au zonation; Ag zonation; Pb zonation; Zn zonation; As zonation; Sb zonation; Cu zonation; Mo zonation

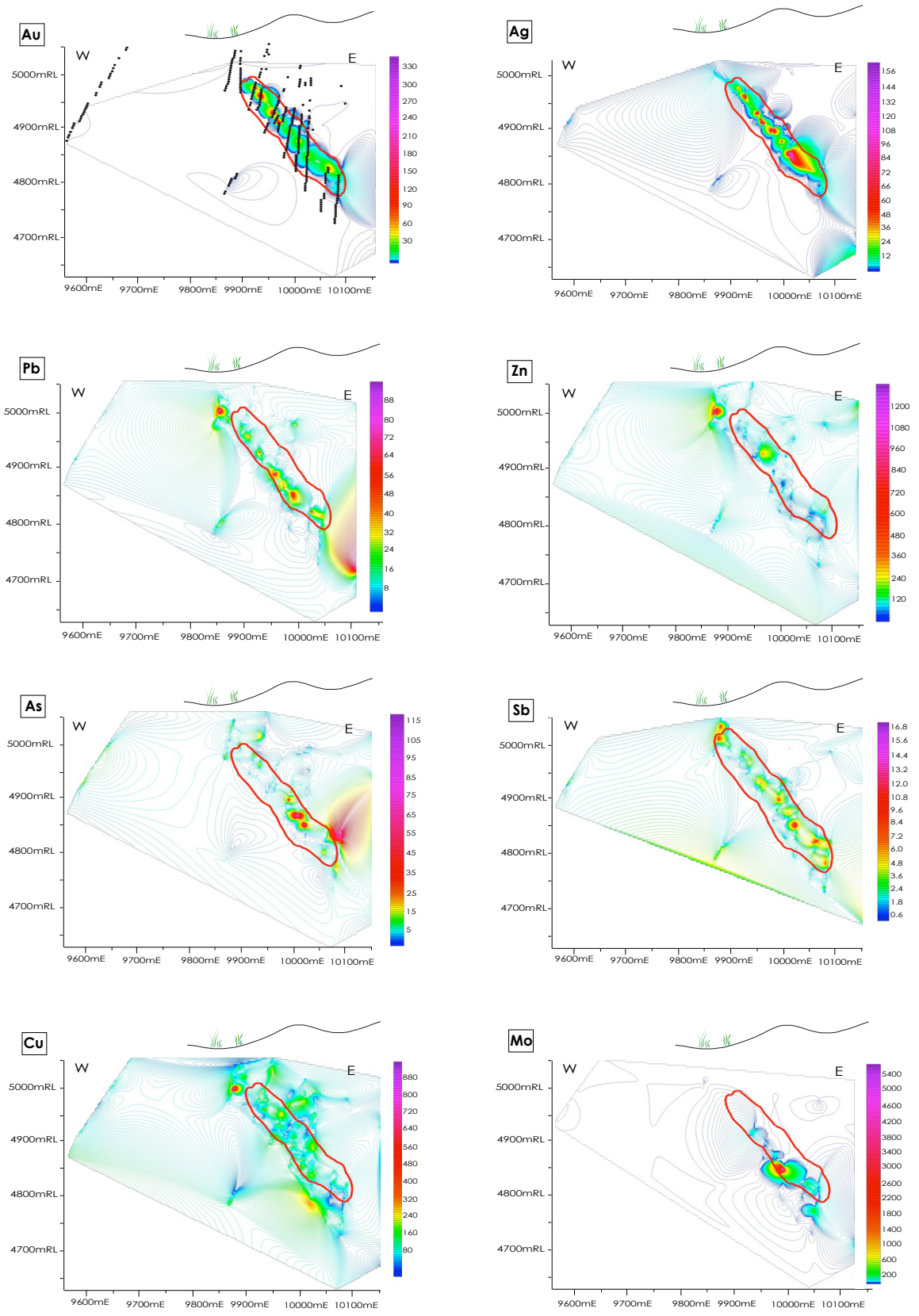

Fig. 4.41 Metal zonation section 19800mN Metal values obtained from diamond drill core assays on section 19800mN. Assay locations shown as black dot points (sample locations are consistent for all figures on this cross section). Red outlines depict Au anomaly. Au zonation; Ag zonation; Pb zonation; Zn zonation; As zonation; Sb zonation; Cu zonation; Mo zonation

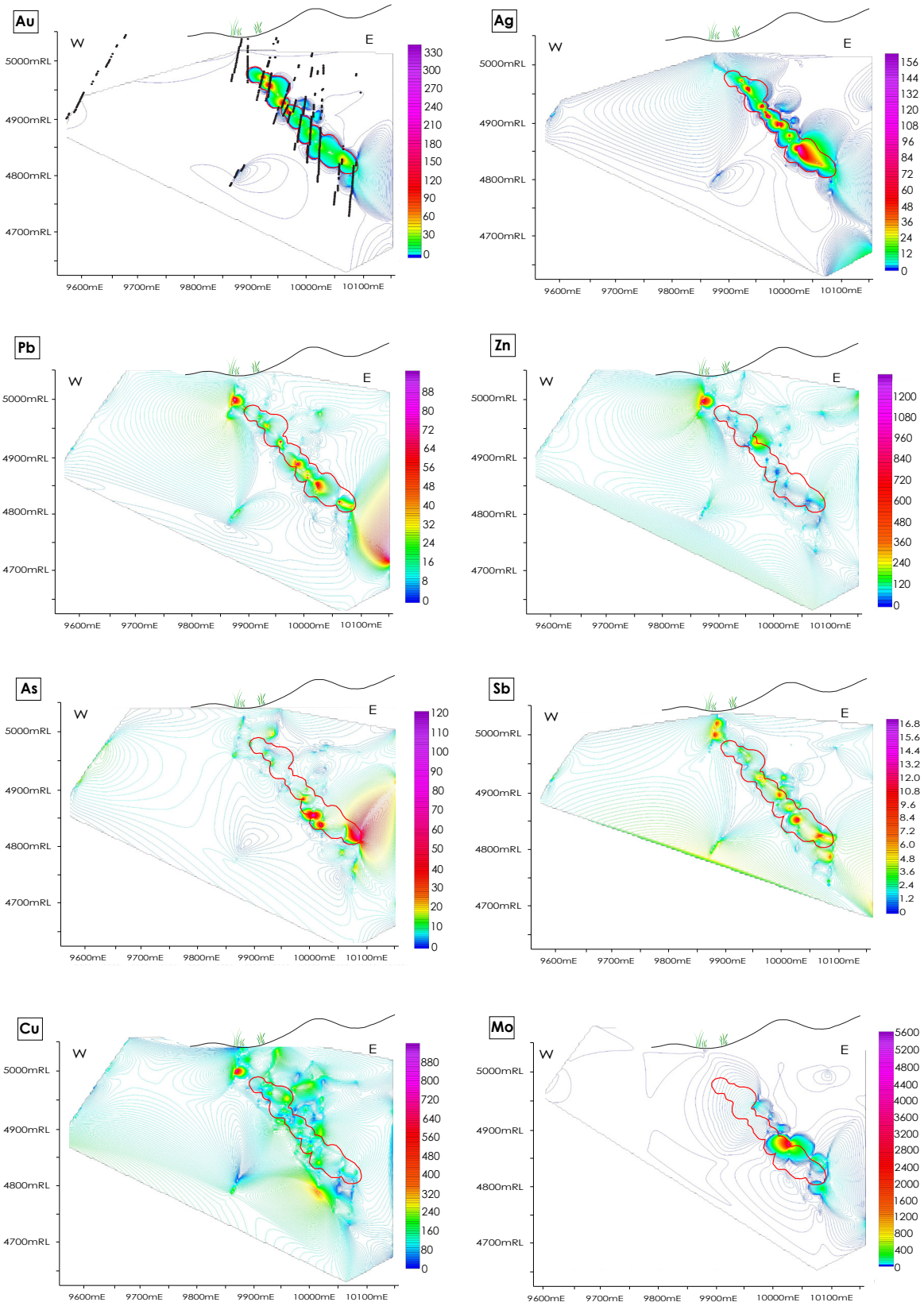

Fig. 4.42 Metal zonation section 19900mN Metal values obtained from diamond drill core assays on section 19900mN. Assay locations shown as black dot points (sample locations are consistent for all figures on this cross section). Red outlines depict Au anomaly. Au zonation; Ag zonation; Pb zonation; Zn zonation; As zonation; Sb zonation; Cu zonation; Mo zonation

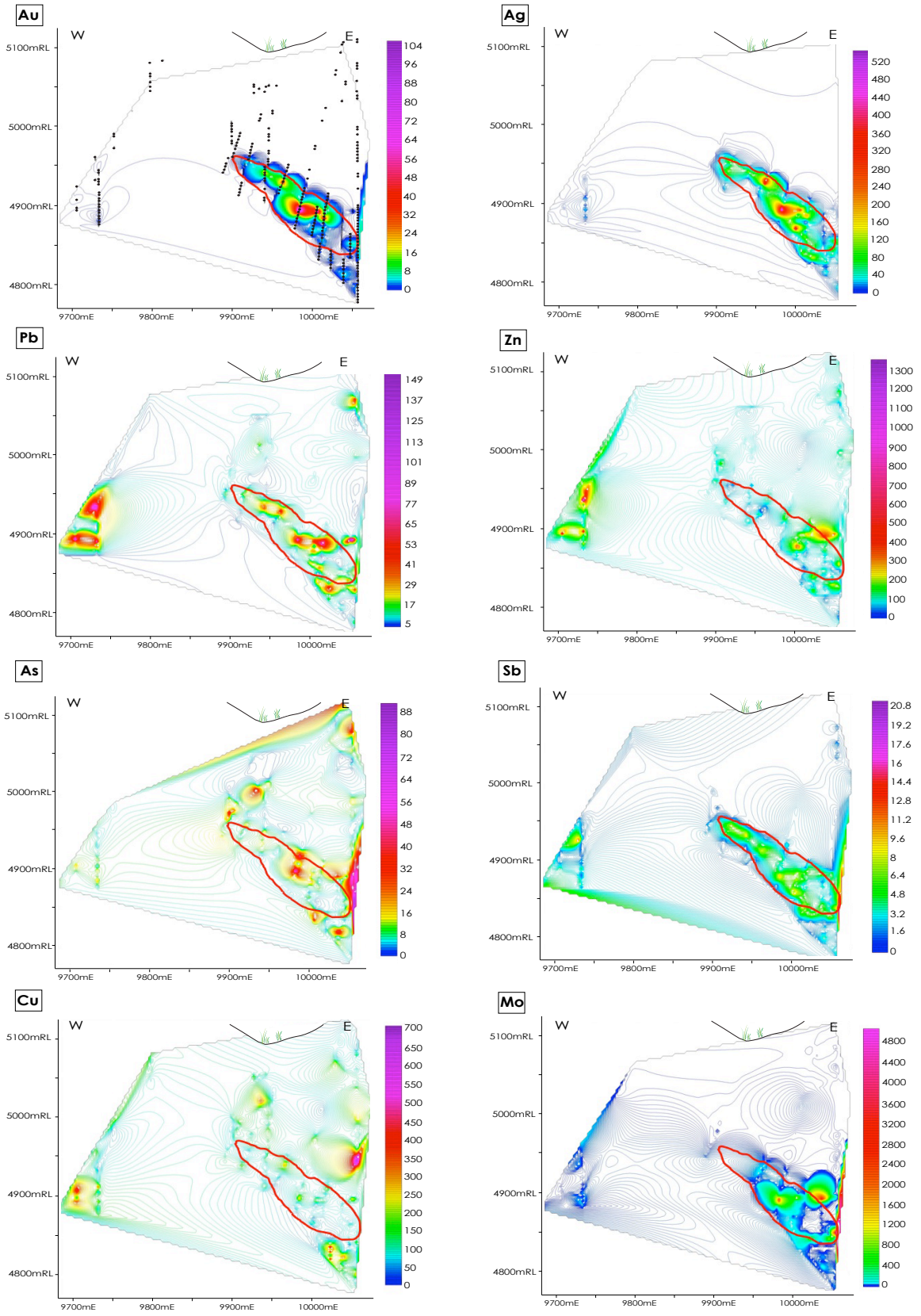

Fig. 4.43 Metal zonation section 20000mN Metal values obtained from diamond drill core assays on section 20000mN. Assay locations shown as black dot points (sample locations are consistent for all figures on this cross section). Red outlines depict Au anomaly. Au zonation; Ag zonation; Pb zonation; Zn zonation; As zonation; Sb zonation; Cu zonation; Mo zonation

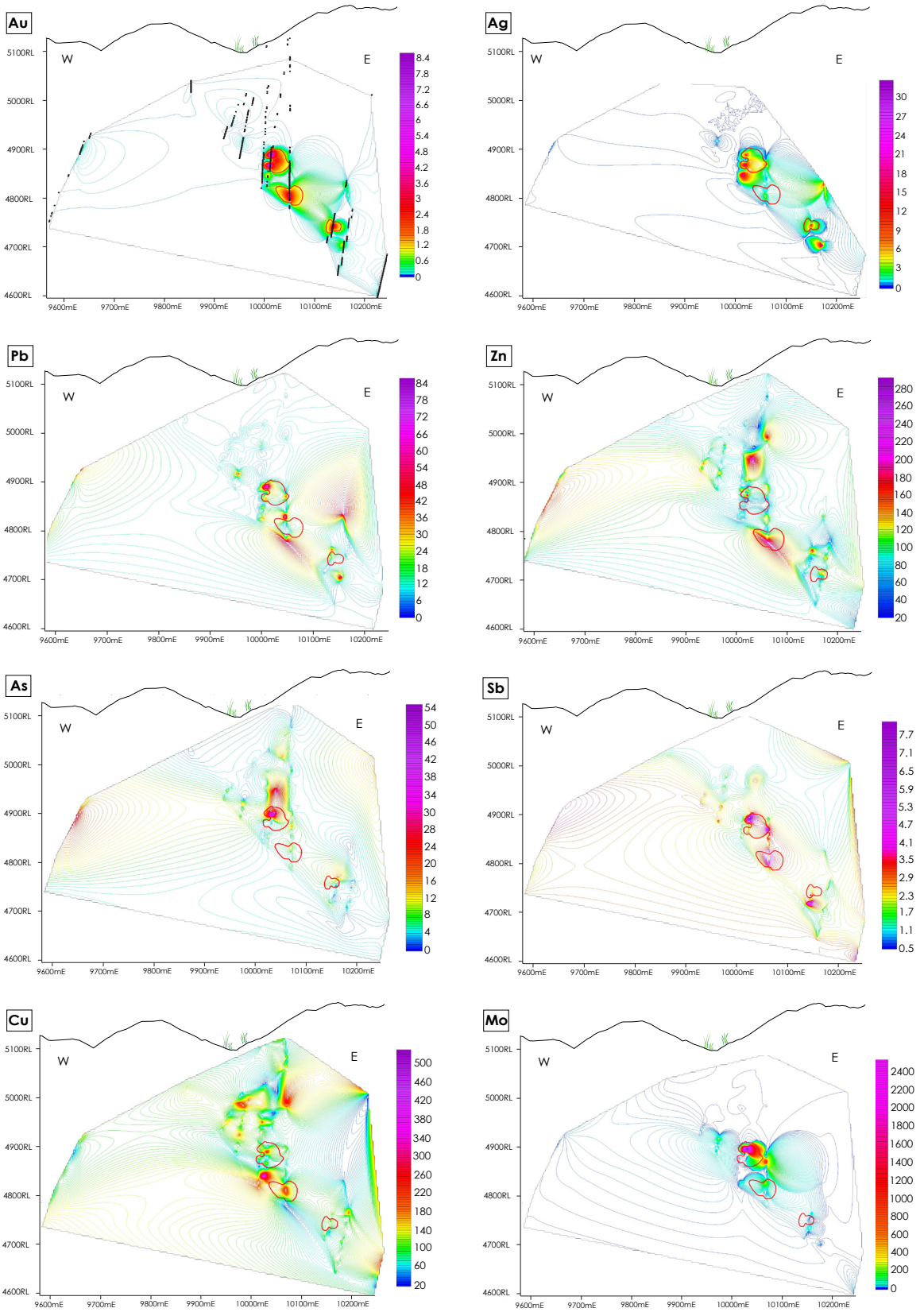

Fig. 4.44 Metal zonation section 20050mN Metal values obtained from diamond drill core assays on section 20050mN. Assay locations shown as black dot points (sample locations are consistent for all figures on this cross section). Red outlines depict Au anomaly. Au zonation; Ag zonation; Pb zonation; Zn zonation; As zonation; Sb zonation; Cu zonation; Mo zonation

A distinct vertical and lateral metal zonation is recognized at the Kencana deposit and some elements provide useful gradients towards targeting the ore zone. Element distribution patterns are discussed below. Metal contouring shows highest assay values along cross sections 19900mN and 20000mN, which intersect the central portion of the vein. To the north, cross section 20050mN shows fewer assay points returning values above LOD values, thus potentially an overall decrease in metal grades. Cross section 19600mN shows an increase in assay values, specifically Cu and Sb concentrations.

4.13 Kencana metal distribution

Precious metal distribution: Gold is the most effective pathfinder element when exploring for Au mineralization. Cross sections through the K1 vein highlight in greater detail the occurrence of Au almost exclusively within the main vein. Gold tends to occur at a slightly deeper RL in a southerly direction (approx 4850mRL; Fig. 4.39) and distribution shifts to the mid levels of the vein towards the north (approx 4890mRL; Fig 4.41). Bonanza grades (>50 ppm) are in localized pods within the main vein and occur at marginally shallower levels towards the south of the vein. Highest Au grades are intersected in cross section 19900mN (up to 330 ppm, Fig. 4.42). In general, the distribution of silver mineralization mimics the pattern of gold mineralization, as electrum is the principal Au- and Ag-bearing mineral. However, some cross sections (19600mN, 19900mN) show that discreet gold and silver mineralization occurs in different areas of the vein, especially higher-grade silver in deeper sections.

The decoupled distribution of gold and silver is shown in Fig. 4.38. Two distinct populations can be observed: Strongly correlated (R=0.982) Au and Ag values (pink population), and increasing Ag values with constant to weakly elevated Au values (R=0.457, black population). Strongly correlated Au and Ag values reflect electrum mineralization in the vein. High Ag values associated with low Au values may be due to the presence of Ag-rich species in the vein, such as aguilarite and naumannite (section 4.7).

Base metal distribution: Base metal values are, in general, low in the K1 vein, reflecting the low temperatures and dilute mineralizing fluid conditions in the Kencana deposit. Values are highest within the vein, although unconstrained anomalies occur at depth. The general trend of base metal mineralization is deeper than the levels at which precious

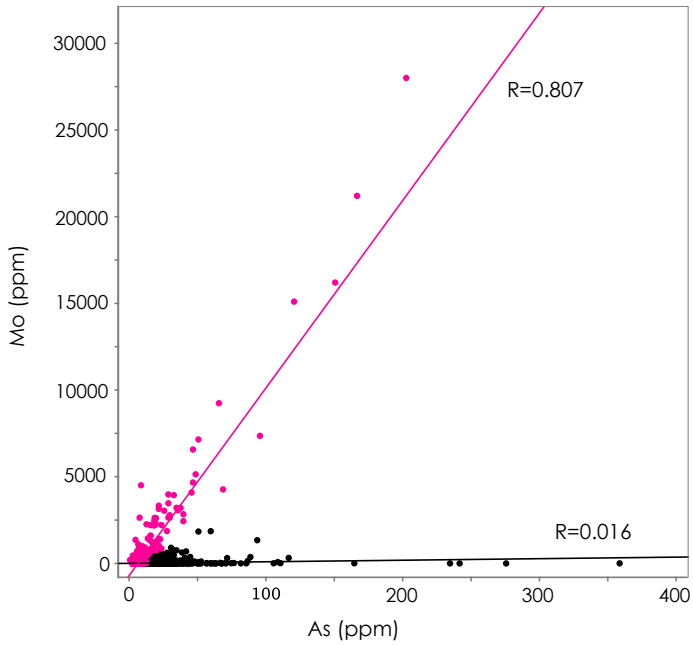

Fig. 4.45 Mo (ppm) vs. As (ppm) plot for metal values from the K1 vein, showing multiple regression and two separate populations. Pink population represents a good correlation (R=0.807) between Mo and As. Black population represents a trend to high As values with constant to low Mo (R=0.016), reflecting mineralization of As-bearing species such as arsenopyrite or tennantite.

metal mineralization is most prevalent (Figs. 4.39-4.44). This trend is due to the differing physiochemical conditions under which these metals preferentially precipitate.

Copper: Copper is very weakly related to Au-Ag mineralization and is present within the boundaries of the 1 g/t Au anomaly, although copper is also weakly enriched both above the vein and more strongly as an unconstrained anomaly at depth below the vein. The principal copper-bearing minerals in the K1 vein are chalcopyrite and bornite (section 4.9). Chalcopyrite mineralization has a close association with electrum in the Kencana vein (section 4.7), which accounts for the Au-Cu association, although some areas of the vein are Au-rich and Cu-poor (Fig. 4.43), suggesting zones of discreet Au mineralization. Copper values are highest in the northern sections of the K1 vein, with maximum grades of 3740 ppm at 19900mN (Fig. 4.42), with a mean of 117 ppm on the same cross section.

Lead: Lead has the strongest positive correlation with gold (and silver) mineralization in the K1 vein. This relationship was also observed at the Gosowong deposit by Olberg, (2001). Lead at Kencana is typically in the galena-clausthalite series, and is typically present in the sulfide-electrum rich bands of type 7, 8 and 9 infill (Section 4.7). In general, the lead grades are well confined to the 1 g/t Au anomaly and values decrease through the surrounding stockwork (e.g. Figs. 4.42 and 4.43). Cross section 20000mN (Fig. 4.43) suggests a zone of Pb mineralization to the west of the section – this is interpreted as interference from

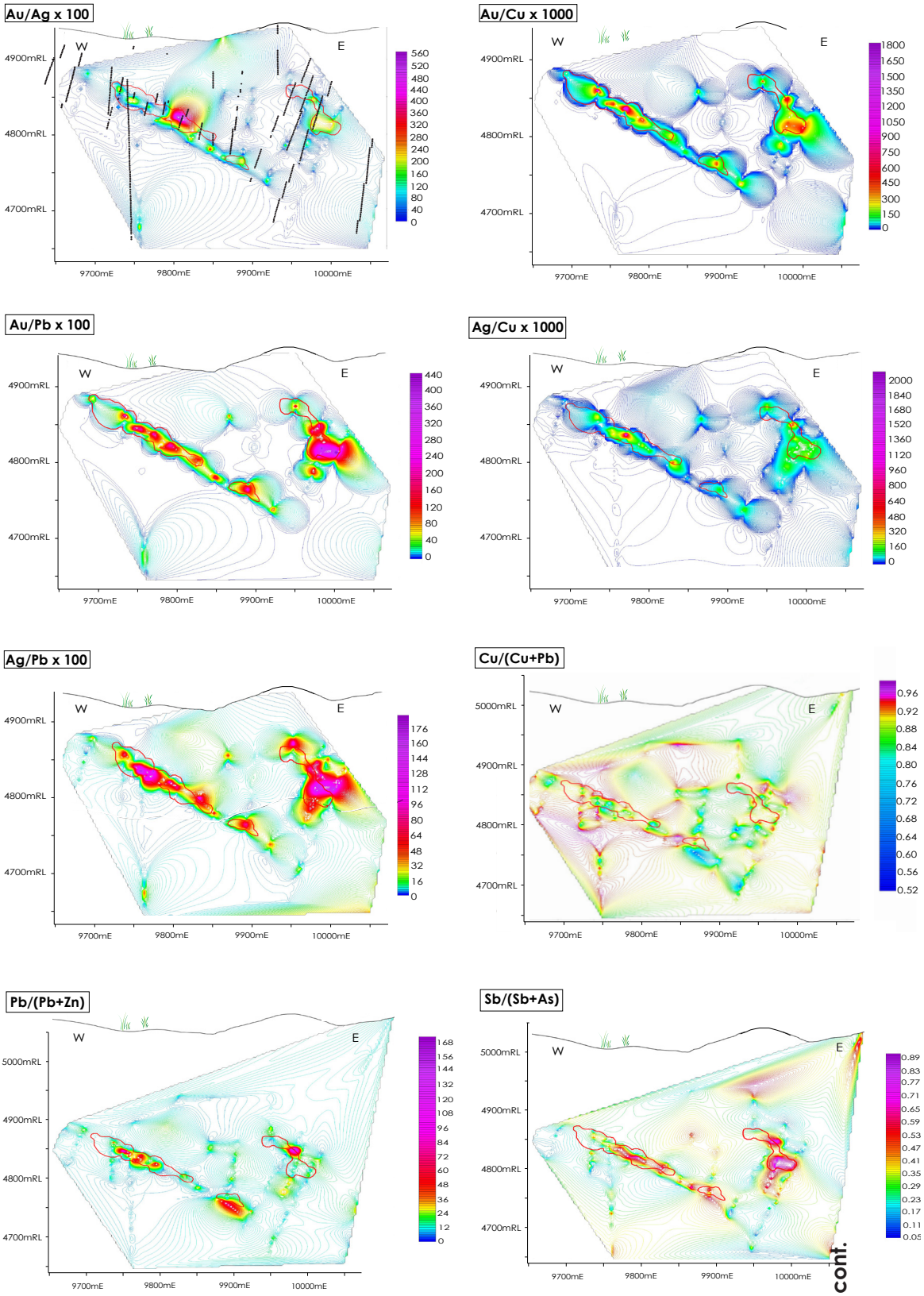

Fig. 4.46 Metal ratio zonation section 19600mN Metal values obtained from diamond drill core assays on section 19600mN. Assay locations shown as black dot points (sample locations are consistent for all figures on this cross section). Red outlines depict Au anomaly. Au/Ag x 100 zonation; Au/Cu x 1000 zonation; Au/Pb x 100 zonation; Ag/ Cu x 1000 zonation; Ag/Pb x 100 zonation, Cu/(Cu+Pb) zonation; Pb/Zn x 100 zonation; Sb/(Sb+As) zonation.

Table 4.1 cont.

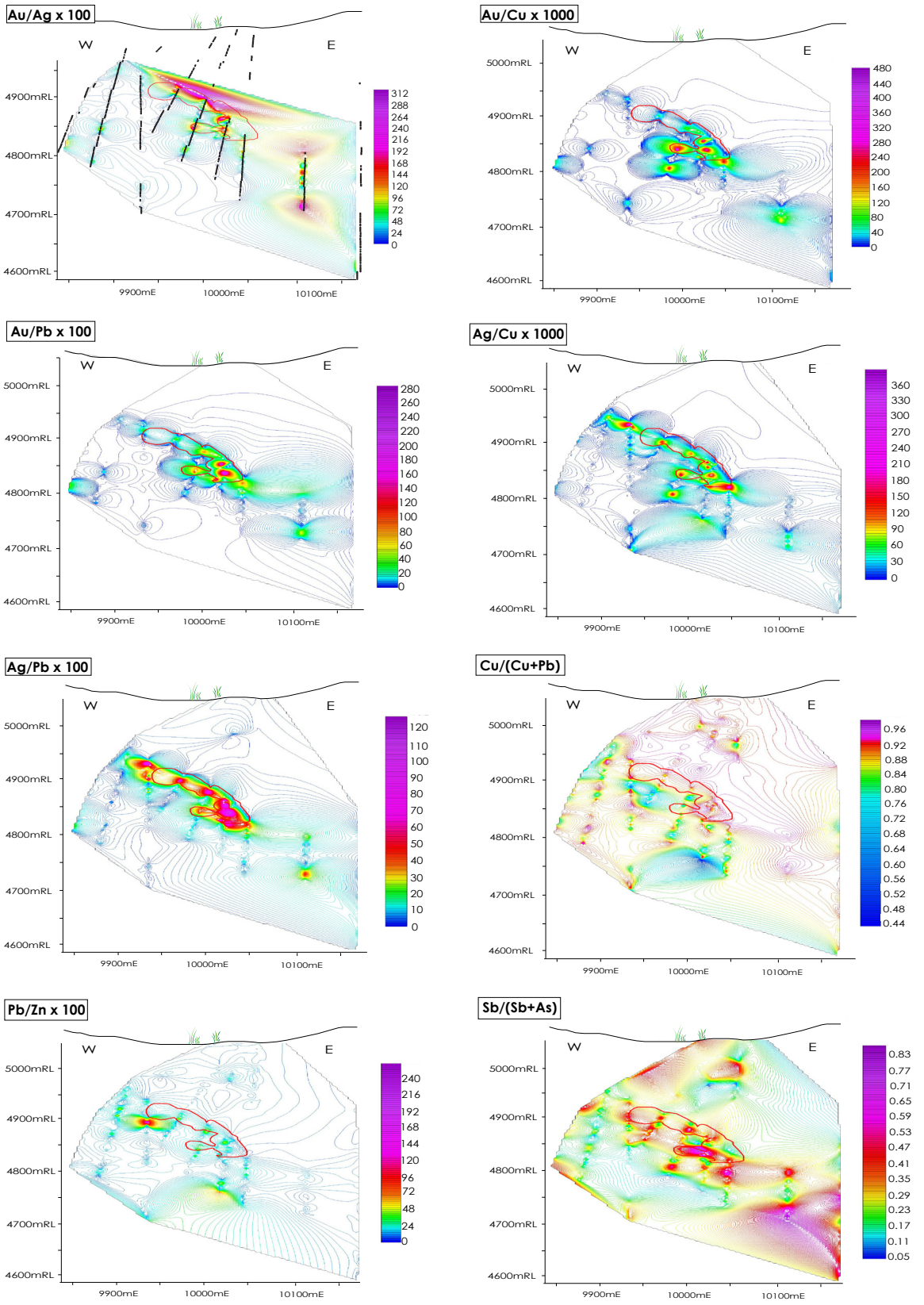

Fig. 4.47 Metal ratio zonation section 19700mN Metal values obtained from diamond drill core assays on section 19700mN. Assay locations shown as black dot points (sample locations are consistent for all figures on this cross section). Red outlines depict Au anomaly. Au/Ag x 100 zonation; Au/Cu x 1000 zonation; Au/Pb x 100 zonation; Ag/ Cu x 1000 zonation; Ag/Pb x 100 zonation, Cu/(Cu+Pb) zonation; Pb/Zn x 100 zonation; Sb/(Sb+As) zonation.

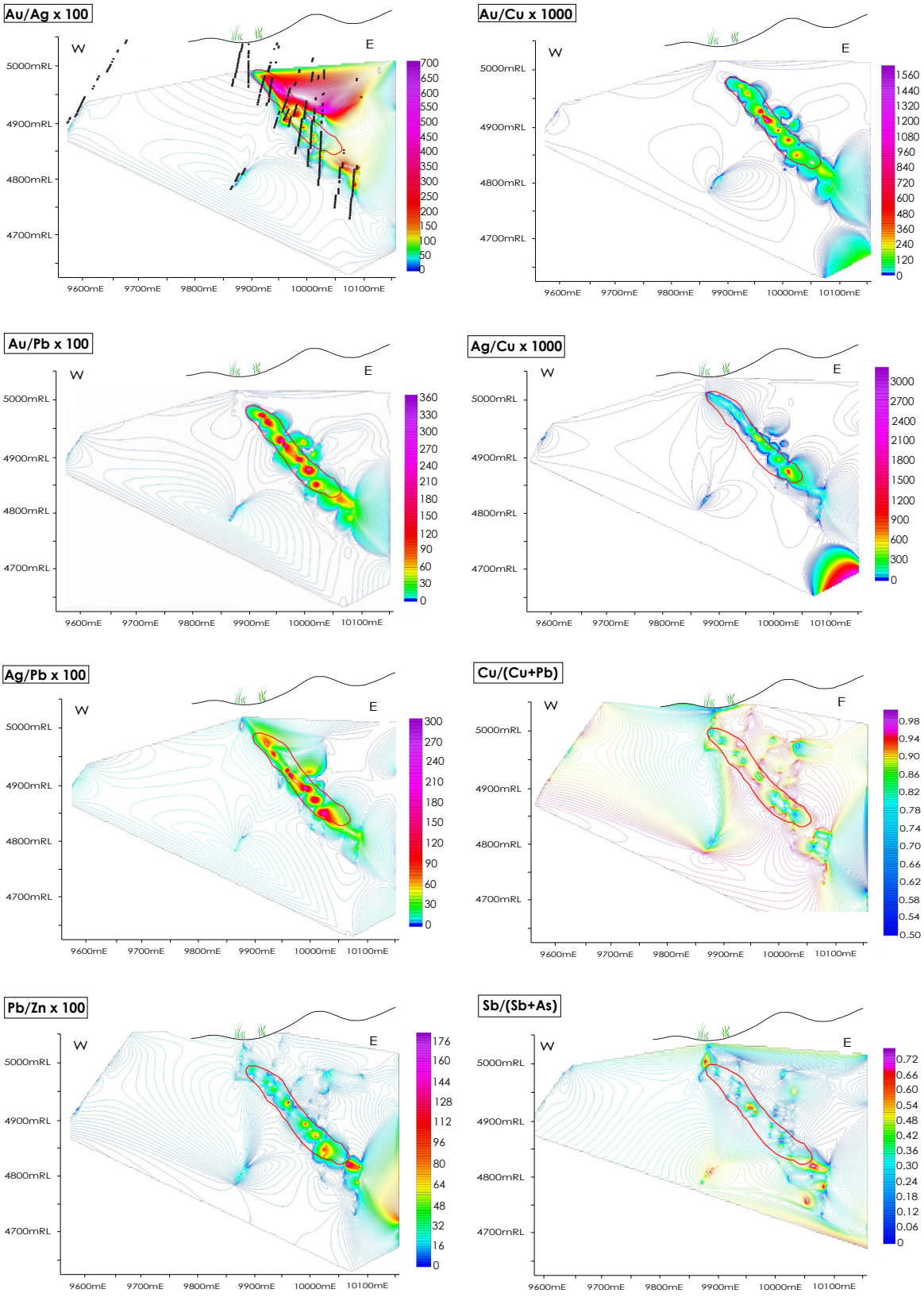

Fig. 4.48 Metal ratio zonation section 19800mN Metal values obtained from diamond drill core assays on section 19800mN. Assay locations shown as black dot points (sample locations are consistent for all figures on this cross section). Red outlines depict Au anomaly. Au/Ag x 100 zonation; Au/Cu x 1000 zonation; Au/Pb x 100 zonation; Ag/ Cu x 1000 zonation; Ag/Pb x 100 zonation, Cu/(Cu+Pb) zonation; Pb/Zn X 100 zonation; Sb/(Sb+As) zonation.

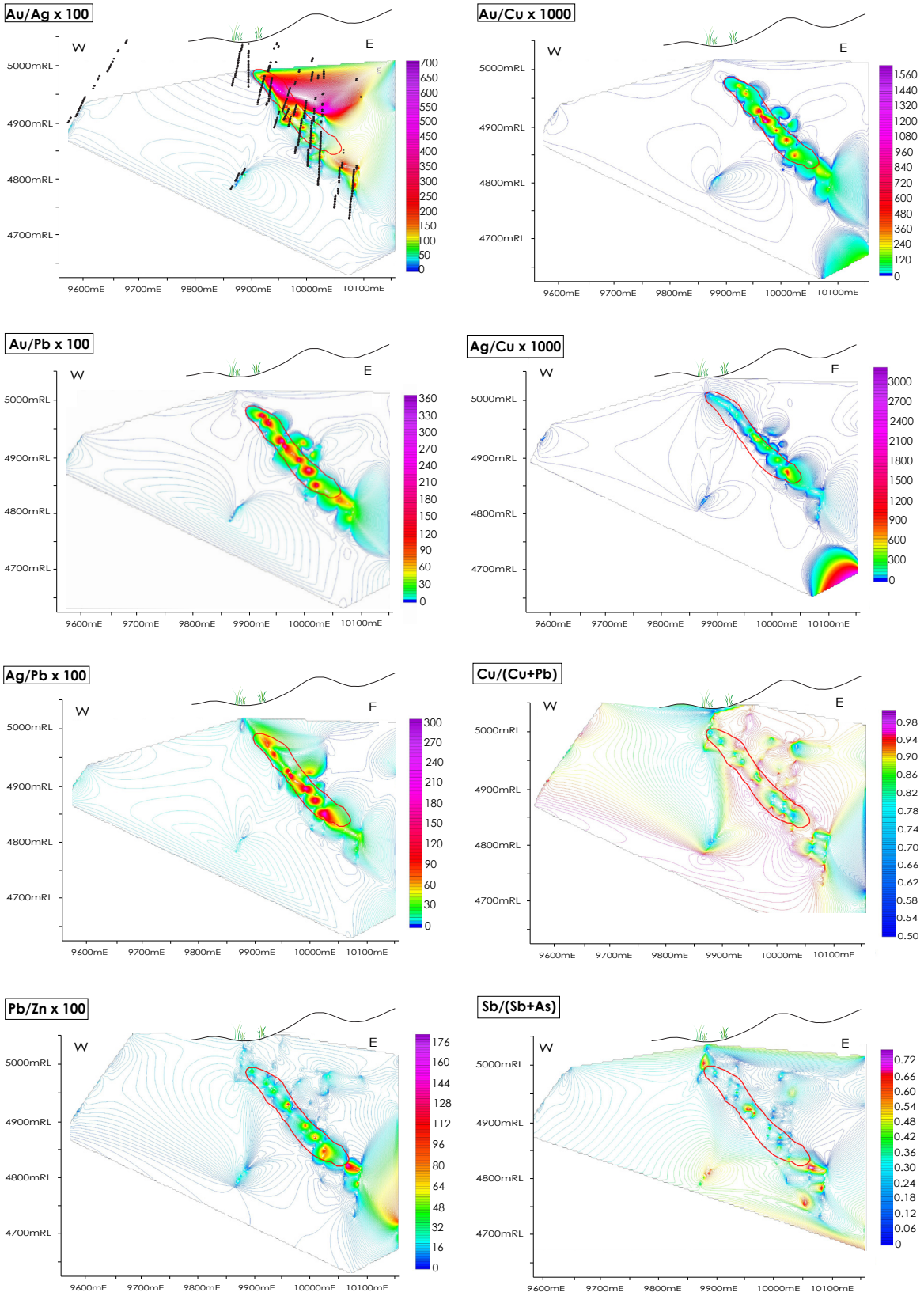

Fig. 4.49 Metal ratio zonation section 19900mN Metal values obtained from diamond drill core assays on section 19900mN. Assay locations shown as black dot points (sample locations are consistent for all figures on this cross section). Red outlines depict Au anomaly. Au/Ag x 100 zonation; Au/Cu x 1000 zonation; Au/Pb x 100 zonation; Ag/ Cu x 1000 zonation; Ag/Pb x 100 zonation, Cu/(Cu+Pb) zonation; Pb/Zn X 100 zonation; Sb/(Sb+As) zonation.

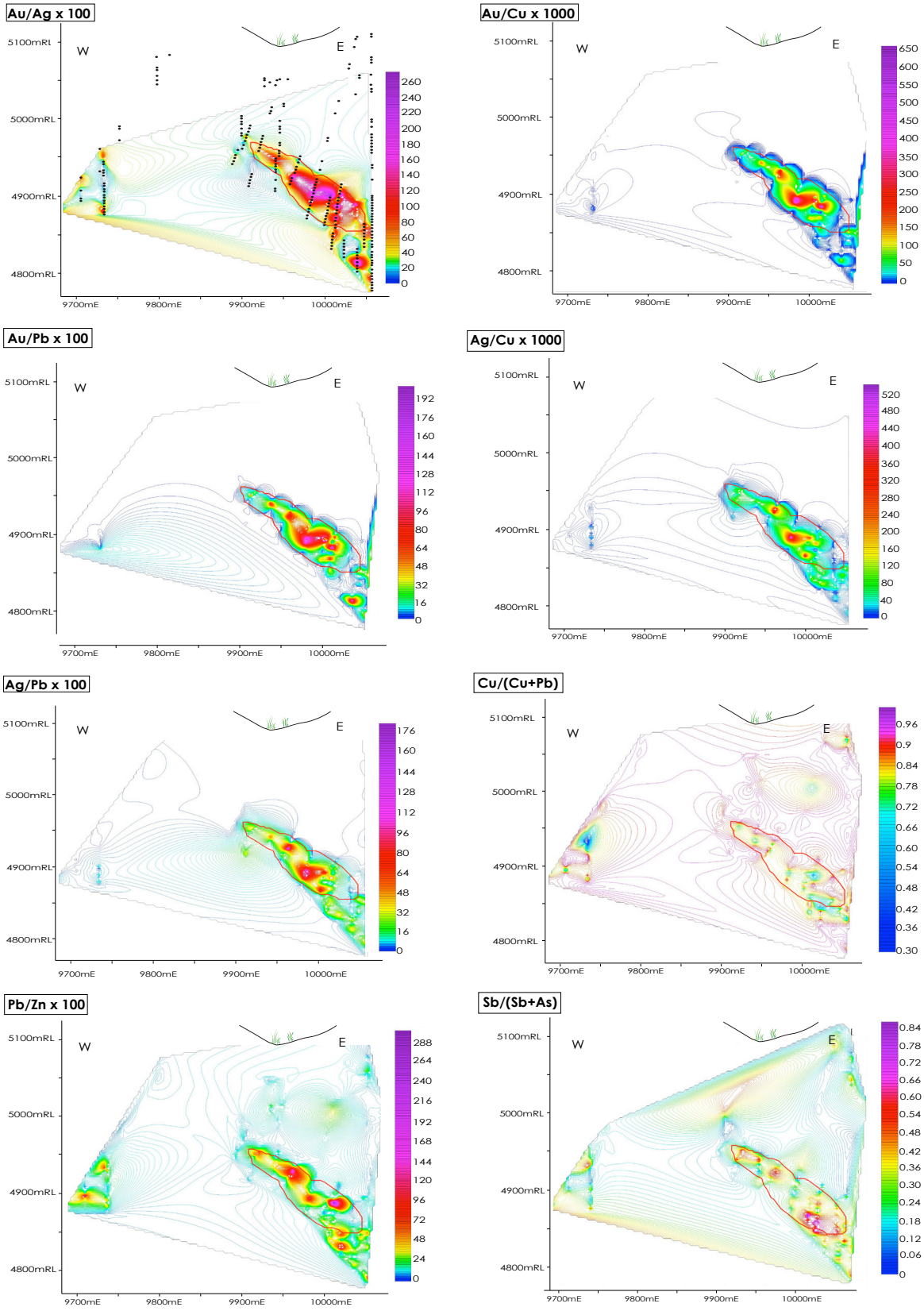

Fig. 4.50 Metal ratio zonation section 20000mN Metal values obtained from diamond drill core assays on section 20000mN. Assay locations shown as black dot points (sample locations are consistent for all figures on this cross section). Red outlines depict Au anomaly. Au/Ag x 100 zonation; Au/Cu x 1000 zonation; Au/Pb x 100 zonation; Ag/ Cu x 1000 zonation; Ag/Pb x 100 zonation, Cu/(Cu+Pb) zonation; Pb/Zn X 100 zonation; Sb/(Sb+As) zonation.

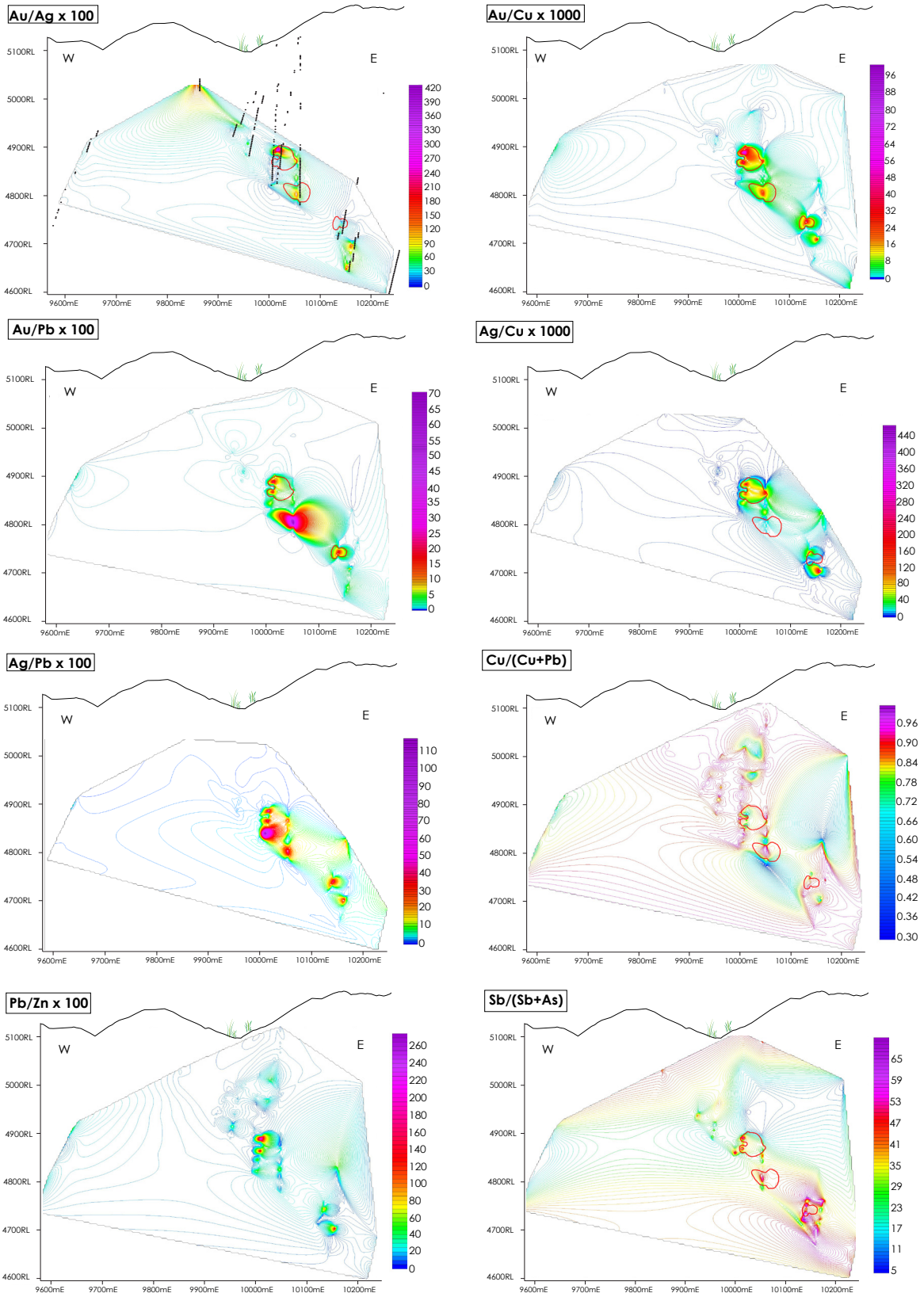

Fig. 4.51 Metal ratio zonation section 20050mN Metal values obtained from diamond drill core assays on section 20050mN. Assay locations shown as black dot points (sample locations are consistent for all figures on this cross section). Red outlines depict Au anomaly. Au/Ag x 100 zonation; Au/Cu x 1000 zonation; Au/Pb x 100 zonation; Ag/ Cu x 1000 zonation; Ag/Pb x 100 zonation, Cu/(Cu+Pb) zonation; Pb/Zn X 100 zonation; Sb/(Sb+As) zonation.

mineralization in the deeper K2 vein structure. Pb grades show a slight overall increase in a northerly direction, from a mean of 20 ppm at 20050mN to 11 ppm at 19600mN.

Zinc: Zinc occurrence in the K1 vein is closely related to Cu, and to a lesser extent, Pb distribution. Zinc grades are of a similar magnitude to Cu grades (80-110 ppm), and values increase marginally in a southerly direction. Zn occurrence is generally closely confined to the main vein zone with the exception of isolated patches associated with Cu mineralization, and interference by the K2 structure in the west of the cross sections (e.g. Fig. 4.43).

Heavy metal distribution: Arsenic distribution is largely confined to the 1 g/t Au anomaly, although most cross sections also show occurrence above the main zone, with values spiking in the hangingwall of the vein. Arsenic content is generally low in the K1 vein, with an average value of 7 ppm, although higher values do occur in isolated spots within and above the vein structure, up to a maximum of 375 ppm along cross section 19900mN (Fig. 4.42). Arsenic distribution does not show a strong correlation with any other metal. Mineralogy studies (section 4.9) show that arsenopyrite is a rare mineral in the vein, as is tennantite, so it is proposed that As could be contained in argillic alteration facies, which may explain the distribution above the vein (Chapter 5). At Gosowong, Olberg (2001) noted that advanced argillic alteration with little or no quartz veining seemed to carry high As values.

Antimony values in K1 are very low, rising to approx. 10 ppm in the ore shoot (Figs. 4.39-4.44). In general, antimony occurrence correlates strongly with precious metal mineralization, although antimony is only present in trace amounts in the vein mineralogy (Section 4.9). Antimony values are zoned with highest grades in the vein, showing a gradual decrease through the stockwork zone to background levels away from the vein (e.g. Figs. 4.39 and 4.41), providing the potential to utilize Sb distribution as a vector to precious metal mineralization. Cross section 19800mN shows a zone of higher Sb values in the deep part of the vein (Fig. 4.41). This correlates weakly with Mo distribution, indicating that Sb could also be contained within the late-stage mineralizing event.

Molybdenum distribution: Molybdenum distribution is controlled by the occurrence of late-stage, molybdenite + quartz-rich shear and breccia infill mineralization (section 4.5). Due to the often discontinuous nature of this type of mineralization, the molybdenum zonation is patchy but generally confined to the 1 g/t Au anomaly, although there are a num-

ber of significant, unconstrained, high-grade zones below the main ore zone (Figs. 4.39 and 4.40) in the southernmost cross sections included in this study. These deep Mo anomalies do not appear to correlate with the distribution any other metal. High Mo values within the vein show the strongest correlation with arsenic (Fig. 4.45), although based on the mineralogy of the Mo-rich vein stage this association is unexplained. Two populations are identified in Fig. 4.45: strongly correlated (R=0.807) Mo and As (pink population), and poorly correlated (R=0.016) increasing As at constant or low Mo values, reflecting arsenopyrite or tennantite mineralization.

4.14 Kencana metal ratio distribution

Metal ratios can be useful in the determination of palaeo-fluid pathways and temperatures of metal precipitation (Olberg, 2001). Metal ratios are more indicative of the physiochemical nature of the mineralizing fluid than metal values, and are independent of vein thickness and the amount of material deposited, unlike metal values (Goodell and Petersen, 1974; Wurst, 2004). Metal ratios are based on the fact that metals precipitate under different physiochemical conditions. By taking the value of a metal that reflects a low temperature depositional environment (e.g. Au, Ag), and dividing it by a metal that reflects a high temperature depositional environment (e.g. base metals), areas of high and low temperature ore deposition can be inferred. Ratios including Au/Ag x 100, Au/Cu x 1000, Au/Pb x 100, Ag/Pb x 100, Ag/Cu x 1000, Cu/(Cu+Pb), Cu/(Cu+Zn), Pb/Zn x 100, and Sb/(Sb+As) are discussed in this chapter. Metal ratio zonation data for cross sections 19600mN-20050mN are shown in Figs. 4.46-4.51.

Au/Ag ratios: Au/Ag x 100 ratios are zoned and decrease strongly away from the main structures, with highest values in the centre of the main vein and toward the top of the structure, indicating higher gold relative to silver at shallower levels in the system (Figs. 4.47 and 4.49), which is consistent with the observations on low sulfidation deposits made by Buchanan (1981), and upheld by Hedenquist et al. (1996); and also reflects trends identified at the Gosowong deposit by Olberg (2001). However, this does not conform to the model proposed by Corbett and Leach (1998), which states that Au/Ag ratios are lower in shallow

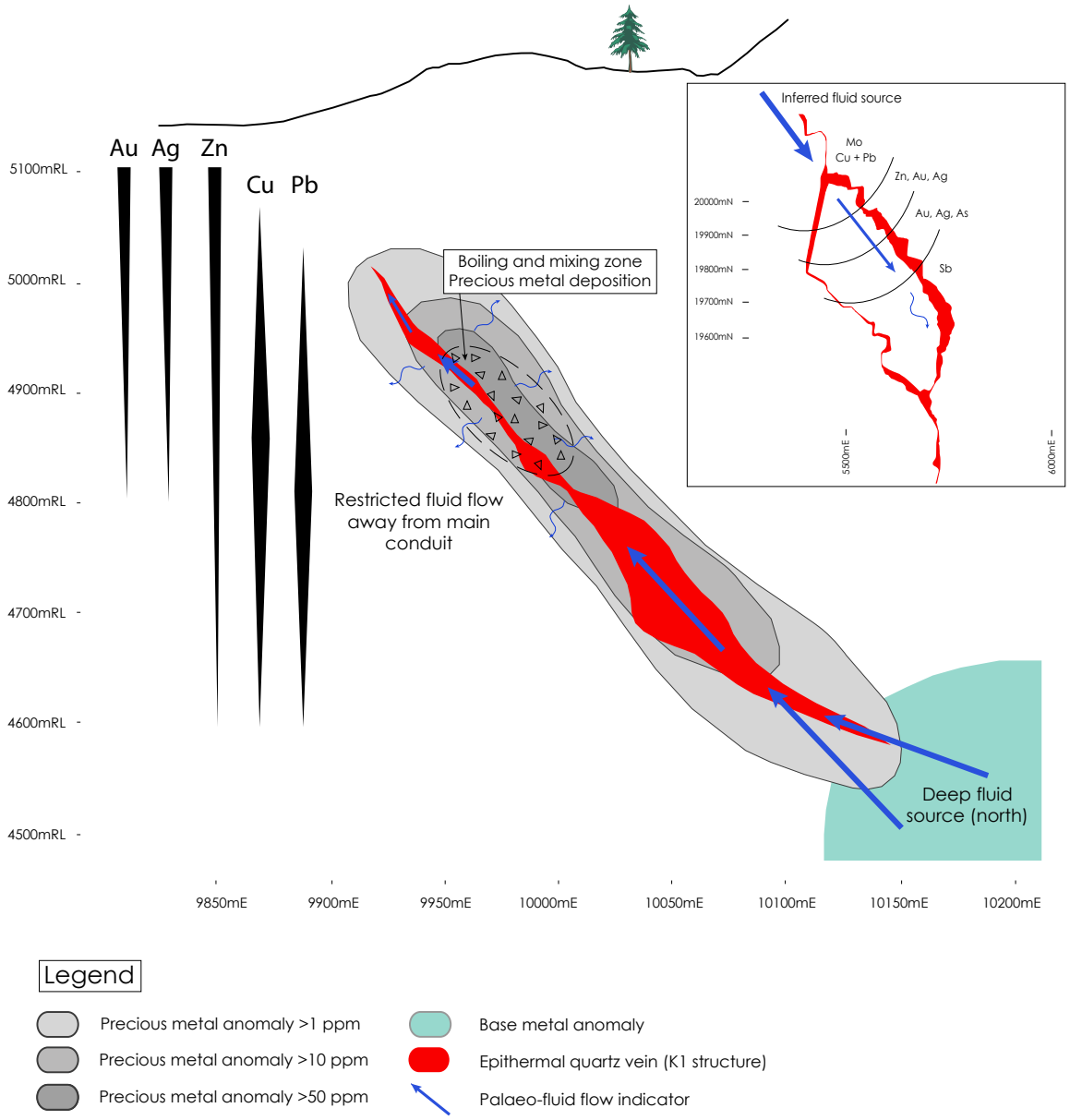

Fig. 4.52 Summary of metal zonation at Kencana Vertical and lateral (inset) metal zonation in the K1 vein, with laterally zoned Au grades. The down-dip extension of the vein is characterized by elevated base metal values and may represent a higher-temperature fluid source for precious metal mineralization at Kencana. Black lines represent relative abundance and elevation of major metal species in the Kencana system. Lateral metal zonation (inset) shows inferred fluid source directions.

and distal portions of the system. Au/Ag ratios are variable within the vein highlighting the decoupled distribution of gold and silver minerals at Kencana.

Au/Base Metal ratios (+ Ag/base metal ratios): Au (Ag) grades are the dominant factor determining the precious metal/ base metal zonation due to the relatively consistent base metal values and the large range of Au and Ag grades. Au/ base metal ratios are highest

within the main structures and decrease away from the centre of the vein. The general distribution of precious/ base metal ratios suggests a decrease in fluid temperature with increased elevation, and restricted lateral flow away from the main structures. Au/Cu x 1000 and Au/Pb x 100 ratios across the Kencana deposit are shown in Figs. 4.45-4.51. Low ratio values also occur at depth below the K1 vein, implying increased amounts of base metal mineralization in the deeper levels of the system (Figs. 4.48 and 4.49), which is consistent with the summary metal values in Table 4.2.

The Au/Cu x 1000 ratio increases upwards and towards the centre of the vein, above 4800mRL (Figs. 4.46 and 4.47). Au/Pb x 100 ratios also increase toward the centre of the vein and decrease with depth away from the vein, along the implied upflow zone from the south-east of the sections (Figs. 4.46-4.48). Ag/ base metal ratios show a similar zonation to the Au/ base metal ratios. Both Au/Cu x 1000 and Ag/Cu x 1000 show that the most Cu-rich areas are in the deepest section of the vein (Figs. 4.47 and 4.49).

Base metal/ base metal ratios: Ratios such as Cu/(Cu+Pb) are used to determine the relative abundance of one base metal compared to another throughout the vein. Evaluating these ratios can be more useful than making interpretations based on single element data, as base metal values in the Kencana deposit are low, and observations can be difficult to make when considering single element zonation. Cu/(Cu+Pb) ratios show low values in the centre of the vein, increasing outwards and particularly at deeper RLs than the Au anomaly (Figs. 4.45 and 4.47), confirming the correlation between Au and Pb. Cross section 19700mN is anomalous in that the vein shows enrichment in Cu relative to Pb, where the Cu is present in the deepest zone of the vein depicted by the Au anomaly, and strong Pb enrichment below the Au anomaly (Fig. 4.46). The ratio is affected by a strong Pb anomaly below the vein dominating the consistently low Cu grades (Fig. 4.40).

Pb/Zn x 100 ratios show zonation around the K1 vein, with high values (Pb enrichment) in the centre of the vein, decreasing through the stockwork to low values (Zn enrichment). High ratio values are encountered along the down-dip extension of the vein, which may indicate a hydrothermal fluid pathway (Figs. 4.49 and 4.50).

Sb/(Sb+As) ratios: Antimony and arsenic are generally associated with the shallower levels of an epithermal system. Ratios show that the distribution of As and Sb is

decoupled, with high values restricted to the main vein depicted by the 1 g/t Au anomaly (Figs. 4.48 and 4.50), confirming the good correlation observed between Sb and Au single element distribution. Sb/(Sb+As) ratios are low along the hangingwall of the K1 structure, corresponding with a spike in arsenic values in the Gosowong assay database at this location (Fig. 4.48). Sb/(Sb+As) ratios may provide a useful tool toward targeting precious metal mineralization in the Kencana district due to the strong zonation produced by these elements.

4.15 Discussion of Kencana metal zonation

The Kencana deposit shows a distinct vertical and lateral metal zonation, which is summarized in Fig. 4.52. Precious metals are enriched at shallow levels of the system (above 4950mRL), and values decrease with depth, where base metal values increase systematically from Zn-rich to Cu- and Pb-rich (Fig. 4.52). Lateral distribution along 6 representative cross-sections shows that the majority of metal occurrence is restricted to the vein structure and the area depicted by the 1 g/t Au anomaly.

Metals, in particular Au and Ag, are generally zoned with high values in the centre of the vein, decreasing outwards through the stockwork zone to background values (e.g. Fig. 4.42). Base metals show moderate enrichment along the down-dip extension of the K1 vein, and together with metal ratio distribution, indicate that hydrothermal fluids may have been sourced from this area (Fig. 4.52). High base metal values in the deeper sections of the vein correspond to the distribution of vein types 7 and 8 which contain abundant base metal sulfide + electrum ± selenide ± sulfosalt ± telluride mineralization (section 4.7). Since Cu and Pb values increase towards the north, a source for base metals is implied to be to the north of Kencana. Highest Mo values are also located along cross sections to the north of the deposit (e.g. 28000 ppm along section 19900mN) and decrease toward the south, inferring a temperature gradient from high to low from north to south across the Kencana deposit.

Zinc values are marginally higher toward the south, which may be the result of deposition from a cooling fluid sourced from the north. The distribution of elevated Pb and Sb values show the strongest correlation with high Au values, and due to the strong zonation exhibited by these elements may provide useful vectors towards precious metal occurrence in the Gosowong goldfield.

Distribution patterns suggest that the K1 structure was an important fluid conduit

and focus for hydrothermal fluids, with restricted flow away from the main vein. Similar trends in the distribution and zonation of precious and base metals were observed at Gosowong (Olberg, 2001), with the exception of molybdenum, which is not present at Gosowong (related to the presence of type 11 infill at Kencana, section 4.4). It is likely that dilation of the north-trending structures in the goldfield created open space and pressure release conducive to boiling and mixing processes, leading to deposition of precious (and base) metals. Increased Au/ base metal ratio values in the centre of the vein suggest lower temperature conditions, corresponding with high Au values.

4.16 Summary

- Kencana (K1 vein) shows a complex, multiphase history of formation with numerous brecciation and vein opening events, resulting in complex overprinting infill stages and crosscutting relationships. Eleven vein and breccia infill types are recognized at Kencana, including wallrock (1), quartz stockwork (2), wallrock breccias with crystalline quartz cement (3), red chalcedony infill (4), massive crystalline quartz (5), massive crystalline quartz breccias (6), cockade-banded quartz-chlorite breccias (7), banded quartz-chlorite (8), banded quartz-adularia (9), grey cryptocrystalline quartz stringer veins (10) and black quartz-molybdenite infill (11).

- Gangue mineralogy is dominated by crystalline, microcrystalline and cryptocrystalline quartz, adularia, chlorite and calcite. Microcrystalline and cryptocrystalline quartz show a variety of textures including colloform and crustiform banding, which are inferred to represent primary growth textures formed during crystal growth or from the deposition of amorphous silica (Dong et al., 1995). Increasing grain size of silica polymorphs from the margins to the centre of individual veins reflects a decrease in the rate of cooling and/ or a decrease in overall fluid flux rate.

- Decreasing fluid flux rates can occur as a result of vein dilation as a result of lower pressure and lower flow rates (Wurst, 2004). Sealing of the vein by deposition of microcrystalline and cryptocrystalline quartz may also decrease flow rates. Complex crustiform

bands are inferred to form by episodic pressure release, where drops in total confining pressure allow fluids to boil, resulting in loss of volatiles, cooling, increase in pH and deposition of gangue (and ore) minerals.

- Mineralogical evidence for boiling is not observed until deposition of type 5 infill, corresponding with formation of wider veins, larger volumes of gangue mineralization and increased Au grade.

- A broad textural zonation from north to south is observed in the K1 vein. Infill types 1, 2 and 3 are distributed throughout the deposit and are particularly prevalent on the margins of the vein. Types 7, 8 and 9 are the main ore-bearing stages and form the bulk of the central section of the vein, particularly below 4950mRL. Type 11 infill is most prevalent to the north of 19900mN, between 4950mRL and 4880mRL. Types 4, 5, 6 and 10 are variably and sporadically distributed across the vein.

- Kencana ore mineralogy is generally typical of low sulfidation epithermal deposits, though several features of the mineral assemblages are less common and may reflect on the metal transportation and depositional processes in the Kencana vein. Multistage, banded veins, hydrothermal breccias and stockworks host ore mineralization, with assemblages dominated by electrum and sulfides, with selenides and lesser tellurides and sulfosalts. Chalcopyrite is the most common sulfide mineral, with selenian-galena, sphalerite, bornite and pyrite in order of decreasing abundance. Other common accessory minerals include aguilarite and molybdenite (in type 11 infill), with trace tennantite, arsenian-pyrite, silver and lead tellurides, naummanite and rare bismuth minerals.

- Ore deposition is interpreted to be the result of a combination of processes, mixing processes are inferred to be of particular importance, based on the presence of high-fineness electrum and selenium-bearing minerals. Evidence for boiling processes are also present at Kencana, including bladed carbonate pseudomorphs and abundant adularia.

- Kencana can be considered a Se-rich epithermal deposit, such as Midas (USA), Hishikari (Japan), and Broken Hills (New Zealand). These deposits are all associated with bimodal volcanism and commonly contain bonanza Au-grades. Selenium substitution in sulfide minerals was also noted at Mt. Muro, and a positive correlation between gold, silver and selenium was recognized at the Pongkor low sulfidation epithermal deposit.

- Eutectic temperatures from primary fluid inclusions range from -24.6 to -18.3°C, inferring formation from fluids dominated by NaCl with minor KCl contribution. Homogenization temperatures for primary inclusions are variable depending on quartz type: crystalline quartz (QX, type 2c) veins range from 203.0 to 248.8°C (155.0 to 257.0°C including data from Coote, (2003)) and salinities range from 0.1 to 0.5 wt% NaCl (equiv.) (0.1 to 0.7 wt% NaCl (equiv.) including data from Coote, (2003)); quartz-adularia (QA, type 9) veins range from 195.8 to 258.7°C (189.0 to 270.0°C including data from Coote, (2003)) and salinities range from 0.0 to 0.8 wt% NaCl (equiv.) (0.0 to 1.0 wt% NaCl (equiv.) including data from Coote, 2003); quartz-chlorite (QC, type 8) veins range from 202.7 to 306.9°C and salinities range from 0.0 to 1.0 wt% NaCl (equiv.). A peak in homogenization temperatures for both QA and QX fluid inclusions is apparent between 200 and 225°C.

- Fluid inclusions from QA and QX vein types are strongly dominated by meteoric water composition, and fluid inclusions from the QC vein types have a slightly increased dilute magmatic component. It is proposed that gold hydrosulfides (in particular, $Au(HS)_2$) are most significant in terms of gold transport in a reduced, dilute magmatic-derived fluid as inferred for Kencana. Boiling assemblages were not observed in this study.

- Minimum pressures of entrapment for fluid inclusions from QX and QA veins (type 2c and 9) were between 10-20 bars. All QX fluid inclusions were trapped between 5 to 40 bars, and all QA fluid inclusions were trapped between 5 to 50 bars. Fluid inclusions from QC type veins show a range of entrapment pressures, with the majority falling in the range 30-50 bars.

- Taking into account uncertainty in the position of the palaeo-water table and the possible influence of boiling, most of the fluid inclusions were trapped 50 to 200 m deeper than their current location which implies that Kencana was uplifted up to 200 m between the time of its formation and the present, or that the water table was at least 200 m higher than the current erosion surface.

- The K1 vein shows a distinct vertical and lateral metal zonation. Precious metals are enriched at shallow levels of the system (above 4950mRL), and values decrease with depth, where base metal values increase systematically from Zn-rich to Cu- and Pb-rich. Lateral distribution along 6 representative cross-sections shows that the majority of metal occurrence is restricted to the vein structure and the area depicted by the 1 g/t Au anomaly. Distribution patterns suggest that the structures are important conduits for focusing hydrothermal fluids, with restricted flow away from the main vein.

- Base metals show moderate enrichment along the down-dip extension of the K1 vein, and together with metal ratio distribution, indicate that hydrothermal fluids may have been sourced from this area. Since Cu, Pb and Mo values increase towards the north, a source for base metals is implied to be to the north of Kencana. Zinc values are elevated toward the centre of the deposit, with high Au and Ag. Antimony and As values are highest toward the south of the K1 vein. This lateral north-south metal zonation is interpreted to represent a hydrothermal fluid temperature gradient.

- Elevated Pb and Sb values show the strongest correlation with high Au values, and due to the strong zonation exhibited by these elements may provide useful vectors towards precious metal occurrence in the Gosowong goldfield.

CHAPTER 5

ALTERATION FACIES, DISTRIBUTION AND GEOCHEMISTRY

5.1 Introduction

Hydrothermal alteration is a product of fluid-rock interaction resulting in replacement of the initial mineral assemblage in a rock, where factors such as permeability, porosity, temperature and fluid composition are variables in controlling the style and intensity of alteration (Brown and Ellis, 1970; De Ronde and Blattner, 1988; Reed, 1997). Hydrothermal alteration may be characterized by the intensity and pervasiveness of the altered rock. Intensity is the degree to which the susceptible primary minerals are converted to secondary minerals (Steiner, 1977; Browne, 1978). Pervasiveness relates to the distribution of alteration as controlled by veinlets at one extreme and the matrix without regard to veinlets at the other (Guilbert and Park, 1986).

Alteration footprints in low sulfidation environments are typically larger than the related ore deposit and thus the recognition of the mineralogical, geochemical and isotopic zonation of alteration may provide a foundation for developing vectors to ore mineralization (Gemmell, 2004). Alteration halos surrounding the ore zone, particularly in vein deposits, typically include a variety of temperature-sensitive clay minerals that can aid in indicating directions of hydrothermal fluid flow (Hedenquist et al., 2000).

In this study, hydrothermal alteration mineralogy at Kencana was determined with the aid of hand specimen and thin section observations, SWIR analysis and K-feldspar staining. Detailed alteration facies zonation was constructed along 9 cross sections across the K1 vein. Alteration facies are determined by the dominant mineral present within the alteration assemblage and a total of ten alteration facies are recognized at Kencana. Representative diamond drill core samples were selected for whole rock alteration geochemistry by XRF and ICP-MS analysis to determine zonation of major and trace elements surrounding the Kencana deposit with the aim of producing geochemical vectors to mineralization.

5.2 District scale alteration

Hydrothermal alteration is widespread in the Gosowong district (Fig. 5.1) and is dominated by a regional, pervasive propylitization (chlorite-epidote-calcite-albite).

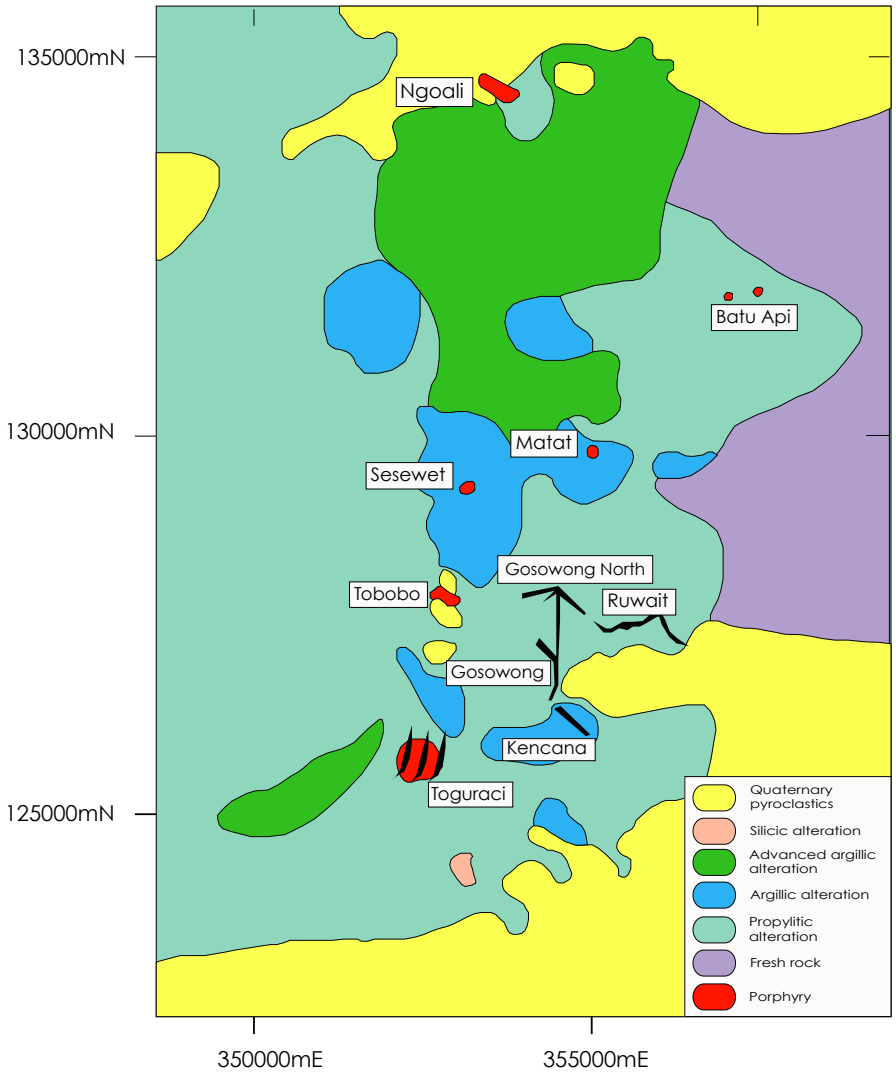

Fig. 5.1 Regional alteration of the Gosowong Goldfield showing distribution of alteration styles and epithermal veining (shown in black). Modified after Olberg et al. (1999).

Locally zones of biotite-magnetite ± chlorite alteration related to the porphyries occur within the propylitic alteration (Richards and Basuki Dwi Priyono, 2004), and argillic alteration through the central corridor of the district, generally confined to ridge outcrops. Erosion is partly responsible for the alteration facies distribution in the Gosowong district, with advanced argillic alteration forming a blanket-like morphology on the ridge tops, suggesting

that this facies may have originally formed an extensive layer covering the district (Olberg, 2001).

Olberg et al. (1999) recognized three major types of hypogene wallrock alteration associated with the Gosowong deposit: (1) silicification (quartz-illite-adularia-pyrite) within the immediate vein zone (<3 m), (2) argillic alteration (illite-quartz-pyrite) enveloping the vein zone, and (3) propylitic alteration (chlorite-epidote-albite-calcite-pyrite) within the footwall and distal to the ore zone. Additionally, advanced argillic (kaolinite-dickite ± alunite) alteration is found at shallow levels toward the south of the Gosowong deposit (Olberg, 2001). Gemmell (2007) recognized zonation of alteration facies around the Gosowong vein from proximal silicic to argillic to vein-related propylitic to distal regional propylitic alteration. Prior to the onset of the Gosowong deposit hydrothermal system, the host rocks in the district were altered to a regional propylitic (epidote, Fe chlorite, albite, pyrite) assemblage. As hydrothermal fluids progressed up the Gosowong fault, vein-related propylitic (epidote, Fe chlorite, smectite, calcite, pyrite) alteration formed within approximately 50 m of the deposit. As the hydrothermal system intensified, argillic (illite, quartz, chalcedony, adularia, Mg-Fe chlorite, smectite, pyrite) alteration formed within a few 10's of meters of the Gosowong fault and overprinted the vein-related and regional propylitic alteration. Silicic (quartz, chalcedony, adularia, illite, Mg chlorite, pyrite) alteration overprints all other types of alteration and is confined to within a few metres of the vein.

5.3 Kencana alteration facies

Nine alteration facies cross sections were constructed in this study and spatial distribution of these cross sections is illustrated in Fig 5.2. This study presents new data for alteration facies zonation along cross sections 19600mN, 19800mN, 19900mN, 20000mN and 20050mN. Previously, Silitonga (2006) carried out preliminary investigations in the alteration mineralogy associated with the Kencana deposit, in which 1200 samples from 19 exploration diamond drill cores were analyzed using SWIR spectral analysis. This data was re-interpreted using the procedure outlined in section 5.3.1 and is included in this study, along with data from new drill core specimens, forming the basis for zonation patterns observed along cross sections 19650mN, 19750mN, 19850mN and 19950mN.

5.3.1 Short-wave infrared spectroscopy (SWIR)

In addition to petrographic determination, SWIR spectra were determined for 2870 new diamond drill core specimens using a portable infrared mineral analyzer (PIMA II) of AusSpec International. Raw spectra were imported into The Spectral Geologist™ (TSG) V.4.0 software package in which inspection of the spectra and extraction of spectral parameters was performed. Spectra were interpreted manually by identification of diagnostic absorption features by their shape, intensity, wavelength position and shape of the overall spectrum (Thompson et al., 1999). Comparison of obtained spectra with library data is a fundamental process in the identification procedure. The USGS compiled SPECMIN 1036 library, containing over 1300 mineral spectra, was used for reference. Automated spectral interpretation features of TSG software were not used in the determination of mineral assemblages in this study due to inconsistencies in results. PIMA studies are limited in the capacity to determine alteration mineralogy of dark coloured, infrared absorbent samples (Wurst, 2004). The mineralogy of these samples was resolved by thin section observations.

5.4 Alteration facies distribution and zonation

Alteration mineralogy as determined by SWIR analysis was contoured and vertical and lateral alteration facies zonation was interpreted from the mineral distribution. Hypogene alteration at Kencana is approximately zoned around the deposit with respect to four major types of alteration: (1) phyllic alteration in the form of pervasive silicification in the immediate vein zone, (2) argillic alteration enveloping the vein zone, (3) propylitic alteration filling fractures, extending up to 50 m from the vein, and (4) argillic alteration and regional propylitic alteration distal to the deposit. Supergene advanced argillic alteration affects the top 5 m of stratigraphy at Kencana. Disruption to vertical and lateral zonation is common where fluid pathways are determined by lithological and structural permeability, and due to the complex overprinting nature of the alteration facies assemblages determined for Kencana.

Alteration mineralogy is shown in Figs. 5.2-5.5.10, as determined from PIMA analysis. Alteration facies interpretations are based on the alteration mineralogy for each cross section, shown with chlorite chemistry in Figs. 5.14-5.22. Alteration facies characteristics,

distribution and implications are summarized in Table 5.1.

5.5 Alteration facies descriptions

Ten main alteration facies are recognized at Kencana and are determined according the dominant alteration minerals present. These facies are the SCG (Argillic 1) facies, ISP (Argillic 2) facies, IC (Argillic 3) facies, QAS (Phyllic) facies, EC (Propylitic 1) facies, CEP (Propylitic 2) facies, P (Sub-propylitic) facies, BM (Calc-potassic) facies, IDP (Intermediate-advanced argillic) facies, and the KH (Advanced argillic facies). Common alteration minerals include quartz, illite, smectite, adularia, halloysite, kaolinite, sericite, chlorite, epidote, prehnite, calcite, and pyrite. Occurrences of gypsum, anhydrite, biotite, magnetite, actinolite, phengite, chalcopyrite, opal, dickite and pyrophyllite were noted but are less common throughout the system, though no sulfates (e.g. gypsum), prehnite, actinolite, dickite, pyrophyllite or opal were detected in thin section or hand specimen observations. The nature and distribution of alteration facies are described below.

5.5.1 Argillic 1 (SCG) alteration facies

The SCG alteration facies is dominated by smectite (mostly montmorillonite) and calcite alteration with minor gypsum. SCG alteration is prevalent at shallow levels and occurs predominantly above 4900mRL in the system (Figs. 5.2-5.10). Areas of SCG alteration below this elevation occur distal to epithermal veining. SCG altered rocks are typically pale to mid-grey, and soft to indurated. Alteration is generally weakly to moderately pervasive, fine-grained and is best developed in coherent andesite lavas and clasts of andesite autobreccias. Primary volcanic textures are generally preserved in SCG altered rocks. Calcite is crystalline and occurs as veinlets and larger (>2 cm) prismatic calcite crystals growing into cavity space.

SCG alteration is overprinted by all alteration facies at Kencana, especially surface KH facies alteration. Rocks affected by supergene KH facies alteration were most likely SCG altered prior to weathering. SCG alteration is often transitional to ISP (Argillic 2) alteration with increasing depth above the Kencana deposit.

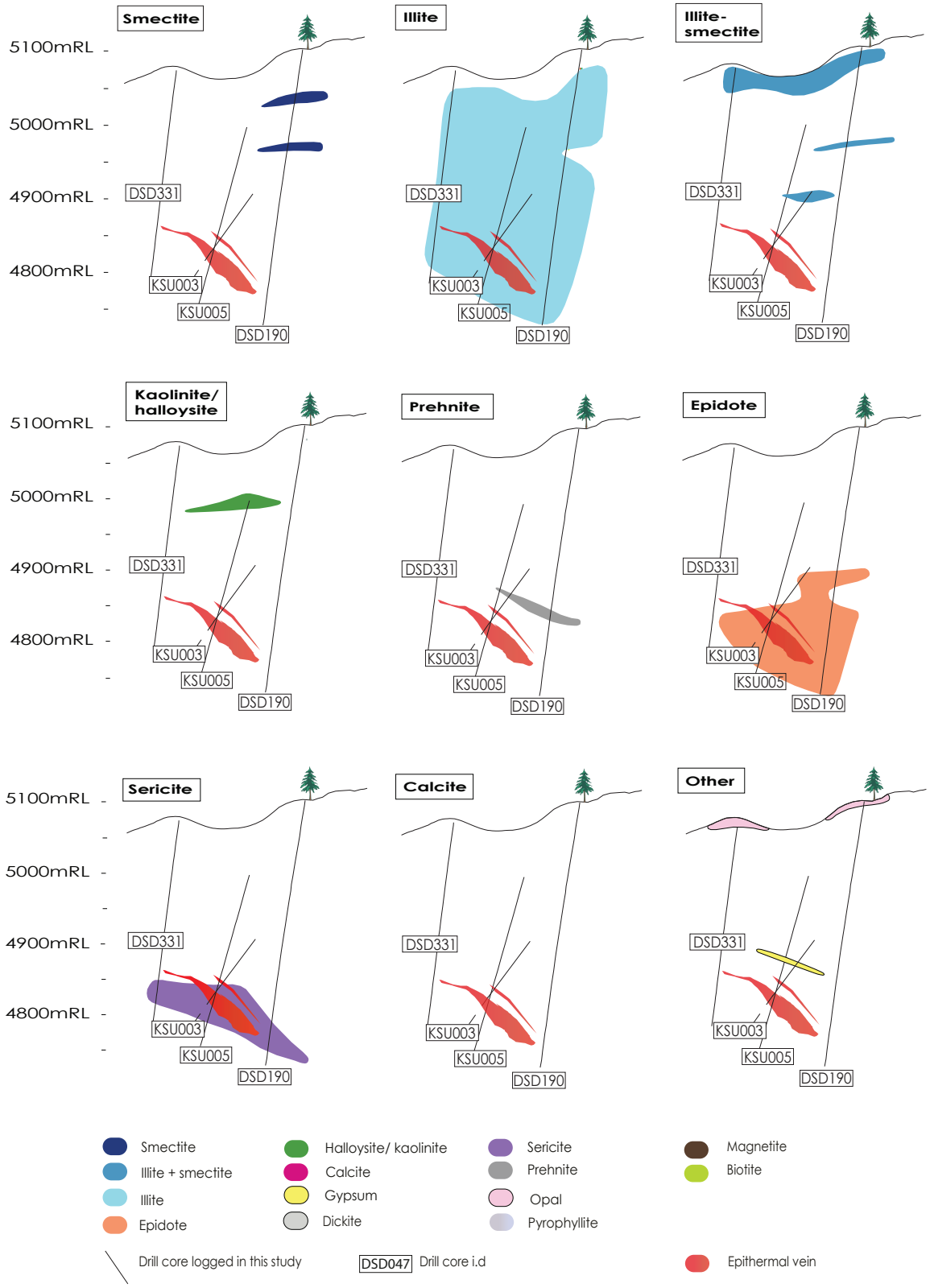

Fig. 5.2 Kencana section 19600mN alteration mineralogy showing the principal hydrothermal alteration minerals and their distribution, as determined by PIMA analysis. Calcite was not observed along this cross section.

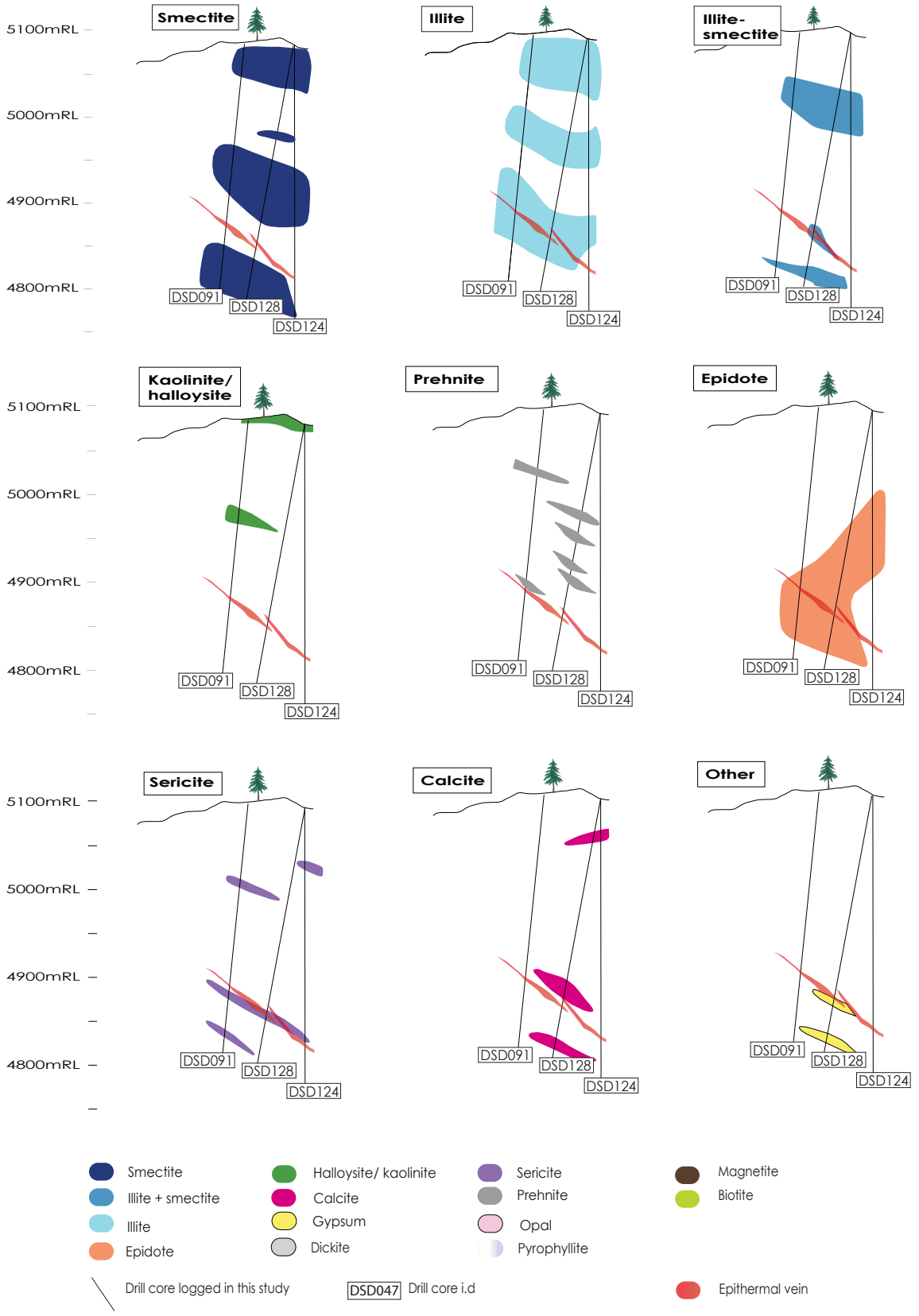

Fig. 5.3 Kencana section 19650mN alteration mineralogy showing the principal hydrothermal alteration minerals and their distribution, as determined by PIMA analysis.

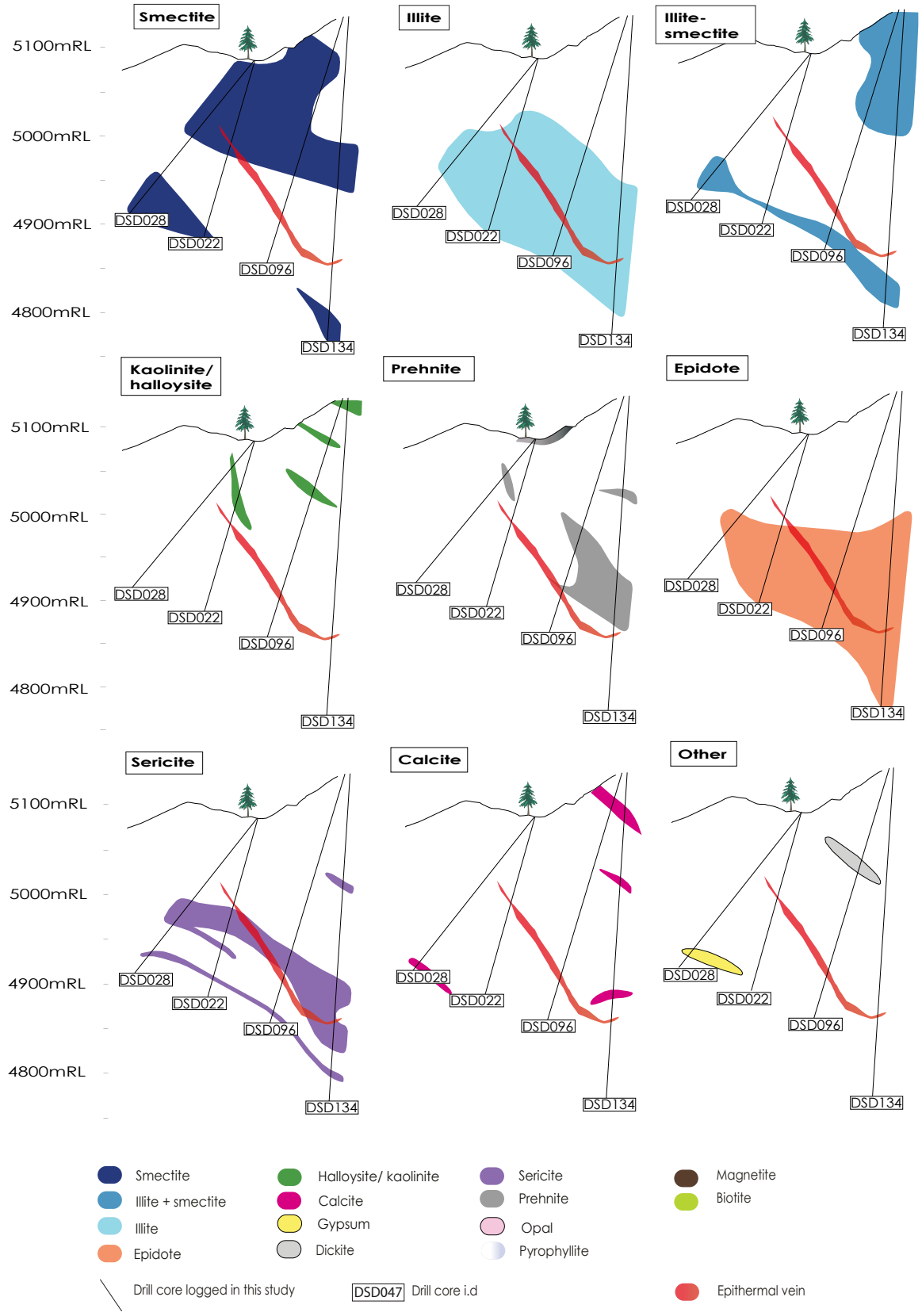

Fig. 5.4 Kencana section 19750mN alteration mineralogy showing the principal hydrothermal alteration minerals and their distribution, as determined by PIMA analysis.

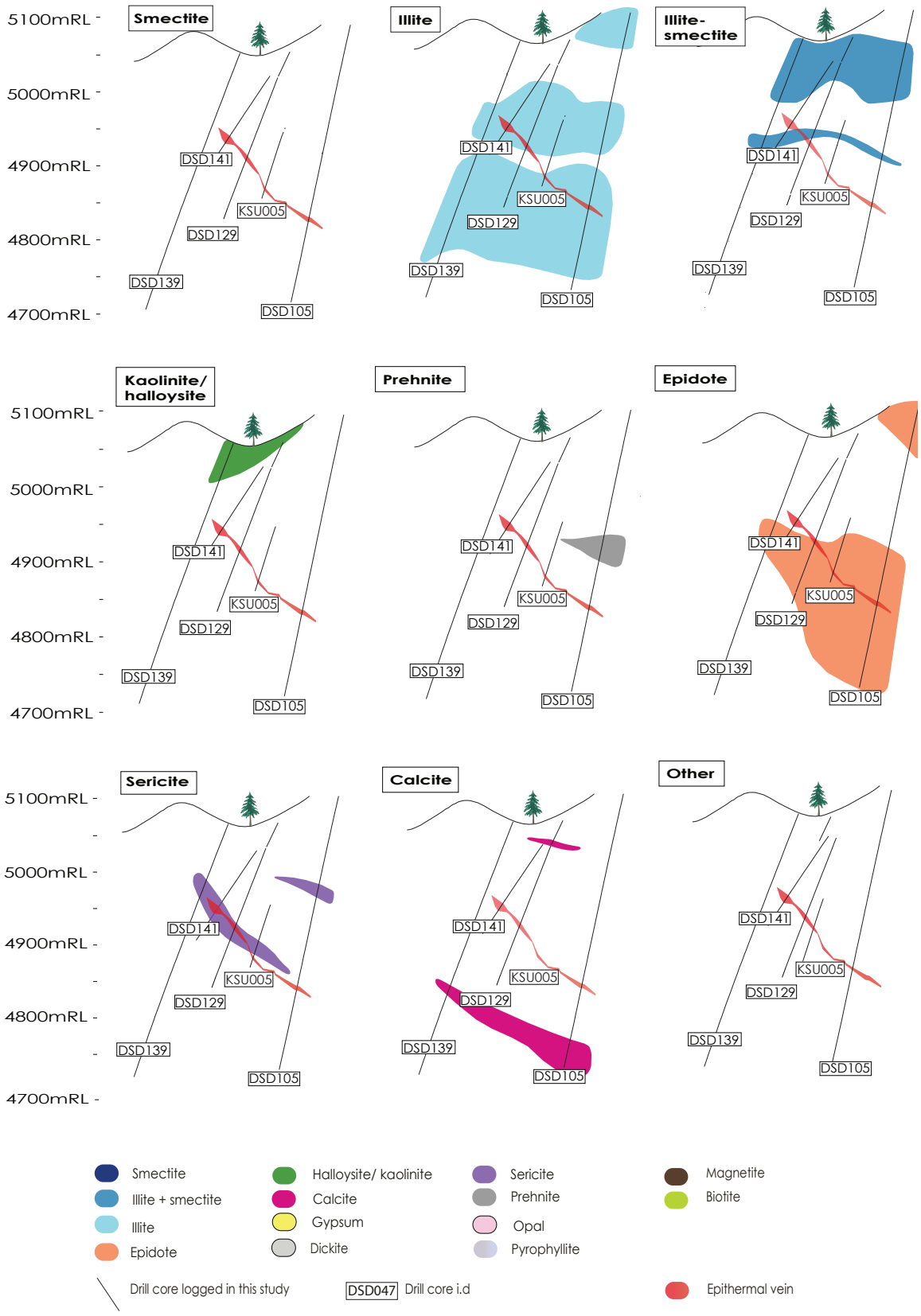

Fig. 5.5 Kencana section 19800mN alteration mineralogy showing the principal hydrothermal alteration minerals and their distribution, as determined by PIMA analysis. Smectite was not observed along this cross section.

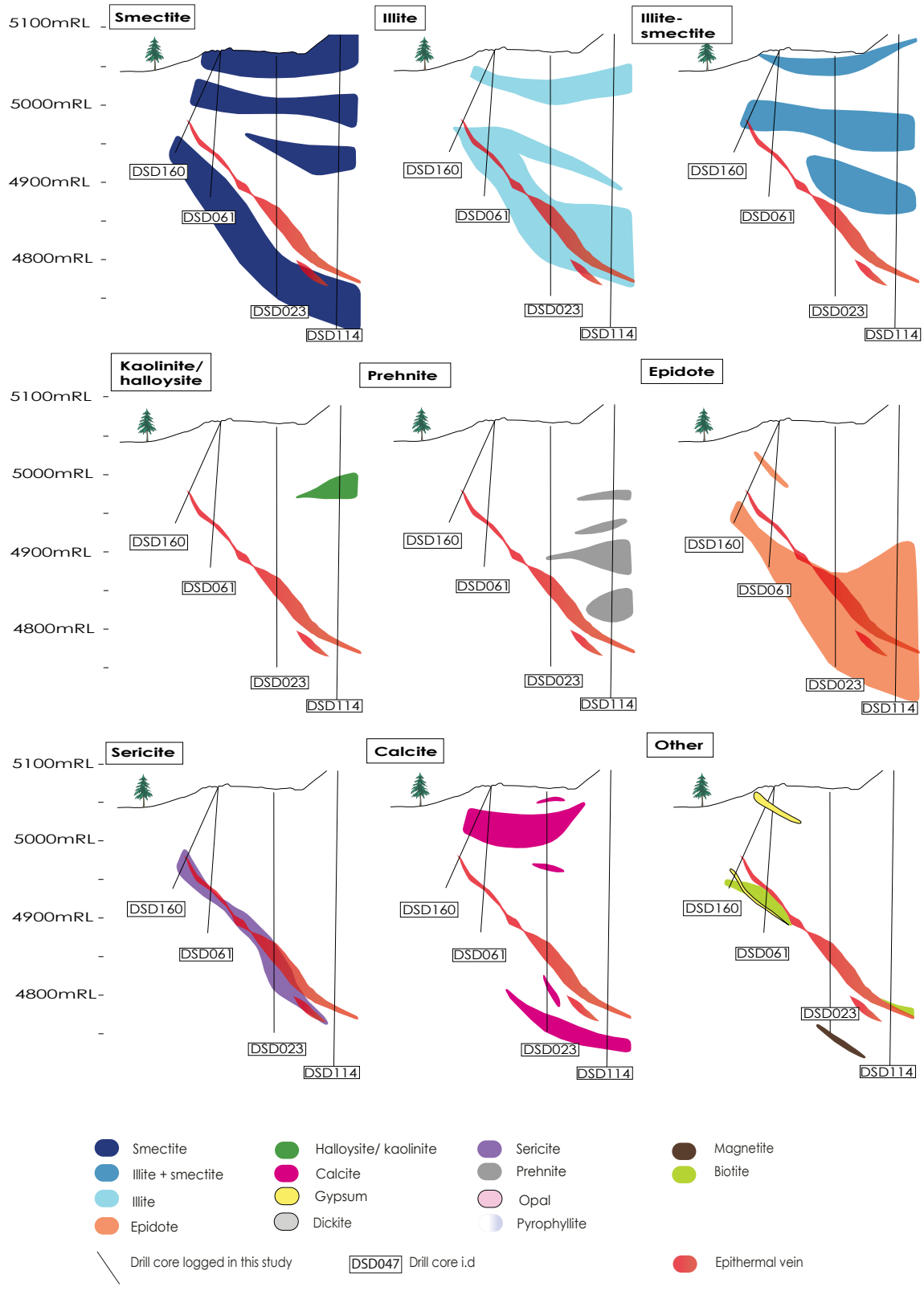

Fig. 5.6 Kencana section 19850mN alteration mineralogy showing the principal hydrothermal alteration minerals and their distribution, as determined by PIMA analysis.

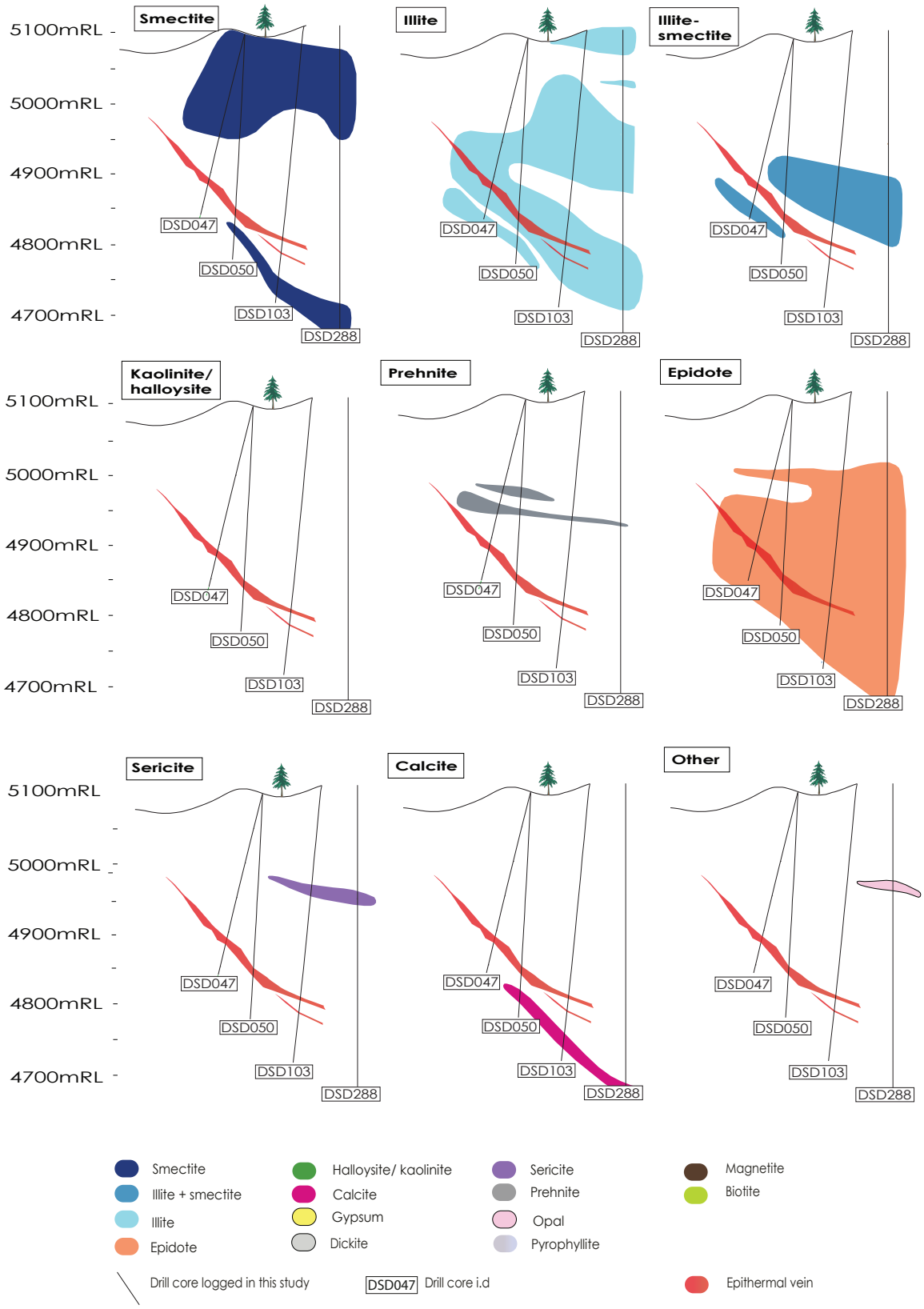

Fig. 5.7 Kencana section 19900mN alteration mineralogy showing the principal hydrothermal alteration minerals and their distribution, as determined by PIMA analysis. Halloysite/ kaolinite was not observed along this cross section.

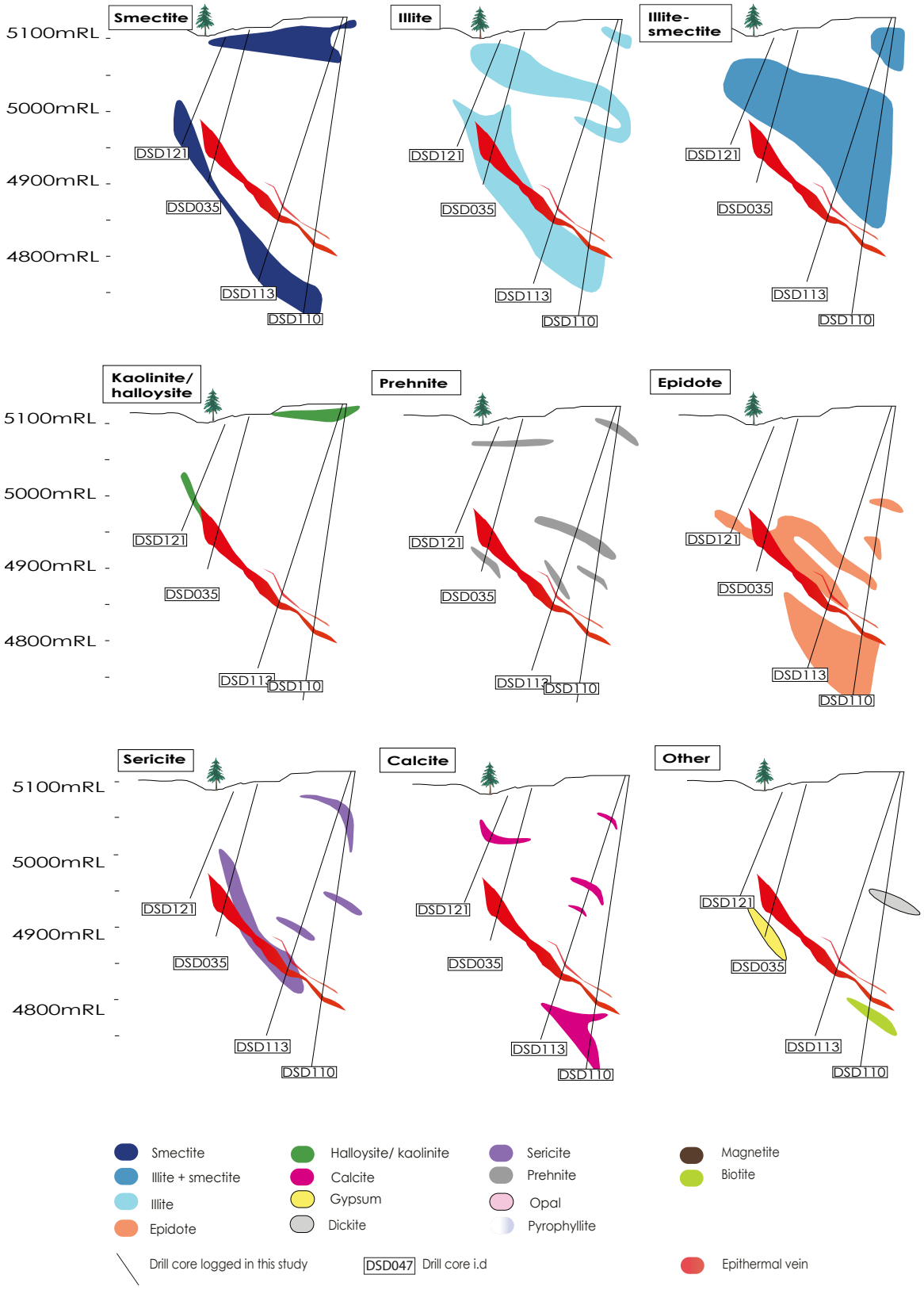

Fig. 5.8 Kencana section 19950mN alteration mineralogy showing the principal hydrothermal alteration minerals and their distribution, as determined by PIMA analysis.

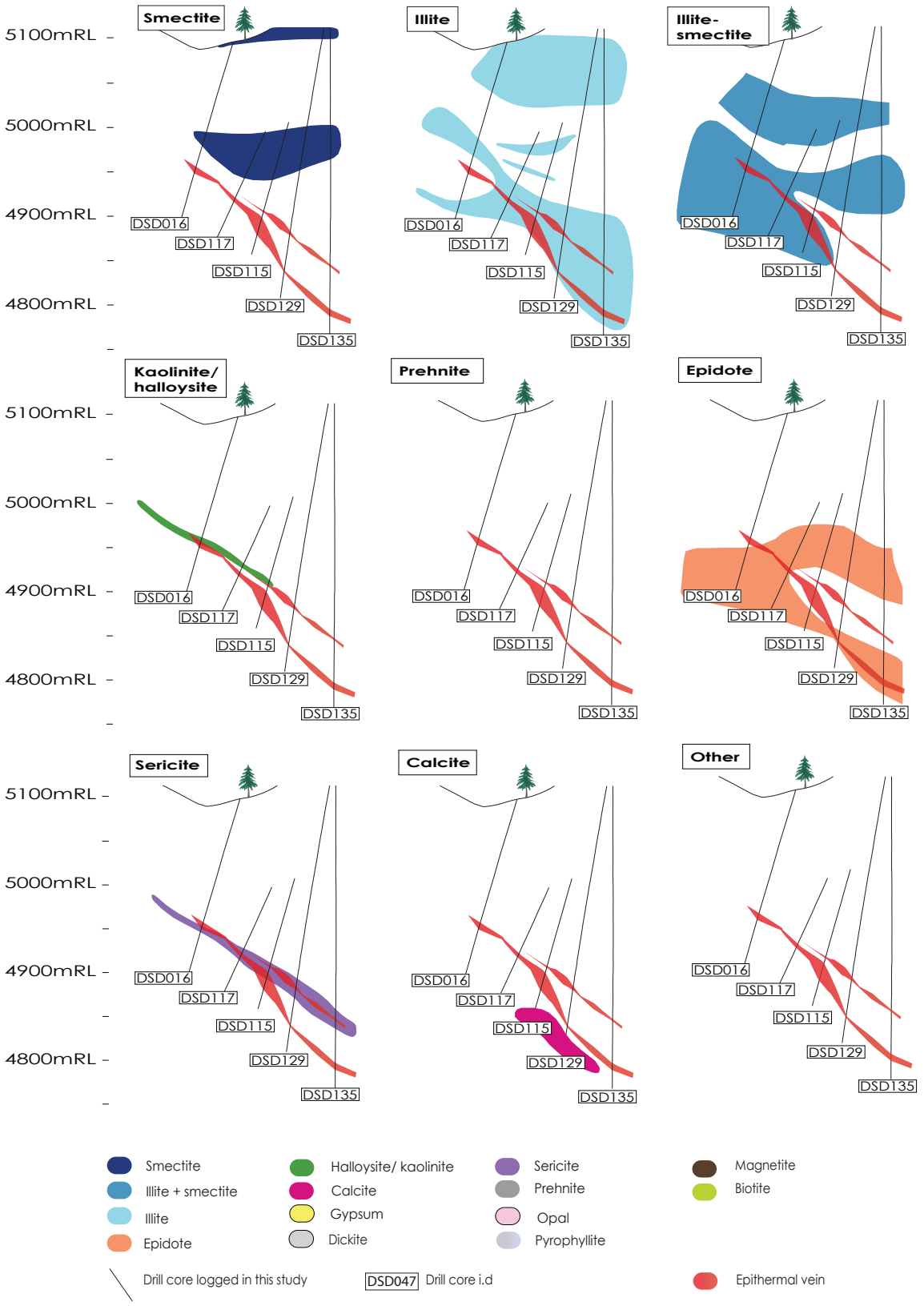

Fig. 5.9 Kencana section 20000mN alteration mineralogy showing the principal hydrothermal alteration minerals and their distribution, as determined by PIMA analysis. Prehnite was not observed along this cross section.

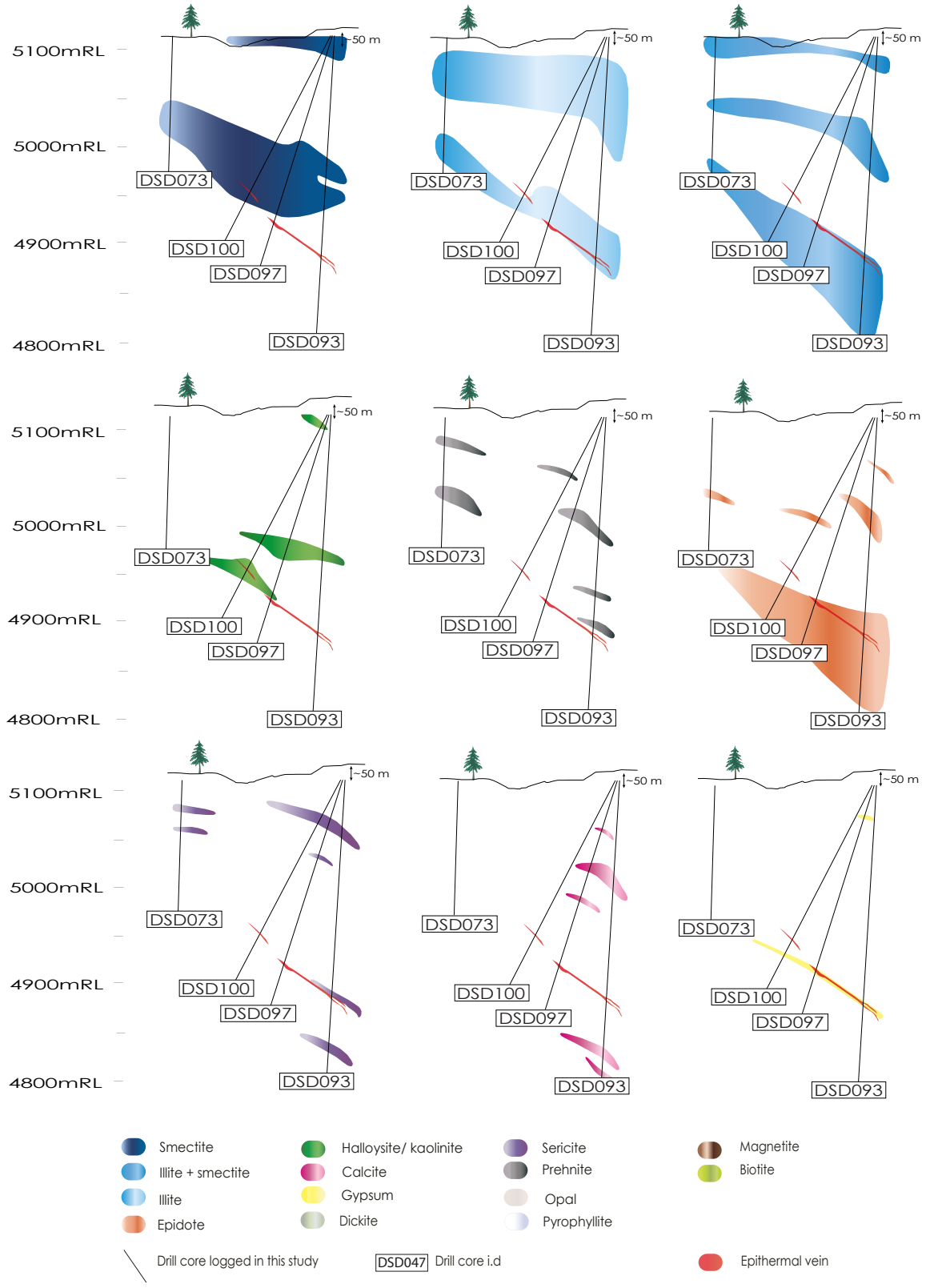

Fig. 5.10 Kencana section 20050mN alteration mineralogy showing the principal hydrothermal alteration minerals and their distribution, as determined by PIMA analysis.

5.5.2 Argillic 2 (ISP) alteration facies

The ISP facies is dominated by illite, smectite, pyrite and chlorite with minor carbonate. ISP altered rocks are fairly soft and pale grey or pale green. Alteration is typically pervasive and partially destructive of primary volcanic texture, although it can be selective (feldspar replacement) or fracture related in hematite-dusted andesite autobreccias (Fig. 5.11). ISP alteration is the most common alteration facies associated with the Kencana deposit and affects all lithologies, though it is best developed in coherent andesite lavas. The dominant clay composition of the assemblage is transitional with proximity to the ore body, with a change from smectite-rich through layered illite-smectite to illite-rich towards the vein. Layered illite-smectite is an alteration product of plagioclase, mafic phenocrysts and adularia that has previously replaced plagioclase phenocrysts (Simpson et al., 2001). It also fills interstitial sites in the groundmass and is a significant in the matrix cement and clasts of volcanic breccias. ISP alteration is often transitional to the IC alteration facies with proximity to the Kencana vein. Chlorite composition in ISP alteration is typically Fe-rich to intermediate, becoming more Mg-rich with depth (Figs. 5.14-5.22).

5.5.3 Argillic 3 (IC) alteration facies

The IC alteration facies is dominated by illite, pyrite and chlorite with minor quartz and adularia. IC altered rocks can be soft and friable, or indurated depending on the affected lithology. IC alteration can be grey, mid to pale green, or white. Pyrite is typically disseminated (~1%) though sporadic veinlets (<0.5 cm) occur in the hangingwall margins of the vein structure. Alteration is typically pervasive but can manifest as illite and/ or chlorite selective replacement of feldspars in andesite units, or as selvedge alteration around minor pyritic or hematitic veins proximal to the deposit in unaltered/ SCG/ ISP altered rocks (Fig. 5.11 A). Coherent andesite units can show total groundmass replacement by illite + adularia with disseminated pyrite. IC alteration intensifies toward the deposit and often forms an envelope extending between 20-50 m surrounding the QAS facies alteration, which hosts the epithermal vein. Though best developed in the hanging-wall above the structure, IC alteration is common in breccia clasts within the Kencana vein.

The argillic 3 alteration facies affects all lithologies at Kencana with the exception of

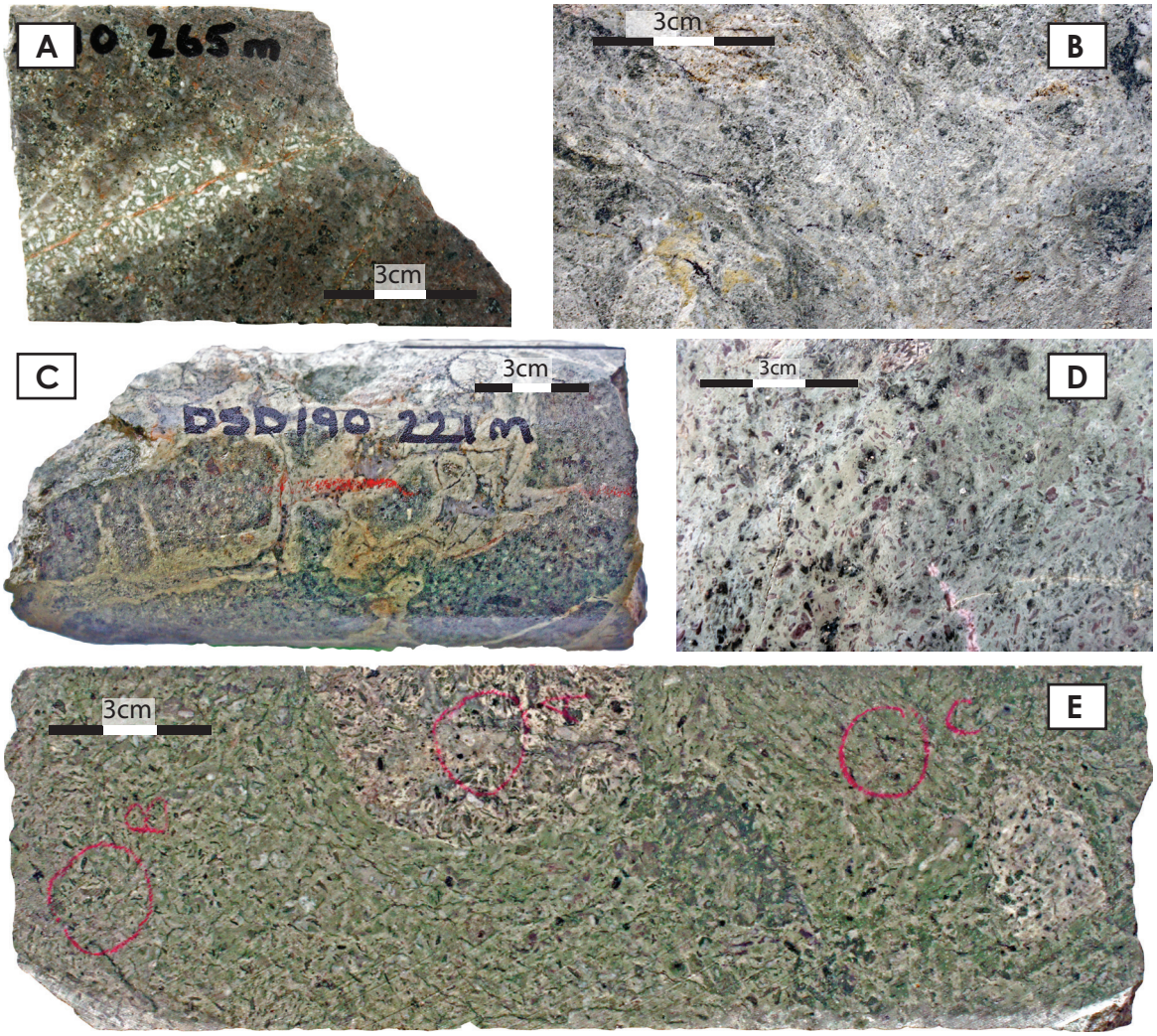

Fig. 5.11 ISP and IC facies alteration

A) Illite-chlorite selvedge alteration of hematite veinlet in hematite-dusted andesite lava. Plagioclase phenocrysts are selectively illite-replaced, from drill core DSD190_265 m; **B)** Texturally destructive pervasive illite-chlorite-pyrite alteration form drill core DSD100_109.5 m; **C)** Illite cemented chlorite-altered andesite breccia with disseminated pyrite and calcite veinlets from drill core DSD190_221 m; **D)** Pervasive strongly illite--smectite-chlorite-pyrite altered crystal-rich volcanics from drill core DSD099_188.8 m; **E)** Pervasive strongly illite-chlorite-pyrite altered breccia. Relict breccia clasts can still be identified, and are more preferentially illite-altered than the chlorite-altered matrix. From drill core DSD288_310 m. Coloured circles on photographs relate to locations for PIMA analysis.

the basaltic unit. IC alteration is overprinted by the QAS and CEP alteration facies. Chlorite chemistry associated with IC alteration is intermediate between Fe- and Mg-rich (see Figs. 5.14-5.22)

5.5.4 Phyllic (QAS) alteration facies

The phyllic alteration facies is dominated by quartz, adularia, sericite and pyrite. QAS altered rocks are found marginal to IC altered rocks in close proximity to the Kencana

vein, forming an envelope extending approximately 10 m from the deposit and following the approximate geometry and dip of the vein. Lesser volumes of QAS alteration also occur in shear zones above the vein in association with prehnite facies and EC alteration. Silicification is generally pervasive, affecting all lithologies and overprinting all alteration styles at Kencana, though it is best developed in coherent andesite lavas. Rocks affected by QAS alteration are very hard and typically preserve primary volcanic texture, where not obscured by earlier alteration (Fig. 5.12). Sericite is fine-grained and cannot be detected in hand sample, requiring microscopy and SWIR analysis for detection. Fine-grained adularia selectively replaces feldspar phenocrysts in both andesite and volcaniclastic units, and pervasively alters the groundmass of andesite lavas (Fig. 5.12). Adularia distribution is determined by Na-cobaltinitrate staining, and is significantly more widespread than hand sample observations imply. Pyrite is disseminated and abundance increases with proximity to the deposit.

5.5.5 Propylitic 1 (EC) alteration facies

The EC alteration facies is dominated by epidote ± chlorite ± pyrite ± adularia with minor quartz and calcite. The propylitic 1 alteration facies forms a wide regional footprint around the Kencana deposit and as such EC alteration is widely spread across the region. However, EC alteration is the dominant facies below 5000mRL, and increases in abundance and intensity toward the vein. EC alteration ranges from pale to dark green and largely affects the non-permeable coherent lithologies at Kencana. In the clastic units, EC alteration is disseminated and typically manifests as selective replacement of feldspar phenocrysts.

Epidote occurs either as a pervasive alteration of groundmass, or, with proximity to the deposit, fills fractures with calcite and quartz (Fig. 5.13 A and B). Fracture controlled epidote increases in abundance towards the Kencana vein and always occurs in the coherent lithologies beneath the host structure, particularly the basaltic unit, where EC alteration is transitional to CEP alteration. Fracture controlled epidote alteration crosscuts earlier pervasive EC alteration. EC alteration is transitional to IC alteration. EC alteration (particularly fracture controlled EC alteration) overprints the argillic assemblages at Kencana but is overprinted by QAS alteration, and was formed by an earlier event than the P alteration in shallow shear zones.

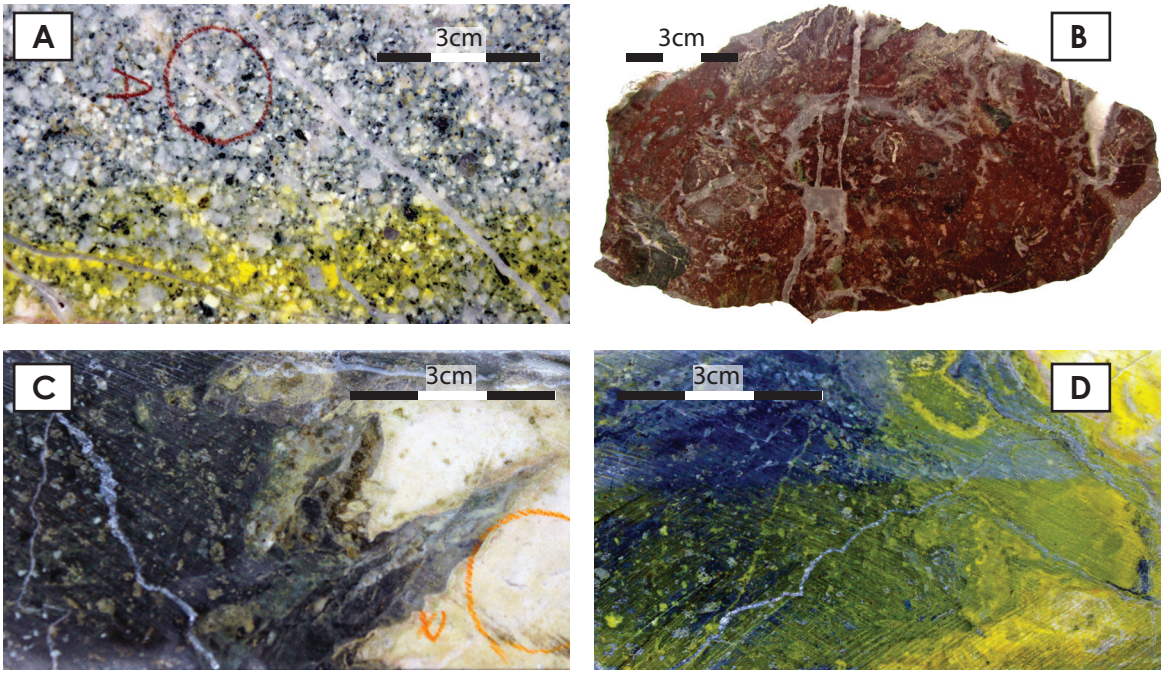

Fig. 5.12 QAS facies alteration

A) Quartz veinlets and pervasive silicification of diorite from drill core DSD117_270 m. Yellow staining highlights adularia distribution, selectively altering plagioclase phenocrysts and some groundmass; **B)** Pervasively silicified hematitic sandstone with quartz veinlets and propylitic-illitic altered fragments from underground face Sub2 UC01 S075; **C)** Propylitic alteration (selective replacement of feldspars) overprinted by QAS facies alteration (white) with quartz veinlets from drill core DSD105_388 m; **D)** Sodium cobaltinitrite staining of C) highlighting adularia distribution from drill core DSD105_388 m. Adularia selectively replaces plagioclase phenocrysts and is pervasively associated with quartz.. Coloured circles are related to locations for PIMA analysis.

5.5.6 Propylitic 2 (CEP) alteration facies

The propylitic CEP alteration facies is dominated by epidote ± calcite ± pyrite with minor quartz. CEP alteration ranges from mid to dark green and rocks affected by CEP alteration are generally indurated. CEP alteration occurs in two locations surrounding the deposit: Below the Kencana vein where CEP alteration is typically the only facies present, and in shear zones above the vein between 5050-5000mRL in association with sub-propylitic and phyllic alteration. CEP alteration below the vein is unconstrained in depth and typically manifests as fractures filled with epidote ± crystalline calcite ± quartz and a pervasively epidote-calcite altered groundmass (Fig 5.13 C and D). CEP alteration is most intense in the basaltic unit, though it does affect coherent andesites and volcaniclastic sandstones higher in the stratigraphy. CEP altered veinlets and fractures overprint the regional propylitic 1 alteration at Kencana.

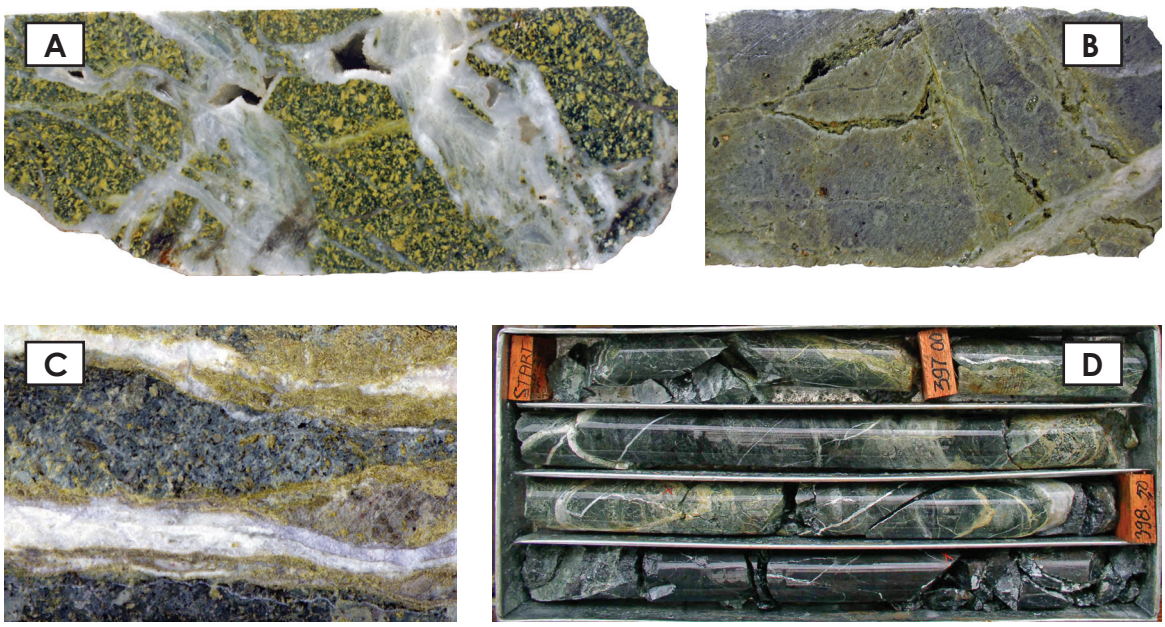

Fig. 5.13 EC and CEP alteration facies

A) Epidote altered diorite with quartz vein stockwork from drill core DSD288_433 m. Epidote selectively alters plagioclase phenocrysts and occurs along fractures with calcite (EC facies); **B)** Fracture controlled epidote-chlorite alteration (EC facies) with quartz vein and overprinted by pervasive silicification from drill core DSD048_353 m; **C)** Fracture controlled epidote+calcite alteration (CEP facies) parallel to and crosscut by quartz veins from drill core DSD105_419 m. Plagioclase phenocrysts are selectively replaced by epidote in a chlorite altered groundmass; **D)** Drill core showing weakly sheeted quartz vein stockwork with abundant fracture controlled epidote (CEP facies), overprinted by pervasive silicification from drill core DSD325_m. Quartz veins crosscut epidote alteration. Some weakly argillic zones show overprinting by epidote alteration.

5.5.7 Sub-propylitic (P) alteration facies

The sub-propylitic prehnite alteration facies consists of prehnite ± gypsum with minor chlorite and is hosted in shear zones above the Kencana deposit, particularly toward the north of the system (from 19850mN). Alteration is pale grey to pale green and often overprints puggy illite-smectite clays. Gypsum occurrence was identified by PIMA analysis and was not detectable in hand specimen or thin section observations. Sub-propylitic altered shear zones are often associated with earlier calcite ± epidote ± pyrite alteration.

5.5.8 Calc-potassic (BM) alteration facies

The BM alteration facies is dominated by biotite ± magnetite ± actinolite with minor albite. Biotite and magnetite are fine grained and rely on microscopy and PIMA analysis for detection. BM alteration is typically black to dark green and rocks affected by BM alteration are mostly coherent andesites and basaltic andesite. Magnetite occurs as veinlets (~0.3 cm thick) crosscutting earlier (propylitic and argillic) alteration styles. Magnetite veinlets

were observed in drill core DSD139 at a depth of 234 m to the end of hole. Magnetite veinlets have also been observed in exploration drill cores to the south of the Kencana deposit although the lateral extent of their distribution is as yet unconstrained (Chambers, pers. comm., 2010). Calc-potassic alteration occurs proximal to the deposit and extends up to 15 m from the vein, though generally it occurs less than 3 meters from epithermal mineralization.

5.5.9 Intermediate-advanced argillic (IDP) alteration facies

Intermediate-advanced argillic alteration in the Kencana system comprises illite ± dickite ± pyrophyllite or kaolinite. IDP alteration is volumetrically minor in comparison to other alteration facies at Kencana, and occurs in shear zones above the vein at approximately 4950mRL. Samples containing pyrophyllite do not contain illite and vice versa. IDP alteration is only observed in core samples from the deposit and as a result, observations are limited due to strong weathering. IDP alteration ranges from pale grey to white where samples contain kaolinite, and rocks affected by IDP alteration are very soft and friable. IDP alteration is generally destructive of primary volcanic texture.

5.5.10 Advanced argillic (KH) alteration facies

The advanced argillic alteration facies consists of kaolinite or halloysite with pyrite and minor opal and illite. KH alteration is strongly pervasive and destructive of primary texture, and produces soft, friable rocks that appear bleached white. Identification of the original rock type is difficult given the nature of this alteration. This facies is most prominent in the near-surface oxidized zone (< 10 m from surface), where halloysite-predominant alteration is a product of supergene weathering, and is often characterized by red-orange Fe-oxide staining. Advanced argillic alteration overprints all other alteration facies, with the exception of pervasive silica alteration (QAS facies). Hypogene kaolinite alteration occurs in shear zones overlying the main K1 structure in association with pyrite and illite, and following the upward projection of the vein towards the surface. Opal was not detected in hand specimen, however PIMA analysis suggests that opal occurs in the KH facies at surface along cross section 19600mN (Fig. 5.2). Opal is also detected in minor volumes in shear zones

along cross section 19900Mn (Fig. 5.7).

Paragenesis

Prior to initiation of the Kencana hydrothermal system, host rocks in the district were altered to a regionally extensive propylitic assemblage of Fe-chlorite, albite, pyrite ± epidote. This style of alteration selectively replaces the plagioclase phenocrysts and/or groundmass crystals in both the coherent or volcaniclastic lithologic units. Dilation along the K1 fault created structurally controlled permeability, leading to a wide zone (up to 100 m) of vein-related propylitic alteration, which overprints regional propylitic alteration (EC facies). Argillic alteration (ISP transitional to IC facies alteration) followed and overprinted the propylitic alteration, though some CEP alteration overprints argillic assemblages, reflecting the complex history of repeated structural dilation along the fault. The argillic alteration is most intense within 25 m from the Kencana vein. Silicic alteration formed during the most intense phase alteration and vein mineralization, and is confined to an envelope <10 m from the vein, and overprints all other types of alteration. Advanced and intermediate-advanced argillic alteration (IDP and KH facies) form in shear zones above the deposit.

5.6 Discussion of alteration mineralogy, facies and distribution at Kencana

Alteration at Kencana is generally typical of low-sulfidation epithermal deposits, dominated by quartz-adularia-sericite, and illite to smectite clay assemblages (Hedenquist et al., 2000). These minerals reflect the near-neutral pH and reduced composition of the ore fluid. Interstratified illite-smectite and smectite clays plus kaolinite occur on the margins of the system, as well as within the ore zone, commonly as supergene alteration products of hydrothermal sericite (Hedenquist et al., 2000).

Alteration mineralogy as determined by SWIR analysis was contoured and vertical and lateral alteration facies zonation was interpreted from the mineral distribution (Figs. 5.14-5.22). Hypogene alteration at Kencana is approximately zoned around the deposit with respect to four major types of alteration: (1) phyllic alteration (QAS facies) in the form of pervasive silicification and quartz-adularia-sericite alteration in the immediate vein zone, (2) argillic alteration (IC facies) enveloping the vein zone, (3) high temperature propylitic

alteration (CEP facies) filling fractures, extending up to 50 m from the vein, and (4) low-temperature argillic alteration and regional propylitic alteration (SCG, ISP and IC facies) distal to the deposit. Supergene advanced argillic alteration (KH facies) affects the top 5-10 m of stratigraphy at Kencana. Disruption to vertical and lateral zonation is common where fluid pathways are determined by lithological and structural permeability, and due to the complex overprinting nature of the alteration facies assemblages determined for Kencana.

Propylitic facies are spatially discreet, with EC facies alteration forming a wide footprint largely above the vein, and CEP alteration confined to a narrow zone around the vein and more commonly as a poorly constrained zone below the vein, primarily affecting basaltic volcaniclastic units (Figs. 5.14-5.22).

The presence of opal in KH facies alteration along cross section 19600mN (Fig. 5.2) may suggest a hypogene origin for advanced argillic alteration in this location. Though other typical minerals are not present, it is possible that the cross section could represent the edge of a steam-heated zone of advanced argillic alteration. It is proposed that any further steam-heated alteration would occur further to the south and more investigation and sampling is needed to determine this.

The centre and margins of the deposits show slightly different characteristics in terms of the distribution of alteration mineralogy, which may prove useful in exploring for epithermal deposits in the Gosowong district. The deposit margins show a higher abundance of KH facies alteration proximal to the vein, contain opal in advanced argillic alteration at surface and shear zones are characterized by more illite-smectite, KH facies alteration and sub-propylitic facies alteration. The centre of the deposit displays a higher abundance of EC and BM facies alteration, and shear zones are characterized by more QAS and CEP facies alteration, as well as dickite which is found in shear zones in the centre of the deposit.

Several variables can influence mineral precipitation in hydrothermal systems: concentrations of aqueous species or gases, host rock compositions, reaction kinetics, duration of hydrothermal activity, degree of equilibrium, permeability, temperature, pressure, redox and acidity (Corbett and Leach, 1998; Cooke et al., 2000; Pass, 2010). While this invariability can result in a complex combination of factors influencing mineral deposition, known

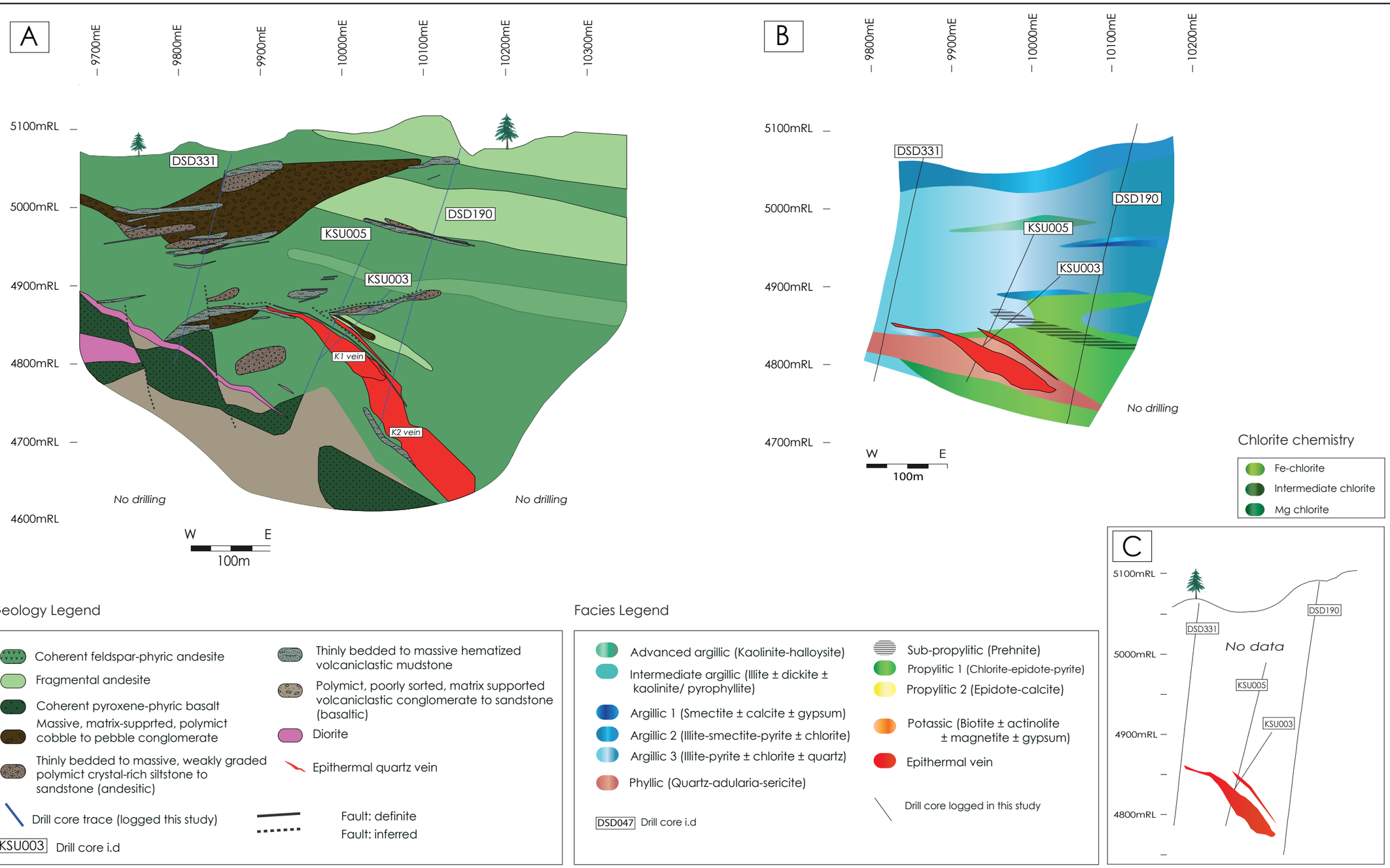

Fig. 5.14 Section 19600mN alteration assemblage distribution (right) shown with geology section (left). Facies distribution displays a blanket of advanced argillic alteration at the surface. Argillic assemblages are smectite- to illite-dominated with increasing depth. Shear zones above the vein are characterized by advanced argillic, sub-propylitic and argillic 1+2 assemblages. Proximal to the vein is a broad zone of propylitic 1 alteration. Phyllic alteration envelopes the vein. Chlorite alteration (inset) is not available for this cross section due to lack of suitable samples. Alteration style is generally not related to lithology. Alteration study not extended to K2 vein.

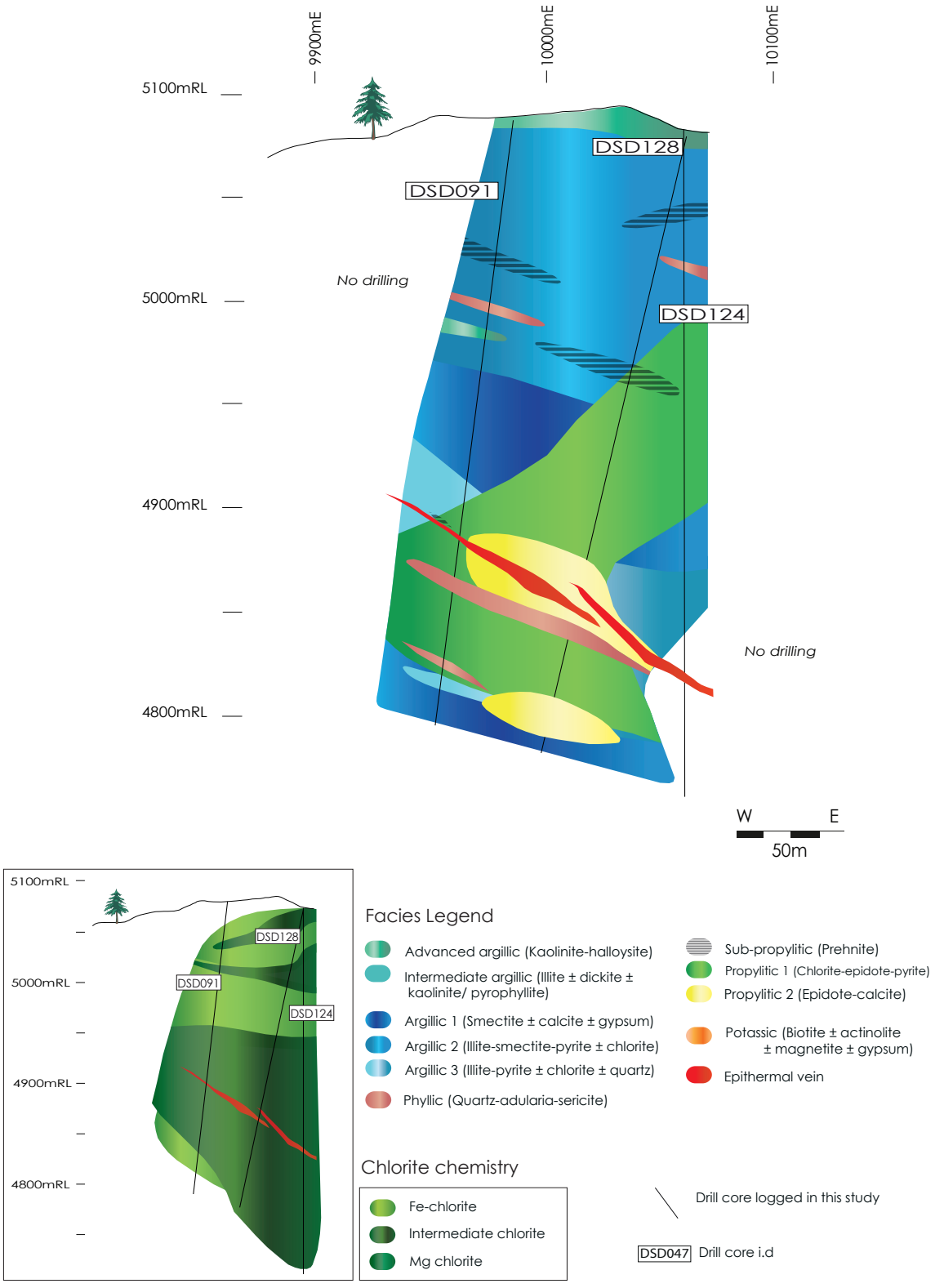

Fig. 5.15 Section 19650mN alteration assemblage distribution displaying a blanket of advanced argillic alteration at the surface. Argillic assemblages are variably interlayered illite-smectite dominated to smectite-dominated and illitic with proximity to the vein. A broad zone of propylitic 1 alteration is proximal to the vein. Propylitic 2 alteration envelopes the vein with a zone of phyllic alteration immediately underlying the structure. Shear zones above the vein are characterized by sub-propylitic, phyllic and advanced argillic assemblages. Chlorite alteration (inset) is broadly vertically zoned from Fe-rich to intermediate composition chlorite surrounding the vein.

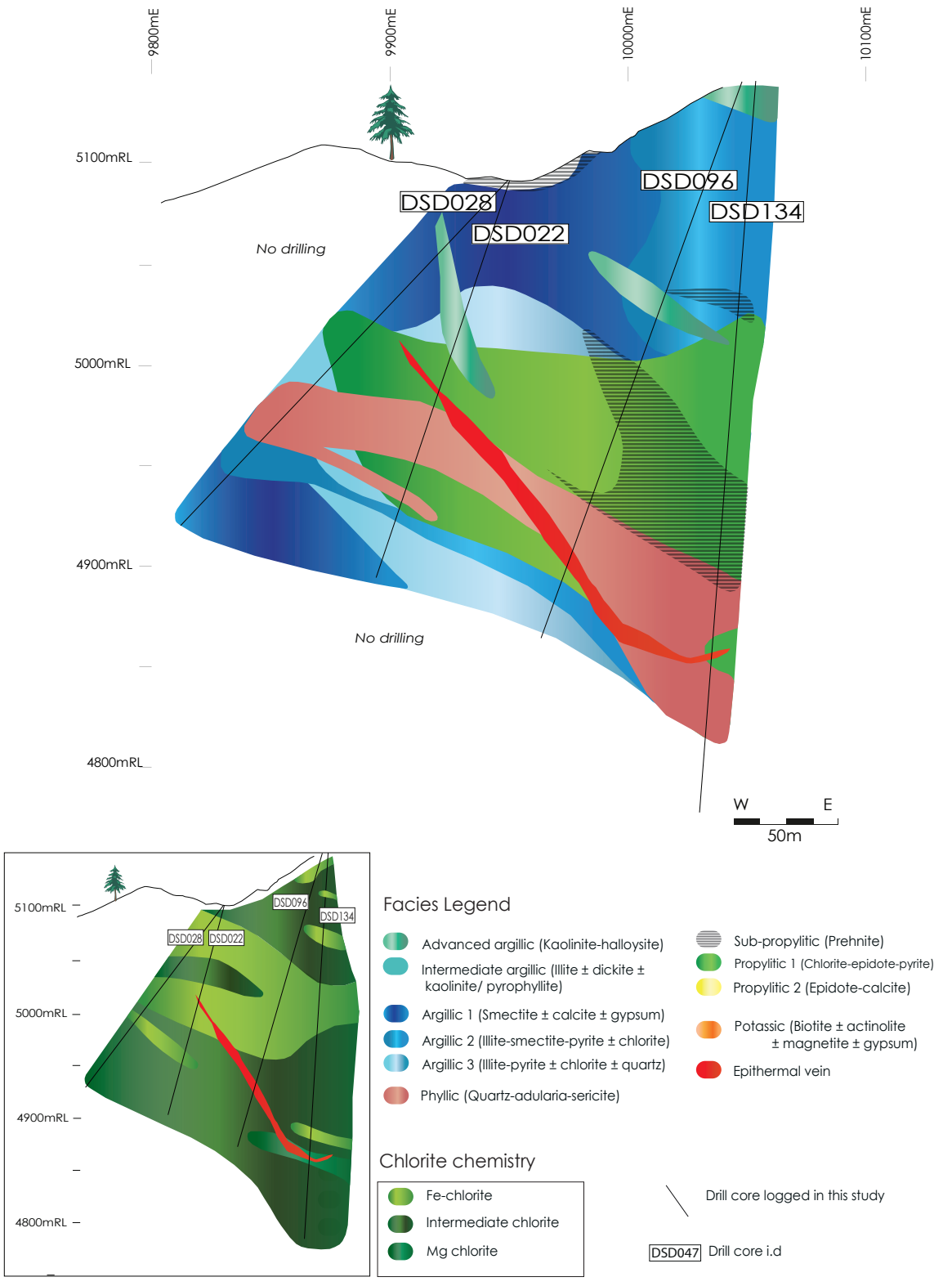

Fig. 5.16 Section 19750mN alteration assemblage distribution displaying a blanket of advanced argillic and sub-propylitic alteration at the surface. Argillic assemblages are zoned from smectite-rich to illite-rich towards the vein. A broad zone of propylitic 1 alteration is proximal to the vein. Phyllic alteration envelopes the vein. Shear zones above the vein are characterized by sub-propylitic and advanced argillic assemblages. Chlorite alteration (inset) is broadly vertically zoned from Fe-rich to intermediate composition chlorite surrounding the vein.

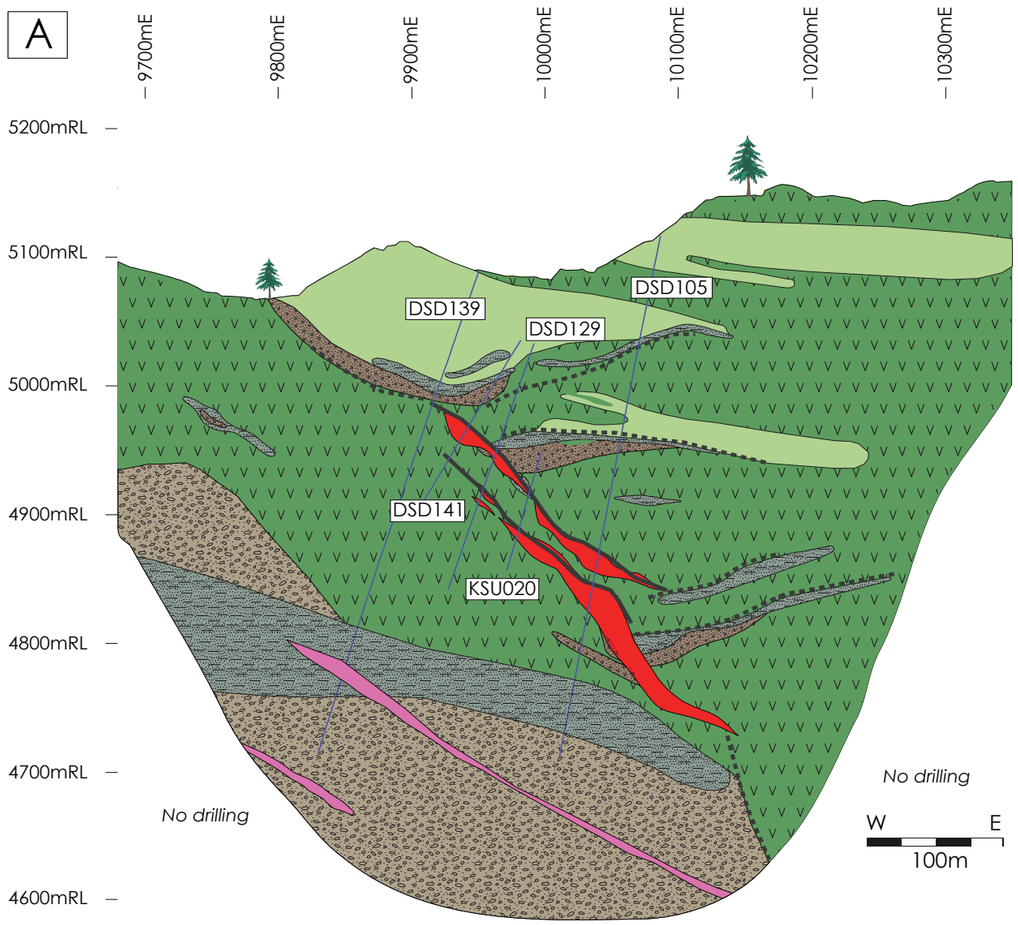

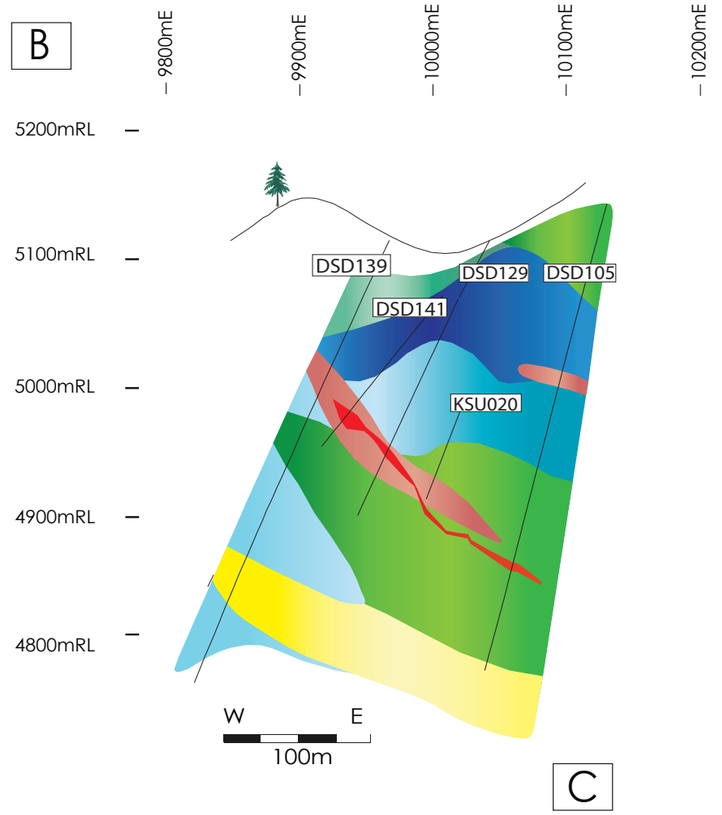

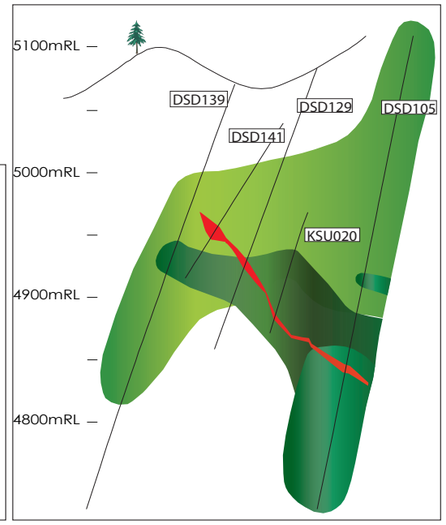

Geology Legend

- Coherent feldspar-phyric andesite
- Fragmental andesite
- Coherent pyroxene-phyric basalt
- Massive, matrix-supprted, polymict cobble to pebble conglomerate
- Thinly bedded to massive, weakly graded polymict crystal-rich siltstone to sandstone (andesitic)
- Thinly bedded to massive hematized volcaniclastic mudstone
- Polymict, poorly sorted, matrix supported volcaniclastic conglomerate to sandstone (basaltic)
- Diorite
- Epithermal quartz vein
- Drill core trace (logged this study)
- KSU003 Drill core i.d
- Fault: definite
- Fault: inferred

Facies Legend

- Advanced argillic (Kaolinite-halloysite)
- Intermediate argillic (Illite ± dickite ± kaolinite/ pyrophyllite)
- Argillic 1 (Smectite ± calcite ± gypsum)
- Argillic 2 (Illite-smectite-pyrite ± chlorite)
- Argillic 3 (Illite-pyrite ± chlorite ± quartz)
- Phyllic (Quartz-adularia-sericite)
- Sub-propylitic (Prehnite)
- Propylitic 1 (Chlorite-epidote-pyrite)
- Propylitic 2 (Epidote-calcite)
- Potassic (Biotite ± actinolite ± magnetite ± gypsum)
- Epithermal vein
- Drill core logged in this study
- DSD047 Drill core i.d

Fig. 5.17 Section 19800mN alteration assemblage distribution (right) shown with geology section (left). Facies distribution a blanket of advanced argillic alteration with propylitic 1 assemblage alteration at the surface. Argillic assemblages are transitional from smectite to illite-dominated with proximity to the vein. Shear zones above the vein are characterized by sub-propylitic alteration. Proximal to the vein, the propylitic 1 assemblage is dominant. The vein is enveloped by phyllic alteration, and below the vein is located a deep zone of propylitic 2 alteration. Chlorite alteration (inset) is vertically zoned from Fe-rich through intermediate composition to Mg-rich chlorite at depth. Alteration style is largely continuous regardless of lithology.

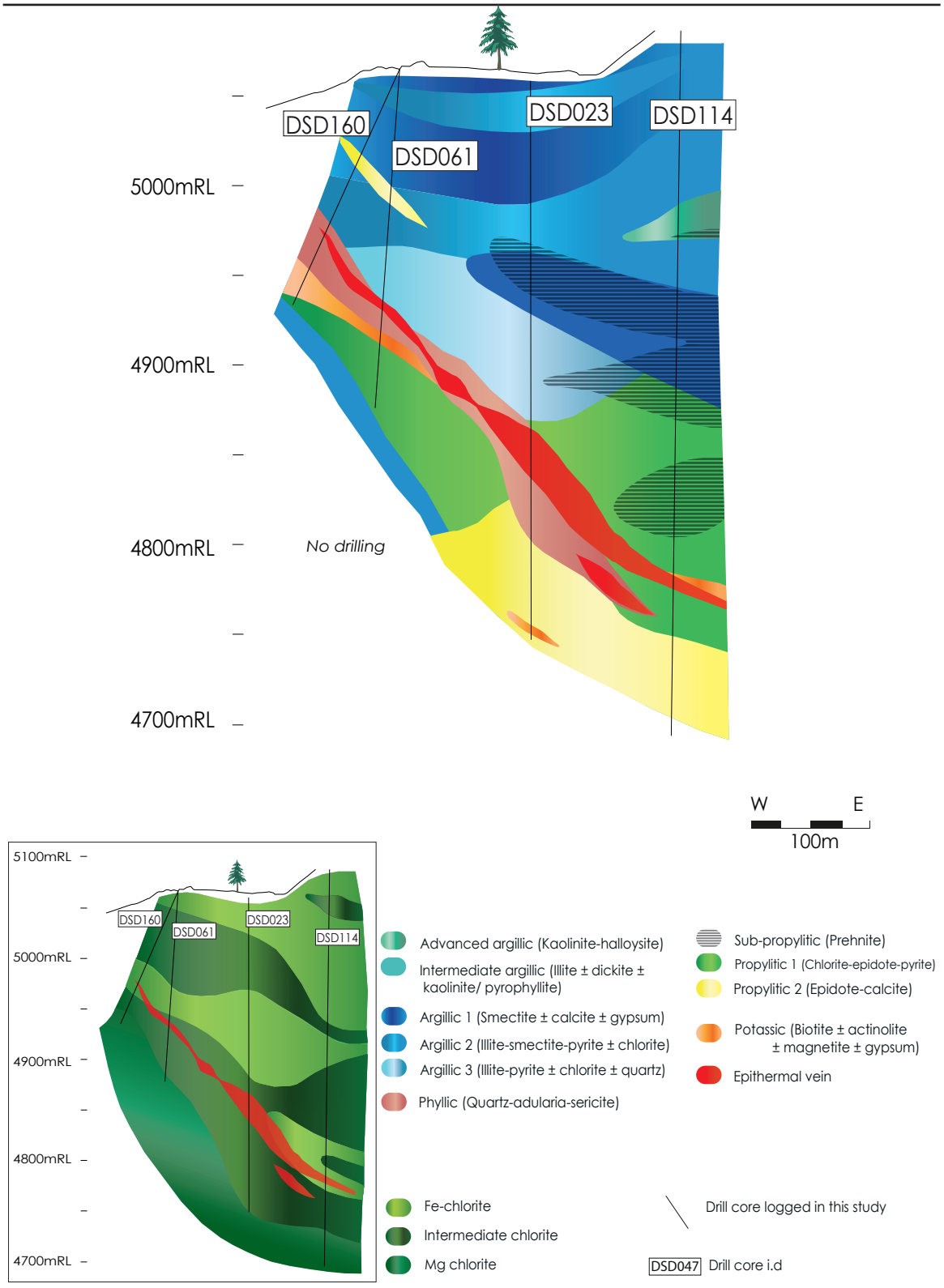

Fig. 5.18 Section 19850mN alteration assemblage distribution displaying a vertical zonation from smectite -dominated argillic assemblages (Argillic 1+2) to illite-dominated assemblages (Argillic 3) with proximity to the vein. Shear zones are characterized by sub-propylitic alteration. Proximal to the vein, propylitic 1 assemblage dominates, and the vein is enveloped by phyllic alteration and minor potassic assemblages. Below the vein is a zone of propylitic 2 alteration. Chlorite alteration (inset) is vertically zoned from Fe-rich through intermediate composition to Mg-rich chlorite at depth.

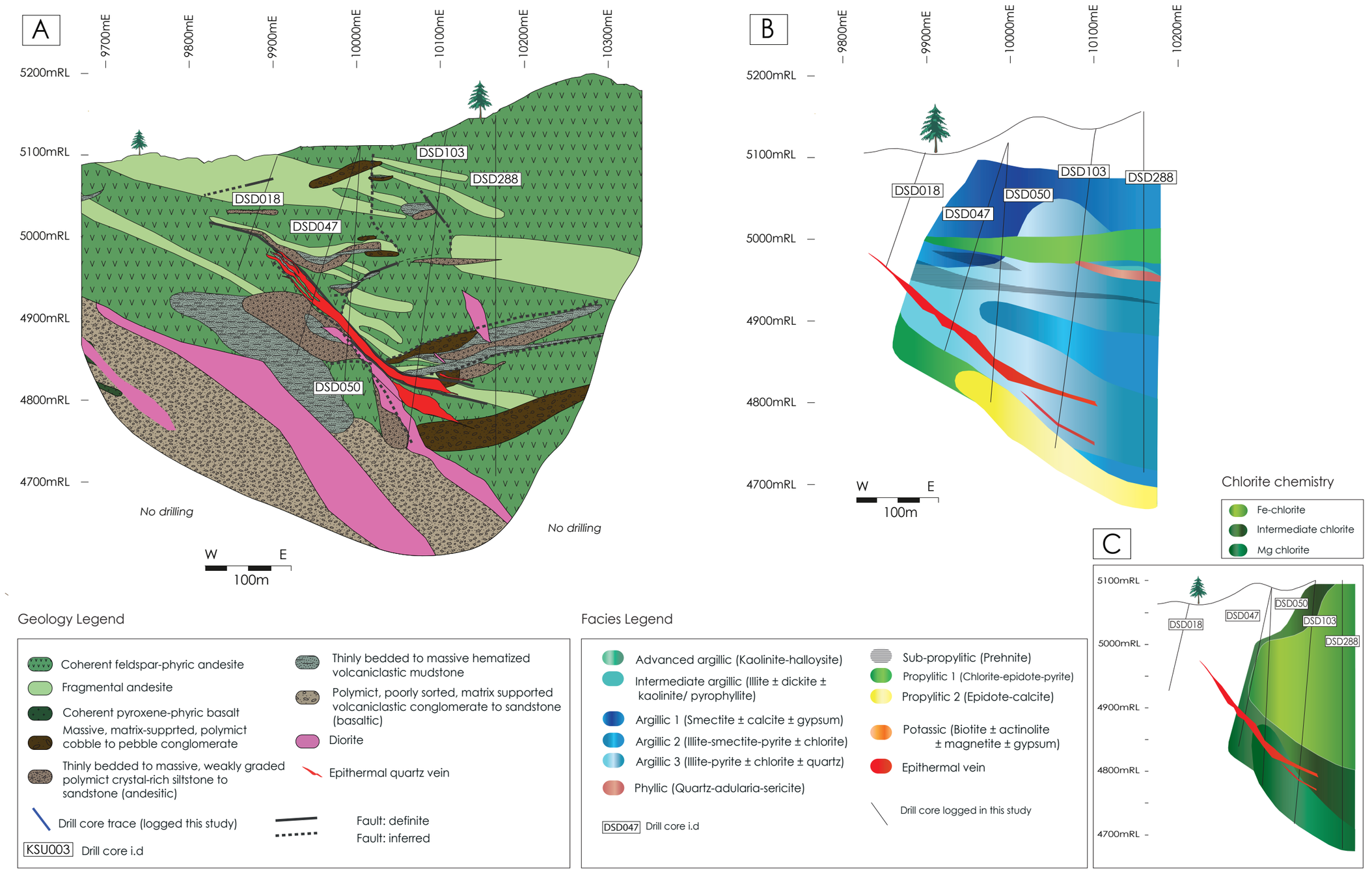

Fig. 5.19 Section 19900mN alteration assemblage distribution displaying a broad vertical zonation from smectite-dominated argillic assemblages (Argillic 1+2) to illite-dominated argillic alteration (Argillic 3). Shear zones above the vein are marked by sub-propylitic, phyllic and intermediate argillic alteration. Below the vein, propylitic 1+2 assemblages are dominant. Chlorite alteration (inset) is vertically zoned from Fe-rich, through intermediate composition to Mg-rich chlorite at depth.

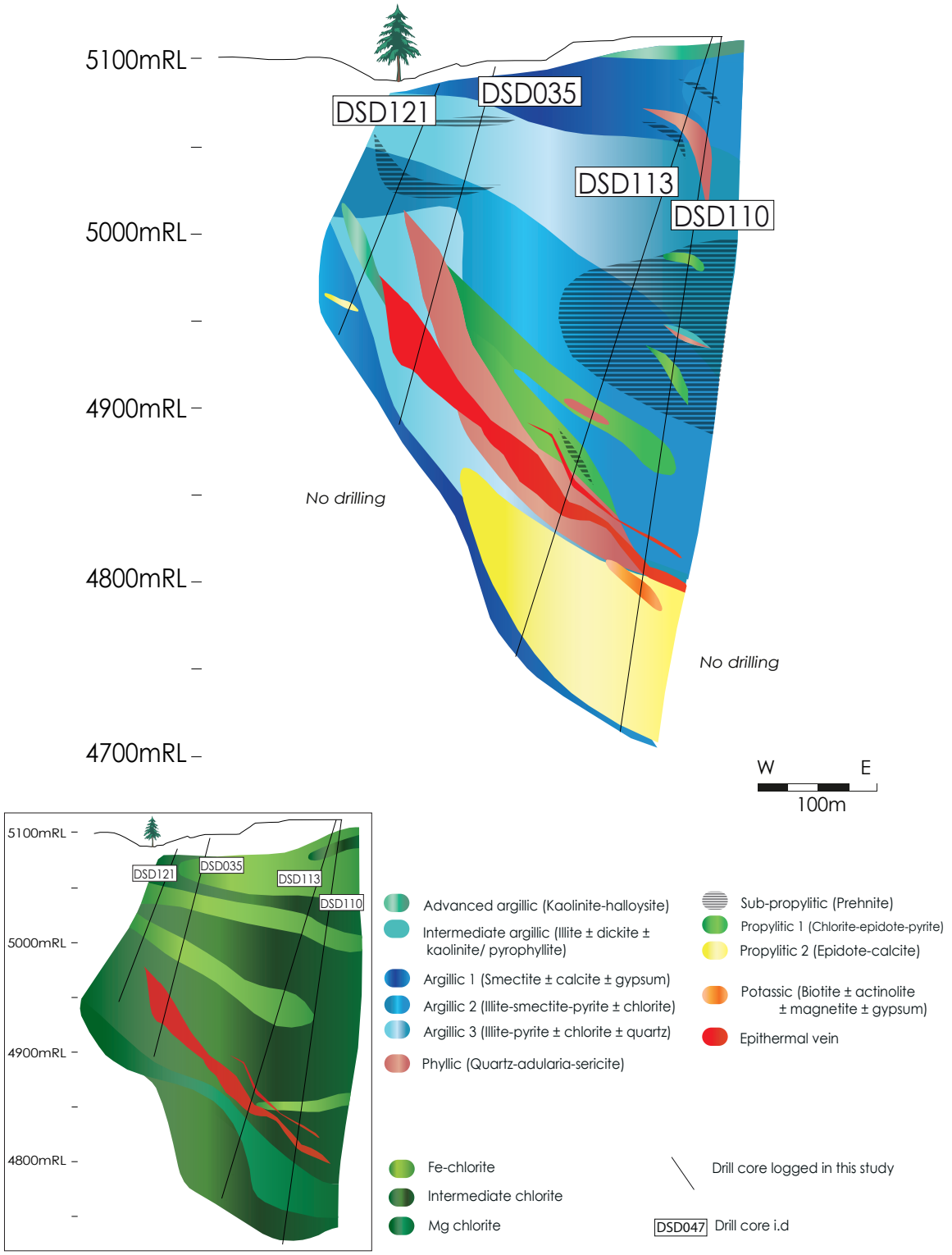

Fig. 5.20 Section 19950mN alteration assemblage distribution displaying a blanket of advanced argillic alteration at surface, through variably smectite to illite rich argillic assemblages overprinted by sub-propylitic, phyllic and intermediate argillic shears. Propylitic 1 alteration occurs in a zone up to 25 m above the vein, and an envelope of phyllic alteration immediately surrounds the vein. A deep zone of propylitic 2 alteration occurs below the vein, with limited potassic alteration. The outflow zone is marked by a zone of advanced argillic alteration continuing along the upward extension of the vein. Chlorite alteration (inset) is broadly vertically zoned from Fe-rich, through intermediate composition to Mg-rich at depth.

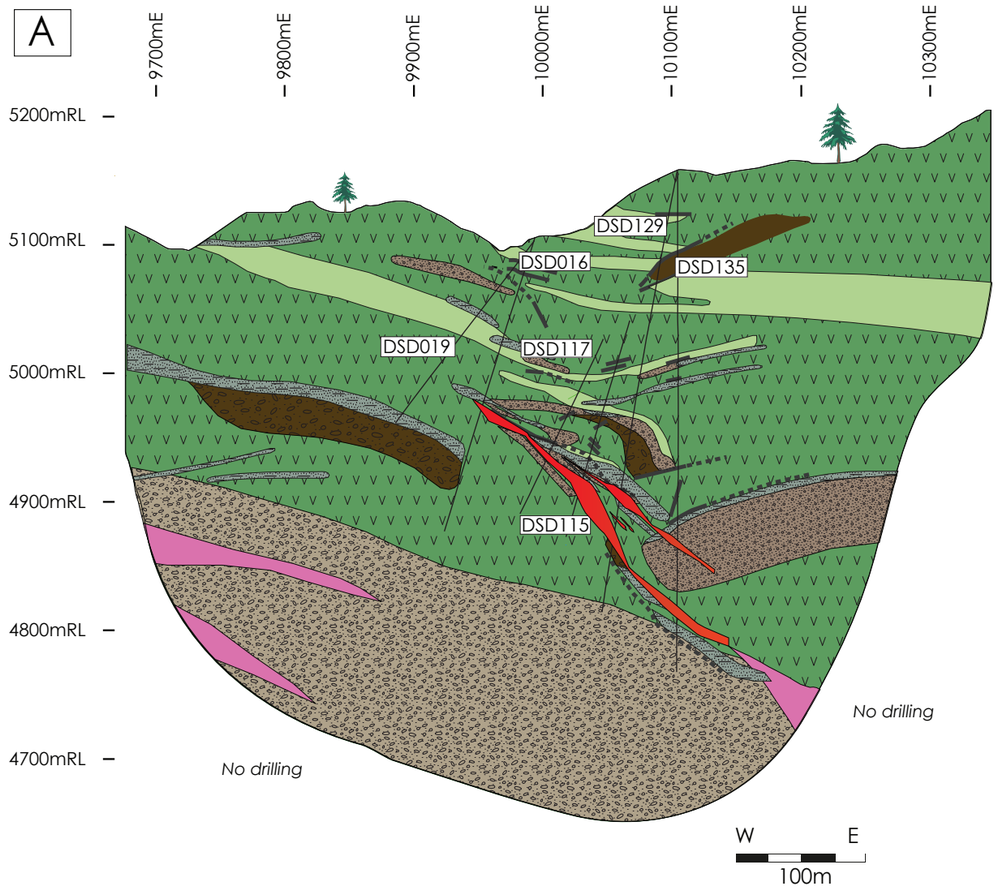

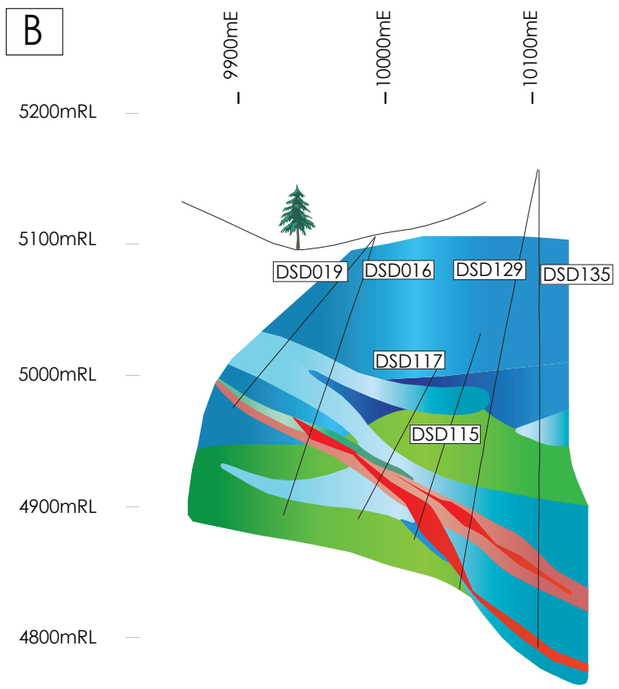

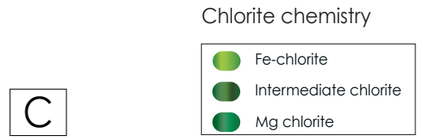

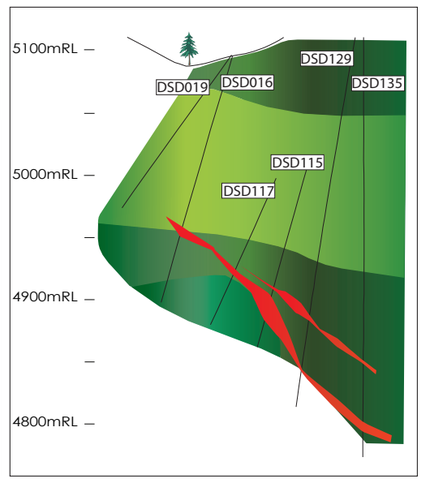

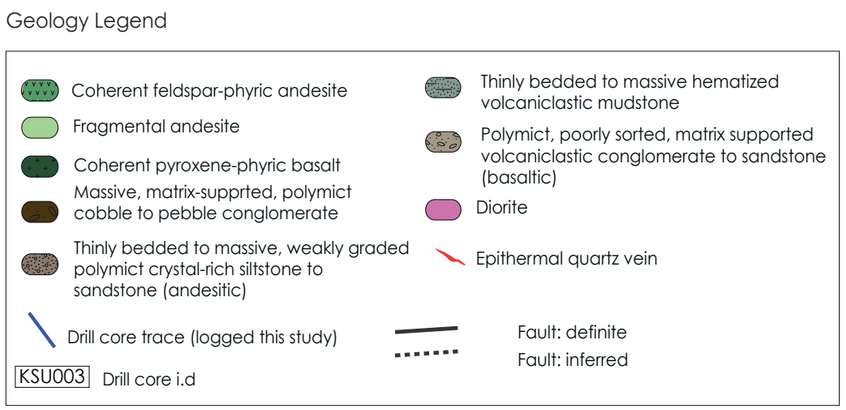

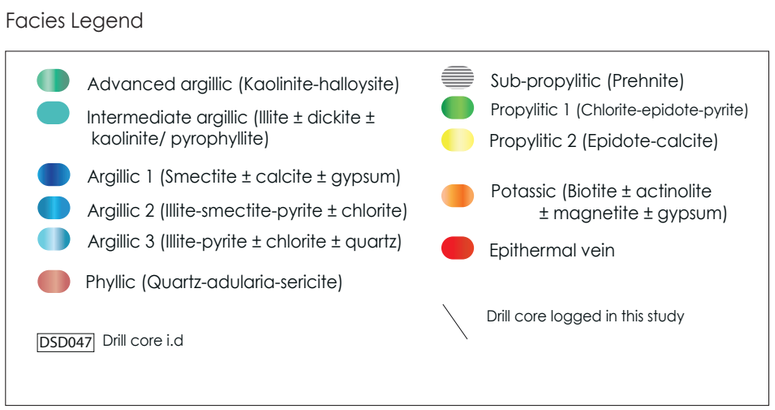

Fig. 5.21 Section 20000mN alteration assemblage distribution (right) shown with geology section (left). Facies distribution displays a zoned alteration around the K1 vein from regional smectite-dominated argillic assemblages (Argillic 1+2), to illite-dominated assemblages (Argillic 3), with proximal propylitic alteration and an envelope of phyllic alteration immediately surrounding the vein. The outflow zone is marked by a zone of advanced argillic alteration continuing along the upward extension of the vein. Chlorite alteration (inset) is zoned from intermediate composition at surface to Fe-rich, through intermediate composition around the vein and a zone of Mg-rich chlorite at depth. Alteration style is generally continuous regardless of lithology.

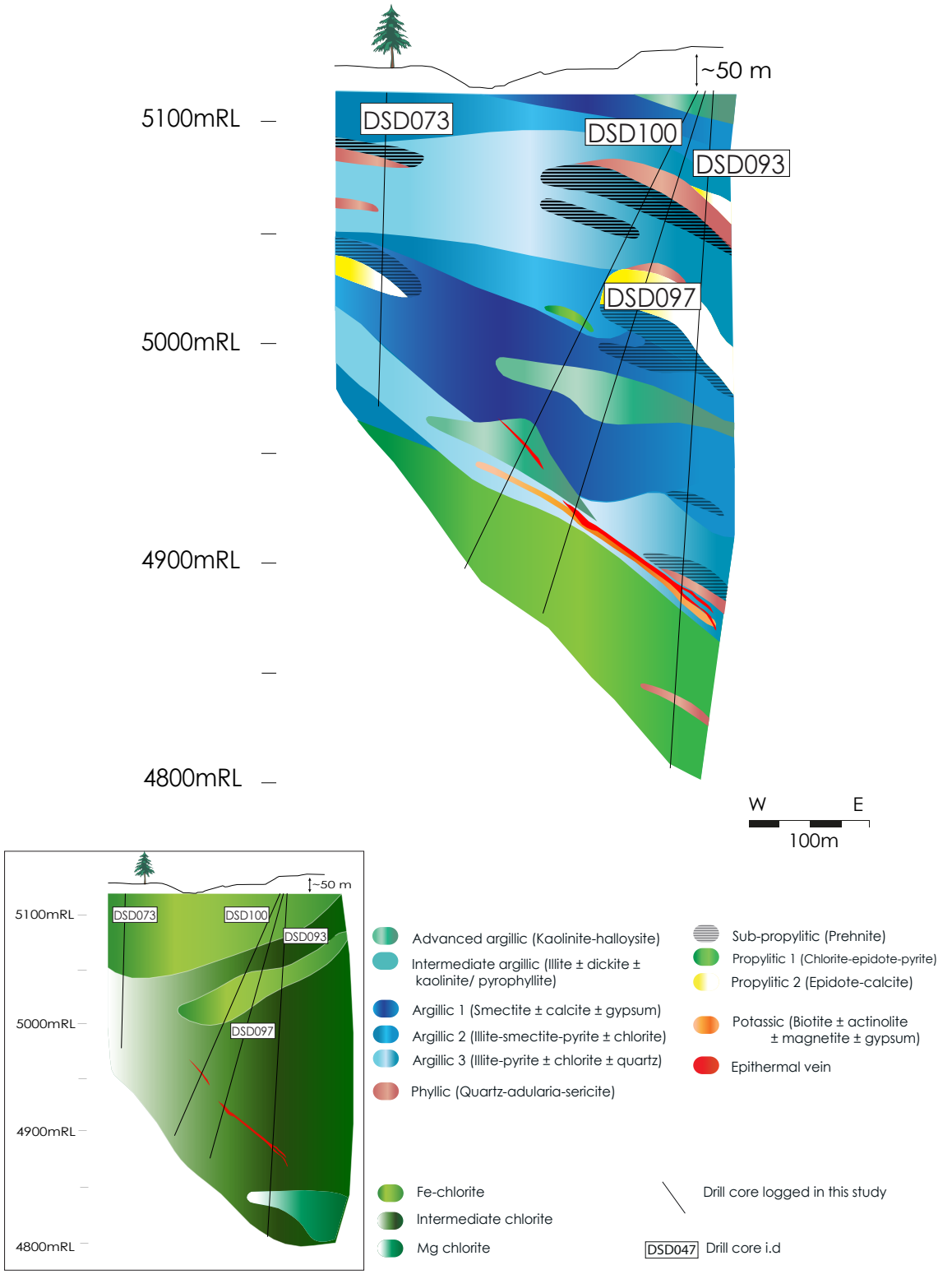

Fig. 5.22 Section 20050mN alteration assemblage distribution displaying intermittent zones of smectite and illite-dominated argillic assemblages (Argillic 1-3) overprinted by shear zones characterized by phyllic, sub-propylitic and propylitic 2 assemblages. The vein is associated with a thin envelope of potassic alteration, and the outflow zone is marked by a zone of advanced argillic alteration continuing along the upward extension of the vein. Chlorite alteration (inset) is vertically zoned from Fe-rich at surface through intermediate composition to deep Mg-rich chlorite.

conditions from active geothermal systems and experimental modeling can be used to determine the physio-chemical conditions of ore deposition and hydrothermal fluid (Henley and Ellis, 1983; Hedenquist and Houghton, 1987; Reyes, 1990; Cooke et al., 1996; Pass, 2010).

The alteration halo to the ore zone includes a variety of temperature-sensitive minerals that can help to indicate locations of palaeofluid flow. Temperature stability ranges for common hydrothermal minerals are shown in Fig. 5.23 A. A general trend in increasing temperature towards the ore zone can be interpreted for the Kencana deposit, with smectite-dominated assemblages (20-200ºC) transitional to illite-dominated assemblages (220-310ºC), with increasing abundance of chlorite, epidote, albite and sericite, which infer a palaeofluid temperature of >200ºC (Fig. 5.23). Temperature stability ranges for hydrothermal minerals can be used to determine approximate temperature stability ranges for Kencana alteration facies. Inferred fluid palaeotemperatures for Kencana alteration facies are shown in Fig. 5.23 B and form over the ranges: SCG facies (80-200°C), KH facies (80-310°C), IDP facies (60-360°C), QAS facies (60-480°C), IC facies (80-480°C), P facies (240-410°C), BM facies (140-430°C), and EC and CEP facies (200-420°C), where ranges are defined by major and accessory minerals in each facies. Alteration facies zonation generally reflects the decreasing hydrothermal fluid temperature with distance from the upflow zone and mineralized structure. BM facies alteration (one of the highest temperature facies) is commonly found in the upflow zone. It is not clear whether BM facies alteration forms early in the system as intrusion-related alteration similar to that found at the porphyries at Toguraci and to the north of the goldfield, or as a late-stage phase related to the inferred higher temperature molybdenite-black quartz mineralization. Local variations in facies distribution, and thus fluid palaeotemperature, are dependent on features including permeability, porosity and faulting.

Mineralogy an also be used to estimate fluid acidity. Alteration assemblages at Kencana plot along a trend from higher temperature, near-neutral conditions (potassic and propylitic alteration) to acidic conditions at lower temperature (argillic alteration) (Fig. 5.24). Acidic conditions are reflected in the argillic IDP and KH facies present in shear zones above the vein, suggesting a progression to higher acidity and lower temperature as hydrothermal activity waned. KH facies alteration also marks the outflow zone of the vein, where ad-

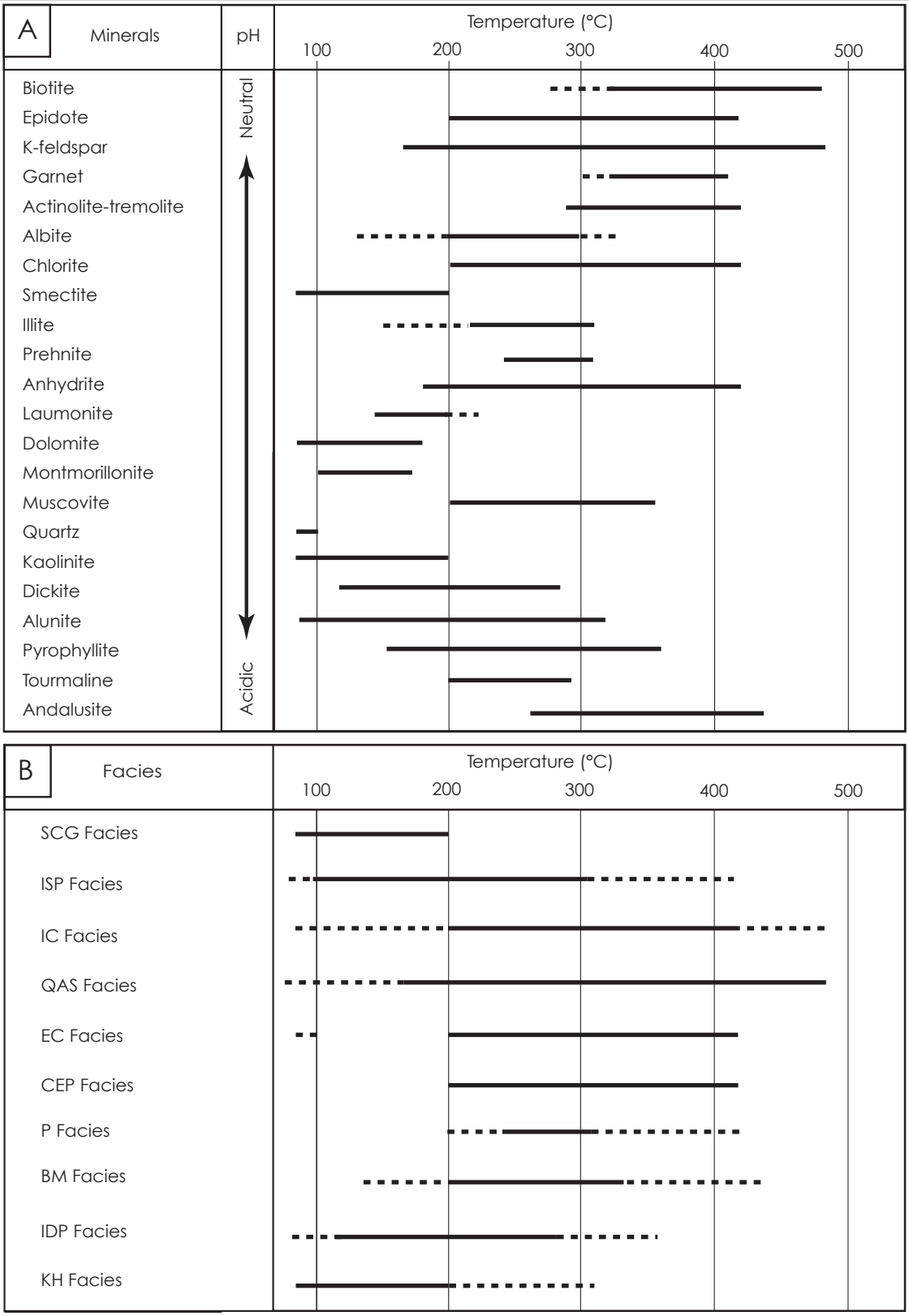

Fig 5.23 A) Temperature stability ranges of hydrothermal minerals deduced empirically from active geothermal systems and experimental modeling (Hemley et al., 1980; Henley and Ellis, 1983; Bird et al., 1984; Hedenquist and Houghton, 1987; Reyes, 1990). Minerals are arranged by stability with respect to pH. Modified from Pass (2010); **B)** Temperature stability ranges for Kencana alteration facies determined by major (bold lines) and accessory (dashed lines) minerals for each assemblage.

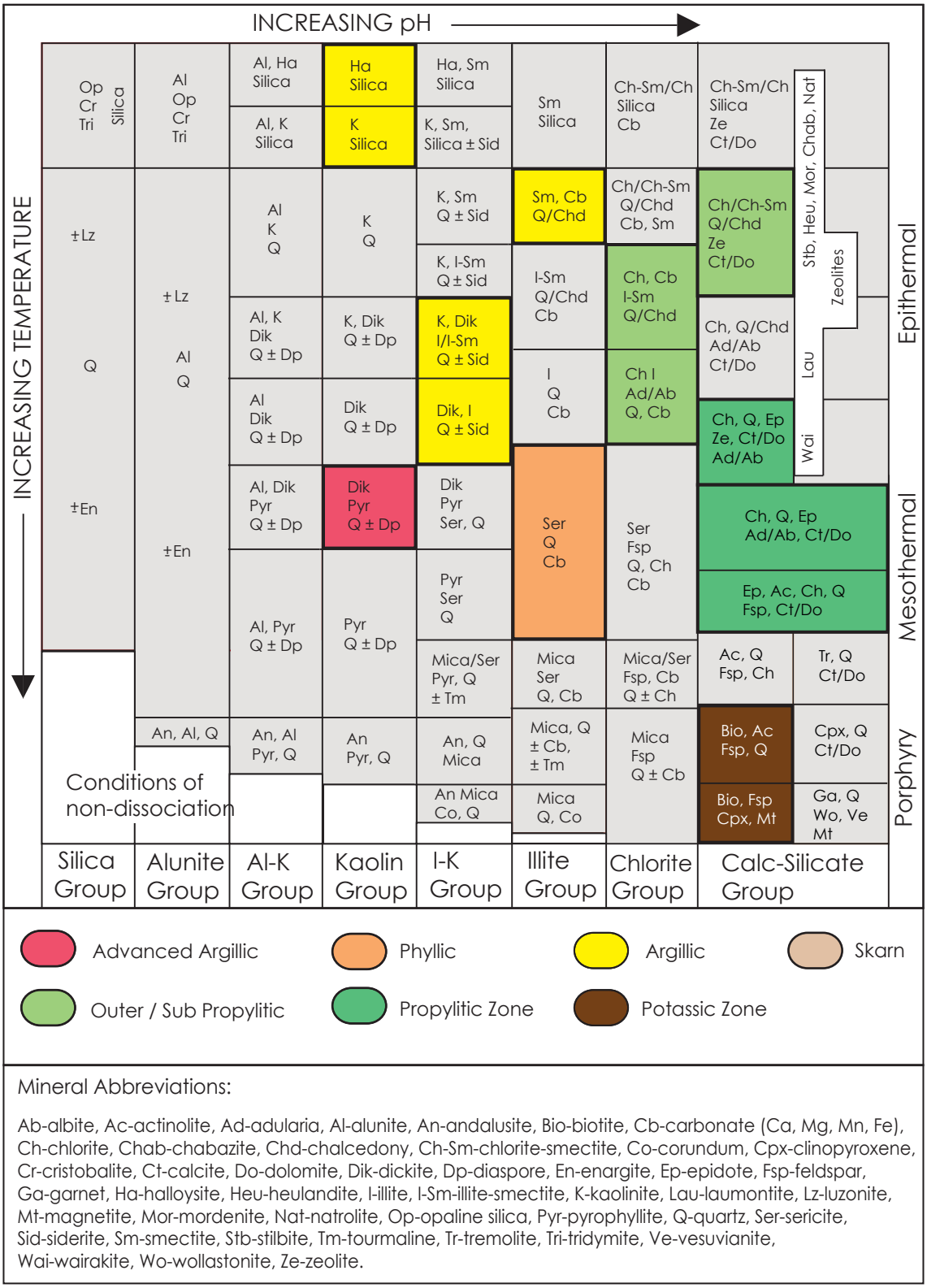

Mineral Abbreviations:

Ab-albite, Ac-actinolite, Ad-adularia, Al-alunite, An-andalusite, Bio-biotite, Cb-carbonate (Ca, Mg, Mn, Fe), Ch-chlorite, Chab-chabazite, Chd-chalcedony, Ch-Sm-chlorite-smectite, Co-corundum, Cpx-clinopyroxene, Cr-cristobalite, Ct-calcite, Do-dolomite, Dik-dickite, Dp-diaspore, En-enargite, Ep-epidote, Fsp-feldspar, Ga-garnet, Ha-halloysite, Heu-heulandite, I-illite, I-Sm-illite-smectite, K-kaolinite, Lau-laumontite, Lz-luzonite, Mt-magnetite, Mor-mordenite, Nat-natrolite, Op-opaline silica, Pyr-pyrophyllite, Q-quartz, Ser-sericite, Sid-siderite, Sm-smectite, Stb-stilbite, Tm-tourmaline, Tr-tremolite, Tri-tridymite, Ve-vesuvianite, Wai-wairakite, Wo-wollastonite, Ze-zeolite.

Fig. 5.24 Common alteration mineralogy in hydrothermal systems modified from Corbett and Leach (1998). Approximate temperature and pH ranges: Potassic and skarn (high T: >300°C, pH ≥7), propylitic (280°–300°C, pH ~5–>7), outer/sub propylitic (250°–<200°C, pH~5–>7), phyllic (250°–200°C, pH 4–6), argillic (250°–>200°C, pH 4–6), advanced argillic (high to low temperatures, pH <4). Temperature and pH ranges taken from Corbett and Leach (1998) text. Alteration mineral assemblages found at Kencana are shown in colour.

vanced argillic alteration extends towards surface from the upper end of the vein. This zone reflects the more acidic conditions and lower temperature of the fluid after boiling, mixing and sulfide precipitation within the vein.

There is chemical and stable isotope evidence from hot springs (Waiotapu, New Zealand) that cold groundwater also acts as a diluent at shallow levels, and very near the surface steam-heated acid sulfate waters can mix with the upflow. Boiling of deep chloride fluids prior to dilution results in the stabilization of K-feldspar. In contrast, dilution at shallower depths by the steam-heated waters (both CO_2-rich and acid sulfate) leads to the water compositions initially shifting to K-mica (and interstratified illite-smectite) stability, and to kaolinite stability with further dilution and temperature decrease (Hedenquist, 1991). The composition and distribution of these fluids are consistent with alteration mineralogy and zonation observed at Kencana. Boiling of deep chloride fluid is very common in the upper 1–2 km of the upflow zone of most geothermal systems, though it may be quenched by mixing with marginal waters, either cold groundwater in high relief terrane, or steam-heated waters in areas of lower relief (Hedenquist, 1991). CO_2-rich steam-heated waters are common on the margins of systems and generally underlie the near-surface, acid sulfate steam-heated waters. Interaction with CO_2-rich waters will form K-mica and interstratified clays, while acid sulfate waters cause kaolinite and even alunite to form. The former assemblage is commonly associated with typical low sulfidation epithermal gold mineralization as wallrock alteration, where gold-bearing veins comprise adularia and illite. Contrastingly, kaolinite is rare, and alunite absent, from a direct spatial and genetic association with gold mineralization in this environment (Hedenquist, 1991). This implies that mixing of deep, neutral pH chloride fluid with surficial acid sulfate waters does not commonly lead to ore-grade gold deposition. Mixing with (and cooling by) CO_2-rich, steam-heated waters leads to clay stability, accounting for the large halo of clay alteration and low-grade metal anomalies surrounding the vein. In contrast, mixing with surficial acid sulfate waters is unlikely to cause precious metal mineralization because the chloride fluids have already lost the majority of their gold through deeper boiling and dilution (Hedenquist, 1991).

In this section, several alteration minerals common to Kencana are discussed relative

Table 5.1 Summary of alteration facies

Alteration facies	Description	Distribution	Associated facies	Interpretation
ARGILLIC 1 (SCG) FACIES	- Dominated by smectite (montmorillonite) and calcite, minor gypsum - Pale to mid-grey, soft to indurated rocks - Weak to moderately pervasive alteration - Primary volcanic textures generally preserved Best developed in coherent andesite lavas and clasts of andesite autobreccias	- Prevalent at shallow levels - Occurs predominantly above 4900mRL - SCG alteration below 4900mRL occurs distal to epithermal mineralization	- Overprinted by all other alteration facies, particularly KH alteraion - Transitional to ISP alteration with inceasing depth (hanginwall)	**Distal, low temperature (80-200°C), near-neutral to weakly acidic fluids**
ARGILLIC 2 (ISP) FACIES	- Dominated by illite, smectite, pyrite, chlorite and minor carbonate - Soft, pale grey to pale green rocks - Pervasive alteration - Some feldspar replacement) or selvedge alteration in hematite-dusted andesite autobreccias - Destructive of primary volcanic texture - Inter-layered illite-smectite fills interstitial sites in the groundmass; significant in the matrix cement and clasts of volcanic breccias. - Clay composition change from smectite-rich through layered illite-smectite to illite-rich towards the vein. - Most common Kencana alteration facies Best developed in coherent andesite lavas	- Vertically and laterally widespread across the Kencana system	Often transitional to the IC alteration facies with proximity to the Kencana vein. Overprints regional propylitic (EC alteration)	**Distal, low temperature (80-200°C), near-neutral to weakly acidic fluids to proximal, higher temperature (220-310°C) fluids; high water-rock ratios**
ARGILLIC 3 (IC) FACIES	- Dominated by illite, pyrite and intermediate composition chlorite, with minor quartz and adularia. - Grey, mid to pale green or white rocks; oft and friable to indurated (lithology dependent) - Typically pervasive but can manifest as illite and/ or chlorite selective replacement of feldspars in andesite units, or as selvedge alteration around minor pyritic or hematitic veins proximal to the deposit in unaltered/ SCG/ ISP altered rocks. - Pyrite is typically disseminated (~1%) though sporadic veinlets (<0.5 cm) occur in the hanging-wall margins of the vein structure.	- Intensifies toward the deposit; often forms an envelope extending between 20-50 m surrounding QAS facies alteration - Best developed in the hanging-wall above the structure. - Common in breccia clasts within the Kencana vein. Affects all lithologies at Kencana with the exception of the basaltic unit.	Overprinted by QAS and CEP alteration facies.	**Low to high temperature (80-480°C), near-neutral to acidic fluids; high water-rock ratios**

Table 5.1 cont. Summary of alteration facies

Alteration facies	Description	Distribution	Associated facies	Interpretation
PHYLLIC (QAS) FACIES	- Pyrite is disseminated and abundance increases with proximity to the deposit - Fine-grained adularia selectively replaces feldspar phenocrysts in both andesite and volcaniclastic units, and pervasively alters the groundmass of andesite lavas. - Dominated by quartz, adularia, sericite and pyrite - Rocks are very hard, primary volcanic texture typically preservewd here not obscured by earlier alteration - Silicification is pervasive, best developed in coherent andesite lavas	- Fills shear zones above the K1vein - Close proximity to the Kencana vein, forming an envelope extending approxi-mately 10 m from the deposit and following the approximate geometry and dip of the vein.	- Marginal to IC facies alteration - Occurs with prehnite facies and EC alteration in shear zones	**Proximal alteration; mid to high temperature (60-480°C), near-neutral fluids.** **Adularia may be an indicator for boiling**
PROPYLITIC 1 (EC) FACIES	- Dominated by epidote ± chlorite ± pyrite ± adularia with minor quartz and calcite. - Pale to dark green - Affects the non-permeable coherent lithologies at Kencana - Pervasive alteration of groundmass, or, with proximity to the deposit, fills fractures with calcite and quartz - CLASTIC UNITS: EC alteration is disseminated and typically manifests as selective replacement of feldspar phenocrysts.	- Forms a wide regional footprint around the Kencana deposit - Dominant facies below 5000mRL, and increases in abundance and intensity toward the vein - Fracture controlled epidote increases in abundance towards the Kencana vein and always occurs in the coherent lithologies beneath the host structure (particularly the basaltic unit)	- Often transitional to the IC alteration facies - Overprints argillic facies - Overprinted by QAS, ISP and CEP facies	**Distal to proximal, high temperature fluids (200-420°C, epithermal-mesothermal transition); near-neutral fluids;**
PROPYLITIC 2 (CEP) FACIES	- Dominated by epidote ± calcite ± pyrite with minor quartz - Mid to dark green, indurated rocks - Fractures filled with epidote ± crystalline calcite ± quartz and a pervasively epidote-calcite altered ground-mass	- In the footwall fo the K1 vein (depth unconstrained) - Between 5050-5000mRL in shear zones - Most intense in basaltic units	- Overprints EC and argillicalteration facies - Overprinted by QAS alteration	**Proximal, high temperature fluids (200-420°C, epithermal-mesothermal transition); near-neutral fluids;**
SUB-PROPYLITIC (P) FACIES	- Prehnite ± gypsum with minor chlorite - Pale grey to green	- In hangingwall shear zones, particularly north of 19850mN	- Overprints puggy ISP and SCG clays - Occurs in association with earlier CEP alteration	**Hydrothermal fluids depositing prehnite have aCO_2 <0.01 moles. High temperature fluid (240-410°C)**
CALC-POTASSIC (BM) FACIES	- Dominated by biotite ± magnetite ± actinolite with minor albite - Pervasive, fine grained, black to dark green, indurated rocks (basaltic andesite and coherent andesites) - Fractures filled with magnetite (3 mm)	- Upflow zone - Proximal to the K1 vein (typically <3 m, but up to 15 m), predominantly in the footwall (from 230 m) - Lateral distribution to the south of Kencana unconstrained	- Overprints argillic and propylitic facies - Overprinted by QAS facies alteration	**Mid to high temperature (140-430°C), magmatic fluid, accompanying porphyry-style mineralization**
ADVANCED ARGILLIC (KH) FACIES	- Kaolinite OR halloysite with pyrite and minor illite and opal (PIMA detection) - Strongly pervasive; soft, friable rocks bleached white - Strongly oxdised near surface - Primary volcanic texture not preserved	- Halloysite alteration <10 m from current surface - Kaolinite alteration in hangingwall shear zones (especially the vein outflow zone)	- Overprints all facies except QAS alteration	**- Near surface: supergene weathering** **- Outflow zone: Acid waters after boiling** **- Low to mid temperature fluids (80-310°C)**

Table 5.1 cont. Summary of alteration facies

Alteration facies	Description	Distribution	Associated facies	Interpretation
INTERMEDIATE-ADVANCED ARGILLIC (IDP) FACIES	- Illite ± dickite ± pyrophyllite or kaolinite - Samples containing pyrophyllite do not contain illite and vice versa. - Pale grey to white (kaolinite samples), very friable rocks, strongly weathered - Destructive of primary texture - Volumetrically minor	- Hangingwall shear zones (4950mRL)		**Low to mid temperature (60-360°C), late-stage acid fluids**

to their occurrence and the physio-chemical conditions that they formed under.

Illite and smectite: Illite alteration is common throughout the various argillic assemblages at Kencana both proximal and distal to ore, and reflects high water-rock ratios (Thompson and Thompson, 1998). Illite is gradational to interlayered illite-smectite and smectite with distance from the vein, though a zone of illite alteration roughly parallel to vein dip is present across the deposit at approximately 5050mRL (Fig. 5.20). Illite alteration is variable from 30-95% volume of the protolith, with most intensely altered samples occurring proximal to ore. Illite (and smectite) variably replace plagioclase phenocrysts, adularia and minor albite, as well as flooding the groundmass of coherent andesites. Illite is very common in the epithermal environment, and forms due to the reaction of host rocks with weakly acidic to near neutral fluids at temperatures of 220-310ºC (Wurst, 2004). Smectite reflects fluids of a similar acidity but lower temperature (<200ºC).

Sericite: Sericite is a highly ordered form of illite, produced by the interaction of host rocks with a near neutral fluid at temperatures greater than 200ºC (Henley and Ellis, 1983; Corbett and Leach, 1998; Wurst, 2004). The presence of adularia with sericite in the QAS facies may be an indicator for boiling (Browne, 1978; Hedenquist, 1990; Dong and Morrison, 1995; Wurst, 2004).

Kaolinite and halloysite: Kaolinite and halloysite at Kencana predominantly occur in shear zones above the vein and in the top 5 m of stratigraphy (Figs. 5.14-5.22). Kaolinite

is formed during the interaction of host rocks with an acidic fluid at temperatures <200ºC. The presence of pyrite (altered to orange iron oxyhydroxides in the near-surface profile) together with kaolinite suggests a supergene origin (Simpson and Mauk, 2011). Halloysite is formed in response to the weathering and hydration of clays in the supergene environment (Corbett and Leach, 1998), although halloysite has been known to form under low temperature hydrothermal conditions (Jansen, 2011). The blanket-like morphology of halloysite and kaolinite alteration paralleling the ground surface and overprinting previous alteration also suggests that the alteration is supergene in origin.

Pyrite: Pyrite is the most common sulfide mineral in the alteration halo at Kencana (minor chalcopyrite is sometimes found). Pyrite occurs in almost every rock from weakly to intensely altered, and in the weathered surface profile containing kaolinite or halloysite, where it has been altered to orange iron oxyhydroxides. Pyrite occurs as fine grained, anhedral to euhedral cubic grains disseminated through the groundmass, or occasionally as veinlets (2 mm wide) in association with the IC alteration facies.

Chlorite: Chlorite alteration is widespread and occurs in several alteration facies at Kencana. Chlorite alteration principally affects the groundmass of altered rocks, though amphibole and less commonly, plagioclase phenocrysts are replaced. Chlorite also occurs with clays as selvedge alteration along minor fractures within coherent units. Chlorite chemistry displays a vertical zonation from Fe-rich through intermediate composition to Mg-rich with depth, with epithermal mineralization generally occurring within the zone of intermediate chlorite composition (as determined by PIMA and microprobe analysis (data in appendix); Figs. 5.14-5.22). Several factors, including temperature, pressure and $f0_2$, as well as bulk rock composition and the chemistry of co-existing silicate assemblages are responsible for the Fe:Mg ratio of chlorite (de Cariat et al., 1993). Chlorite is not a good indicator for fluid palaeotemperature, forming from fluids of ambient temperature to >300°C, but chlorite presence does infer a near-neutral fluid pH of 6-7 (Lawless et al., 1997).

Epidote: Epidote occurs either as a pervasive alteration of groundmass (with calcite), or, with proximity to the deposit, fills fractures with calcite±chlorite and quartz (as at Gosowong and Waitekauri goldfield, Gemmell, (2007); Simpson and Mauk, (2011)). The intensity of epidote alteration increases towards the vein, reflecting the higher fluid tempera-

ture closer to the main conduit for flow (K1 vein). Epidote forms in near-neutral conditions with temperatures >200°C, bordering the epithermal-mesothermal fields on Fig. 5.24.

5.7 Alteration whole rock geochemistry

This section describes the geochemical signature of the alteration facies at the Kencana deposit, including relative enrichments and depletions in mobile elements in the host rock package. The objective of this study was to determine the geochemical zonation surrounding the Kencana deposit, and thus potential vectors to mineralization elsewhere in the goldfield. Due to the blind nature of the deposits, this type of investigation can prove highly useful for exploration teams. 218 diamond drill core samples were selected from a representative suite of rocks including all the major lithofacies and alteration assemblages at Kencana along 3 cross sections (20000mN, 19900mN and 19600mN) and were assayed for various major and trace elements using X-ray fluorescence (XRF) and inductively coupled plasma mass spectrometry (ICP-MS) techniques. Data are presented in the appendix. Data are compared to least altered rocks from the Kencana deposit to allow determination of geochemical trends, and the geochemical zonation around the K1 vein.

5.7.1 Sampling and analytical techniques

Major and trace element concentrations of altered samples were determined by XRF and ICP-MS techniques at the School of Earth Sciences at the University of Tasmania (UTAS). Sample preparation was also undertaken at UTAS. A total of 218 samples from 3 cross sections were analyzed for major and trace elements. Samples were crushed using a steel jaw crusher to produce fragments <0.5 cm. Crushed samples were ground in a tungsten carbide mill to produce fine rock powder of <200 μm. The mill was cleaned with 1-2 passes of high purity quartz sand between each run of samples. Approximately 1 g of each sample was ignited, firstly at 500°C for 4 hours and subsequently at 1000°C overnight. Loss on ignition (LOI) was determined by weighing the sample before and after ignition. XRF analysis included major elements as oxides (SiO_2, Al_2O_3, CaO, Fe_2O_3, K_2O, MgO, MnO, Na_2O, Ti_2O, P_2O_5, and S) and selected trace elements (As, Ba, Cr, Cu, Ni, Pb, Rb, Sr, V, Y, Zn, and Zr) using pressed powder pills. Both suites of elements were determined using a Phillips

1480 automated XRF under the guidance of Phil Robinson.

An additional suite of trace elements, including Ag, Be, Bi, Cd, Cs, Ga, La, Mo, Nb, Pb, Sc, Sn, Ta, Te, Th, Tl and U, were analyzed using an Agilent 7700x ICP-MS under the guidance of Ian Little. A high pressure Pico-Trace digestion using HF/ H_2SO_4 followed by $HClO_4$ was used to dissolve the samples according to the methods described by Yu et al., (2001). The final solution was made in 2% nitric acid. In-house standards (TasBAS and TasGRAN) and two international reference rocks (AGV-1 and GSD-12) were used during analysis.

5.7.2 Previous work

Prior to this study, Gemmell (2007) conducted a geochemical study at the Gosowong deposit which determined a zonation for the alteration geochemistry as determined by XRF and ICP-MS analyses of altered volcanic rocks from diamond drill core samples from the Gosowong deposit (Fig. 5.25). Gemmell (2007) concluded elemental concentrations were variable depending on location:

(1) At surface, Hg, Au, Ag, Pb, Mo, Tl, As, K_2O, and Li were enriched and the alteration index (AI) had high values; CaO, MgO, Fe_2O_3, Sr, and Na_2O was depleted, and the chlorite-carbonate-pyrite index (CCPI) had low values.

(2) Proximal to the deposit, Au, Ag, K_2O, As, Cu and Pb were enriched, whereas Na_2O was depleted.

(3) In the alteration halo, K_2O, Mo, Tl, As and S was enriched, and the AI had high values; Na_2O and Sr were depleted and the CCPI had low values.

(4) Along the downward extension of the Gosowong fault zone, K_2O, Tl, Ba and Li were enriched and the S/ Na_2O ratio had high values (Gemmell, 2007).

5.8 Kencana major and trace element alteration geochemistry

Geochemical data were contoured along the cross sections with Surfer® software by natural neighbour method with an anisotropy ratio of 1, and 3 m grid spacing. Major and trace element zonation surrounding the K1 vein is displayed in Figs. 5.26-5.28.

Elemental concentrations at Kencana were also found to vary depending on location

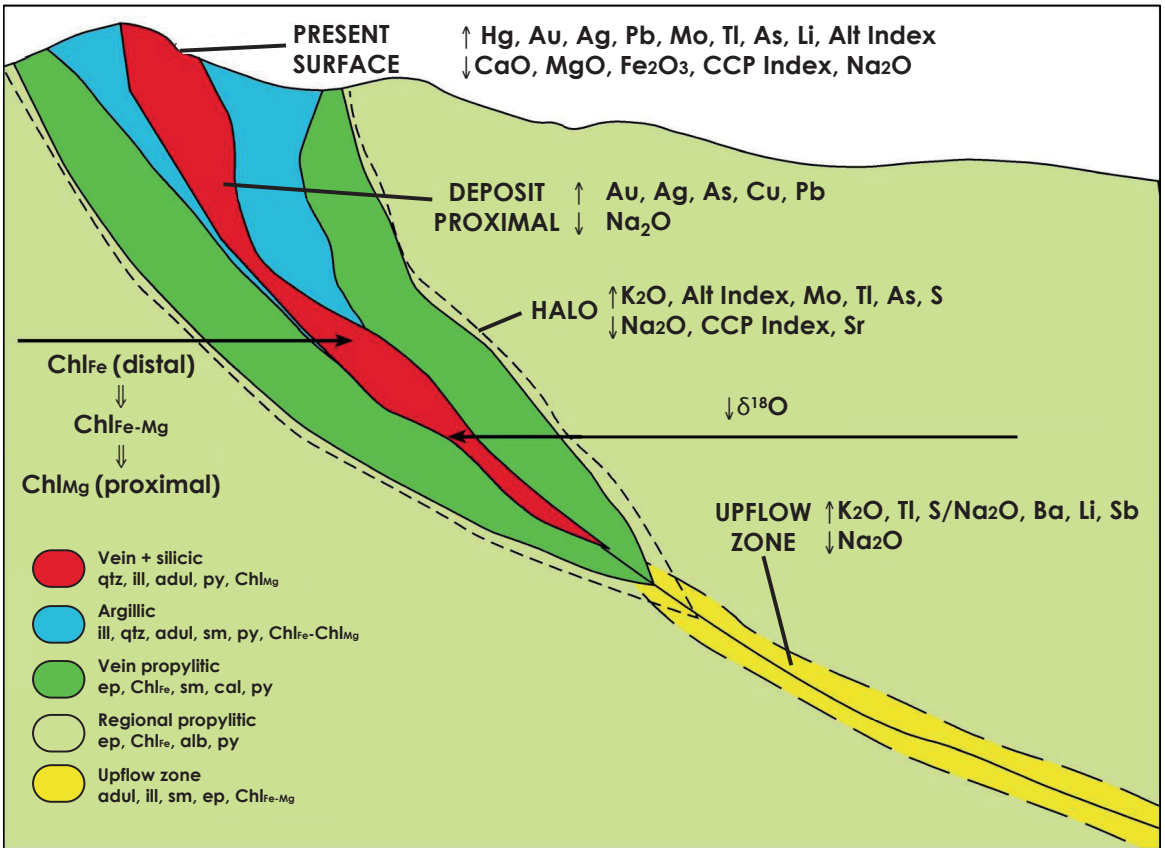

Fig. 5.25 Schematic representation of the mineralogical and geochemical zonation associated with the Gosowong vein deposit, including the alteration halo, downward extension of the fault zone, and at the surface. Small up and down arrows indicate an increase or decrease in respective element concentration or alteration index. Abbreviations: qtz = quartz, ill = illite, adul = adularia, alb = albite, cal = calcite, chlFe = iron-rich chlorite, chlMg- Fe = magnesium-iron–rich chlorite, chlch chlorite, ep = epidote, py = pyrite, sm = smectite; Alt Index = alteration index, CCPI = chlorite-carbonate-pyrite index. From Gemmell, 2007.

and relative position of the cross section through the deposit (section 19600mN is marginal to the system; sections 19900mN and 20000mN transect the centre of the system):

1) Within the vein, Ag, K_2O, Cu, Pb, and Rb have high values and V, Sr, Tl and Na_2O have low values in the centre of the system, and Mo, Sb, Tl, Li and Rb have high values along the margins of the deposit.

2) In the upflow zone, Ag, K_2O, Rb, Tl, MgO, Sb, Li and Mo have high values in the centre of the system. The element zonation along the deposit margins could not be determined in this study due to lack of drilling.

3) In the outflow zone (defined as the vein-parallel vertical extension of the vein, manifesting as shear zones and stockwork), As, Na_2O, Sr and Mn have high values in the centre of the system, and K_2O and Li have high values along the margins of the deposit

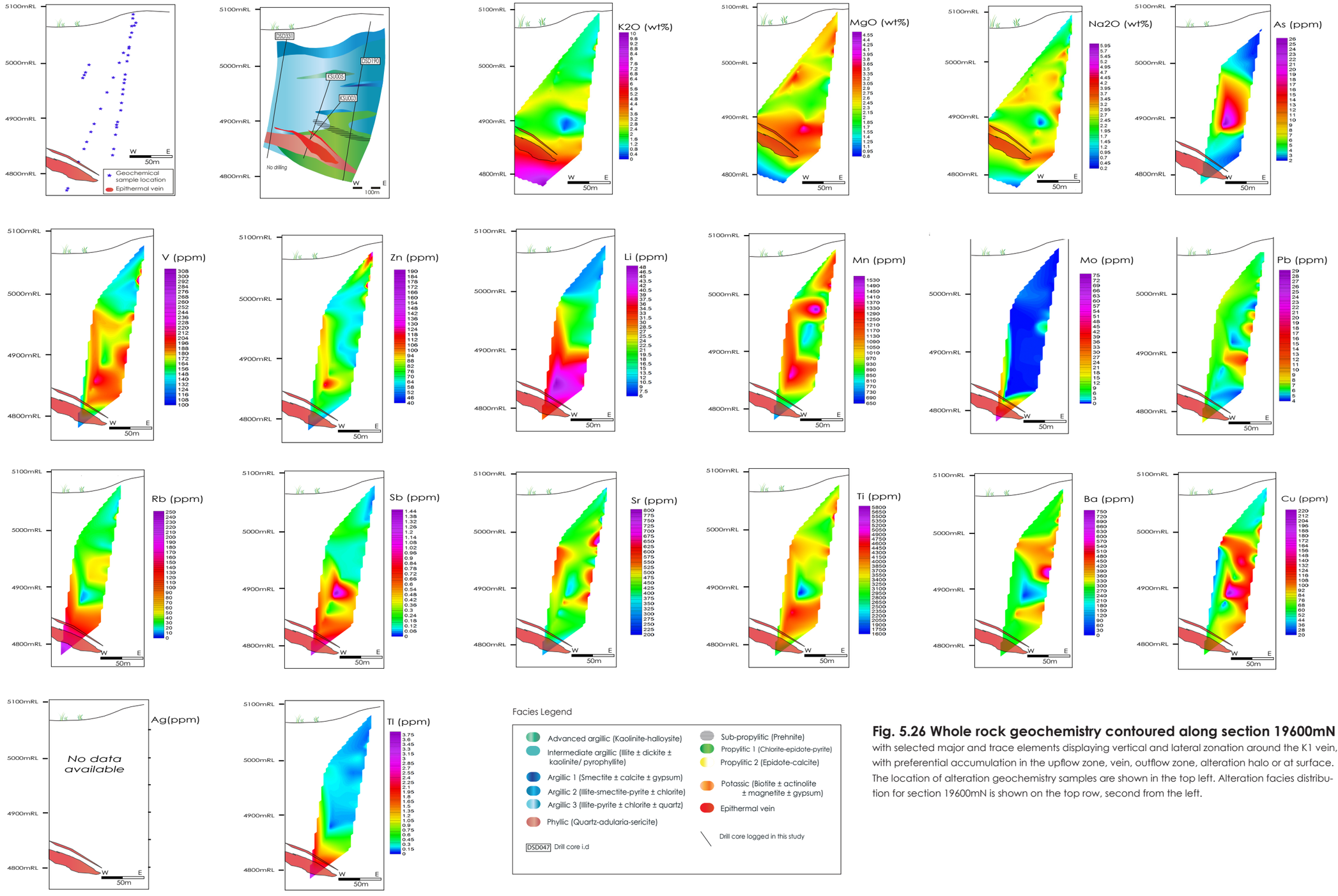

Fig. 5.26 Whole rock geochemistry contoured along section 19600mN with selected major and trace elements displaying vertical and lateral zonation around the K1 vein, with preferential accumulation in the upflow zone, vein, outflow zone, alteration halo or at surface. The location of alteration geochemistry samples are shown in the top left. Alteration facies distribution for section 19600mN is shown on the top row, second from the left.

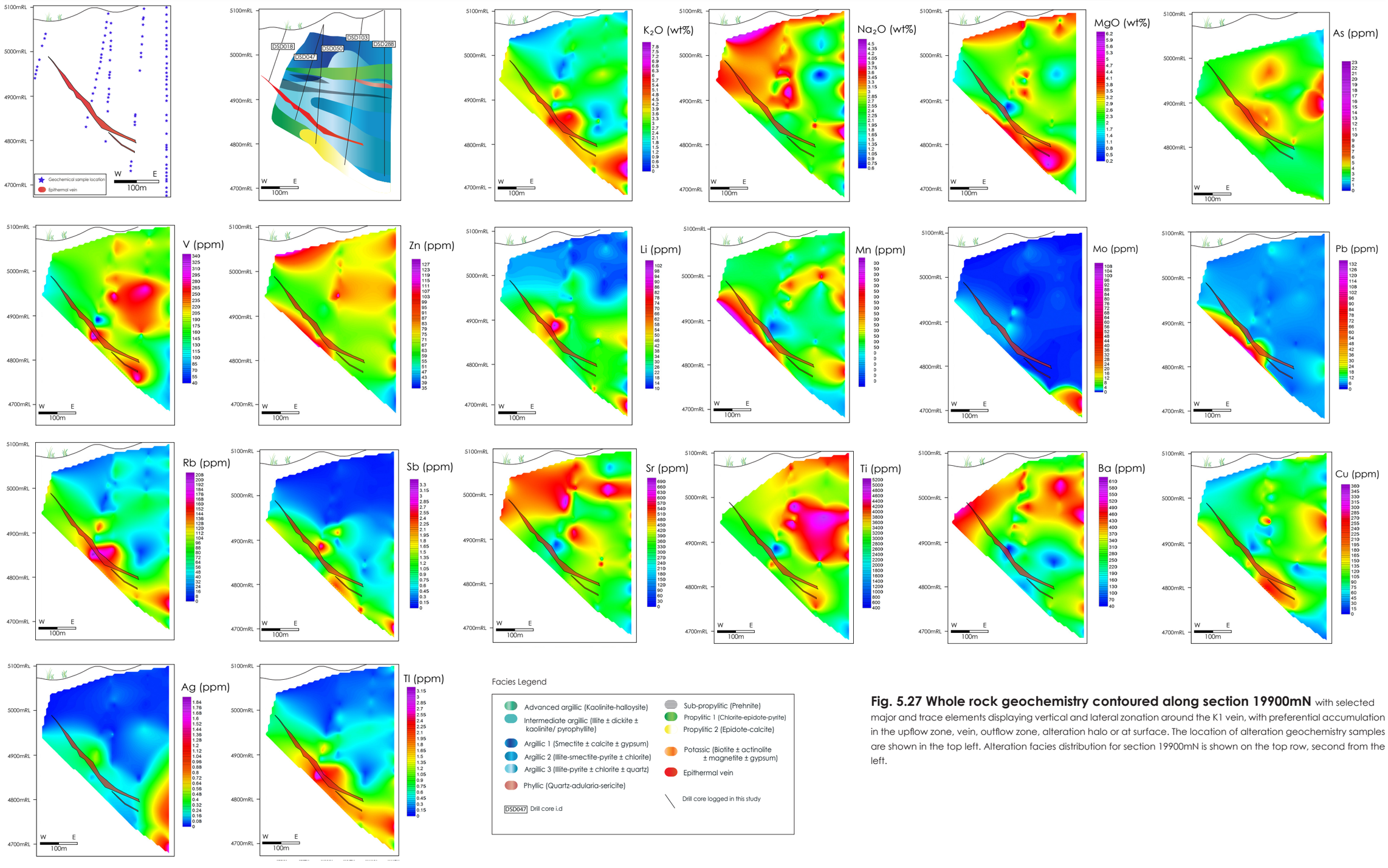

Fig. 5.27 Whole rock geochemistry contoured along section 19900mN with selected major and trace elements displaying vertical and lateral zonation around the K1 vein, with preferential accumulation in the upflow zone, vein, outflow zone, alteration halo or at surface. The location of alteration geochemistry samples are shown in the top left. Alteration facies distribution for section 19900mN is shown on the top row, second from the left.

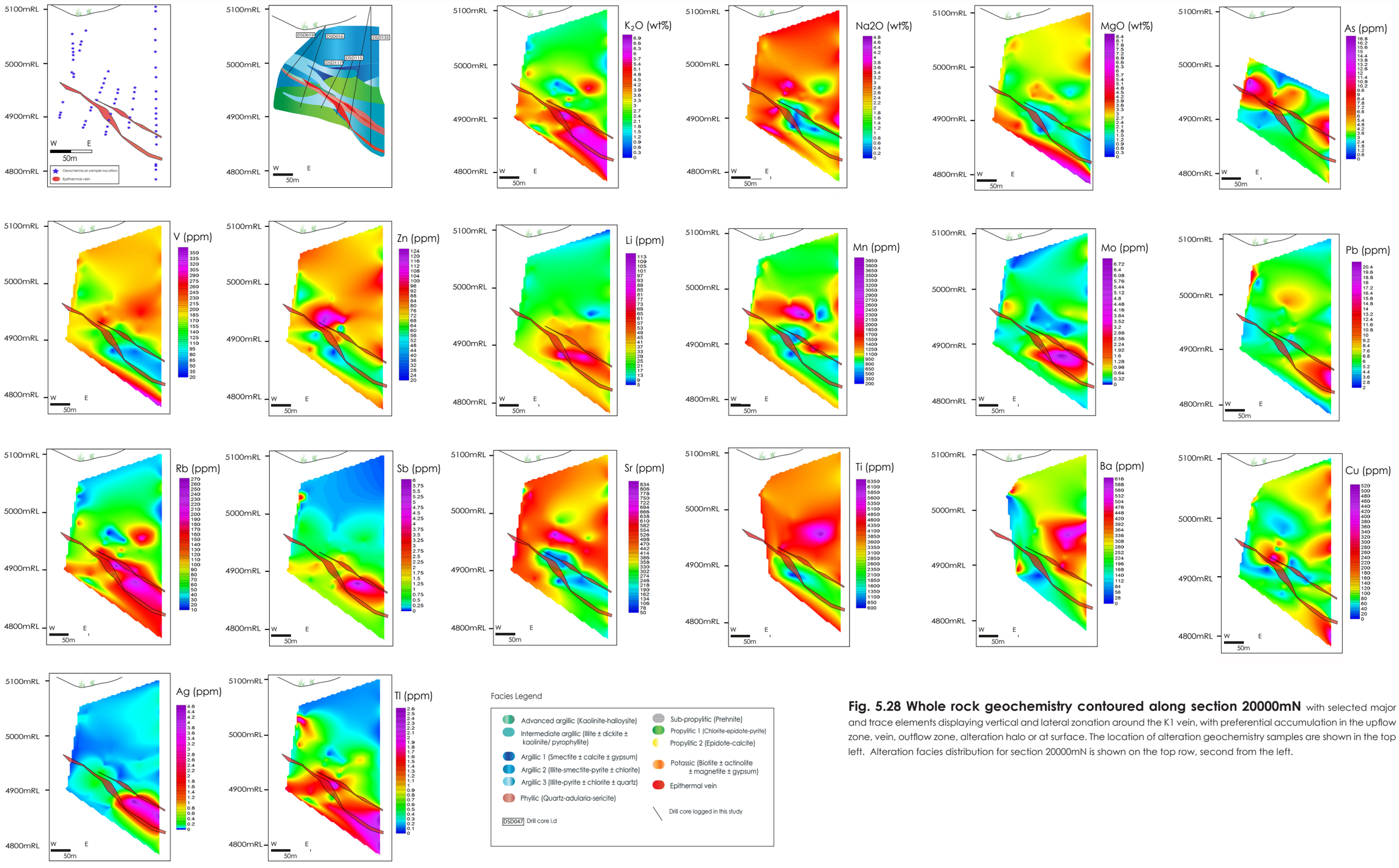

Fig. 5.28 Whole rock geochemistry contoured along section 20000mN with selected major and trace elements displaying vertical and lateral zonation around the K1 vein, with preferential accumulation in the upflow zone, vein, outflow zone, alteration halo or at surface. The location of alteration geochemistry samples are shown in the top left. Alteration facies distribution for section 20000mN is shown on the top row, second from the left.

4) In the alteration halo, Ba, Ti, V and Zn have high values and Rb, Sb and Tl have low values for the centre of the system, and As, Mn, Ti, Ba, Na_2O, Zn, Pb, Cu and Sr have high values for the margin of the deposit.

Major and trace element zonation is largely a function of the host rock lithology and permeability, variable alteration style and mineralization within the vein. Certain alteration facies display distinct geochemical signatures (Figs. 5.26-5.28). ISP and EC alteration are enriched in Zn V and MgO, with sporadic enrichment in Na_2O and Cu where adularia and chalcopyrite occur in these facies. EC alteration is also associated with enriched Sr and Ba. QAS facies alteration is enriched in K_2O, Na_2O, Li and Rb. Sub-propylitic (P facies) alteration along section 19600Mn appears enriched in As and Sb (Fig. 5.26), though this facies is not encountered along sections 19900mN and 20000mN, so this observation cannot be verifed.

Element zonation at Kencana is different to that for Gosowong; however, certain elements can still be used as pathfinders to ore for both systems. Ag, Pb, Cu and K_2O are enriched within the vein and proximally to the deposit. Li (and Rb) values at Kencana have a good correlation with K_2O values, reflecting the substitution of Li for K_2O in adularia. At Gosowong, Tl was found to substitute for K_2O in adularia and consequently can be used as a pathfinder element towards mineralization (Gemmell, 2007). At Kencana, Tl and K_2O show a good correlation in the vein (Figs. 5.26-5.28) but statistically show a poor correla-

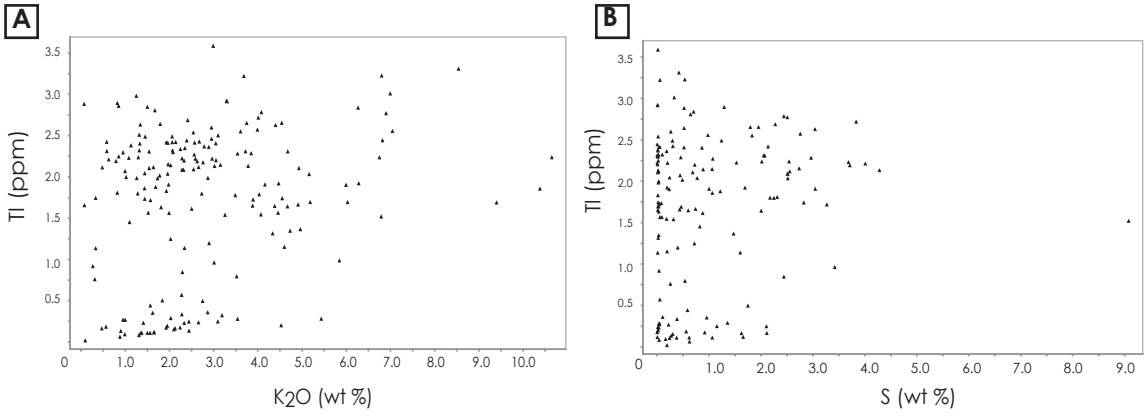

Fig. 5.29 A) Correlation between K2O (wt%) and Tl (ppm). Data scatter represents a Spearman correlation coefficient of 0.17. **B) Correlation between S (wt%) and Tl (ppm).** Data scatter represents a Spearman correlation coefficient of 0.091.

tion, suggesting that they are not contained within the same mineral (i.e adularia; Fig. 5.29). Tl also has no statistical correlation with sulfur, implying that Tl is not contained in sulfide minerals in the vein (Fig. 5.29).

Element associations and their relationship to alteration assemblages are discussed in section 5.9. Major and trace element variability can also be determined relative to calculated distance to vein, and relative to the alteration index and chlorite-carbonate-pyrite indices.

5.8.1 Alteration Index and Chlorite-Carbonate-Pyrite Index

The alteration index (AI), developed by Ishikawa et al., (1976), measures the intensity of alteration in felsic volcanic rocks on determination of $100(MgO + K_2O) / (MgO + K_2O + CaO + Na_2O)$. The index reflects the hydrothermal alteration of Na-plagioclase to sericite and/ or illite and chlorite (Large et al., 2001). Though originally developed for VHMS systems and felsic rocks, the index is equally applicable to epithermal systems (Gemmell, 2002) and intermediate to mafic volcanic settings (Gemmell and Large, 1992). AI values vary from 20 to 60 for unaltered rocks and between 50 and 100 for hydrothermally altered rocks, where AI=100 represents complete feldspar replacement by sericite and/or chlorite (Large et al., 2001). The chlorite-carbonate-pyrite index (CCPI), (defined as $100(MgO + FeO) /(MgO + FeO+ K_2O + Na_2O)$, measures the degree of (Fe, Mg)-chlorite, (Fe, Mg)-carbonate and/ or pyrite alteration (Large et al., 2001).

The alteration box plot, which combines the AI and CCPI was developed by Large et al., (2001), originally for use in VHMS systems. The box plot shows the whole-rock geochemistry of a sample in relationship to alteration mineralogy and the extent of metasomatism. Least altered volcanics plot toward the centre of the diagram, with increasingly altered samples plotting towards the end-member alteration mineral species that characterizes the alteration type (Gemmell, 2007). The alteration box plot has been shown to be applicable in several studies in the low sulfidation epithermal environment (e.g. Gosowong, Gemmell, 2002; Mt. Muro, Indonesia, Wurst, 2004).

The alteration box plot was used to determine the geochemical signature of alteration trends at Kencana. The alteration box plot for whole-rock alteration geochemical sam-

Fig. 5.30 Alteration box plot of the alteration index [AI = 100x(MgO + K_2O)/(MgO + K_2O + CaO + Na_2O)] vs. the chlorite-carbonate-pyrite index [CCPI = 100x(MgO + FeO)/(MgO + FeO + K_2O + Na_2O)] for the Kencana whole-rock geochemical data. Samples are plotted according to alteration style as determined by PIMA analysis. Data from the appendix. The boxes for unaltered andesite-basalt and dacite are from Large et al., (2001).

ples from Kencana is plotted in Fig. 5.30. Samples are plotted according to alteration style (propylitic, argillic, hematitic, least altered/ fresh samples). Three major alteration trends are identified: 1) argillic alteration generally plots along a trend from least altered rocks to the bottom right of the box plot towards the bottom right of the diagram (illite point); 2) chlorite-pyrite-(sericite) alteration and hematized samples plot along a trend from least altered rocks to the right of the diagram (chlorite-pyrite point to chlorite-pyrite + illite); and 3) propylitic alteration containing epidote plots along a trend from least altered rocks towards the top left of the diagram (epidote-calcite point). Some samples plot along different trends than those identified by PIMA analysis, due to the patchy nature of alteration and complex overprinting relationships in the Kencana host package. Samples recorded as propylitic altered were not divided into chlorite and epidote-bearing categories, though this distinction is easily inferred by observing the trends in Fig. 5.30. Silicic altered samples were not included in this study.

Alteration box plots are presented in Figs. 5.31-5.33, where selected elements are plotted in order to identify the geochemical signature of various alteration styles. By determining the geochemical trends of alteration styles, it is possible to delineate geochemical vectors towards mineralization, particularly in deposits with zoned alteration assemblages,

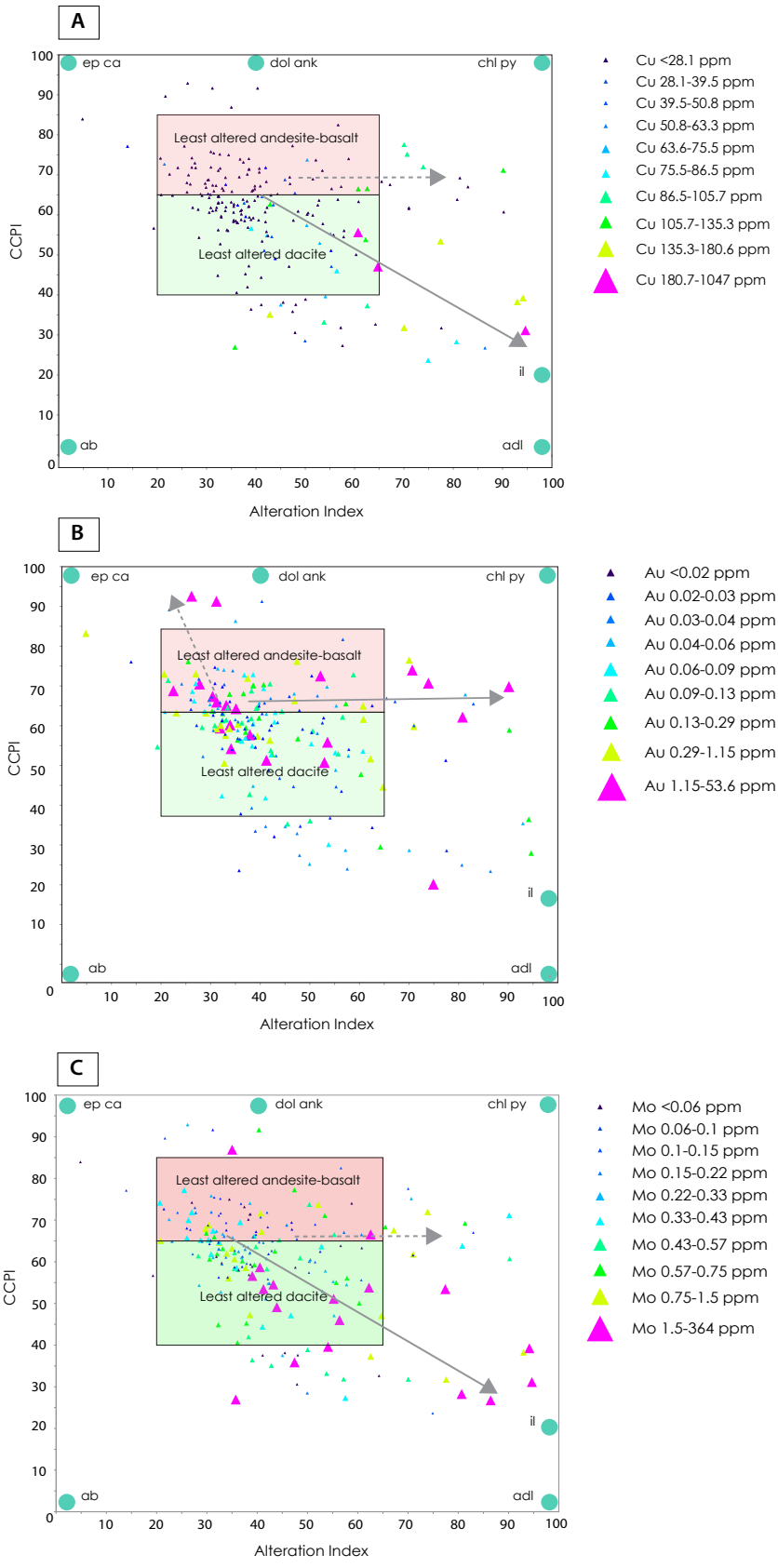

Fig 5.31 Alteration box plots with major and trace element alteration geochemistry

A) Alteration box plot highlighting copper values (ppm).

B) Alteration box plot highlighting gold values (ppm).

C) Alteration box plot highlighting molybdenum values (ppm).

Mineral abbreviations: Ab = albite; Ep = epidote; Ca = calcite; Dol = dolerite; Ank = ankerite; Chl = chlorite; Py = pyrite; Il = illite; adl = adularia

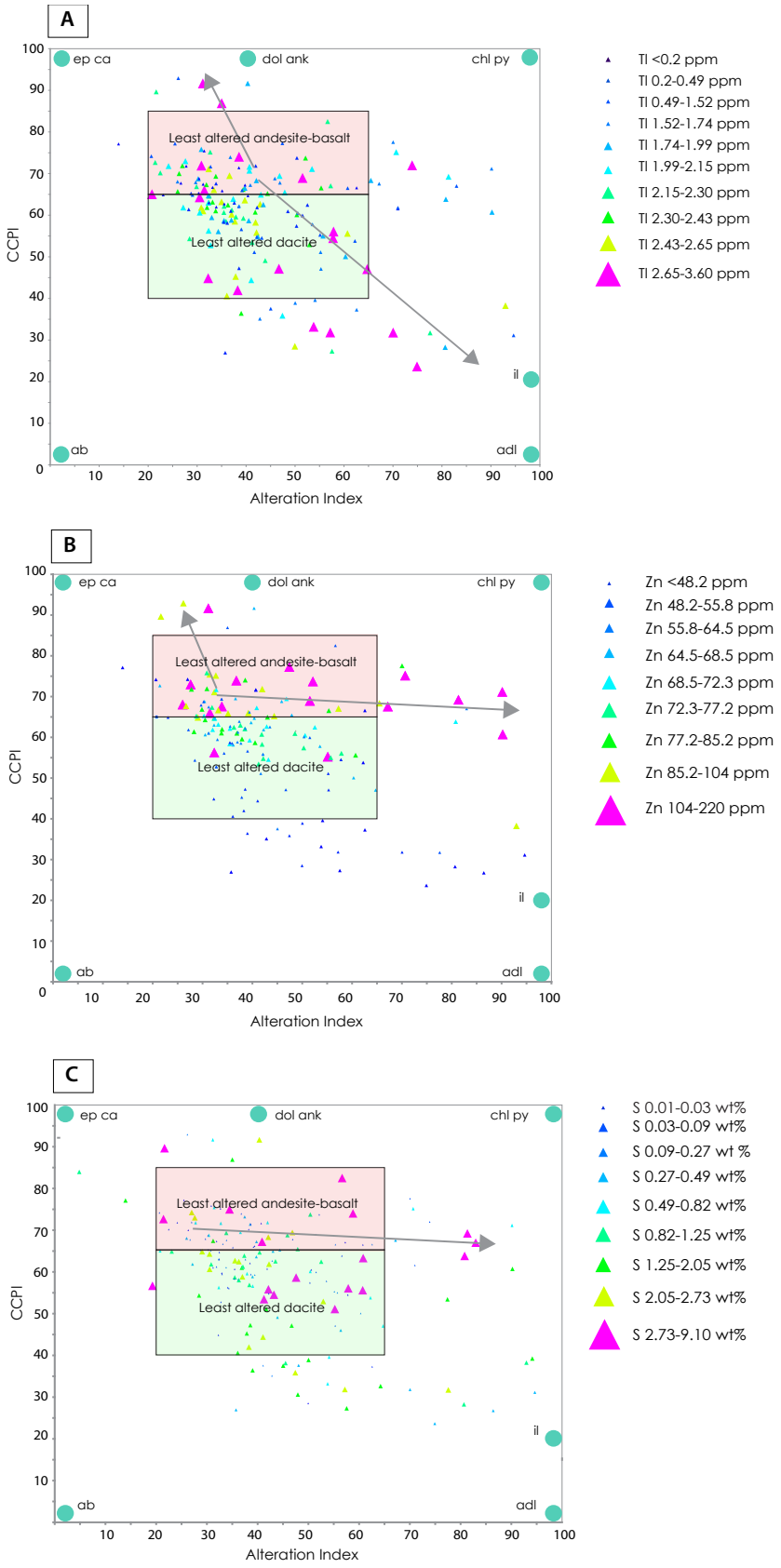

Fig 5.32 Alteration box plots with major and trace element alteration geochemistry

A) Alteration box plot highlighting thallium values (ppm).

B) Alteration box plot highlighting zinc values (ppm).

C) Alteration box plot highlighting sulfur values (wt %).

Mineral abbreviations: Ab = albite; Ep = epidote; Ca = calcite; Dol = dolerite; Ank = ankerite; Chl = chlorite; Py = pyrite; Il = illite; adl = adularia

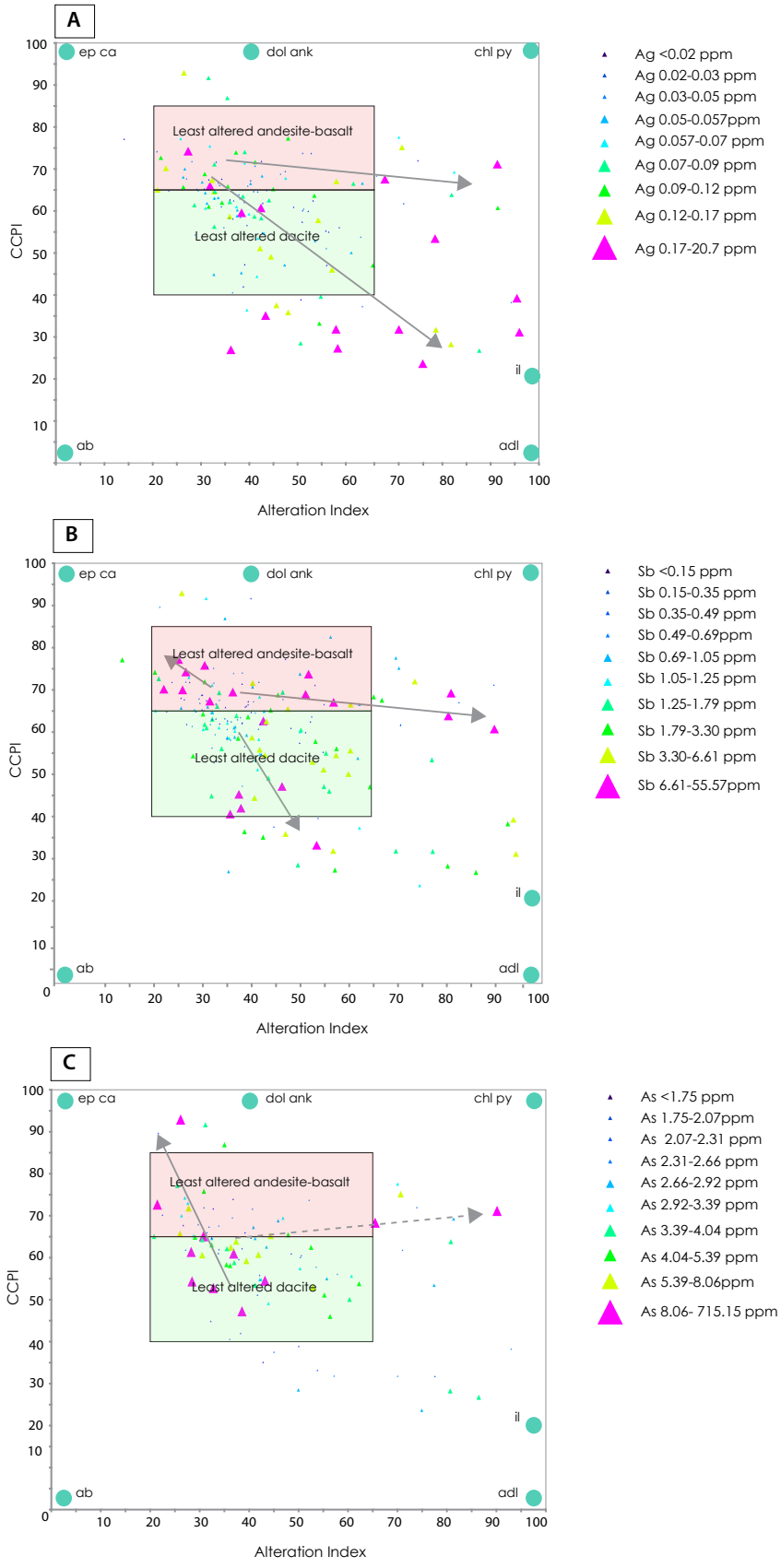

Fig 5.33 Alteration box plots with major and trace element alteration geochemistry

A) Alteration box plot highlighting silver values (ppm).

B) Alteration box plot highlighting antimony values (ppm).

C) Alteration box plot highlighting arsenic values (ppm).

Mineral abbreviations: Ab = albite; Ep = epidote; Ca = calcite; Dol = dolerite; Ank = ankerite; Chl = chlorite; Py = pyrite; Il = illite; adl = adularia

as at Kencana (Wurst, 2004). The distribution of high values highlights the trends that are significant for each element.

Copper values are lowest in unaltered rocks, and show a general increase towards illite alteration (Fig. 5.31 A). A weak positive trend is also present in chlorite-pyrite-(sericite) alteration. Propylitic alteration is not significant for copper mineralization.

Gold is enriched in rocks along the chlorite-pyrite (sericite) trend from the least to most intensely altered rocks exhibiting this alteration style (Fig. 5.31 B). The propylitic alteration trend is also significant for Au, from least to most intensely propylitic altered rocks. Argillic alteration is only weakly significant for Au mineralization.

Mo is strongly enriched along the argillic (illite) trend, and weakly enriched along the chlorite-pyrite-(sericite) trend (Fig. 5.31 C). Mo therefore shows a general association with Cu in terms of alteration assemblage associations, but not with Au.

The distribution of elevated Tl is scattered, however the argillic and propylitic trends are the most significant, from least to most intensely altered rocks (Fig. 5.32 A). At Gosowong, Th was found to substitute for K_2O in adularia (Gemmell, 2007), though this trend is not reflected in the alteration box plot or statistically in Fig. 5.29, though both K_2O and Tl are enriched within the vein (Figs. 5.26-5.28). However, samples containing the most abundant adularia at Kencana also contain abundant quartz veins and veinlets, and for this reason could not be included in the analytical study, which may skew the data away from the adularia alteration trend.

Zinc values are highest in the chlorite-pyrite-(sericite) trend and propylitic trend from least to most intensely altered rocks (Fig. 5.32 B). Zn is interpreted to substitute for Fe in chlorite, which is present in these alteration styles. The argillic alteration trend shows no elevated Zn values.

The distribution of high sulfur values is scattered, though S values are highest along the chlorite-pyrite-(sericite) trend, and to a lesser extent, the propylitic trend (Fig. 5.32 C). S values are high for weakly argillic altered rock, though values show a general decrease with more intense argillic alteration. S values reflect pyrite alteration, which occurs in almost all alteration facies at Kencana, as well as mineralization of sulfide species within the vein.

Ag values are low overall in whole rock samples, however, high values reflect the

argillic and chlorite-pyrite-(sericite) trends (Fig. 5.33 A). This highlights the differing distribution of Au and Ag values in the Kencana system (as described in Chapter 4).

Sb values are highest along the chlorite-pyrite-(sericite) and weakly altered propylitic trends (Fig. 5.33 B). Some high Sb values are also found in weakly argillic altered rocks, though values appear to decrease in both the propylitic and argillic trends with increasing alteration intensity. It is suggested that highest Sb values would be found in samples containing abundant quartz (not analysed), as Sb is enriched within the vein (most likely in tennantite-tetrahedrite series minerals) according to the element zonation in Figs. 5.27 and 5.28.

Like Sb, As values are highest in weakly altered rocks along the propylitic and chlorite-pyrite-(sericite) trends (Fig. 5.33 C). Weakly elevated values are also present in intensely argillic altered rocks. The As trend is also similar to the trends exhibited by Au, though As values are highest in the weakly altered equivalents. For this reason, As can be considered a good distal pathfinder for Au mineralization.

Overall, Cu, Mo, Tl and Ag show an affinity for argillic alteration, an alteration style which is not reflected in high Au values, which are preferentially elevated in the chlorite-pyrite-(sericite) and propylitic trends. Trends displayed in Fig. 5.31-5.33 suggest that As is the best distal pathfinder for Au mineralization with respect to the AI and CCPI, given that As values are enriched in the weakly altered equivalents of intensely altered rocks containing high Au values.

5.8.2 Mass change calculations

The mass changes (i.e. gain or loss) of elements due to hydrothermal alteration were quantified using the modification of Gresens' general metasomatic equation (Gresens, 1967) described by Mauk and Simpson (2007). The mass gain or loss of an element (ΔX) can be determined using the equation: $\Delta X = [(XA^i/XB^i) \times XB] - XA$

where XA^i/XB^i = the ratio of an immobile element in fresh and altered rock; XA = concentration of an element in fresh rock and XB = concentration of an element in altered rock (Mauk and Simpson, 2007).

A fundamental requirement when making these calculations is that the original composition of the altered rock is identical to that of the unaltered equivalent; otherwise the

mass gain or loss of an element will be a hybrid of hydrothermal alteration and variations in the rock's original composition (Gresens, 1967; Mauk and Simpson, 2007). At Kencana, least altered rocks were used for comparison as there were no unaltered equivalents in the area (as at Golden Cross; Mauk and Simpson, 2007).

Mass change calculations were performed for andesitic units, based on the average of two least altered samples (DSD016_77.0 and DSD103_98.6). Mass change calculations were not performed on basalts due to the lack of least altered samples, and volcaniclastic units were discounted from the study due to the uncertainty in the protolith of the sediments. Zirconium is considered immobile in all calculations. Calculated mass changes are presented as grams per 100 cubic centimetres (g/100 cm^3) for the major elements and grams per cubic metre (g/m^3) for the trace elements.

5.9 Discussion of alteration geochemistry

The gain of K and loss of Ca and Na account for much of the mass transferred in shallow hydrothermal systems (Giggenbach, 1984; Simpson and Mauk, 2011). K-metasomatism can be represented by molar (*m)* K/(2Ca+Na+K). Increasing *m*K/(2Ca+Na+K) in altered rocks indicates Ca and/ or Na loss relative to K (Warren et al., 2007; Booden et al., 2011), where a rock that has lost all Ca and Na has an *m*K/(2Ca+Na+K) value of 1 (Simpson and Mauk, 2011).

The process of K-metasomatism is also represented in Fig. 5.34, which plots *m*K/Al against *m*(2Ca+Na+K)/Al. Phases that contain no K, Ca, Na, and Al plot at the origin but their occurrence does not affect where samples are located in this compositional space (e.g. The amount of pyrite has no affect on where the data will plot). The line extending from 1.0 to 1.1 (plagioclase-adularia line) represents the range of feldspar compositions and mixtures with biotite. Fresh felsic rocks plot on or near this line as determined by their K/Al molar ratio, and unaltered rocks plot to the right of the line. The green box represents unaltered andesite compositions from the Taupo Volcanic Zone, NZ (Warren et al., 2007). The *m*K/Al value decreases with increasing amounts of interlayered illite-smectite, and samples with *m*K/Al <0.2 to 0.33 that contain smectite will plot away from the line of slope 1 in proportion to the amount of Ca and Na contained in smectite. Samples with *m*K/Al values <0.2

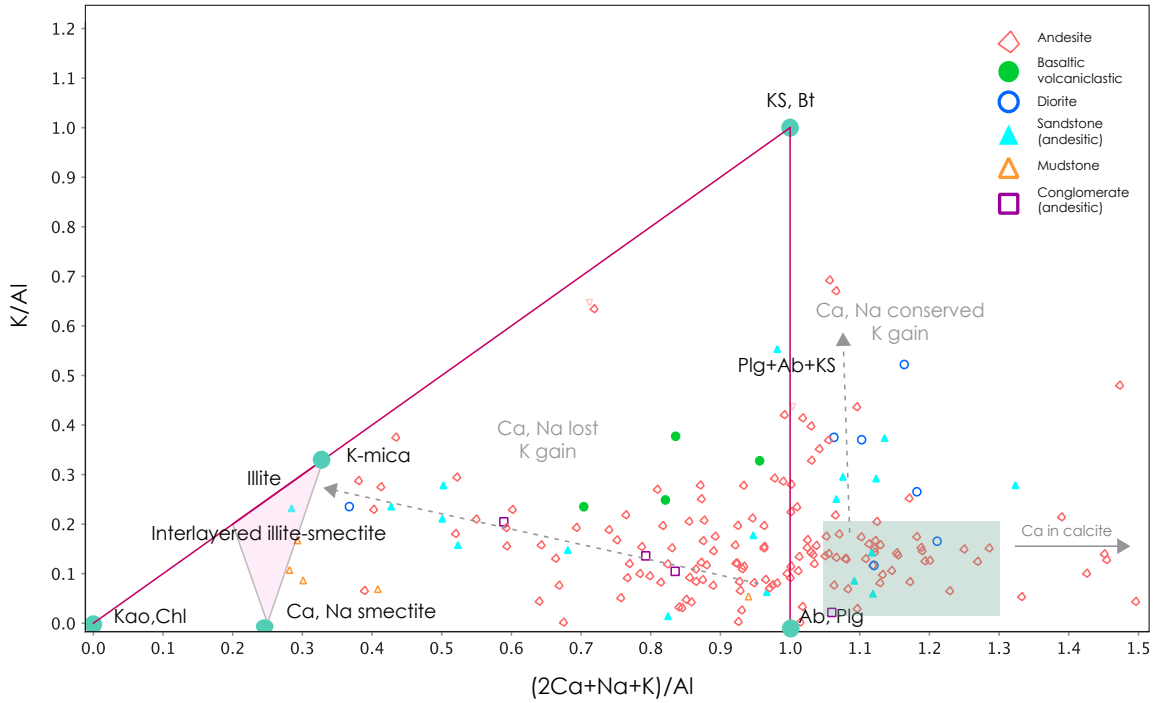

Fig. 5.34 Molar element ratio plot of (2Ca+Na+K)/Al vs. K/Al for rocks hosting the K1 vein.
Mass transfer processes are shown by grey dashed arrows. Alteration minerals are plotted at their respective compositions. The green box represents typical fresh rocks from the Taupo volcanic zone, New Zealand (Warren et al., 2007). Mineral abbreviations: Kao = kaolinite; Chl = chlorite; Plg = plagioclase; Ab = albite; KS = potassium feldspar; Bt = biotite.

to 0.33 that plot along the line of slope 1 likely contain kaolinite and/or Al-bearing chlorite (Warren et al., 2007). The proportion of Al contained in chlorite, rather than the Fe or Mg content, determines the degree to which its presence causes data points to shift toward the origin.

If Al is assumed to be immobile, rocks affected by K-metasomatism plot above and to the left of fresh rock compositions, with *m*K/Al values equal to or greater than the starting composition, reflecting K addition accompanied by loss of Ca and Na, represented by the equations:

(1) $NaAlSi_3O_8 + K^+ \rightarrow KAlSi_3O_8 + Na^+$

albite K-feldspar

(2) $Na_2CaAl_4Si_8O_{24} + 2H^+ + 2K^+ \rightarrow KAlSi_3O_8 + KAl_3Si_3O_{10}(OH)_2 + 2SiO_2 + 2Na^+ + Ca^{2+}$

plagioclase K-feldspar K-mica quartz

Conversion of K-feldspar to K-mica or illite, interlayered illite-smectite, and smectite lowers molar K/Al values of the rock, but this does not necessarily mean lesser effects of

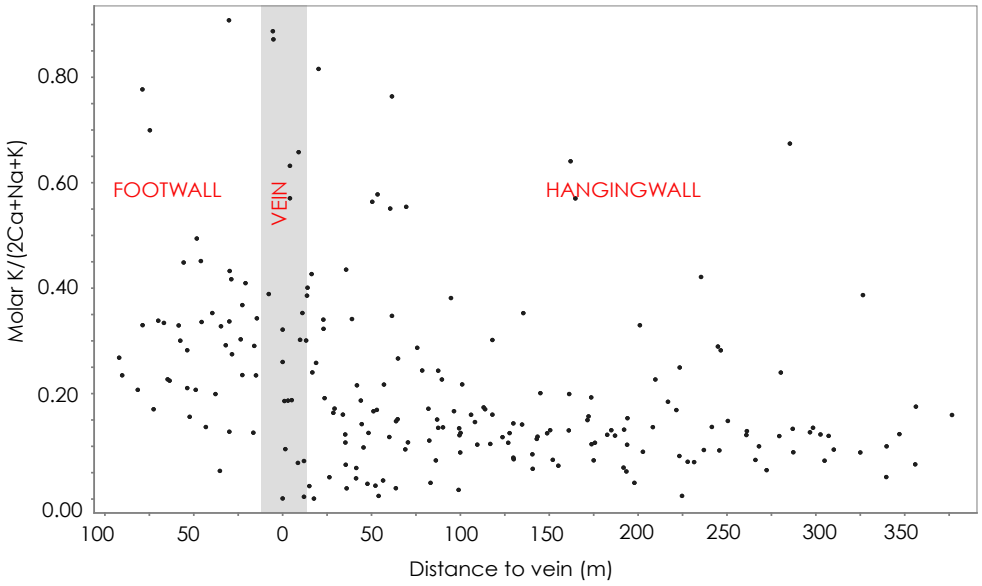

Fig. 5.35 K-metasomatism plotted relative to distance to the K1 vein, showing a general increase from background *m*K/(2Ca+Na+K) values of approximately 0.18 to 0.8 within 50 m of the vein. Values are highest within the vein itself, reflecting the greatest abundance of K-feldspar (adularia). High values above the vein reflect the position of shear zones with increased K-feldspar occurrence. Grey box represents average vein thickness of 10 m.

These trends are reflected in Fig. 5.34, where samples from Kencana are plotted according to lithology. Two major trends can be identified in the data, with andesites, sandstone and conglomerates undergoing Ca and Na loss with K gain, reflecting the alteration of plagioclase to illite and smectite. Mudstones follow a similar trend at lower K values, and basaltic andesites show higher K gain. Diorites show a trend of conserved Ca and Na with K gain, reflecting alteration of plagioclase to K-feldspar (adularia). Several andesite samples plot to the right of the unaltered box, reflecting Ca addition in calcite, as Na addition in the epithermal environment is known to contribute only minor Na to the rock (Giggenbach, 1984; Warren et al., 2007). Little conversion of K-feldspar to K-mica or illite occurs in altered samples from Kencana according to Fig. 5.29.

K-metasomatism is known to increase with proximity to the vein (Fig. 5.35). Selected pathfinder elements are also plotted relative to *m*K/(2Ca+Na+K) values to determine the geochemical signature accompanying K-metasomatism (Fig. 5.36). High As and Sb relative to *m*K/(2Ca+Na+K) values can be used as distal pathfinders to ore mineralization, as these elements are enriched at low *m*K/(2Ca+Na+K) values, where precious metals (e.g. Au) are

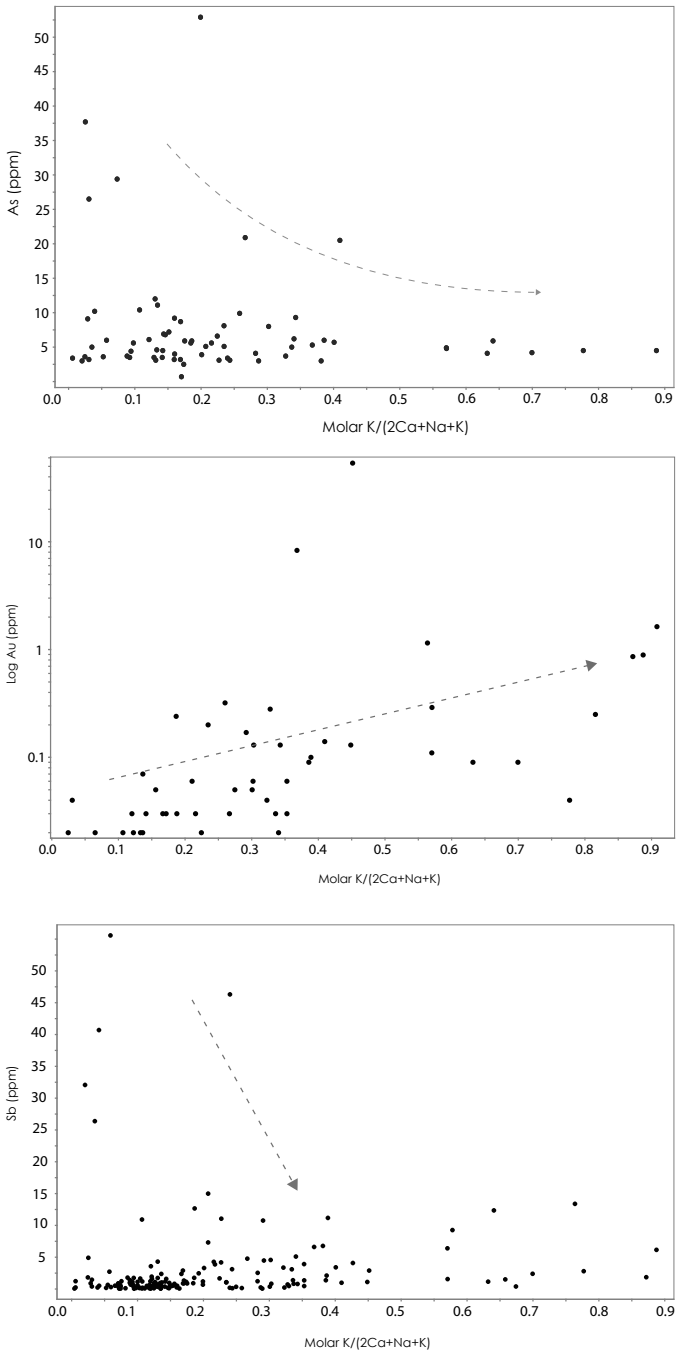

Fig. 5.36 Molar K/(2Ca+Na+K) values plotted against Au and pathfinder elements

A) Arsenic grades decrease with increasing levels of K-metasomatism in the host rock package, to a background of approx. 5 ppm at maximum *m*K/(2Ca+Na+K) values. Geochemical zonation in section 5.8 suggested As values are highest in the regional halo and within the vein. Highest *m*K/(2Ca+Na+K) values are calculated in host rock samples and therefore it can be assumed that maximum As values may not be represented here. Similarly, maximum K_2O values are not represented here, as adularia is most abundant within the vein.

B) Log gold grades show a general increase with increasing levels of K-metasomatism in the host rock package, from a background level of <0.1 ppm to 1 ppm with maximum *m*K/(2Ca+Na+K) values. Highest Au grades are associated with medium *m*K/(2Ca+Na+K) values, which is a factor of sampling (real highest Au grades are associated with quartz and adularia mineralization, and thus could not be included in this study).

C) Antimony grades show a sharp decrease with increasing *m*K/(2Ca+Na+K) values from >40 ppm to a background level of approx. 10 ppm at *m*K/(2Ca+Na+K) = 0.4. The relationship of Sb to *m*K/(2Ca+Na+K) values is similar to that of As.

enriched at higher *m*K/(2Ca+Na+K) values (Fig. 5.36).

The next section describes the enrichment and depletion patterns for selected elements. Mass losses and gains relative to major and trace elements for propylitic altered andesite samples are displayed in Fig. 5.37. Overall, the magnitude of mass changes is greater with proximity to the vein (Fig. 5.37). Mass gains range from ~5-10 g/100 cm^3 to >500 g/100 cm^3 for major elements, and from ~300 to >600 g/m^3 for trace elements with proxim-

ity to the vein. Mass losses are greatest in the hangingwall between 150-300 m from the vein. Though samples were identified as propylitic in hand specimen, the complex overprinting nature of alteration facies at Kencana means that various trends can be identified in the data and attributed to alteration facies other than EC and CEP (propylitic) facies.

Potassium and rubidium: Potassium shows a moderate gain in altered rocks, though the pattern of enrichment is variable with distance from the vein. In general, the greatest K enrichment is in the hangingwall within 50 m of the vein, corresponding to an increase in abundance of K-feldspar in this area, and correlating with the presence of QAS facies alteration in which adularia is most abundant. K gains are also apparent in andesites hosting shear zones above the vein. K loss is overall a minor process (typically of the order of 2-3 g/100 cm^3), but does occur distally from the vein in the hangingwall, where adularia is less abundant and shows alteration to illite, a reaction that results in the loss of K. Rubidium mimics the enrichment pattern of K, reflecting the substitution of Rb for K in adularia and illite (Mauk and Simpson, 2007). Overall, K and Rb gains are higher in the in the centre of the system along cross sections 19900mN and 20000mN than along 19600mN, which is on the fringes of the system.

Sodium: Na displays minor gain due to formation of albite and paragonite. In the hangingwall from 150-300 m from the vein, Na is lost due to replacement of plagioclase by hydrothermal minerals, in particular K-feldspar and clays (Fig. 5.37).

Strontium and barium: Strontium is variably enriched and depleted, though overall Sr follows a similar pattern to K (and Rb). Some strong Sr gains in the hangingwall distally to the vein in the shallow parts of the stratigraphy reflect calcite alteration as part of the distal argillic and propylitic facies (SCG and EC facies; e.g. a gain of ~1500 g/m^3 between 300 and 370 m; Fig. 5.37), as well as the occasional presence of crystalline calcite in surficial KH facies alteration. Sr also shows strong gains below the vein, corresponding to K gains and formation of calcite as part of the CEP alteration facies. Strontium mass transfer shows no particular differentiation between the central and marginal sections of the system. Barium is also variably enriched and depleted through the system, but gains are reflected in carbonate alteration (calcite mineralization) and K-metasomatism. Barium shows overall distal mass

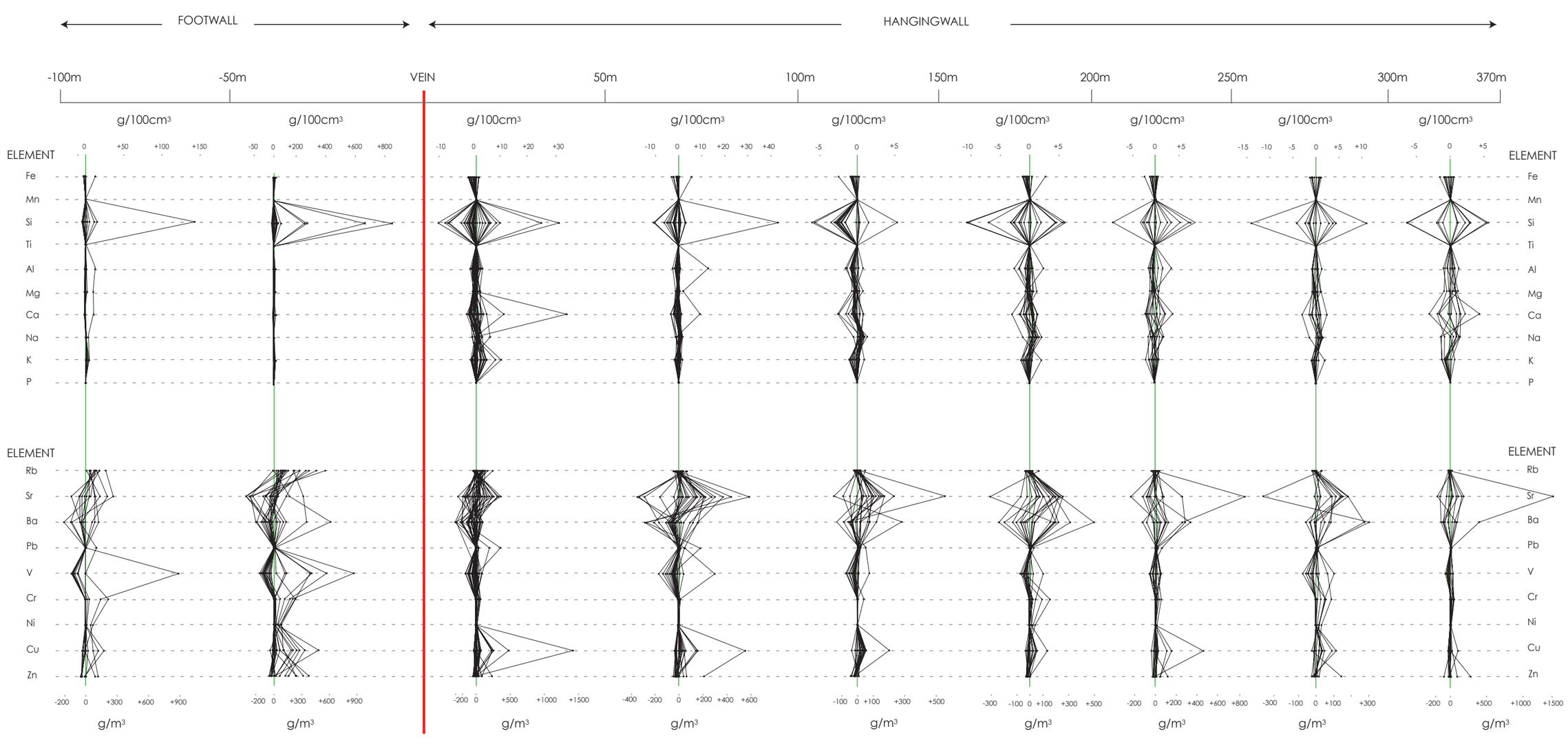

Fig. 5.37 Mass gains and losses of major and trace elements in the andesitic host package of the K1 vein plotted in 50m intervals from hangingwall to footwall. Only propylitic altered samples are included in the analysis (EC and CEP facies). Elements that have been added to the rock have positive values on the X axis, and those that have been lost have negative values on the X axis. Relatively immobile elements (such as Ti, Mn, P) show no mass change. Each black circle represents an individual sample. Major element mass changes are reported in g/100 cm^3, and trace element mass changes are reported in g/m^3.

gain, with an enriched zone in the hangingwall approximately 50-200 m from the vein, and greatest enrichment in the footwall up to 50 m from the vein (Fig. 5.37).

Silicon: Gains or losses of Si are relative to the combined concentrations of this element in both igneous and alteration minerals (Mauk and Simpson, 2007). Si gains and losses related to igneous minerals (such as plagioclase) may be significant at Kencana given the variably aphanitic to porphyritic nature of the phenocrysts in andesite units. The sampling technique excluded all veins and veinlets from whole rock samples. This conservative approach underestimates the total mass of Si that was added to the Kencana system. Overall silicon shows a large gain, with greatest values in proximity to the vein (<100 m from the vein, in the footwall and hangingwall; Fig. 5.37), where the majority of samples gained at least 1% Si (equivalent to 5 g/cm$^{3)}$. The largest gain was calculated at 614 g/cm^3 between 0 and -50 m from the vein in the footwall of the K1 structure, representing strong pervasive silicification of the sample. Si gain is greatest along cross section 19900mN, and losses are greatest along cross section 19600mN.

Calcium: Ca gain is a function of carbonate (predominantly calcite and epidote) and smectite alteration. Ca gains and losses are variable through the stratigraphy, depending on the locations of these hydrothermal phases. Ca losses are a result of the alteration of plagioclase to K-feldspar (equation 2, section 5.9) and largest losses typically occur within 200 m of the vein (Fig. 5.37). Despite Ca losses, Ca gains are greatest within 100 m of the vein in the hangingwall, reflecting the high proportion of smectite and epidote alteration in propylitic altered rocks in this area. Ca gain is greatest along section 19600mN, though calcite was not a common alteration mineral determined by PIMA analysis along this cross section.

Iron: Iron mainly occurs in chlorite with pyrite and chalcopyrite. Fe gain and loss is principally determined by chlorite abundance and chemistry, with Fe loss in the footwall of the deposit caused by the predominance of Mg- chlorite. Fe shows greatest loss proximal to the vein (<50 m; Fig. 5.37), where chlorite has been replaced by quartz and clay minerals, even though pyrite is still common.

Other hydrothermal minerals responsible for mass change in the Kencana system are chlorite (gains in vanadium, chromium, zinc and magnesium), Al-bearing clays, magnetite

(gain in vanadium), galena (gain in lead), chalcopyrite (gain in copper), and sphalerite (gain in zinc). Titanium, manganese and phosphorus show no mass change and are assumed to be relatively immobile in the hydrothermal environment at Kencana.

Patterns of elemental change observed at Kencana show that K-metasomatism (K gain) is accompanied by Si (and Rb) gain proximal to the vein, and losses of Ca and Na commonly characterize the areas affected by K-metasomatism (Warren et al., 2007). Mass change patterns are affected due to the lack of sampling of veinlets and veins together with rock. Vein sampling may change the enrichment patterns of Si, K, Ca (and Au) as these primarily occur in veins in the Kencana system.

Patterns of mass gain and loss observed at Kencana are similar to those determined for the El Peñón deposit, Chile (Warren et al., 2007), the Mt. Muro deposit, Indonesia (Warren et al., 2007), the Martha and Favona deposits, New Zealand (Simpson et al., 2003), and Gosowong (Gemmell, 2007). It should be noted that differences in host lithology affect the absolute amount of elemental losses and gains in these deposits, however all deposits show a consistent gain in K and Rb, whereas Na and to a lesser extent Ca are lost tens to hundreds of metres from the epithermal vein (Mauk and Simpson, 2007).

5.10 Summary

• Alteration at Kencana can be divided into ten main facies: SCG (Argillic 1) facies, ISP (Argillic 2) facies, IC (Argillic 3) facies, QAS (Phyllic) facies, EC (Propylitic 1) facies, CEP (Propylitic 2) facies, P (Sub-propylitic) facies, BM (Calc-potassic) facies, IDP (Intermediate-advanced argillic) facies, and KH (Advanced argillic facies).

• Common alteration minerals include quartz, illite, smectite, adularia, halloysite, kaolinite, sericite, chlorite, epidote, prehnite, calcite, and pyrite. Occurrences of gypsum, anhydrite, biotite, magnetite, actinolite, phengite, chalcopyrite, opal, dickite and pyrophyllite were noted but are less common throughout the system.

• Hypogene alteration at Kencana is approximately zoned around the deposit with respect to four major types of alteration: (1) phyllic alteration (QAS facies) in the form of pervasive silicification and quartz-adularia-sericite alteration in the immediate vein zone, (2) argillic

alteration (IC facies) enveloping the vein zone, (3) high-temperature propylitic alteration (CEP facies) filling fractures, extending up to 50 m from the vein, and (4) low-temperature argillic alteration and regional propylitic alteration (SCG, ISP and IC facies) distal to the deposit. Supergene advanced argillic alteration (KH facies) affects the top 5 m of stratigraphy at Kencana.

• The centre and margins of the deposit show slightly different characteristics in terms of the distribution of alteration mineralogy, which may prove useful in exploring for epithermal deposits in the Gosowong district. The deposit margins show a higher abundance of KH facies alteration proximal to the vein, contain opal in advanced argillic alteration at surface and shear zones are characterized by more illite-smectite, KH facies alteration and sub-propylitic facies alteration. The centre of the deposit displays a higher abundance of EC and BM facies alteration, and shear zones are characterized by more QAS and CEP facies alteration, as well as dickite which is found in shear zones in the centre of the deposit.

• The presence of opal in KH facies alteration along cross section 19600mN may suggest a hypogene origin for advanced argillic alteration in this location. It is possible that the cross section could represent the edge of a steam-heated zone of advanced argillic alteration. It is proposed that any further steam-heated alteration would occur further to the south and more investigation and sampling is needed to determine this.

• Elemental concentrations at Kencana vary depending on location and relative position through the deposit (central or marginal):

1) Within the vein, Ag, K_2O, Cu, Pb, and Rb have high values and V, Sr, Tl and Na_2O have low values in the centre of the system, and Mo, Sb, Tl, Li and Rb have high values along the margins of the deposit.

2) In the upflow zone, Ag, K_2O, Rb, Tl, MgO, Sb, Li and Mo have high values in the centre of the system. The element zonation along the deposit margins could not be determined in this study due to lack of drilling.

3) In the outflow zone (defined as the vein-parallel vertical extension of the vein,

manifesting as shear zones and stockwork), As, Na_2O, Sr and Mn have high values in the centre of the system, and K_2O and Li have high values along the margins of the deposit

4) In the alteration halo, Ba, Ti, V and Zn have high values and Rb, Sb and Tl have low values for the centre of the system, and As, Mn, Ti, Ba, Na_2O, Zn, Pb, Cu and Sr have high values for the margin of the deposit.

• Element zonation at Kencana is different to that for Gosowong; however, certain elements can still be used as pathfinders to ore for both systems. Ag, Pb, Cu and K_2O are enriched within the veins and proximally to the deposits. Li (and Rb) values at Kencana have a good correlation with K_2O values. At Gosowong, Tl substitutes for K_2O (in adularia) and consequently can be used as a pathfinder element towards mineralization (Gemmell, 2007); however at Kencana Tl and K_2O show very poor correlation and it is assumed little substitution of Tl into adularia occurs. However, Tl is still a useful pathfinder element at Kencana as values are enriched within the vein.

• Three major alteration trends are identified with respect to the AI and CCPI: 1) argillic alteration; 2) chlorite-pyrite-(sericite) alteration; and 3) propylitic alteration. Cu, Mo, Tl and Ag show an affinity for argillic alteration, which is not reflected in high Au values (preferentially elevated in the chlorite-pyrite-(sericite) and propylitic trends). Arsenic is the best distal pathfinder for Au mineralization with respect to the AI and CCPI, given that As values are enriched in the weakly altered equivalents of intensely altered rocks containing high Au values.

• K-metasomatism is shown to quantitatively increase towards the deposit. High As and Sb values relative to *m*K/(2Ca+Na+K) values can be used as distal pathfinders to ore mineralization, as these elements are enriched at low *m*K/(2Ca+Na+K) values, where precious metals (e.g. Au) are enriched at higher *m*K/(2Ca+Na+K) values.

CHAPTER 6

GENETIC MODEL

6.1 Introduction

This chapter summarizes the geologic history and hydrothermal evolution of the Kencana low sulfidation epithermal deposit. This thesis aimed to document the geology of the Kencana deposit, to use geochemical methods to constrain the signature of alteration and ore mineralization, fluid compositions and sources, to understand the timing of volcanic and hydrothermal processes, and to propose a genetic model for mineralization. The preceding chapters provided insights into the evolution of the Kencana deposit, with particular focus on the K1 vein. Conclusions and findings of the previous five chapters are combined in this chapter to construct an ore deposit model. The volcanic-hydrothermal evolution of the Kencana deposit is relevant to understanding and exploring for other low sulfidation epithermal gold deposits in volcanic settings.

6.2 Volcanic emplacement and structural setting

An essential precursor to the formation of the Kencana deposit was the formation of a favourable stratigraphic and structural setting. The Halmahera arc is a N- to NE-trending volcanic arc of basaltic and andesitic composition, forming a chain of stratiform calc-alkaline volcanic islands offshore of western Halmahera and cones transecting the NW arm of the island. The current arc began activity within the last 1 Ma and is built upon the deformed and partly eroded andesites and basaltic volcanic rocks of the Neogene arc, which host Gosowong goldfield epithermal mineralization, including the Kencana deposit. Inception of the Neogene arc began at approximately 11 Ma (Hall et al., 1995), underlain by Cretaceous, Eocene and Oligocene arc volcanic rocks forming the western arm of Halmahera island. The opposing Sangihe and Halmahera Arcs have been actively converging since the late Pliocene (Hall, 2000). This double convergence zone is a globally unique example of arc-arc collision, with the Molucca Sea plate dipping east beneath Halmahera and west beneath the Sangihe

Arc, forming an inverted U-shape (Fig. 2.2).

Andesites and diorites in the Gosowong goldfield are closely temporally related, with andesite emplacement at 3.73 ± 0.22 Ma followed by diorite intrusion at ~3.50 Ma (Micklethwaite, 2010). Interlayered coherent andesite and basalt flows and monomict breccias (autobreccias) and tuffs are interpreted to have formed in the volcanic slope environment in subaerial to submarine (sub-lacustrine) conditions (Fig. 3.10). The upper part of the stratigraphic sequence is characterized by numerous beds of monomict and polymict volcaniclastic rocks (mudstones, sandstones and conglomerates) formed by extensive reworking of volcanic rocks, followed by a transition to dacitic volcanism, represented by flow and fall deposits (Fig. 2.7 A). The sequence is covered by Recent ignimbrites. Diorite dykes crosscut both coherent volcanic and volcaniclastic units, with rare peperitic contacts where intrusion occurs into mudstone.

Volcanic and volcaniclastic rocks hosting the Kencana deposit define a moderately east-dipping stratigraphy with westward-rotated units offset by post-mineralization faulting. Five principal lithofacies are identified: 1) plagioclase-phyric coherent and clastic andesite facies; 2) plagioclase-phyric coherent basalt facies; 3) sedimentary facies; 4) intrusive facies and 5) fiamme-bearing facies.

North-trending 2.9 Ma Pliocene extensional structures within the Gosowong Formation host low sulfidation epithermal Au mineralization, with the Kencana deposit interpreted to be hosted in a NW-trending step-over segment of the N-trending Gosowong fault (Fig. 2.8; Micklethwaite, 2010). These are interpreted to have formed between, and become compartmentalized between, major NW-trending structures in the Pliocene dextral wrench, reflecting shallow reactivation of Miocene arc and arc-inversion, N- to NNE-trending, arc-parallel structures (Fig. 2.5; Global Ore Discovery, 2010).

6.3 Hydrothermal system evolution and ore deposition

The onset of hydrothermal activity at Kencana was initiated by extension causing dilation along N- and NW-trending structures. Hydrothermal activity at Kencana began by 2.9 Ma as determined by $^{40}Ar/^{39}Ar$ geochronology of adularia, forming part of a district epithermal mineralization event including formation of the Gosowong and Toguraci dep-

soits. Ascending magmatic fluids associated with arc magmatism combined with circulating meteoric waters (as indicated by fluid inclusion study) to provide precious metal-bearing solutions dominated by a meteoric component (Fig. 4.34 D). Structures provided effective conduits for focusing fluid flow and the host rock sequence provided variations in permeability, porosity and rheology, in particular the hematized mudstone units, which effectively acted as aquacludes and restricted vein dilation. Eleven breccia and infill types are recognized at Kencana, including wallrock (1), quartz stockwork (2), wallrock breccias with crystalline quartz cement (3), red chalcedony infill (4), massive crystalline quartz (5), massive crystalline quartz breccias (6), cockade-banded quartz-chlorite breccias (7), banded quartz-chlorite (8), banded quartz-adularia (9), grey cryptocrystalline quartz stringer veins (10) and black quartz-molybdenite infill (11).

The first infill stage (type 2, crystalline quartz stockwork) formed in response to rising hot, low salinity (203.0 to 248.8°C, 0.1 to 0.5 wt% NaCl (equiv.), <0.015 m CO_2) hydrothermal fluids permeating the host rock package. The hangingwall and footwall of the K1 vein are characterized by thicker, more abundant type 2 quartz veins, becoming thinner and more sparse away from the main fluid flow pathways. Early hydrothermal activity is marked by a widespread, regional pervasive propylitization (Fe-chlorite, albite, pyrite ± epidote) primarily altering plagioclase feldspars and glassy groundmass in andesites flows and breccias, and basaltic units.

Continued dilation of faults provided a focus for fluid flow. Increasing flow rates, higher temperatures, increasing silica saturation of hydrothermal fluids and increased cooling rates of silica gels are represented by a transition from crystalline quartz-dominant to microcrystalline and cryptocrystalline quartz-dominant vein types in the K1 vein paragenetic sequence. High flow rates and effective mechanisms of quartz precipitation are represented by high volumes of quartz mineralization in infill types 4 and 5. Rapid crystallization caused sealing of fissures, which were subsequently re-opened by further dilation and brecciation. Banded quartz textures formed as a result of this episodic pressure release (particularly in infill types 4, 8 and 9) and are particularly prevalent during the mid to late stages of the system, which is represented by voluminous quartz and sporadic sulfide deposition.

Dilation along the K1 fault created structurally controlled permeability, leading to a

wide zone (up to 100 m) of vein-related propylitic (epidote-calcite-pyrite) alteration, which overprints regional propylitic alteration (EC facies). Argillic alteration (ISP transitional to IC facies alteration) followed and overprinted the propylitic alteration, though some CEP alteration overprints argillic assemblages, reflecting the complex history of repeated structural dilation along the fault. Illite and chlorite alteration associated with these infill stages indicate high fluid to rock ratios with weakly acidic to near-neutral hydrothermal fluids at temperatures of 220-310°C, with a transition to lower temperature, smectite-dominated alteration assemblages more distally from the main fluid flow conduits.

Hydrothermal brecciation was widespread and particularly common in the steeper sections of the vein, with multiple events represented by cross-cutting breccia packages. Brecciation early in the life of the system is represented by jigsaw-fit to crackle breccia wallrock clasts cemented by quartz volumes <40% (infill type 3). Continued brecciation is represented by an increase in quartz cement abundance, decrease in abundance and size of wallrock fragments, and a transition to rotated-fit textures (infill types 6 and 7, and brecciated type 9 infill).

Amethyst is most common in the late bands and infill of type 9 veins, forming coarse crystalline comb texture crystals and infilling vug spaces, after mineral assemblages inferred to form as a result of boiling processes and not directly associated with precious metal deposition. The occurrence of amethyst later in the life of the system is consistent with a hydrothermal fluid that has previously boiled and deposited $Al(OH)^-$ as sericite, illite or adularia, as amethyst formation is possibly promoted by a change from Al-rich to poor conditions (Dennen and Puckett, 1972). The development of coarse comb texture amethyst crystals suggests slow rates of deposition in open space (Dong et al., 1995), a reflection of lower flow rates and possible sealing of the hydrothermal system.

Infill types define a broad textural zonation from north to south in the K1 vein. Infill types 1, 2 and 3 are distributed throughout the deposit and are particularly prevalent on the margins of the vein. Types 7, 8 and 9 are the main ore-bearing stages and form the bulk of the central section of the vein, particularly below 4950mRL. Type 11 infill is most prevalent to the north of 19900mN, between 4950mRL and 4880mRL. Types 4, 5, 6 and 10 are variably and sporadically distributed across the vein (Fig. 4.27). This north-south zonation is

reflected in the distribution of metal assays across the deposit. Copper, Pb and Mo values increase towards the north, inferring a source for base metals to the north of Kencana. Zinc values are elevated toward the centre of the deposit, with high Au and Ag. Antimony and As values are highest toward the south of the K1 vein (Fig. 4.52). This lateral zonation is interpreted to represent a hydrothermal fluid temperature gradient.

Precious and base metal mineralization is associated with the microcrystalline and cryptocrystalline quartz-dominant vein types formed in the mid- to late stages of the system (predominantly infill types 7, 8 and 9), transported in near-neutral, hot, low salinity (195.8 to 258.7°C, 0.0 to 0.8 wt% NaCl (equiv.), <0.015 m CO_2) fluids, with a transition to marginally higher temperatures and salinities through time (202.7 to 306.9°C , 0.0 to 1.0 wt% NaCl (equiv.), <0.015 m CO_2) associated with type 7 and 8 infill. Alteration associated with the main ore bearing phases is characterized by intense pervasive illite and adularia alteration of host rock units <25 m from the K1 structure, and an envelope of QAS (quartz-adularia-sericite) alteration with intense pervasive silicification <10 m from the vein.

Electrum at Kencana is deposited with a variety of sulfides, selenides and sulfosalts, and lesser tellurides. At dilational sites within the conduit, particularly above zones restricted by hematized mudstone beds, a combination of mixing and boiling processes (resulting in pressure changes and gas loss, predominantly H_2O with H_2S and CO_2) caused physiochemical changes in hydrothermal fluids (e.g. pH, salinity, sulfur fugacity, temperature) and prompted precious and base metal precipitation with quartz, adularia and chlorite. Gold hydrosulfides (in particular, $Au(HS)_2^-$) are most significant in terms of Au transport at Kencana. Boiling is a process that affects the stability of gold hydrosulfide and triggers gold precipitation due to H_2S loss. Evidence for boiling at Kencana is supported by the presence of bladed quartz pseudomorphs and adularia within the vein, though boiling assemblages were not observed in fluid inclusions. Textural and mineralogical evidence for boiling is first observed in type 5 infill, which is paragenetically coincident with the onset of metal precipitation in the K1 vein (Fig. 4.28). Gases driven off during boiling (such as H_2S and CO_2) condense into meteoric water at shallow levels in the system (in permeable shear zones above the vein, and near-surface along cross section 19600mN), forming cool acid sulfate waters responsible for formation of intermediate argillic and hypogene advanced argillic alteration.

Opal along cross section 19600mN is inferred to have formed at the water table as silica precipitated from ascending silica-rich hydrothermal fluids. There is, however, uncertainty in the timing of formation of advanced argillic assemblages, in particular the near-surface alteration containing opal. Given the distribution of these assemblages at the southern end of the deposit, it is possible that there is a second zone of upwelling of hydrothermal fluid here, though it seems more likely that the assemblages are the result of post-mineral hydrothermal fluids migrating through the host rock package.

Mixing is also an important process for gold deposition, where gold transported as hydrosulfide complexes is destabilized and gold precipitation triggered by mixing with oxidised meteoric waters (and reduced hydrothermal fluids buffered to more oxidized conditions by hematized mudstone units). This process is supported by the presence of high fineness of electrum (Spycher and Reed, 1995), and selenium substitution in sulfides (Reyes, 2002; Wurst, 2004; Simon et al., 1997) in the K1 vein.

The final stage of mineralization at Kencana is marked by poorly crystalline, dark, fine-grained black breccia matrix and vein infill (type 11), characterized by quartz and molybdenite with galena, Ag-selenides and pyrite. Type 11 infill cross-cuts all previous infill types and often occurs along the hangingwall or footwall margins and in zones where there are marked changes in permeability, porosity and rheology between adjacent units. The marked change in the mineralization style and mineral assemblage may reflect input of fluids from a separate source, or a pulse of magmatic fluid late in the system with less dilution by meteoric water than those that formed previous infill types.

6.4 Late stage magmatism, uplift and erosion

After hydrothermal activity ceased at Kencana, a period of magmatism, followed by uplift and erosion, occurred. Pliocene dacitic volcanic and volcaniclastic rocks form the unmineralized Kayasa Formation which overlies the Gosowong Formation to the north and east of the Kencana deposit. The youngest unit is represented by extensive Quaternary ignimbrite deposits covering much of the southeast of the district. A supergene alteration profile characterized by a kaolinite-halloysite-(Fe-oxyhydroxide) blanket 5-10 m thick has formed in the oxidized zone at the current ground surface, representing a weathering profile formed

in the intense tropical climate.

Pressure estimates used to calculate minimum depth of entrapment infer that most fluid inclusions were trapped 50 to 200 m deeper than their current location, which implies that Kencana was uplifted up to 200 m between the time of its formation and the present, or that the water table was at least 200 m higher than the current erosion surface (given the uncertainty in the position of the palaeowater table), which is consistent with observations from the Gosowong deposit (Olberg, 2001).

CHAPTER 7

CONCLUSIONS

7.1 Conclusions

The main conclusions derived from the study of the Kencana Au-Ag low sulfidation epithermal deposit are as follows:

- The Kencana deposit (4.4 Mt @ 27.9 g/t Au, containing 4 Moz Au) forms part of the Gosowong goldfield on Halmahera island, Eastern Indonesia, which contains three bonanza grade Au low sulfidation epithermal deposits (Gosowong, Toguraci and Kencana), hosted by a sequence of basaltic to andesitic coherent and volcaniclastic facies of upper Miocene to Pliocene age. The heat source for epithermal activity is provided by magmatism along the Miocene Halmahera Arc.
- Five principal lithofacies are identified in the Kencana deposit: 1) Plagioclase-phyric coherent and clastic andesite facies (plagioclase-phyric coherent andesite and plagioclase-phyric monomict andesite breccia); 2) Plagioclase-phyric coherent basalt facies; 3) Sedimentary facies (hematitic mudstone; polymict, matrix-supported conglomerate and polymict, basaltic matrix-supported conglomerate); 4) Intrusive facies (diorite) and 5) Fiamme-bearing facies (dacitic ignimbrite). These facies represent proximal deposition of coherent lavas in the volcanic slope environment, with extensive re-working of flows and ash deposits to form volcaniclastic units in a shallow, regressive sub-lacustrine depositional environment. Intrusive facies cross-cut the basaltic and andesitic volcanic pile and form peperitic contacts with hematized mudstones.
- Kencana is hosted by two main sub-parallel NW-trending fault structures, (K1 and K2) dipping ~46°E, joined by numerous major and minor link structures, such as K-link (KL), that exhibit a steeper dip than the main K1 and K2 structures. The structures provide a host for epithermal mineralization, and veins appear best developed along

lithological boundaries, particularly where rheological differences exist (e.g. mudstone/volcanic rock contact). The NW-trending structures are step-over segments between 2.9 Ma extensional N-trending normal faults, including the structure hosting the Gosowong deposit ~1 km to the north.

- The K1 vein shows a complex, multiphase history of formation with numerous brecciation and opening events, resulting in complex overprinting infill stages and crosscutting relationships. Eleven infill types are recognized at Kencana, including wallrock (1), quartz stockwork (2), wallrock breccias with crystalline quartz cement (3), red chalcedony infill (4), massive crystalline quartz (5), massive crystalline quartz breccias (6), cockade-banded quartz-chlorite breccias (7), banded quartz-chlorite (8), banded quartz-adularia (9), grey cryptocrystalline quartz stringer veins (10) and black quartz-molybdenite infill (11).
- A broad textural zonation from north to south is observed across the K1 vein. Infill types 1, 2 and 3 are distributed throughout the deposit and are particularly prevalent on the margins of the vein. Types 7, 8 and 9 are the main ore-bearing stages and form the bulk of the central section of the vein, particularly below 4950mRL. Type 11 infill is most prevalent to the north of 19900mN, between 4950mRL and 4880mRL. Types 4, 5, 6 and 10 are variably and sporadically distributed across the vein.
- Kencana ore mineralogy is generally typical of low sulfidation epithermal deposits, though several features of the mineral assemblages are less common and may reflect on the metal transportation and depositional processes in the Kencana vein. Gold occurs as inclusions and complex intergrowths of high-fineness electrum in multistage, banded veins, hydrothermal breccias and stockworks, predominantly in infill types 7, 8 and 9. Ore assemblages dominated by electrum and sulfides, with selenides and lesser tellurides and sulfosalts. Chalcopyrite is the most common sulfide mineral, with selenian-galena, sphalerite, bornite and pyrite in order of decreasing abundance. Other common accessory minerals include aguilarite and molybdenite (in type 11 infill), with trace tennantite, arsenian-pyrite, silver and lead tellurides, naummanite and rare bismuth minerals.
- Gangue mineralogy is dominated by crystalline, microcrystalline and cryptocrystalline quartz, adularia, chlorite and calcite. Microcrystalline and cryptocrystalline quartz show

a variety of textures including colloform and crustiform banding, likely representing primary growth textures formed during crystal growth or from the deposition of amorphous silica. A general transition from early coarse crystalline quartz to micro- and cryptocrystalline quartz dominant assemblages is observed in the paragenetic sequence of the K1 vein, reflecting an increase in the rate of silica precipitation in silica-saturated fluids (likely in response to boiling conditions). The increasing grain size of silica polymorphs from the margins to the centre of individual veins reflects a decrease in the rate of cooling, cessation of boiling and/ or a decrease in overall fluid flux rate in each individual vein cycle.

- Physiochemical conditions of ore deposition vary through the formation of the deposit. Fluid inclusion data indicate that early crystallline quartz (type 2c) was precipitated from near-neutral, hot, low salinity, low CO_2 (203.0 to 248.8°C, 0.1 to 0.5 wt% NaCl (equiv.), <0.015 m CO_2) fluids. Temperatures and salinities increase with time through the formation of the deposit, with quartz-adularia (type 9) mineralization forming in marginally hotter, more saline conditions (195.8 to 258.7°C, 0.0 to 0.8 wt% NaCl (equiv.), <0.015 m CO_2), with a transition to 202.7 to 306.9°C, 0.0 to 1.0 wt% NaCl (equiv.), <0.015 m CO_2 fluids associated with precious metal deposition in type 7 and 8 infill. The range of peak homogenization temperatures for both type 2c and 9 infill are between 200 and 225°C.
- Mineralizing fluids are strongly dominated by meteoric water, with a marginally increased magmatic input during formation of type 7 and 8 infill. Ore deposition is interpreted to be the result of a combination of processes (mixing, boiling and cooling), though mixing processes are inferred to be of particular importance, based on the presence of high-fineness electrum and selenium-bearing minerals. Evidence for boiling processes is also present at Kencana, including bladed carbonate pseudomorphs and abundant adularia, though boiling assemblages were not observed in the fluid inclusion study.
- Hydrothermal fluids were sourced from the down-dip extension of the K1 vein, flowing upwards through the dilating structure. Metal distribution is vertically and laterally zoned at the Kencana deposit, with precious metals enriched at shallow levels of the system (above 4950mRL), and base metal values increasing systematically with depth.

Metals are generally confined to NW-trending dilational structures and high values are coincident with the 1 g/t Au anomaly, with restricted hydrothermal fluid flow and low metal values away from the main veins. Lateral zonation implies a hydrothermal fluid temperature gradient with a metal source to the north of the Kencana deposit.

- On a deposit scale, alteration assemblages are dominated by quartz, illite, smectite, adularia, halloysite, kaolinite, sericite, chlorite, epidote, prehnite, calcite, and pyrite. Gypsum, anhydrite, biotite, magnetite, actinolite, phengite, chalcopyrite, opal, dickite and pyrophyllite were noted but are less common. Ten alteration facies are recognized: SCG (Argillic 1) facies, ISP (Argillic 2) facies, IC (Argillic 3) facies, QAS (Phyllic) facies, EC (Propylitic 1) facies, CEP (Propylitic 2) facies, P (Sub-propylitic) facies, BM (Calc-potassic) facies, IDP (Intermediate-advanced argillic) facies, and KH (Advanced argillic) facies.
- Alteration minerals are approximately zoned around the K1 vein, reflecting a trend in increasing temperature of hydrothermal fluids towards the ore zone. Smectite-dominated assemblages (20-200°C) are transitional to illite-dominated assemblages (220-310°C), with increasing abundance of chlorite, epidote, albite and sericite toward the vein, inferring palaeofluid temperatures of >200°C. Zonation is also observed in the distribution of alteration facies: (1) phyllic alteration (QAS facies) in the form of pervasive silicification and quartz-adularia-sericite alteration in the immediate vein zone, (2) argillic alteration (IC facies) enveloping the vein zone, (3) high-temperature propylitic alteration (CEP facies) filling fractures, extending up to 50 m from the vein, and (4) low-temperature argillic alteration and regional propylitic alteration (SCG, ISP and IC facies) distal to the vein. Supergene advanced argillic alteration (KH facies) blankets the top 5 m of stratigraphy at Kencana and represents intense tropical surface weathering.
- The geochemical signature of altered rocks hosting the Kencana deposit is variable depending on position relative to the mineralized structure: 1) Within the vein, Ag, K_2O, Cu, Pb, and Rb have high values and V, Sr, Tl and Na_2O have low values in the centre of the system, and Mo, Sb, Tl, Li and Rb have high values along the margins of the deposit; 2) In the upflow zone, Ag, K_2O, Rb, Tl, MgO, Sb, Li and Mo have high values in the centre of the system; 3) In the outflow zone, As, Na_2O, Sr and Mn have high values in the centre of the system, and K_2O and Li have high values along the margins of the deposit;

and 4) In the alteration halo, Ba, Ti, V and Zn have high values and Rb, Sb and Tl have low values for the centre of the system, and As, Mn, Ti, Ba, Na_2O, Zn, Pb, Cu and Sr have high values for the margin of the deposit.

- Patterns of elemental change observed at Kencana show that K-metasomatism (K gain) is accompanied by Si (and Rb) gain proximal to the vein, and losses of Ca and Na commonly characterize the areas affected by K-metasomatism. Patterns of mass gain and loss observed at Kencana are similar to those determined for the El Peñón deposit, Chile, the Mt. Muro deposit, Indonesia, the Martha and Favona deposits, New Zealand, and Gosowong.
- It is proposed that a sub-class of low sulfidation epithermal deposits (Se-rich low sulfidation epithermals), characterized by bonanza-grade Au, bimodal volcanism and a Se-rich ore mineral assemblage, such as Midas (USA), Hishikari (Japan), and Broken Hills (New Zealand), can be considered, and that Kencana is a classic example of such a deposit. It is proposed that as well as similarities in their general geological setting, these deposits may form under similar physiochemical conditions, including the relatively more oxidized conditions than typical for low sulfidation systems for which deposition of selenium-bearing minerals requires, possibly reflecting the importance of mixing as a mechanism for ore deposition.

7.2 Exploration Implications

The final aim of this project was to determine criteria that may aid in the exploration and discovery of further low sulfidation Au mineralization in the Gosowong goldfield. Several features observed in the Kencana deposit may be useful for helping to vector towards mineralized zones in the goldfield, and other low sulfidation epithermal districts:

- Epithermal mineralization at Kencana is best developed along lithologic contacts, particularly where rheologic differences occur. In particular, hematized mudstone units are critical in controlling the dilation of the epithermal structure and mineralization is best developed above zones constricted by these mudstones. Mapping and correlation of mudstone units may provide target zones for further dilational sites.
- Elevated Pb and Sb values show the strongest correlation with high Au values, and due

to the strong zonation exhibited by these elements may provide useful vectors towards precious metal occurrence in the Gosowong goldfield.

- The presence of Se-rich minerals in the ore assemblage at Kencana suggests that Se may be a useful pathfinder to further Au mineralization. Currently, Se is not included in the routine assay suite for exploration drillcore in the Gosowong goldfield, though this may prove a useful vector to ore.
- The lateral metal zonation from high to low temperature from north to south across the deposit, and the proposed source of hydrothermal fluids to the north of the Kencana deposit may provide the basis for delineation of a target area for further mineralization. Late, Mo-bearing type 11 infill and general increase in base metal values with depth may indicate the prospect of a more magmatic-derived, porphyry-style deposit deeper in the stratigraphy to the north of Kencana.
- The geochemical signature of altered rocks hosting epithermal mineralization at Kencana is different to that for Gosowong; however, certain elements can still be used as pathfinders to ore for both systems and thus can be considered potential regional vectors to ore. Ag, Pb, Cu and K_2O are enriched within the veins and proximally to the deposits. Li (and Rb) values at Kencana have a good correlation with K_2O values. At Gosowong, Tl substitutes for K_2O (in adularia) and consequently can be used as a pathfinder element towards mineralization (Gemmell, 2007). Though Tl and K_2O show poor correlation at Kencana, Tl values are still highest within the vein and thus Tl is still a useful pathfinder element at Kencana.
- Potassium metasomatism (represented by mK/(2Ca+Na+K) values) quantitatively increases towards the Kencana deposit. High As and Sb values relative to mK/(2Ca+Na+K) values can be used as distal pathfinders to ore mineralization, as these elements are enriched at low mK/(2Ca+Na+K) values, where precious metals (e.g. Au) are enriched at higher mK/(2Ca+Na+K) values.
- The centre and margins of the Kencana deposit show different characteristics in terms of the distribution of alteration mineralogy which could be used to determine relative position within an ore body. The deposit margins show a higher abundance of KH facies alteration proximal to the vein, contain opal in advanced argillic alteration at surface

and shear zones are characterized by more illite-smectite, KH facies alteration and sub-propylitic facies alteration. The centre of the deposit displays a higher abundance of EC and BM facies alteration, more complex overprinting of facies, and shear zones are characterized by more QAS and CEP facies alteration, as well as dickite which is found in shear zones above the vein in the centre of the deposit.

REFERENCES

Arancibia, G., Matthews, S.J., Cornejo, P., Pırez de Arce, C., Zuluaga, J.I., and Kasaneva, S., 2006, $^{40}Ar/^{39}Ar$ and K-Ar geochronology of magmatic and hydrothermal events in a classic low-sulphidation epithermal bonanza deposit: El Peñon, northern Chile: Mineralium Deposita, v. 41, p. 505–516.

Barton, P.B., Jr., and Skinner, B.J., 1979, Sulfide mineral stabilities, in Barnes, H.L., ed., Geochemistry of hydrothermal ore deposits, 2nd ed.: New York, Wiley-Interscience, p. 278–403.

Bates, R.L., and Jackson, J.A., (eds.) 1987, Glossary of Geology: American Geological Institute, Alexandria, VA, 3rd edition, 788 p.

Begbie, M.J., Spörli, K.B., and Mauk, J.L., 2007, Structural evolution of the Golden Cross epithermal Au-Ag deposit, New Zealand: Economic Geology, v. 102, p. 873–892.

Benton, R., 2004, Kencana Resource Information: Internal company report for PT. Nusa Halmahera Minerals, 5 p.

Berry, R.F., 2012, personal communication, Hobart, University of Tasmania.

Bird, D.K., Schiffman, P., Elders, W.A., Williams, A.E., and McDowell, S.D., 1984, Calc-silicate mineralization in active geothermal systems: Economic Geology, v. 79, p. 671-695.

Bodnar, R.J., 1993, Revised equation and table for determining the freezing point depression of H_2O–NaCl solutions: Geochimica et Cosmochimica Acta, v. 57, p. 683–684.

Booden, M.A., Mauk, J.L., and Simpson, M.P., 2011, Quantifying metasomatism in epithermal Au-Ag Deposits: A case study from the Waitekauri Area, New Zealand: Economic Geology, v. 106, p. 999–1030.

Braithwaite, R.L., and Faure, K., 2002, The Waihi epithermal gold-silver-base metal sulfide-quartz vein system, New Zealand: Temperature and salinity controls on electrum and sulfide deposition: Economic Geology, v. 97, p. 269-290.

Braund, K., 2006, Geology, geochemistry and paragenesis of the Royal, Crown, and Roses pride low sulphidation epithermal quartz vein structures, Cracow, South-east Queensland: Unpublished Masters thesis, University of Queensland, 442 p.

Braxton, D.P., 2007, Boyongan and Bayugo porphyry Cu-Au deposits, NE Mindanao, Phil-

ippines: geology, geochemistry, and tectonic evolution: Unpublished Ph.D thesis: Hobart, Australia, University of Tasmania, 277 p.

Brown, P.E., 1989, FLINCOR; a microcomputer program for the reduction and investigation of fluid-inclusion data: American Mineralogist, v. 74, n. 11–12, p. 1390–1393.

Brown, P.E., 1998, Fluid inclusion modeling for hydrothermal systems: in Richards, J.P., and Larsen, P.B., (eds.), Techniques in hydrothermal ore deposits geology, v. 10, Reviews in Economic Geology, p. 151-171.

Browne, P.R.L., 1978, Hydrothermal alteration in active geothermal fields: Annual Reviews, Earth and Planetary Sciences, v. 6, p. 229-250.

Browne, P.R.L., and Ellis, A.J., 1970, The Ohaaki-Broadlands hydrothermal area, New Zealand: Mineralogy and related geochemistry: American Journal of Science, v. 269, p. 97–215.

Buchanan, L.J., 1981, Precious metal deposits associated with volcanic environment in the southwest: Arizona Geological Society Digest, v. 14, p. 237–262.

Cardwell, R.K., Isacks, B.L., and Karig, D.E., 1980, The spatial distribution of earthquakes, focal mechanism solutions and subducted lithosphere in the Philippine and northeastern Indonesian islands. The tectonic and geologic evolution of Southeast asian seas and islands: Geophysical monograph 23, Hayers, D.E., (ed.), p. 1-35. American Geophysical Union, Washington.

Carlile, J.C., Davey, G.R., Kadir, I., Langmead, R.P., and Rafferty, W.J., 1998, Discovery and Exploration of the Gosowong Epithermal Gold Deposit, Halmahera, Indonesia: Journal of Geochemical Exploration, v. 60, p. 207-227.

Casadevall, T., and Ohmoto, H., 1977, Sunnyside Mine, Eureka mining district, San Juan County, Colorado; geochemistry of gold and base metal ore deposition in a volcanic environment: Economic Geology, v. 72, p. 1285-1320.

Cathles, L.M., Erendi, A.H., and Barrie, T., 1997, How long can a hydrothermal system be sustained by a single intrusive event?: Economic Geology, v. 92, p. 766–771.

Chambers, C., 2010, personal communication, Brisbane, Newcrest Mining Ltd.

Christie, A.B., Simpson, M.P., Brathwaite, R.L., Mauk., J.L., and Simmons, S.F., 2007, Epithermal Au-Ag and related deposits of the Hauraki goldfield, Coromandel volcanic zone, New Zealand: Economic Geology, v. 102, p. 785–816.

Cooke, D.R., and Bloom, M.S., 1990, Epithermal and subadjacent porphyry mineralization, Acupan, Baguio District, Philippines; a fluid-inclusion and paragenetic study: Journal of Geochemical Exploration, v. 35, p. 297-340.

Cocker, H.A., Mauk, J.L, and Rabone, S.D.C., (2012), The origin of Ag–Au–S–Se minerals

in adularia-sericite epithermal deposits: constraints from the Broken Hills deposit, Hauraki Goldfield, New Zealand: Mineralium Deposita, v. 47, p. 1-18

Cooke, D.R., and Bloom, M.S., 1990, Epithermal and subjacent porphyry mineralization, Acupan, Baguio district, Philippines: A fluid-inclusion and paragenetic study: Journal of Geochemical Exploration, v. 35, p. 297-340.

Cooke, D.R., and McPhail, D.C., 2001, Epithermal Au-Ag-Te mineralization, Acupan, Baguio District, Philippines; numerical simulations of mineral deposition: Economic Geology, v. 96, p. 109-131.

Cooke, D.R., and Simmons, S.F., 2000, Characteristics and genesis of epithermal gold deposits: reviews in Economic Geology, v. 13, p. 221-244.

Coote, J.A.R., 2003, Petrological studies of diamond drill core from the gold mineralised Kencana vein system, Gosowong district, Halmahera, Indonesia; Applied Petrological Services: Unpublished report prepared for PT. Nusa Halmahera Minerals, 85 p.

Coote, J.A.R., 2005, Petrological studies of diamond drill core from the southeast Kencana epithermal gold project, Gosowong district, Halmahera, Indonesia; Applied Petrological Services: Unpublished report prepared for PT. Nusa Halmahera Minerals, 34 p.

Coote, J.A.R., 1996, Studies of host rock, vein structure and gangue and ore mineralogy in drill core from the Gosowong gold deposit, Halmahera: Applied Petrological Sciences Report 26, Unpublished report prepared for PT. Puncakbaru Jayatama.

Corbett, J.G., and Leach, T. M., 1998, Southwest Pacific rim gold-copper systems: Structure, alteration, mineralisation: Society of Economic Geologists Special Publication, v. 6, p. 237.

Coupland, T., Sims, D., Singh, V., Benton, R., Wardiman, D., and Carr, T., 2009, Understanding geological variability and quantifying resource risk at the Kencana Underground Gold Mine, Indonesia: Proceedings, Seventh International Mining Geology Conference, p. 169-186 (The Australasian Institute of Mining and Metallurgy: Melbourne).

Darman, H., and Hasan Sidi, F., ed., 2000, An Outline of the Geology of Indonesia: Indonesian Association of Geologists, p. 131-139.

Davey, G.R., Carlile, J.C., Olberg, D.J., and Langmead, R.P., 1997. Discovery of the Gosowong epithermal quartz-adularia vein gold deposit, Halmahera, eastern Indonesia: Australian Mineral Foundation New Generation Gold Mines '97 Conference, Perth, Western Australia, November, 1997, Proceedings, p. 3.1–3.15.

Dennen, W.H., and Puckett, A.M., 1972, On the chemistry and colour of amethyst: The Canadian Mineralogist, v. 11, p. 448-456.

de Cariat, P., Hutcheon, I., and Walshe, J.L., 1993, Chlorite geothermometry: Clays and Clay Minerals, Vol. 41, No. 2, p. 219-239.

de Ronde, C.E.J., and Blattner, P., 1988, Hydrothermal alteration, stable isotopes, and fluid inclusions of the Golden Cross epithermal gold deposit, Waihi, New Zealand: Economic Geology, v. 83, p. 895–917.

Diamond, L.W., 2001, Review of the systematics of CO_2–H_2O fluid inclusions: Lithos, v. 55, p. 69–99.

Dong, G., and Morrison, G.W., 1995, Adularia in epithermal veins, Queensland; morphology, structural state and origin: Mineralium Deposita, v. 30, p. 11-19.

Dong, G., and Morrison, G.W., and Jaireth, S., 1995, Quartz textures in epithermal veins, Queensland; classification, origin and implication: Economic Geology, v. 90, p. 1841-1856.

Dowling, K., and Morrison, G., 1989, Application of quartz textures to the classification of gold deposits using North Queensland examples: Economic Geology Monographs, v. 6, p. 342-355.

Einaudi, M.T., 1977, Environment of ore deposition at Cerro de Pasco, Peru: Economic Geology, v. 72, p. 893-924.

Einaudi, R.H., Hedenquist, J.W., and Inan, E.E., 2003, Sulfidation of fluids in active and extinct hydrothermal systems: transitions from porphyry to epithermal environments in Simmons, S.F., and Graham, I., ed., Volcanic, geothermal and ore forming fluids: Society of Economic Geologists Special Publication, no. 10, p. 315-343.

Eramet, 2009, www.eramet.fr

Fitzgerald, F., and Leonard, G., 1999, Report on exploration undertaken, Central Gosowong District, Halmahera, Indonesia, unpublished report for PT Puncakbaru Jayatama, 192 p.

Fournier, R.O., 1985, The behaviour of silica in hydrothermal solutions: Geology and Geochemistry of Epithermal Systems (eds. Berger, B.R., and Bethke, P.M.,): Reviews in Economic Geology, v. 2, p. 45-59.

Gemmell, J.B., 2002, Hydrothermal alteration associated with the Gosowong low sulfidation epithermal Au-Ag vein deposit: ARC-AMIRA P588 Final report 2, p. 1.1-1.11.

Gemmell, J.B., 2004, Low and intermediate-sulfidation epithermal deposits: 24ct Gold Workshop, CODES Special Publication, no. 5, p. 57-63.

Gemmell, J.B., 2007, Hydrothermal alteration associated with the Gosowong epithermal Au-Ag deposit, Halmahera, Indonesia: Mineralogy, geochemistry and exploration implications: Economic Geology, v. 102, p. 893–922.

Gemmell, J.B., and Large, R.R., 1992, Stringer system and alteration zones underlying the Hellyer volcanogenic massive sulfide deposit, Tasmania, Australia: Economic Geology, v.

87, p. 620-649.

Gemmell, J.B., Simmons, S.F., and Zantop, H., 1988, The Santo Nino silver-lead-zinc vein, Fresnillo District, Zacatecas, Mexico: Part 1. Structure, vein stratigraphy and mineralogy: Economic Geology, v. 83, p. 1597-1618.

Giggenbach, W.F., 1984, Mass transfer in hydrothermal alteration systems: Geochimica et Cosmochimica Acta, v. 48, p. 2693–2711.

Gill, J.B., 1981, Orogenic Andesites and Plate Tectonics: Springer-Verlag, Berlin, 390 p.

Global Ore Discovery, 2010, Low sulphidation epithermal system analysis and targeting, Gosowong COW, Halmahera Indonesia: Unpublished report prepared for Newcrest Mining Ltd., 107 p.

Golden Peaks Resources, 2010, www.relianceresources.com

Goldstein, R.H., and Reynolds, T.J., 1994, Systematics of fluid inclusions in diagenetic minerals: SEPM Short Course Notes, v. 31.

Goodell, P. C., and Petersen, U., 1974, Julcani Mining District, Peru: A Study of Metal Ratios: Economic Geology, v. 69, p. 347-361.

Gresens, R.L., 1967, Composition-volume relationships of metasomatism: Chemical Geology, v. 2, p. 47-55.

Groff, J., Heizler., M.T., McIntosh, W.C., and Norman, D.I., 1997, $^{40}Ar/^{39}Ar$ dating and mineral paragenesis for Carlin-type gold deposits along the Getchell trend, Nevada: evidence for cretaceous and tertiary gold mineralization: Economic Geology, v. 92, p. 601–622.

Guilbert, J.M., and Park, C.F., 1986, The geology of ore deposits: W.H. Freeman and Company, New York, 985 p.

Hakim, A.S and Hall, R., 1991, Tertiary Volcanic Rocks From the Halmahera Arc, Eastern Indonesia: Journal of South East Asian Earth Sciences, v. 6, p. 271-284

Hall, R., 1987, Plate boundary evolution in the Halmahera region, Indonesia: Tectonophysics, v. 144, p. 337-352.

Hall, R., 2000, Neogene History of Collision in the Halmahera region, Indonesia: Proceedings of the Indonesian Petroleum Association, 27th Annual Convention and Exhibition, p. 487-493..

Hall, R., 2001, Cenozoic geological and plate tectonic evolution of SE Asia and the SW Pacific: Computer-based reconstructions, model and animations: Journal of Asian Earth Sciences, v. 20, p. 353-431.

Hall, R., 2002, Cenozoic geological and plate tectonic evolution of SE Asia and the SW Pacific: computer-based reconstructions, model and animations: Journal of Asian Earth Sciences, v. 20, p. 353-431.

Hall, R., Ali, J.R., Anderson, C.D., and Baker, S.J., 1995, Origin and motion history of the Philippine Sea Plate: Tectonophysics, v. 251, p. 229–250.

Hall, R., Audley-Charles, M.G., Banner, F.T., Hidayat, S., and Tobing, S.L., 1988, Basement rocks of the Halmahera region, eastern Indonesia: A Late Cretaceous-early Tertiary arc and fore-arc: Journal of the Geological Society, v. 145, p. 65–84.

Hall, R., and Nichols, G.J., 1990, Terrane amalgamation at the boundary of the Philippine Sea Plate: Tectonophysics, v. 181, p. 207-222.

Hall, R., and Smyth, H.R., 2008, Cenozoic arc processes in Indonesia: Identification of the key influences on the stratigraphic record in active volcanic arcs, in Draut, A.E., Clift, P.D., and Scholl, D.W., eds., Formation and Applications of the Sedimentary Record in Arc Collision Zones: Geological Society of America Special Paper 436, p. 27–54.

Hamilton, W., 1979, Tectonics of the Indonesian region: USGS Professional Paper, no. 1078, 345 p.

Hannington, M.D., and Scott, S.D., 1989, Gold mineralization in volcanogenic massive sulfides: implications of data from active hydrothermal vents on the modern sea floor: Economic Geology Monographs, v. 6, p. 491-507.

Heald, P., Foley, N.K., and Hayba, D.O., 1987, Comparative anatomy of volcanic-hosted epithermal deposits; acid-sulfate and adularia-sericite types: Economic Geology, v. 82, p. 1-26.

Hedenquist, J.W., 1987, Volcanic related hydrothermal systems in the circum-Pacific basin and their potential for mineralization: Mining Geology, v. 37, p. 347-364.

Hedenquist, J.W., 1990, The thermal and geochemical structure of the Broadlands-Ohaaki geothermal system: Geothermics, v. 19, p. 151- 185.

Hedenquist, J.W., 1991, Boiling and dilution in the shallow portion of the Waiotapu geothermal system: Geochimica et Cosmochimica Acta, v. 55, p. 2753-2765.

Hedenquist, J.W., Arribas, A., and Gonzalez-Urien, E., 2000, Exploration for epithermal gold deposits: Reviews in Economic Geology, v. 13, p. 221–244.

Hedenquist, J.W., and Henley, R.W., 1985, The importance of CO_2 on freezing point measurements of fluid inclusions: evidence from active geothermal systems and implications for epithermal ore deposition: Economic Geology, v. 80, p. 1379–1406.

Hedenquist, J.W., and Houghton, B. F., 1987, Epithermal gold mineralization and its volcanic environments: Sydney, University of Sydney, Earth Resources Foundation, 422 p.

Hedenquist, J.W., Izawa, E., Arribas, A., and White, N.C., 1996, Epithermal gold deposits: styles, characteristics and exploration: Resource Geology, Special Publication 1, poster and booklet.

Hedenquist, J.W., and Lowenstern, J.B., 1994, The role of magmas in the formation of hydrothermal ore deposits: Nature, v. 370, p. 519–527.

Hemley, J.J., Montoya, J.W., Marinenkoa, J.W., and Luce, R.W., 1980, Equilibria in the System Al_2O3-SiO_2-H_2O and Some General Implications for Alteration/Mineralization Processes: Economic Geology, v. 75, p. 210-228.

Henley, R.W., 1985, The geothermal framework for epithermal systems: Reviews in Economic Geology, v. 2, p. 1-24.

Henley, R.W., and Ellis, A.J., 1983, Geothermal systems ancient and modern; a geochemical review: Earth-Science Reviews, v. 19, p. 1-50.

Hudson, D.M., 2003, Epithermal alteration and mineralization in the Comstock district, Nevada: Economic Geology, v. 98, p. 367–386.

Ibaraki, K., and Suzuki, R., 1993, Gold-silver quartz-adularia veins of the Main, Yamada and Sanjin deposits, Hishikari gold mine - A comparative study of their geology and ore deposits, in Shikanzono, N., Naito, K., and Izawa, E., (eds.), High Grade Epithermal Gold Mineralization, the Hishikari Deposit: Resource Geology Special Issue 14, p. 1-11.

Ishikawa, Y., Sawaguchi, T., Iwaya, S., and Horiuchi, M., 1976, Delineation of prospecting targets for Kuroko deposits based on modes of volcanism of underlying dacite and alteration halos: Mining Geology, v. 26, p. 105–117 (in Japanese with English abs.).

Jansen, N.H., 2012, Geology and genesis of the Cerro la Mina porphyry-high sulfidation prospect, Mexico: Unpublished Ph.D thesis, University of Tasmania, 222 p.

Kamilli, R.J., and Ohmoto, H., 1977, Paragenesis, zoning, fluid inclusion, and isotopic studies of the Finlandia Vein, Colqui District, central Peru: Economic Geology, v. 72, p. 950-982.

Kuenen, P.H., 1935, Contributions to the geology of the East Indies from the Snellius expedition, Part I, Volcanoes: Leidse Geol. Mededel. v. 7, p. 273 331.

Large, R.R., Gemmell, J.B., Paulick, H., and Huston, D., 2001, The alteration box plot: A simple approach to understanding the relationship between alteration mineralogy and lithogeochemistry associated with VHMS deposits: Economic Geology, v. 96, p. 957–972.

Lawless, J.V., White, P.J., Bogie, I., Paterson, L.A., and Cartwright, A.J., 1997, Epigenetic magmatic-related mineral deposits: exploration based on mineralisation models. Unpublished lecture notes for Kingston Morrison seminars, Manila and Jakarta, September 1997.

Leach, T.M., 2005, Comments on the alteration and mineralisation at the Gosowong Project, Halmahera Island, Indonesia: Unpublished report prepared for PT. Nusa Halmahera Minerals, 54 p.

Leavitt, E.D., Spell, T.L., Goldstrand, P.M., and Arehart, G.B., 2004, Geochronology of the Midas low-sulfidation gold-silver deposit, Elko County, Nevada: Economic Geology, v. 99, p. 1665-1686.

Lindgren, W., 1933, Mineral Deposits: New York, McGraw-Hill, 930 p.

Love, D., Clark, A., Hodgson, C., Mortensen, J., Archibald, D., and Farrar, E., 1998, The timing of adularia–sericite-type mineralization and alunite–kaolinite-type alteration, Mout-Skukum epithermal gold deposit, Yukon territory, Canada, $^{40}Ar/^{39}Ar$ and U–Pb geochronology: Economic Geology, v. 93, p. 437-462

Macpherson, C.G., and Hall, R., 1999, Tectonic controls of geochemical evolution in arc magmatism of SE Asia: Australasian Institute of Mining and Metallurgy Publication Series 4/99, p. 359-367.

Macpherson, C.G., and Hall, R., 2002, Timing and tectonic controls in the evolving orogen of SE Asia and the Western Pacific and some implications for ore genesis; in Blundell, D.J., Neubauer, F., and Von Quadt, A., (eds), The Timing and Location of Major Ore Deposits in an Evolving Orogen: Geological Society, London, Special Publications, v. 204, p 49-67.

Marjoribanks, R., 1997, Geological Interpretation of the Gosowong Region Halmahera Island, Indonesia: Unpublished Report prepared for PT. Nusa Halmahera Minerals.

Matchan, E., and Phillips, D., 2011, New $^{40}Ar/^{39}Ar$ ages for selected young (<1 Ma) basalt flows of the Newer Volcanic Province, southeastern Australia: Quaternary Geochronology, v. 6, p. 356-368.

Mauk, J.L., and Simpson, M.P., 2007, Geochemistry and stable isotope composition of altered rocks at the Golden Cross epithermal Au-Ag deposit, New Zealand: Economic Geology, v. 102, p. 841–871.

McDougall, I., and Harrison, T.M., 1999, Geochronology and thermochronology by the $^{40}Ar/^{39}Ar$ Method, Second Edition: New York, Oxford University Press, 269 p.

McKee, E., and Noble, D., 1989, Cenozoic tectonic events, magmatic pulses, and base and precious metal mineralization in the Central Andes, in: Ericksen, G.E., Cañas Pinochet, M.T., and Reinemund, J.A., (eds), Geology of the Andes and its relation to hydrocarbon and mineral resources: Houston, Texas, Circum-Pacific Council for Energy and Mineral Resources Earth Sciences Series, no. 11, p. 189–194.

McPhie, J., 2012, personal communication, Hobart, University of Tasmania.

McPhie, J., Doyle, M., and Allen, R., 1993, Volcanic textures: a guide to the interpretation

of textures in volcanic rocks: Hobart, CODES, University of Tasmania, 196 p.

Micklethwaite, S., 2010, Structural architecture, development and tectonic setting of the Gosowong Goldfield: Unpublished report prepared for Newcrest Mining Ltd., 197 p.

Micklethwaite, S., and Silitonga, D.E., 2011, Transient Kinematic Changes in Epithermal Systems: Toguraci Deposit, Halmahera: Society for Geology Applied to Mineral Deposits 11th Biennial Meeting, Antofagasta, Chile, September, Proceedings, p. 738-740.

Morris, J.D., Jezek, P.A., Hart, S.R. and Gill, J.B. 1983, The Halmahera island arc, Molucca Sea collision zone, Indonesia: a geochemical survey, in Hayes, D.E.(ed.) The Tectonic and Geologic Evolution of South-East Asian Seas and islands, Part 2: American Geophysical Union Monograph no. 23, p. 373-387.

Morrison, G., 2007, A geological domain model for the Kencana deposit and its application to near-mine exploration: Klondike Exploration Services, Unpublished report prepared for PT. Nusa Halmahera Minerals, 26 p.

Nash, J.T., 1972, Fluid inclusion studies of some gold deposits in Nevada: U.S Geological Survey Prof. Paper 800-C, p. C15-C19.

Newcrest Mining Limited, 2010, www.newcrest.com.au; written communication.

Olberg, D.J., 2001, Ore shoot targeting in the Gosowong vein zone, Halmahera, Indonesia: Unpublished Masters of Economic Geology thesis, University of Tasmania, 227 p.

Olberg, D.J, Rayner, J., Langmead R.P., and Coote, J.A.R., 1999, Geology of the Gosowong epithermal gold deposit, Halmahera, Indonesia, East Indonesia: Australasian Institute of Mining and Metallurgy Publication Series 4/1999, p. 179–186.

Parsons, I., Brown, W.L., and Smith, J.V., 1999, Ar/Ar thermochronology using alkali feldspars: real thermal history or mathematical mirage of microtexture?: Contributions to Mineralogy and Petrology, v. 136, p. 92-110.

Pass, H.E., 2010, Breccia-hosted chemical and mineralogical zonation patterns of the Northeast Zone, Mt. Polley Cu-Ag-Au alkalic porphyry deposit, British Columbia, Canada: Unpublished Ph.D thesis, CODES, University of Tasmania, 260 p.

Renne, P.R., Swisher, C.C., Deino, A.L., Karner, D.B., Owens, T.L., and DePaolo, D.J., 1998, Intercalibration of standards, absolute ages and uncertainties in $^{40}Ar/^{39}Ar$ dating: Chemical Geology, v. 145, p. 117-152.

Reyes, A.G., 1990, Petrology of Philippines geothermal systems and the application of alteration mineralogy to their assessment: Journal of Volcanology and Geothermal Research, v. 43, p. 279–309.

Reyes, A.G, Trompetter, W., Britten, K., and Searle, J., 2002, Mineral deposits in the Rotokawa geothermal pipelines, New Zealand: Journal of Volcanology and Geothermal Re-

search, v.119, p. 215-239.

Reed, M.H., 1997, Hydrothermal alteration and its relationship to ore fluid composition, in: Barnes, H.L., (ed.) Geochemistry of Hydrothermal Ore Deposits: John Wiley & Sons, Inc., New York, p. 303-365

Reed, M.H., and Spycher, N.F., 1985, Boiling, cooling, and oxidation in epithermal systems; a numerical modeling approach: Reviews in Economic Geology, v. 2, p. 249-272.

Richards, T.H, 2006, Gosowong Goldfield: Transverse Faults and Mineralisation: Unpublished internal company prepared for PT. Nusa Halmahera Minerals, 11 p.

Richards, T.H., and Basuki Dwi Priyono, M.D., 2004, Discovery of the Toguraci epithermal Au-Ag deposits, Gosowong goldfield, Halmahera Island, East Indonesia: Australasian Institute of Mining and Metallurgy Publication Series 5/2004, p. 359–366.

Richards, T.H., Ketut Gede Suyadnya, I., Tyasmudadi, N., Darmawan, D., and Muryanto, A., 2005, The discovery of the Kencana low sulfidation epithermal deposit, Gosowong goldfields, Halmahera, Island, East Indonesia: NewGen Gold Conference, Perth, Western Australia, November 2005, Proceedings, p. 151–167.

Sanematsu, K., Watanabe, K., Duncan, R., and Izawa, E., 2004, Mineralization ages using $^{40}Ar/^{39}Ar$ dating and the precipitation of gold in the Hishikari epithermal gold deposit, Japan, in: International Association of Volcanology and Chemistry Earth's Interior (IAVCEI) General Assembly, Pucón, Chile, Abstract (CD-ROM).

Sawkins, F.J., O'Neil, J.R., and Thompson, J.M., 1979, Fluid inclusion and geochemical studies of vein gold deposits, Baguio District, Philippines: Economic Geology, v. 74, p. 1420-1434.

Seward, T.M., 1991, The hydrothermal chemistry of gold, in Foster, R.P., (ed.) Gold metallogeny and exploration: Glasgow, Blackie and Son, p. 37–62.

Silitonga, D.E., 2006, The alteration and mineralization zonation based on core data analysis in the K1 vein, Kencana deposit, Gosowong Goldfield, Halmahera, North Maluku, Indonesia: Unpublished Bachelor of Science thesis, Padjadjaran University, 51 p.

Sillitoe, R.H., 1977, Metallic mineralization affiliated to subaerial volcanism: A review, in Volcanic processes in ore-genesis: London, Institution of Mining and Metallurgy and Geological Society, p. 99-116.

Sillitoe, R.H., and Hedenquist, J.W., 2003, Linkages between volcanotectonic settings, ore-fluid compositions, and epithermal precious-metal deposits: Society of Economic Geologists Special Publication no. 10, p. 315-343.

Simmons, S.F., and Browne, P.R.L., 2000, Hydrothermal minerals and precious metals in the Broadlands-Ohaaki geothermal system; implications for understanding low-sulfidation

epithermal environments: Economic Geology, v. 95, p. 971-999.

Simmons, S.F., and Christenson, B.W., 1994, Origins of calcite in a boiling geothermal system: American Journal of Science, v. 294, p. 361–400.

Simmons, S.F., White, N.C., and John, D.A., 2005, Geological characteristics of epithermal precious and base metal deposits: Economic Geology 100TH Anniversary Volume, p. 485–522.

Simon, G., Kesler, S.E., and Essene, E.J., 1997, Phase relations in selenides, sulfides, tellurides and oxides; II. Applications to selenide bearing ore deposits: Economic Geology, v. 92, p. 468-484.

Simpson, M.P., and Mauk, J.L., 2011, Hydrothermal Alteration and Veins at the Epithermal Au-Ag Deposits and Prospects of the Waitekauri Area, Hauraki Goldfield, New Zealand: Economic Geology, v. 106, p. 945–973.

Simpson, M.P., Mauk, J.L., and Castendyk, D.N., 2003, Geochemistry of wall-rock alteration at the Waihi and Favona epithermal deposits, New Zealand: New Zealand Branch of the Australian Institute of Mining and Metallurgy Annual Conference, 36th, Dunedin, New Zealand, 3-5 September, Proceedings, p. 261–270.

Simpson, M.P., Mauk, J.L., and Simmons, S.F., 2001, Hydrothermal alteration and hydrologic evolution of the Golden Cross Epithermal Au-Ag Deposit, New Zealand: Economic Geology, v. 96, p. 773-796.

Sims, D., 2008, The Gosowong Goldfield; 5 Moz and still growing: Proceedings, Terry Leach Symposium, Sydney, October, (Sydney Mineral Exploration Geologists Discussion Group: Sydney), p. 97-106.

Sims, D., and Benton, R., 2009, Life on the Rollercoaster – Mining and Milling the Kencana K1 Orebody, Indonesia: Proceedings, Seventh International Mining Geology Conference, p. 319-327 (The Australasian Institute of Mining and Metallurgy: Melbourne).

Spycher, N.F., Reed, M.H., 1989, Evolution of a Broadlands-type epithermal ore fluid along alternative P-T paths - implications for the transport and deposition of base, precious, and volatile metals: Economic Geology, v. 84, p. 328–359.

Steiger, R.H., Jäger, E., 1977, Subcomission on geochronology: Convention on the use of decay constants in geo- and cosmochronology: Earth and Planetary Science Letters, v. 36, p. 359-362.

Steiner, A., 1977, The Wairakei geothermal area, North Island, New Zealand: New Zealand Geological Survey Bulletin 90, 136 p.

Sukamto, R., Apandi. T., Supriatna. S., and Yasin, A., 1981, The geology and tectonics of Halmahera island and surrounding areas, in Barber, A.J., and Wiryosuyono, S., (eds.), The

Geology and Tectonics of Eastern Indonesia: Special Publication of the Indonesian Geology Resource Development Centre, v. 2, p. 349-362.

Thompson , A.J.B., Hauff, P.L., and Robitaille, A.J., 1999, Alteration mapping in exploration: Application of short-wave infrared (SWIR) spectroscopy: Society of Economic geologists Newsletter, no. 39, p. 16-27.

Uyeda, S., and Ben-Avraham, Z., 1972, Origin and development of the Philippine Sea: Nature v. 240, p. 176-178.

van Leeuwen, T.M., 1994, 25 years of mineral exploration and discovery in Indonesia: Journal of Geochemical Exploration, v. 50, p 13-90.

Vasconcelos, P., 1998, $^{40}Ar/^{39}Ar$ analyses, Gosowong prospect area, Halmahera: University of Queensland, internal company report prepared for PT. Nusa Halmahera Minerals/ Newcrest Mining Ltd, 69 p.

Walsh, J.J., and Watterson, J., 1991, Geometric and kinematic coherence and scale effects in normal fault systems: Journal of the Geological Society, London, Special Publications, v. 56, p. 193-203.

Warmada, I.W., Lehmann, B., and Simandjuntak, M., 2003, Polymetallic sulfides and sulfosalts of the Pongkor epithermal gold-silver deposit, West Java, Indonesia: The Canadian Mineralogist, v. 41, p. 185-200.

Warren, I., Simmons, S.F., and Mauk, J.L., 2007, Whole-rock geochemical techniques for evaluating hydrothermal alteration, mass changes, and compositional gradients associated with epithermal Au-Ag mineralization: Economic Geology, v. 102, p. 923–948.

White, J. D. L., McPhie, J., and Skilling, I., 2000, Peperite: a useful genetic term: Bulletin of Volcanology, v. 62, p. 65-66.

White, N.C., and Hedenquist, J.W., 1990, Epithermal environments and styles of mineralization: Variations and their causes, and guidelines for exploration: Journal of Geochemical Exploration, v. 35, p. 445–474.

Wurst, A.T., 2004, Geology and genesis of the Permata-Batu Badinding-Hulubai, and Kerikil Au-Ag low sulfidation epithermal deposits, Mt. Muro, Kalimantan, Indonesia: Unpublished Ph.D. thesis, University of Tasmania, 423 p.

Yu, Z., Robinson, P., Townsend, A.T., Munker, C., and Crawford, A.J., 2000, Determination of geological materials for trace element determination of using ICP-MS, Geostandards Newsletter: The Journal of Geostandards and Geoanalysis, v. 25, p. 199-217.

Zhang, Y., and Frantz, J.D., 1987, Determination of the homogenization temperatures and densities of supercritical fluids in the system NaCl–KCl–CaCl2–H2O using synthetic fluid inclusions: Chemical Geology, v. 64, p. 335–350